

# **Diagenetic controls on sandstones of the Stuttgart Formation – consequences for the porosity evolution of hydrothermal reservoirs in the North German Basin**

Dissertation

for the award of the degree  
*"Doctor rerum naturalium (Dr. rer. nat.)"*  
of the Georg-August University Göttingen

within the doctoral program Geoscience  
of the Georg-August University School of Science (GAUSS)

submitted by

Sebastian Niegel

from Borna (near Leipzig), Deutschland

Göttingen, 29.03.2023



Supervisory committee:

Prof. Dr. Martin Sauter

Department of Applied Geology,  
Georg-August University Göttingen

Dr. Matthias Franz

Department of Applied Geology,  
Georg-August University Göttingen

Thesis committee:

Referent: Prof. Dr. Inga Moeck

Department of Applied Geology,  
Georg-August University Göttingen

Co-referent: Prof. em. Dr. Reinhard Gaupp

Institute of Geosciences,  
Friedrich Schiller University Jena

Co-referent: Dr. Matthias Franz

Department of Applied Geology,  
Georg-August University Göttingen

Other members of the thesis committee:

Prof. Dr. Martin Sauter

Department of Applied Geology,  
Georg-August University Göttingen

Prof. Dr. Jonas Kley

Department of Structural Geology  
and Geodynamics,  
Georg-August University Göttingen

Dr. Markus Wolfgramm

Department 430 of Ministry for  
Climate Protection, Agriculture,  
Rural Areas and Environment,  
Mecklenburg-Vorpommern

Dr. Bettina Wiegand

Department of Applied Geology,  
Georg-August University Göttingen

Date of the oral examination: 09.05.2023



---

# Abstract

The present dissertation is part of the R&D project *GeoPoNDD*, which deals with the potential use of the six main Mesozoic geothermal reservoir complexes in Northern Germany. The hydrothermal reservoirs of the Stuttgart Formation, which have been poorly explored, were evaluated in the previous *Sandsteinfazies* project using an extensive database of cores, wireline logs and seismic data. This subsurface facies and thickness mapping of the Lower and Upper Schilfsandstein Members revealed a fluvio-deltaic environment prograding from the northern and southern margins toward this subsidence center. The resulting subsurface facies maps and samples of different facies types are the basis of this dissertation.

This study focused on petrography and diagenesis in the reservoirs of the Stuttgart Formation (Middle Keuper). Therefore, an extensive petrographic analysis of the Lower and Upper Schilfsandstein Members was carried out, leading to a mineralogical and diagenetic characterization of different facies types. Associated to the deposition of sandstones in distinct fluvio-deltaic environments, four diagenetic pathways – Delta Channel, Delta Plain, Fluvial Channel and Floodplain Diagenesis Types – are indicated by systematic variations of detrital and authigenic assemblages. In response to the evolution of the North German Basin, high permeabilities of sandstones of the Delta Channel and Fluvial Channel Diagenesis Types are related to the subsequent control of depositional and diagenetic regimes on porosity evolution. The proposed model of cementation-controlled burial diagenesis, followed by dissolution-controlled retrograde diagenesis (uplift) and low to moderate reburial corresponds to the Mesozoic–Cenozoic evolution of larger areas of the North German Basin.

Due to the documented diagenetic pathways, parageneses and the low to intermediate grain packaging seems to be not in agreement with the burial history of the Stuttgart Formation in the North German Basin. To reconstruct the basin evolution, i.a. isotopic and microthermal investigations were done. A reactive transport modelling for the possible formation of the analcime was also realized. The calculated formation temperatures of authigenic dolomite and quartz of up to 200 °C, as evidenced by fluid inclusions, indicate greater maximal burial depths of the Stuttgart Formation than previously known. To explain this discrepancy, different hypotheses are discussed. The subsequent uplift from deep to shallow burial depth, associated to latest Jurassic–Cenozoic structural differentiation and inversion of the North German Basin, triggered substantial dissolution processes that mainly affected carbonate cementations. A

possible second prograde diagenesis was documented by U/Pb dating of carbonate cementations, followed by a second reburial phase. Further dissolution and cementation processes were associated with this basin evolution. This opened pore spaces and contributed to the evolution of secondary porosity. Moderate post-inversion reburial rates resulted in only negligible mechanical compaction and reduction of secondary porosity.

Improved knowledge of diagenetic pathways and burial history, exemplified by sandstones of the Stuttgart Formation, will contribute significantly to improved predictions for other Mesozoic hydrothermal reservoir, i.e. Rhaetian reservoirs, in the North German Basin. Thus, better predictions regarding to the reservoir quality also minimize the exploration risk.

Geothermal exploitation of the Lower or Upper Schilfsandstein Members is limited due to locally highly variable reservoir quality (thicknesses, porosities, and permeabilities) resulting from different facies types and their characteristic diagenetic processes.

The stratigraphic, lithological, petrographic as well as petrophysical data finally led to aquifer maps of the Lower and Upper Schilfsandstein Members, which were made available to the public in the Geothermal Information System (GeotIS). This set of maps is intended to minimize exploration and financial risks for deep, geothermal reservoirs in the North German Basin in the future.

# Acknowledgement

This thesis was funded by the Federal Ministry for Economic Affairs and Climate Action (BMWK, grant number 0325920), which covered all the expenses I needed for this research.

My special thanks go to Dr. Matthias Franz for the opportunity to work on the *GeoPoNDD* project, his suggestions and exemplary supervision. I would like to thank Prof. Dr. Martin Sauter for his supervision and support in difficult phases during the promotion. I would also like to thank Dr. Graciela Sosa, Dr. Alfons van den Kerkhof and Dr. Markus Wolfgramm for their expertise in questions concerning the petrography, mineralogy and diagenesis of the investigated samples.

Further acknowledgements related to the studies can be found in the respective chapters.

Moreover, I would like to thank all my friends and fellow students who made my doctoral study so pleasant. Special thanks go to my parents, who have always supported me and without whom I would not be in the fortunate position to study and do my PhD.

# Content

<b>Abstract .....</b>	<b>i</b>
<b>Acknowledgement.....</b>	<b>iii</b>
<b>Content .....</b>	<b>iv</b>
<b>Chapter I.....</b>	<b>1</b>
<b>1 Introduction .....</b>	<b>1</b>
1.1 Motivation.....	1
1.2 Working area and data base .....	3
1.2.1 Working area.....	3
1.2.2 Data base.....	4
1.3 Approach of research .....	5
1.4 Structure of this thesis .....	6
References .....	7
<b>Chapter II.....</b>	<b>9</b>
<b>2 Deep geothermal resources of the North German Basin: The hydrothermal reservoirs of the Stuttgart Formation (Schilfsandstein, Upper Triassic) .....</b>	<b>9</b>
2.1 Introduction .....	10
2.2 Geological setting.....	12
2.3 An exploration scheme for Mesozoic hydrothermal reservoirs.....	14
2.4 Stratigraphic control on the reservoirs of the Stuttgart Formation .....	18
2.5 Subsurface facies mapping .....	20
2.5.1 Sea-level control .....	20
2.5.2 Morphology .....	23
2.5.3 Facies analysis.....	24
2.5.3.1 Facies associations the Lower Schilfsandstein.....	24
2.5.3.2 The Lower Schilfsandstein fluvio-deltaic system.....	31
2.5.3.3 Facies associations of the fluvial Upper Schilfsandstein.....	35
2.5.3.4 The Upper Schilfsandstein distributive fluvial system .....	37
2.6 Reservoir quality .....	40
2.6.1 Granulometry .....	40



2.6.2	Detrital mineralogy of sandstones .....	41
2.6.3	Authigenic mineralogy of sandstones .....	44
2.6.4	Porosity and permeability .....	45
2.6.5	Reservoir quality mapping .....	46
2.7	Seismic exploration and mapping .....	50
2.7.1	Example 1: Horn Graben (German North Sea) .....	50
2.7.2	Example 2: Wolin Block (Baltic Sea) .....	52
2.8	Discussion .....	54
2.8.1	Controls on deposition and preservation of the Stuttgart Formation .....	54
2.8.2	Drainage pattern .....	56
2.8.3	The Stuttgart Formation: a deep geothermal reservoir? .....	57
2.9	Concluding remarks .....	58
	References .....	59
A	Appendix .....	71
<b>Chapter III .....</b>		<b>72</b>
<b>3</b>	<b>Depositional and diagenetic controls on porosity evolution in sandstone reservoirs of the Stuttgart Formation (North German Basin) .....</b>	<b>72</b>
3.1	Introduction .....	73
3.2	Geological setting .....	75
3.2.1	The Central Euroean Basin System .....	75
3.2.2	The Stuttgart Formation .....	77
3.3	Working areas, data base and methods .....	78
3.4	Results .....	81
3.4.1	Granulometry .....	84
3.4.1.1	Lower Schilfsandstein Member .....	84
3.4.1.2	Upper Schilfsandstein Member .....	85
3.4.2	Detrital mineralogy .....	86
3.4.2.1	Schilfsandstein cores .....	86
3.4.2.2	Schilfsandstein outcrops .....	90
3.4.3	Compaction, intergranular volume and porosity .....	92
3.4.3.1	Schilfsandstein cores .....	92
3.4.3.2	Schilfsandstein outcrops .....	95
3.4.4	Authigenic mineralogy .....	96
3.4.4.1	Schilfsandstein cores .....	96
3.4.4.2	Schilfsandstein outcrops .....	107

3.5	Discussion.....	107
3.5.1	Diagenesis of the Stuttgart Formation .....	107
3.5.1.1	Depositional regime .....	109
3.5.1.2	Eogenetic regime .....	109
3.5.1.3	Mesogenetic regime.....	111
3.5.1.4	Telogenetic regime.....	112
3.5.2	Constraints on burial and uplift history.....	113
3.5.2.1	Maximum burial temperature and depth .....	113
3.5.2.2	Uplift and reburial .....	116
3.6	Conclusions .....	117
	References .....	119
<b>Chapter IV</b>	<b>.....</b>	<b>139</b>
<b>4</b>	<b>From eo- to telogenesis in sandstone diagenesis: constraints from fluid inclusions, stable isotopes and U/Pb dating of authigenic cementations ..</b>	<b>139</b>
4.1	Introduction .....	140
4.2	Data set and methods .....	140
4.2.1	Samples.....	140
4.2.2	SEM-EDX and CL .....	141
4.2.3	Microthermometry .....	142
4.2.4	Stable isotopes.....	142
4.2.4.1	Carbon and oxygen isotopes.....	142
4.2.4.2	Sulphur isotopes .....	143
4.2.5	U/Pb dating of carbonates.....	143
4.2.6	Reactive transport modelling.....	144
4.3	Results.....	147
4.3.1	Detrital mineralogy .....	147
4.3.2	Compaction and contact strength, intergranular volume and porosity..	149
4.3.3	Diagenesis and authigenic mineralogy .....	149
4.3.4	Microthermometry .....	150
4.3.5	Stable isotopes.....	154
4.3.5.1	Carbon and oxygen isotopes.....	154
4.3.5.2	Sulphur isotopes .....	157
4.3.6	U/Pb dating of carbonates.....	157
4.3.7	Reactive transport modelling.....	159
4.4	Discussion.....	160

---

4.4.1	Origin of authigenic carbonates and quartz .....	160
4.4.1.1	Stable isotopes of calcite and dolomite .....	160
4.4.1.2	Microthermometry of dolomite and quartz .....	164
4.4.1.3	U/Pb dating of carbonates .....	165
4.4.2	Origin of authigenic sulphates .....	167
4.4.3	Origin of authigenic analcime .....	169
4.4.4	Explanation for higher formation temperatures .....	169
	References .....	172
<b>Chapter V</b>	.....	<b>179</b>
<b>5</b>	<b>Diagenetic controls on sandstone reservoirs of the Exter Formation (Rhaetian) – preliminary results .....</b>	<b>179</b>
	References .....	188
<b>Curriculum Vitae</b>	.....	<b>191</b>







# Chapter I

## 1 Introduction

### 1.1 Motivation

This work is part of the joint project *GeoPoNDD* funded by the Federal Ministry for Economic Affairs and Climate Action (BMWK, grant numbers 0325920). The general idea of the project is to characterize Mesozoic geothermal reservoirs in Northern Germany and to work out their potential and to minimize their exploration risk. Thus, the project contributes, especially in the development of methods, processes and decision support tools, to the cost-effective use of heat from geothermal reservoirs in Northern Germany. Based on the distribution, formation and the evaluation of hydraulic properties, a map series of individual geothermal horizons is created and points to potential maps with high or low geothermal potential. By integrating the potential maps into the Geothermal Information System (GeotIS, [www.geotis.de](http://www.geotis.de)), exploration predictions for individual locations will be improved.

The most suitable Mesozoic aquifers for geothermal use in the North German Basin are the Middle Buntsandstein, Stuttgart Formation, Rhaetian, Lower Jurassic, Aalenian, and Lower Cretaceous (Fig. 1.1; Feldrappe et al., 2007, 2008; Wolfgramm et al., 2008).

Facies distribution and diagenesis are of essential relevance for the evolution and potential of geothermal reservoirs. Most of these reservoirs have already been studied regarding to their depositional environment and resulted in subsurface facies maps (Franz, 2020). So far, the diagenesis has not been studied in detail at any of these reservoirs. Therefore, the aim was to investigate the diagenesis of a first Mesozoic reservoir exemplarily.

The focus of this study is on the comparatively immature sediments of the Stuttgart Formation (Schilfsandstein), which show high porosities and permeabilities despite present-day burial depths of up to 1600 m. The same phenomenon is observed in other Mesozoic reservoirs, i.e. the Rhaetian reservoirs. This detailed study aims to reconstruct the influence of tectonics or facies on the preservation of reservoir suitability resulting from low compaction and high porosity. The fluvio-deltaic and brackish-marine sediments of the Stuttgart Formation are good candidates for such a study because of the small-scale facies shift, the relatively short depositional period of 1 Myr (Miller et al., 2017), and the basin-wide distribution.

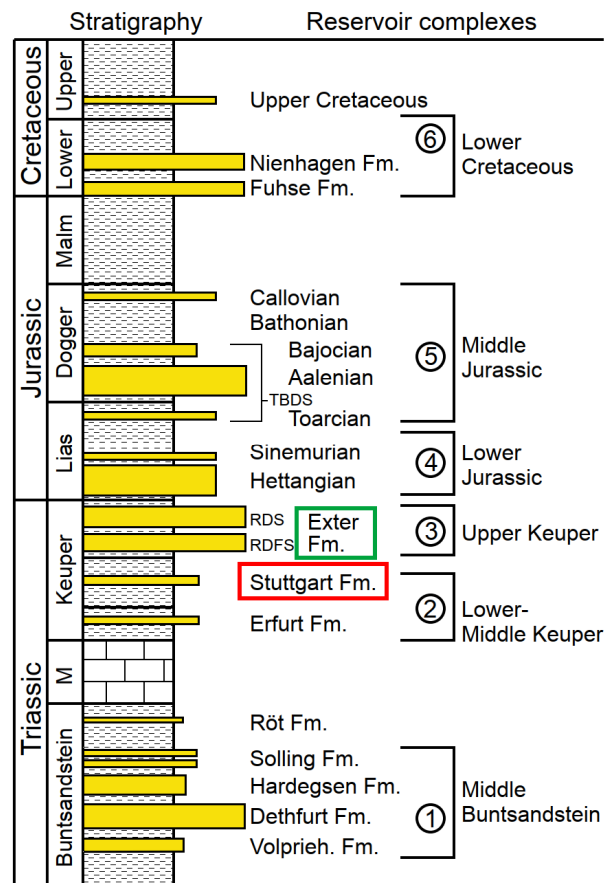


Fig. 1.1 Mesozoic reservoir complexes investigated within the R&D projects *Sandsteinfazies* and *GeoPoNDD* and studied in this thesis; modified from Franz (2020); red box - main subject of this thesis, green box – Mesozoic reservoir with the highest potential for geothermal use.

Starting from the generated subsurface facies maps and the sampled lithofacies types of the previous *Sandsteinfazies* project (FKZ 0325285, chapter II), a detailed mineralogical-petrographical study was carried out to determine the characteristics of the diagenetic modifications of various facies types (chapter III). Chemical analyses on selected authigenic minerals will be used to characterise in more detail with respect to formation temperatures, depths and chemism (chapter IV). Based on these results, a reconstruction of the basin evolution in the Northeast German Basin is given to provide a model for further Mesozoic reservoirs (chapter V).

On the basis of the obtained petrographic and hydraulic properties of the sediments, potential maps of the reservoirs were prepared (chapter II), which were published in the Geothermal Information System ([www.geotis.de](http://www.geotis.de)).



## **1.2 Working area and data base**

### **1.2.1 Working area**

The Schilfsandstein (Jäger, 1827) is known as the Stuttgart Formation based on the DSK (2005). The facies pattern and depositional environment are very controversial and highly debated (Wurster, 1964; Dittrich 1989; Bachmann and Beutler 1996; Shukla and Bachmann, 2007).

The Stuttgart Formation extends from present-day Poland, across Germany, to France and northern Switzerland, and plays a crucial role in understanding the development of the Central European Basin.

The investigation of the Stuttgart Formation as a geothermal reservoir was realised for the eastern part of the North German Basin. For a basin-wide petrographic-diagenetic comparison, further samples from the Weserbergland, Thuringia and southern Germany were analysed mineralogically (see chapter III). Due to the diverse and complex development of the German Basin, the samples arise from wells with depths of 240–1600 m (northern Germany) as well as from surface outcrops (Weserbergland, Thuringia, southern Germany) (Fig. 1.2).

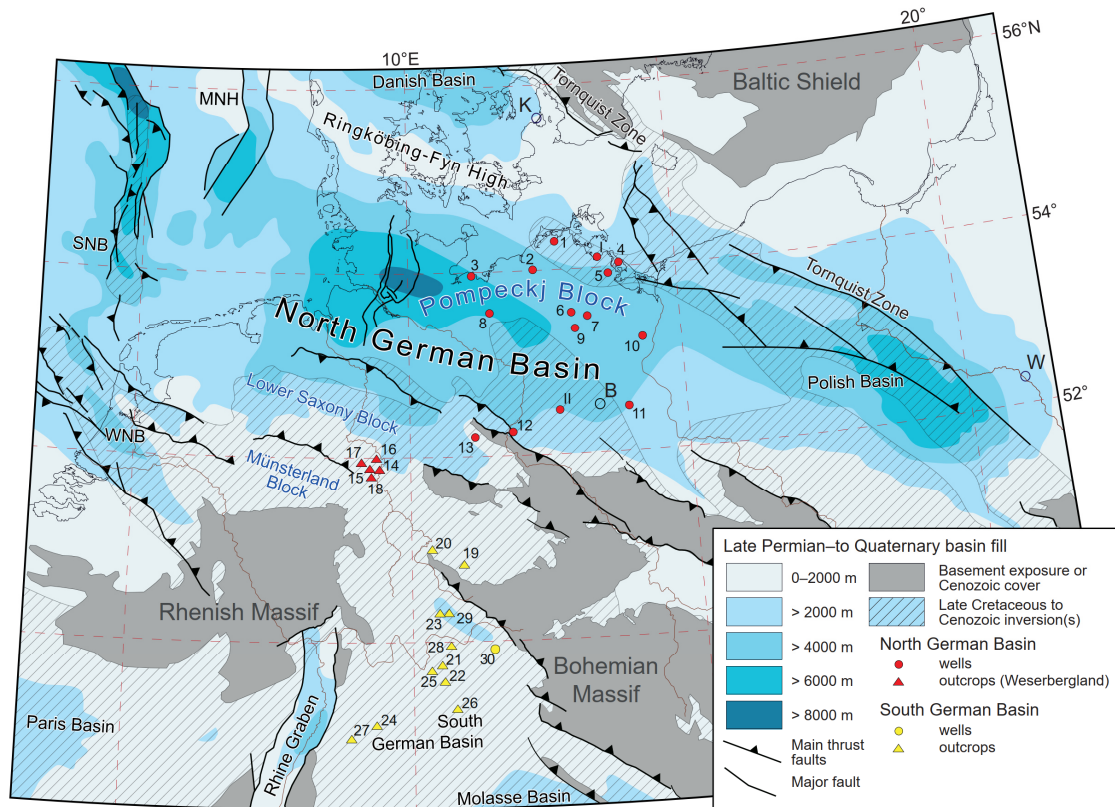


Fig. 1.2: Central European Basin System with subbasins, major fault systems and basement exposures, MNH – Mid North Sea High, SNB – South North Sea Basin, WNB – West Netherlands Basin; modified after Kley and Voigt (2008). Thickness of the Later Permian–Quaternary basin fill according to Ziegler (1990). North Germany: 1 – Kb Barth 6a/65, 2 – Kb Goritz 1/62, 3 – E Klütz 1/65, 4 – E Lütow 3/66, 5 – Kb Wolgast 1/1A/63, 6 – Kb Tarnow 1/65, 7 – Gt Neubrandenburg 2/85, 8 – Kb KSS 1/66, 9 – Kb Brustorf 1/62, 10 – Kb Gartz 1/65, 11 – Kb Strausberg 1/63, 12 – Kb Burg 2/61, 13 – Dp Morsleben 52a/95; localities referred to as in the text: I – Loissin 1/70, II – Ketzin storage site (several wells). Weserbergland: 14 – Birkenberg-Polle, 15 – Wiehenberg, 16 – Amelgatzen, 17 – Barntrop, 18 – Osterhagen. Thuringia: 19 – Drei Gleichen area (Arnstadt); 20 – Am Hohnert (Eisenach). South Germany: 21 – Abtswind, 22 – Eulenberg, 23 – Eyershausen, 24 – Heilbronn, 25 – Iphofen, 26 – Lichtenau, 27 – Maulbronn, 28 – Sand am Main, 29 – Trappstadt, 30 – Obersees 1. Figure is from Niegel and Franz (2023).

## 1.2.2 Data base

As part of the *Sandsteinfazies* project (FKZ 0325285), a comprehensive facies study was carried out, which led to a new interpretation of the facies pattern of the Stuttgart Formation (Franz et al., 2018). Based on this, the model of an endorheic basin with fluvio-deltaic and brackish-marine deposits was developed (Franz et al., 2018).

Many samples of different facies types were obtained during this previous study. This extensive data and sample record (e.g. thin sections, granulometric data, poro-perm data) from various wells in the North German Basin was available for petrographic analysis at the beginning of this thesis. Detailed descriptions of the applied methods are explained in the corresponding chapters of this cumulative dissertation.

### 1.3 Approach of research

In the projects *Sandsteinfazies* (grant 0325285) and *GeoPoNDD* (grant 0325920) the potential geothermal reservoirs were evaluated according to the following five steps (see also Fig. 1.3):

1. bio-/sequence-stratigraphic dating
2. reconstruction of the facies areas
3. petrography, petrology and diagenesis of the sediments
4. hydraulic characterisation
5. spatial illustration in thematic maps

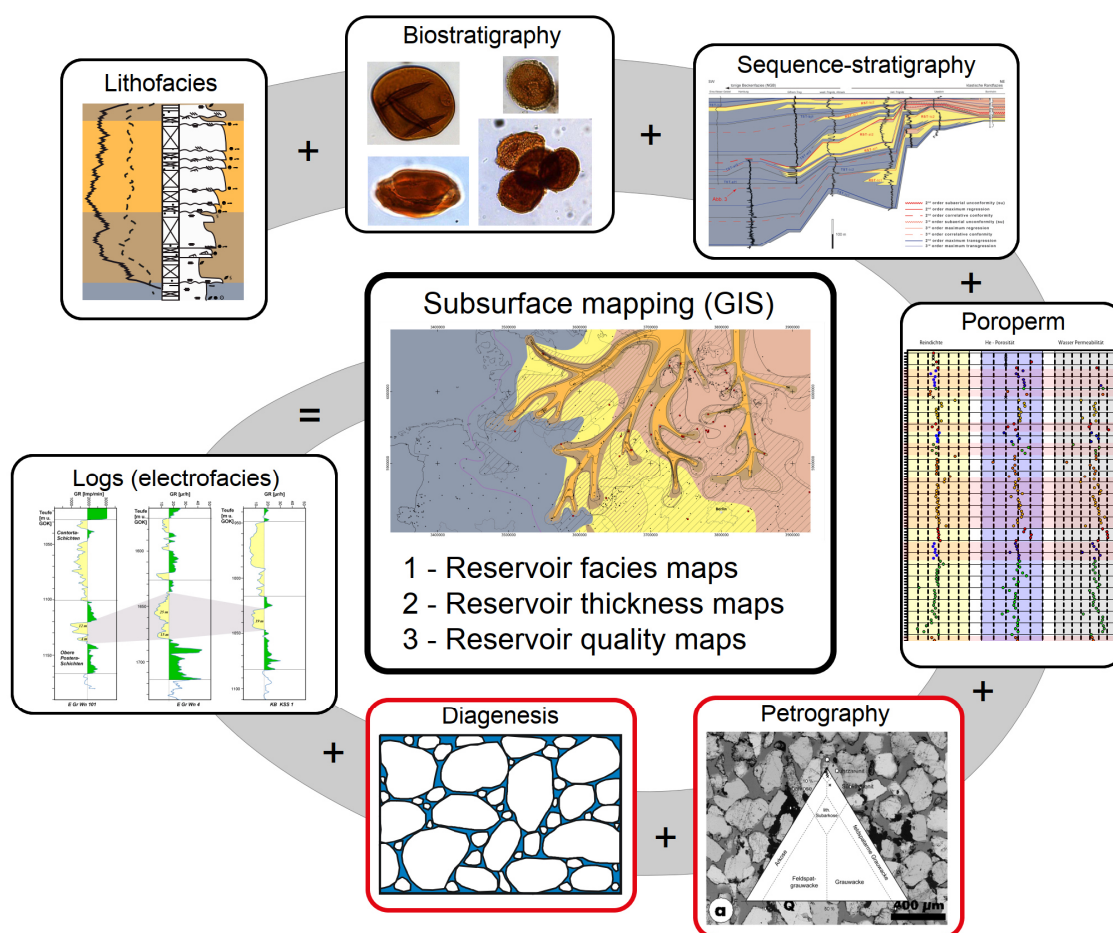


Fig. 1.3: Simplified exploration workflow applied to the Mesozoic reservoirs; modified from Franz et al. (2018); red boxes mark the involvement of this study.

Bio-/sequence-stratigraphic dating (step 1) and reconstruction of the facies areas (step 2) of the Stuttgart Formation were mainly studied in the *Sandsteinfazies* project.

The results of this study were published in Franz et al. (2018; see chapter II). In progress of this thesis, petrography, petrology and diagenesis of the sediments (step 3) were extensively studied, which finally led to a detailed characterisation of the reservoirs of the Stuttgart Formation. Based on the facies analysis and hydraulic properties (step 4), the preparation of potential maps (step 5, chapter II) was realised during the previous *Sandsteinfazies* project. Petrography and diagenesis in chapter II were made during the progress of this thesis. The results of this study are mainly presented in the chapters III to V.

An extensive thin section study (transmitted light and cathodoluminescent microscopy, SEM-EDX, microthermometry/fluid inclusions) is the main work of this dissertation. These data are complemented by geochemical analysis of stable isotopes, determination of salinities in fluid inclusions; carbonate dating and conventional X-ray diffraction (XRD) analysis were applied to bulk rock samples. Based on the data obtained from this study, a reactive transport modelling was realised additionally. Facies reconstructions and maps, granulometric data, porosities and permeabilities of the investigated samples were already available at the beginning of the *GeoPoNDD* project. Detailed explanations of the methods can be found in the corresponding chapters.

#### **1.4 Structure of this thesis**

This doctoral thesis is divided into five chapters.

Chapter I sets the context for the entire topic of this study. The following chapters describe the different subjects of the study and their results.

In chapter II the facies analysis and the generated subsurface facies maps of the Lower and Upper Schilfsandstein Members are published. Furthermore, the potential and spatial distributions of the Stuttgart Formation in northeastern Germany are presented.

Chapter III shows diagenesis types, which have undergone different petrographic and mineralogical formations due to variations in facies and depositional conditions. Additionally, a reconstruction of the basin evolution is given based on authigenic minerals.

Chapter IV deals with unpublished data of the project, which support the reinterpretation of the basin evolution. Special investigations (e.g. stable isotopes, fluid inclusions, carbonate dating) on different authigenic minerals allow conclusions to be

drawn about on the paleofluid evolution (chemism, temperature), which enables the chronological classification of authigenic mineral formation during basin development.

Chapter V highlights the significance of this study for further Mesozoic reservoirs.

## References

- Bachmann, G. H., Beutler, G., 1996. Fluviale Zyklen im Schilfsandstein (Obere Trias) in Neinstedt am Harz. – *Hall. Jb. Geow. B*, 18: 131–140.
- Dittrich, D., 1989. Der Schilfsandstein als synsedimentär-tektonisch geprägtes Sediment – eine Umdeutung bisheriger Befunde. – *Z. dt. geol. Ges.*, 140 (2): 295–310.
- DSK (Deutsche Stratigraphische Kommission, Ed.) (2005): *Stratigraphie von Deutschland, IV: Keuper*. Courier Forschungsinstitut Senckenberg 253, 296 p.
- Feldrappe, H., Obst, K., Wolfgramm, M., 2007. Evaluation of sandstone aquifers of the North German Basin: a contribution to the „Geothermal Information System of Germany“. In: *Abstracts for the European Geothermal Congress. Proceedings European Geothermal Congress 2007*, 8 p.
- Feldrappe, H., Obst, K., Wolfgramm, M., 2008. Die mesozoischen Sandsteinaquifere des Norddeutschen Beckens und ihr Potential für die geothermische Nutzung. *Zeitschrift für Geologische Wissenschaften* 36 (4–5), 199–222, only abstract.
- Franz, M., 2020. Remaining opportunities in hydrothermal reservoirs of the North German Basin – an exploration strategy for improved reservoir predictions and developments, Technische Universität Bergakademie Freiberg, Habilitationsschrift.
- Franz, M., Nowak, K., Niegel, S., Seidel, E., Wolf, M., Wolfgramm, M., 2018. Deep geothermal resources of the North German Basin: The hydrothermal reservoirs of the Stuttgart Formation (Schilfsandstein, Upper Triassic). *Zeitschrift der Deutschen Gesellschaft für Geowissenschaften* 169 (3) 353–387. <https://doi.org/10.1127/zdgg/2018/0164>.
- Jäger, G. F. v., 1827.: *Über die Pflanzenversteinerungen welche in dem Bausandstein von Stuttgart vorkommen*. – 40 p., VIII Bl. : III.; Stuttgart.
- Kley, J., Voigt, T., 2008. Late Cretaceous intraplate thrusting in central Europe: effect of Africa–Iberia–Europe convergence, not Alpine collision. *Geology*, 36, 839–842. <https://doi.org/10.1130/G24930A.1>.

- Miller, C.S., Peterse, F., da Silva, A.-C., Baranyi, V., Reichart, G.J., Kürschner, W., 2017. Astronomical age constraints and extinction mechanisms of the Late Triassic Carnian crisis. *Scientific Reports*, 7, No 2557: 1–7. <https://doi.org/10.1038/s41598-017-02817-7>.
- Shukla, U. K., Bachmann, G. H., 2007. Estuarine sedimentation in the Stuttgart Formation (Carnian, Late Triassic), South Germany. – *N. Jb. Geol. Paläontol. Abh.*, 243: 305–323.
- Wolfgramm, M., Rauppach, K., Seibt, P., 2008. Reservoir-geological characterization of Mesozoic sandstones in the North German Basin by petrophysical and petrographical data. *Zeitschrift für Geologische Wissenschaften* 36 (4–5), 249–265.
- Wurster, P., 1964. *Geologie des Schilfsandsteins*. – *Mitt. d. Geol. Staatsinst. Hamburg*, 33: 1–140.
- Ziegler, P. A., 1990. *Geological Atlas of Western and Central Europe*. Shell International Petroleum Maatschappij BV, Den Haag.

# Chapter II

## 2 Deep geothermal resources of the North German Basin: The hydrothermal reservoirs of the Stuttgart Formation (Schilfsandstein, Upper Triassic)

Publication: Franz, M., Nowak, K., Niegel, S., Seidel, E., Wolf, M., Wolfgramm, M., 2018. Deep geothermal resources of the North German Basin: The hydrothermal reservoirs of the Stuttgart Formation (Schilfsandstein, Upper Triassic). *Zeitschrift der Deutschen Gesellschaft für Geowissenschaften* 169 (3) 353–387. <https://doi.org/10.1127/zdgg/2018/0164>

**Authors' edited topics:** This publication was mainly conceptualized and written by Matthias Franz (reconstruction of depositional environments, granulometric analysis of the sediments, sequence stratigraphy, potential analysis as a geothermal reservoir). Kerstin Nowak and Matthias Franz documented the wells, described them macroscopically, and executed facies analysis and interpretation. The microscopic study of the detrital and authigenic minerals was realized by Sebastian Niegel. Elisabeth Seidel and Marco Wolf contributed seismic studies from the North Sea and Baltic Sea areas. Markus Wolfgramm worked on the concept of the publication, the discussion and made important corrections.

## **Abstract**

The enormous geothermal resources of the North German Basin are bound to Palaeozoic petrothermal and Mesozoic hydrothermal reservoirs. Based on previous exploration campaigns, six Mesozoic reservoir complexes were identified among which the hydrothermal reservoirs of the Stuttgart Formation were underexplored so far. To evaluate the potential of these reservoirs, an interdisciplinary exploration strategy was applied to a large database of cores, wireline logs and seismic data. Repeated transgressions from Tethyan waters resulted in formation of inland seas covering large parts of the basin. Accordingly, the deposition of the Stuttgart Formation was primarily controlled by 3<sup>rd</sup>- and 4<sup>th</sup>-order T-R sequences; in particular, the basinwards-directed progradation of the fluvio-deltaic Lower and Upper Schilfsandstein Members are related to lowstands. Within both members, fine- to medium grained sandstones of channel fills and levee–crevasse splay complexes form compound reservoirs representing the main target of geothermal exploration. For the Lower Schilfsandstein, this channel belt reservoir type is characterised by a median thickness of 23 m, median porosity of 22.7 % and median permeability of 443 mD. For the Upper Schilfsandstein, the channel belt reservoir type is characterised by a median thickness of 17 m, median porosity of 24.0 % and median permeability of 546 mD. The quality of these reservoirs is limited by the generally low compositional maturity of sandstones being lithic arkoses and feldspatic litharenites, the partly high content of detrital matrix within pores and substantial diagenetic cementation. The resulting high lateral variability of reservoir qualities contributes to considerable exploration risks. Despite this, reservoirs of high quality could be proven for individual localities where they may be considered alternative option if the development of Upper Keuper or Middle Jurassic hydrothermal reservoirs fails.

## **2.1 Introduction**

The North German Basin (NGB) yields enormous deep geothermal resources commonly subdivided into Palaeozoic petrothermal reservoirs and Mesozoic hydrothermal reservoirs (Rockel et al. 1997, Jung et al. 2002). Following an intense phase of hydrocarbon exploration, the exploration of Mesozoic hydrothermal reservoirs started in the early 1970's in NE Germany. Since, numerous studies have evaluated Mesozoic hydrothermal reservoirs (e.g. Katzung 1984, Diener et al. 1988-92, Wormbs et al. 1988, Katzung et al. 1992, Scholle 1992, Beutler et al. 1994, Schulz & Röhling 2000, Kabus et al. 2003, Feldrappe et al. 2008). These studies focused almost



exclusively on sandstone reservoirs and identified six reservoir complexes within the Mesozoic succession. So far, the depths, temperatures and thicknesses of these reservoir complexes were evaluated in a rather generalised form (see GeotIS; Agemar et al. 2014). As such, the reliable reservoir prediction for under-explored localities is hampered since high-resolution subsurface facies mapping has not been carried out for individual reservoirs. The same refers to sand thickness maps, which are either too low resolution or too generalised (see Feldrappe et al. 2008: Fig. 5c).

The exploitation of geothermal energy started with the development of Rhaetian reservoirs at the sites of Waren (1986) and Neustadt Glewe (1994) (Fig. 2.1). Based on these development examples, the long-term successful operation of hydrothermal reservoirs requires:  $>65\text{ }^{\circ}\text{C}$  reservoir temperature,  $>20\text{ m}$  reservoir net-thickness and  $>500\text{ mD}$  permeability (Rockel et al. 1997). These requirements emphasise the importance of high-resolution subsurface maps illustrating the net-thickness and quality of individual reservoirs and enabling improved reservoir predictions. As such, an exploration strategy was designed to provide high-resolution subsurface facies and thickness maps. In the years 2011–2015, this approach was applied to the Lower to Middle Keuper, Upper Keuper and Middle Jurassic reservoir complexes; it is currently applied to the Middle Buntsandstein, Lower Jurassic and Lower Cretaceous reservoir complexes.

Recently, results of the exploration of the Upper Keuper and Middle Jurassic reservoir complexes were reported by Franz et al. (2015, 2018a), Zimmermann (2015) and Zimmermann et al. (2018) including high-resolution subsurface maps. This contribution details the exploration result of the Schilfsandstein reservoirs (Stuttgart Formation) including sets of high-resolution subsurface facies, reservoir thickness and quality maps as well as two case studies of seismic exploration.

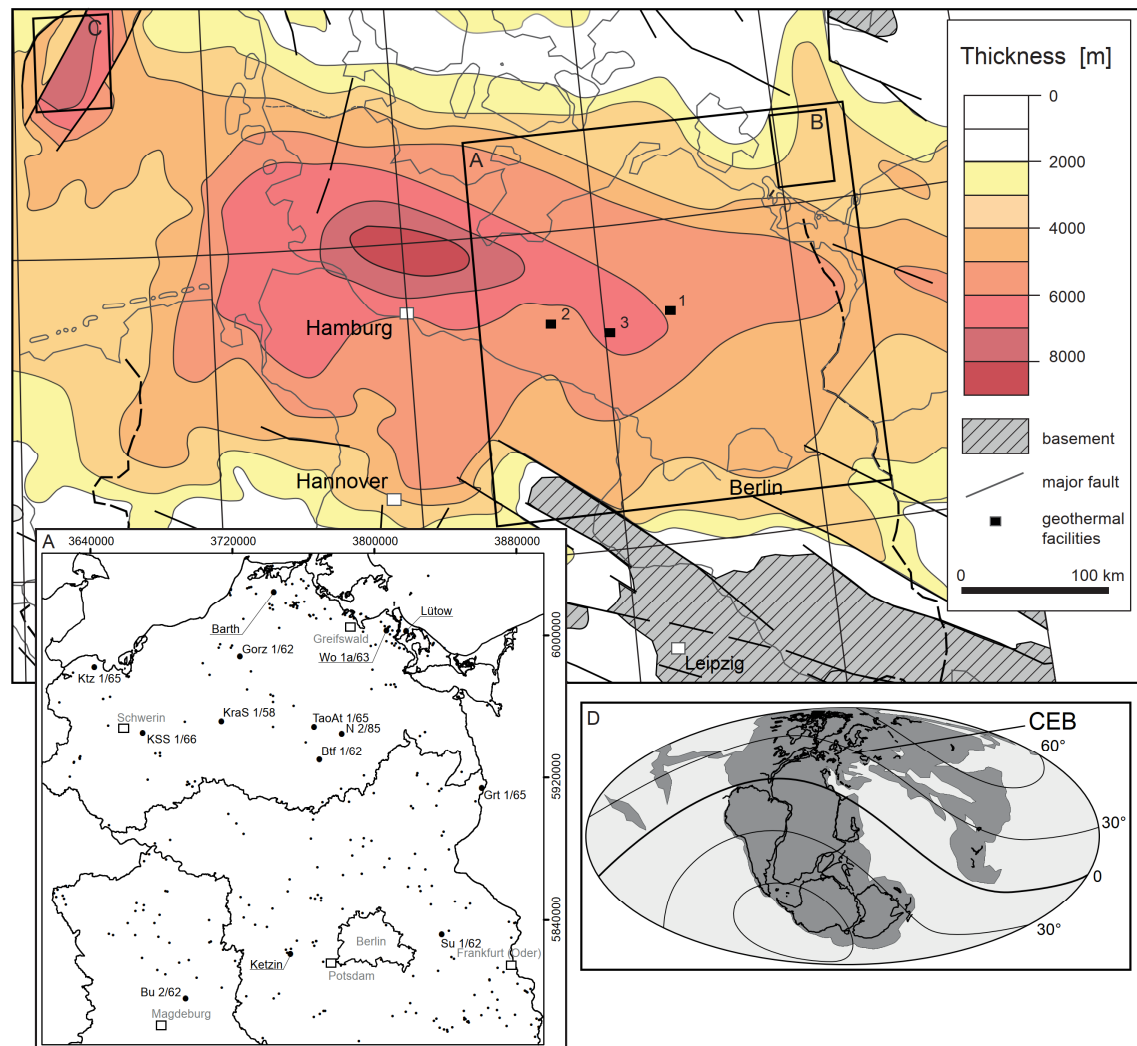


Fig. 2.1: Structure of the North German Basin and sedimentary thickness of Upper Rotliegend to base Quaternary; compiled after Ziegler (1982, 1990). Black squares = Geothermal facilities referred to in the text: 1 = Waren, 2 = Neustadt-Glewe (for details see Franz et al. 2018a), 3 = Parchim 1 (see Fig. 2.2). (A) Working area of subsurface mapping; large dots, small dots = cored wells, logged wells studied herein. (B), (C) Seismic exploration case studies (B = Wolin Block, C = Horn Graben). (D) Late Triassic global palaeogeography (Stampfli, unpubl.).

## 2.2 Geological setting

Following the Variscan Orogeny, the Central European Basin (CEB) formed as a large epicontinental sag basin (Bally & Snellson 1980), or intracontinental (cratonic) basin, with a center to the North of the Variscan Orogen (Bachmann & Grosse 1989, Ziegler 1990, Gast et al. 1998). During its long basin history, the CEB accumulated a succession of considerable thickness, in particular in the North German part of the basin where the Rotliegend to Tertiary basin fill locally exceeds a thickness of 10,000 m (Fig. 2.1; Bachmann & Grosse 1989, Pharaoh et al. 2010). According to this thick basin fill and geothermal gradients of 32–90 K per km of depth, the North German

Basin yields enormous deep geothermal resources (Katzung 2004, Wolfgramm et al. 2014).

The complex history of the CEB was characterised by alternating phases of subsidence, basin reorganisation and salt diapirism (Nöldecke & Schwab 1977, Ziegler 1990, Kley et al. 2008). Consequently, three main stages may be recognised: (1) basin initiation, (2) basin fill, (3) basin differentiation and inversion (Fig. 2.2; Nöldecke & Schwab 1977, Schwab 1985). In particular, the basin differentiation and inversion stage (Late Jurassic to recent) may be further subdivided (Kley et al. 2008).

Petrothermal resources are mainly associated to late Palaeozoic strata of the basin initiation and early basin fill stages; whereas hydrothermal resources are bound to Mesozoic strata of the middle and late basin fill stage. Jung et al. (2002) estimated the total geothermal resources of Germany for electricity production to about 1,200 EJ (Exa Joule =  $10^{18}$  J), the six hundredfold of the total electricity consumption of about 2 EJ in the year 2002. About 96 % of these enormous resources are bound to petrothermal reservoirs, 4 % are bound to faults and 1 % is bound to hydrothermal reservoirs only (Jung et al. 2002). In the NGB, the Mesozoic sandstone reservoirs are commonly grouped to six reservoir complexes: (1) Middle Buntsandstein, (2) Lower to Middle Keuper, (3) Upper Keuper, (4) Lower Jurassic, (5) Middle Jurassic and (6) Lower Cretaceous (Fig. 2.3; Wolfgramm et al. 2008, Franz et al. 2018a).

The Lower to Middle Keuper reservoir complex comprises potential hydrothermal reservoirs in the Lower Keuper (Erfurt Formation) and the Middle Keuper (Stuttgart Formation, Schilfsandstein). The reservoirs of the Stuttgart Formation are situated at depths of 250–1600 m in the eastern part of the NGB. Towards the western part, the depth increases to 2,500 m and more (Feldrappe et al. 2008). Proven depths of more than 5,000 m in the western NGB are related to graben structures and rim synclines. Depths of less than 300 m in the eastern NGB are related to salt diapirs (Baldschuhn et al. 2001, Feldrappe et al. 2008). Accordingly, the temperatures of reservoir fluids vary from 33 °C to, locally, more than 100 °C (Feldrappe et al. 2008).

The typical sandy to shaly lithologies of the Stuttgart Formation occur sandwiched between variegated Keuper shales forming a prominent succession of basin-wide occurrence. The sedimentological research initially focussed on the outcrop areas in the southern CEB (review in Schröder 1977). Since the comprehensive conceptual work of Wurster (1964), the depositional environment of the Stuttgart Formation was subject to animated discussions. Based on intense outcrop analyses in South Germany, Wurster (1964, 1972), Emmert (1965) and Brown and Fisher (1971) argued

for a large delta system, running N-S to NNE-SSW, with a source area in Scandinavia. Later, a deltaic origin was rejected and a fluvial origin became widely accepted (e.g. Heling 1979, Duchrow 1984, Dittrich 1989, Ricken et al. 1998, Shukla et al. 2010).

In the NGB, the Stuttgart Formation was subject to several studies of facies and sedimentology (e.g. Häusser 1972, Häusser & Kurze 1975, Beutler & Häusser 1982, Beutler 1995, Franz 2008, Barnasch 2010, Förster et al. 2010, Shukla et al. 2010, Franz et al. 2014). Based on the evaluation of a large set of well data, Beutler & Häusser (1982), Beutler & Nitsch in DSK (2005) and Barnasch (2010) argued for an exo-rheic drainage and reconstructed a network of broad N-S to NNE-SSW trending channel belts running across the NGB towards South Germany. In agreement with the model of Wurster (1964), this network was considered routing system for detritus of Scandinavian provenance transported to South Germany.

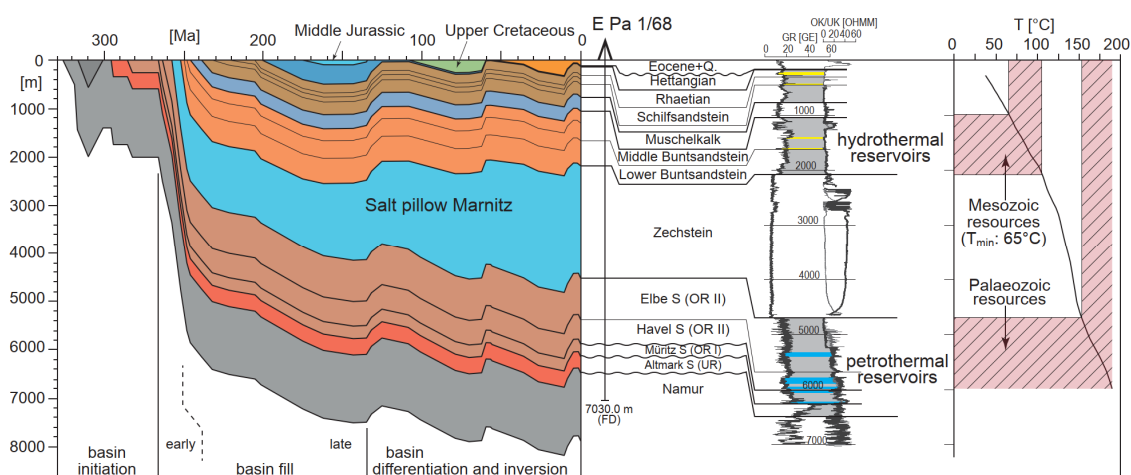


Fig. 2.2: The basin fill of the North German Basin as exemplified by well Parchim 1/68, modified from Franz et al. (2018a). The Zechstein evaporates subdivide Mesozoic from Palaeozoic reservoirs. The former are operated using conventional methods and the latter using unconventional methods subsumed under the term Enhanced Geothermal Systems (EGS). S = Subgroup, UR = Unterrotliegend, OR = Oberrotliegend. For location see Fig. 2.1; temperature from Hoth (1997); subsidence curve modified from Hoth (1997), Friberg (2001), Wolfgramm (2005).

### 2.3 An exploration scheme for Mesozoic hydrothermal reservoirs

The significant reduction of exploration risks and improved prediction of reservoir quality are the two main goals of the exploration scheme designed for Mesozoic hydrothermal reservoirs (Franz et al. 2015). In the years 2011–2015, this exploration scheme was applied to the Lower to Middle Keuper, Upper Keuper and Middle Jurassic reservoir complexes (Franz et al. 2015, Zimmermann 2015, Franz et al. 2018a, this work).

The study on the Lower to Middle Keuper reservoir complex focused only on potential reservoirs of the Stuttgart Formation. In the first step, a detailed core-based litho- and biofacies analysis was applied to 14 wells with complete or partially core recovery of the Stuttgart Formation (Fig. 2.4). Grain-sizes and physical bedding structures were used to define primary and secondary lithofacies types. The integration of biofacies analyses, macro- and micropalaeontology, palynology and partly ichnology led to facies associations. The facies associations were employed to reconstruct the depositional environments of the Stuttgart Formation, in particular the reservoirs of the Lower and Upper Schilfsandstein Members. In the second step, litho- and biostratigraphically dated sections were used to reconstruct the architectures of the Stuttgart Formation along basin centre-to-basin margin transects in order to define genetic surfaces (Franz et al. 2014). These genetic surfaces, for example the maximum regression surface of the Lower Schilfsandstein, provided the base for the construction of subsurface facies maps. In the third step, the granulometry, petrography, diagenesis and hydraulic parameters of reservoirs were studied in order to evaluate the reservoir quality. The granulometry was analysed based on 256 samples (18 wells). Samples were mechanically disintegrated by gently mortar grinding using a wooden pestle. Following optical inspection under binocular microscope the samples were dry sieved with standard mesh sieves according to DIN 4022 standard. The results were classified following Wentworth (1922) and values of mean grain sizes, sorting and skewness were calculated according to Folk & Ward (1957). For petrography and diagenesis, 98 thin sections were investigated by means of transmitted light and cathodoluminescent microscopy and SEM-EDX. Point counting analyses of very fine- to medium-grained sandstones were performed to quantify detrital grains, matrix, authigenics and pore space and to estimate the contact strength according to Füchtbauer (1973). 200-300 point per thin section were counted, the step size was adapted to grain sizes of individual samples.

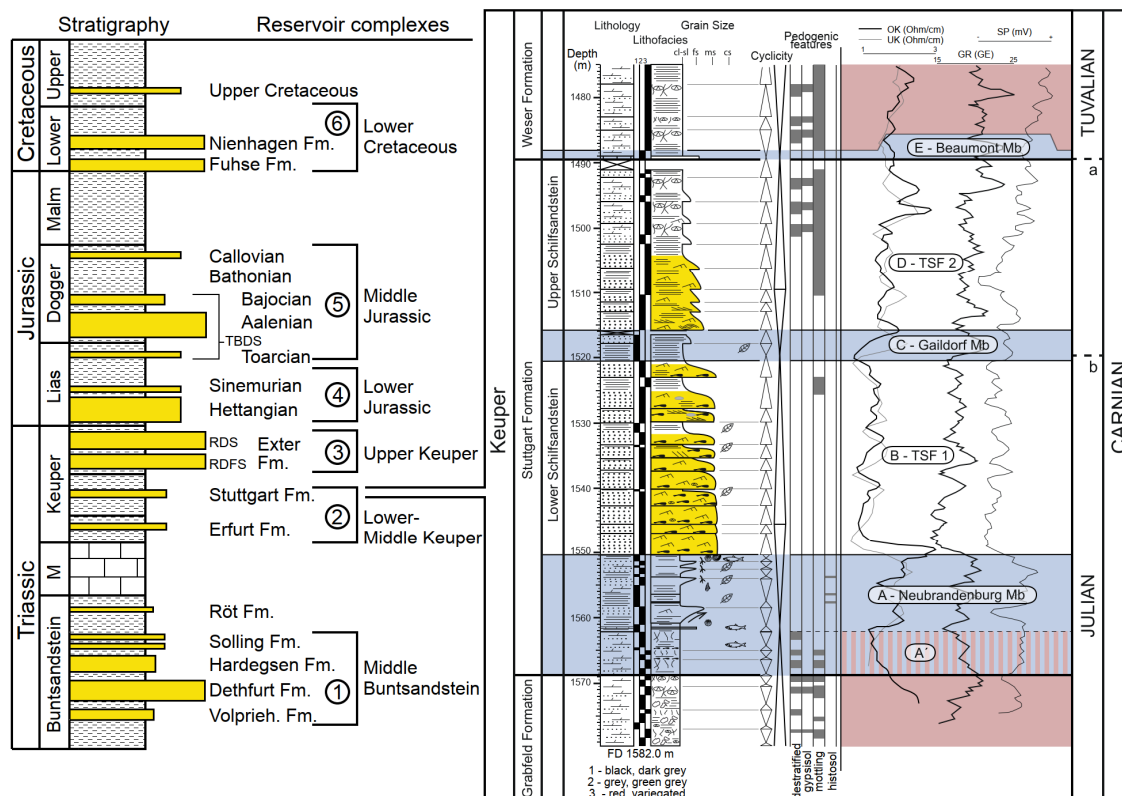


Fig. 2.3: The Mesozoic reservoir complexes of the NGB with herein detailed reservoirs of the Stuttgart Formation exemplified by the Neubrandenburg 2 well. Blue = transgressions, yellow = Lower and Upper Schilfsandstein reservoirs. Correlation of the Julian-Tuvalian boundary: a = according to Kozur & Bachmann (2010), b = modified from Franz et al. (2014). For location see Fig. 2.1.

Sandstones were classified according to Pettijohn (1967) and McBride (1963) and compared to a data set of older and younger sandstones of the NGB (Franz et al. 2018a). The porosity was analysed by 114 measurements of the fluid saturation (Archimedes' principle) and 66 measurements of helium porosity. The permeability was analysed by means of 66 measurements of water permeability at Gesteinslabor Dr. Eberhard Jahns (Heiligenstadt, Germany). Data and parameters of measurements are available upon request. In addition, the permeability was calculated from  $k_f$ -values of 256 grain size analyses using a modified formula of Beyer (1964). This is based on correlations of  $k_f$ -values estimated from lab measurements, thin section analyses and grain size analyses as described by Franz et al. (2015).

For subsurface facies mapping a large data base of more than 300 logged wells was integrated. The results of the core-based facies analysis (corefacies) were transferred to logged wells based on typical motifs of wireline logs (electrofacies). As cored intervals allow a much more detailed facies reconstruction compared to wireline log interpretations, some simplifications were needed. The levee and crevasse splay facies associations, which could be readily distinguished in cored intervals, were summarised

to a levee/crevasse splay complex in wireline logs. In the same way, terminal distributary channels and proximal mouth bars were merged to a distributary/mouth bar complex. For individual wells, the dominant facies association of the upper regressive phases and the maximum regressions were projected onto GIS-based subsurface facies maps of the Lower and Upper Schilfsandstein Members. Concerning the Lower Schilfsandstein, the subsurface map displays the cumulative evolution of deltas from their initial formation up to the approximated final stage. Concerning the Upper Schilfsandstein, the subsurface map displays the maximum progradation and outbuilding of distributive fluvial systems. The Usedom and Ketzin areas were selected for detailed mapping due to tight well spacing in these areas. The results of these studies, in particular the lateral shifting architecture of channel belts, were transferred to parts of the study area with rather limited well control, such as the Darß area. For areas of poor well control, the proven records of channels were linked directly resulting in straight courses of channel belts. For individual areas, the number of channels mapped is related to the well control and thus, the effective number of channels might be higher.

To control the mapped fluvio-deltaic channel belts and characterise their palaeohydraulics, the width of channel belts ( $W_{dcb}$ ) were calculated from the thicknesses of sandy channel fills using empirical equations according to Collinson (1978) and Fielding & Crane (1987). The integration of reservoir quality and subsurface facies resulted in reservoir quality maps localising areas of high, medium and low reservoir qualities. The reservoir qualities were characterised low, medium or high based on threshold values of <10 m, 10–20 m and >20 m reservoir thickness and of <250 mD, 250–500 mD and >500 mD permeability. It is important to note; these maps do not illustrate a possibility of success.

To support the subsurface mapping, two seismic studies were carried out in the German part of the Horn Graben (German North Sea, TUNB project) and Wolin Block (Baltic Sea, USO project). For the Horn Graben, the German Part of the HG97 2D seismic dataset from Maersk was reinterpreted using Paradigm SeisEarth 2017. In 2D seismic sections of this data set, the base of the Stuttgart Formation coincides with a positive reflector (European standard) of medium to strong amplitude. Considerable control on seismic sections is provided by the R1 well situated in the centre of the Horn Graben (see chapter 2.7.1). For the Wolin Block, seismic sections were reinterpreted using the software SeisWare (Seidel et al. 2018) which are part of a larger data set generated by the former PETROBALTIC consortium in the 1970s to 1980s. These data were reprocessed by the SASO working group in the 1990s and more recently by

Central European Petroleum Ltd. (CEP) for prospecting purposes. The interpretation of seismic sections, in which the base of the Stuttgart Formation coincides with a zero-crossing, undulating reflector below the top Keuper reflector, is controlled by the well H2-1/90 at the Wolin Block (see chapter 2.7.2). However, the interpretation of the seismic data is hampered by the appearance of multiples which could not be suppressed during the reprocessing. Due to a missing velocity model, the depth and vertical exaggeration (VE) is calculated assuming a constant interval velocity of 2000 m/s for the Mesozoic succession.

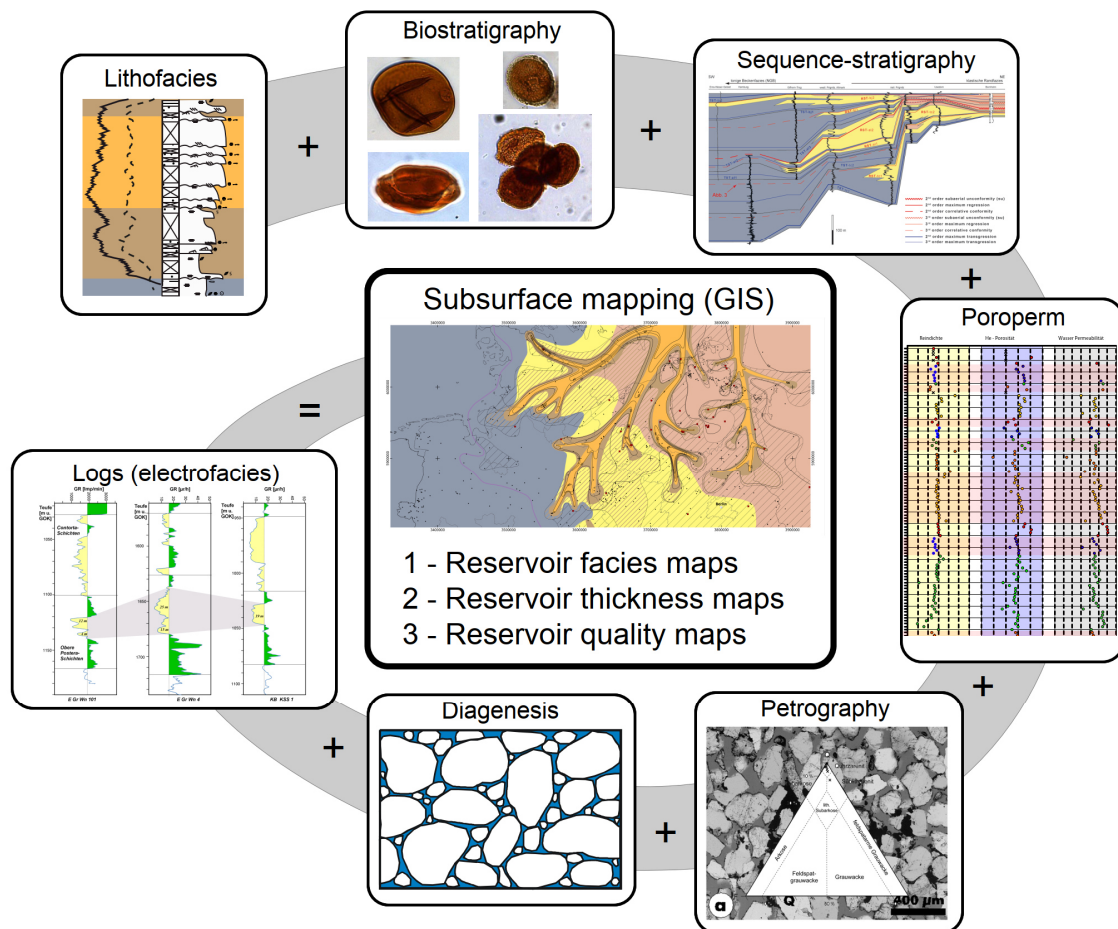


Fig. 2.4: Simplified exploration workflow applied to the reservoirs of the Stuttgart Formation; modified from Franz et al. (2018a).

## 2.4 Stratigraphic control on the reservoirs of the Stuttgart Formation

The prominent but informal stratigraphic term “Schilfsandstein” was replaced by the formal term Stuttgart Formation (Beutler in DSK 2005). The Stuttgart Formation attains an average thickness of 60–70 m in the NGB (Beutler & Häusser 1982). Towards the



South, the average thicknesses decrease to 15–50 m in Thuringia (Dockter & Schubert 2005) and 3–40 m in South Germany (Etzold & Schweizer 2005, Freudenberger 2005). The base of the Stuttgart Formation is defined at the base of the Neubrandenburg Member and the top at the base of the Beaumont Member (Weser Formation) (Fig. 2.3). For more detailed descriptions of stratigraphy and thickness of the Stuttgart Formation in the NGB, the reader is referred to Beutler & Häusser (1982), Beutler in DSK (2005), Franz (2008), Barnasch (2010), and Franz et al. (2014, 2018b).

The deposition of the Stuttgart Formation was controlled and possibly triggered by a series of transgressions into the CEB and resulting in the shaly to dolomitic Neubrandenburg, Gaildorf, and Beaumont Members. Intercalated with these transgression horizons, the shaly to sandy Lower and Upper Schilfsandstein Members represent basinwards-progradations of fluvio-deltaic depositional environments. The framework of 3<sup>rd</sup>- order and 4<sup>th</sup>-order maximum flooding and maximum regression surfaces provides considerable sequence-stratigraphic control to the Stuttgart Formation (Fig. 2.5; Franz et al. 2014).

Biostratigraphic control is provided by conchostracans, ostracods and palynomorphs (Heunisch 1999, Kozur & Bachmann 2010, Kozur & Weems 2010). In particular, the ostracod assemblage recorded in the Neubrandenburg Member enables the time-constrained correlation from the NGB to Thuringia (see Kozur & Bachmann 2010, Franz et al. 2014). Based on biostratigraphic arguments, the entire Stuttgart Formation was correlated with the late Julian upper *Austrotrachyceras austriacum* zone (Bachmann & Kozur 2004, Kozur & Bachmann 2010). However, based on sequence-stratigraphic arguments, Franz et al. (2014) suggested that the upper part of the Stuttgart Formation may range into the early Tuvanian (Fig. 2.3). The time-spans estimated to about 0.8 Myr for the Stuttgart Formation (Kozur & Bachmann 2010) and to about 1.2 Myr for the mid-Carnian episode (Zhang et al. 2015, Miller et al. 2017) are in general agreement.

In the central part of the NGB, the transition from the Grabfeld Formation to the Stuttgart Formation was considered continuous by Franz et al. (2014, 2018b) based on the observation of successive facies shifts between lithologies of the Grabfeld and Stuttgart formations. Moreover, the Stuttgart Formation in the central NGB seems to witness a largely continuous sedimentary record as both, the transgression horizons as well as the Lower and Upper Schilfsandstein could be readily recognised in the wells investigated herein. Towards Thuringia and South Germany, the boundary of the Grabfeld and Stuttgart formation is unconformable (Fig. 2.5; e. g., Bachmann & Wild 1976, Haunschild & Ott 1982). The same refers to the margins of the NGB and

basin-internal highs, such as the Eichsfeld-Altmark Swell, where up to 100 m of the Grabfeld Formation may be missing (Franz 2008, Barnasch 2010). The erosional contact of the Grabfeld and Stuttgart Formations is referred to as Unconformity 2 (D2 sensu Beutler in DSK 2005) or Schilfsandstein Unconformity (Franz et al. 2018b).

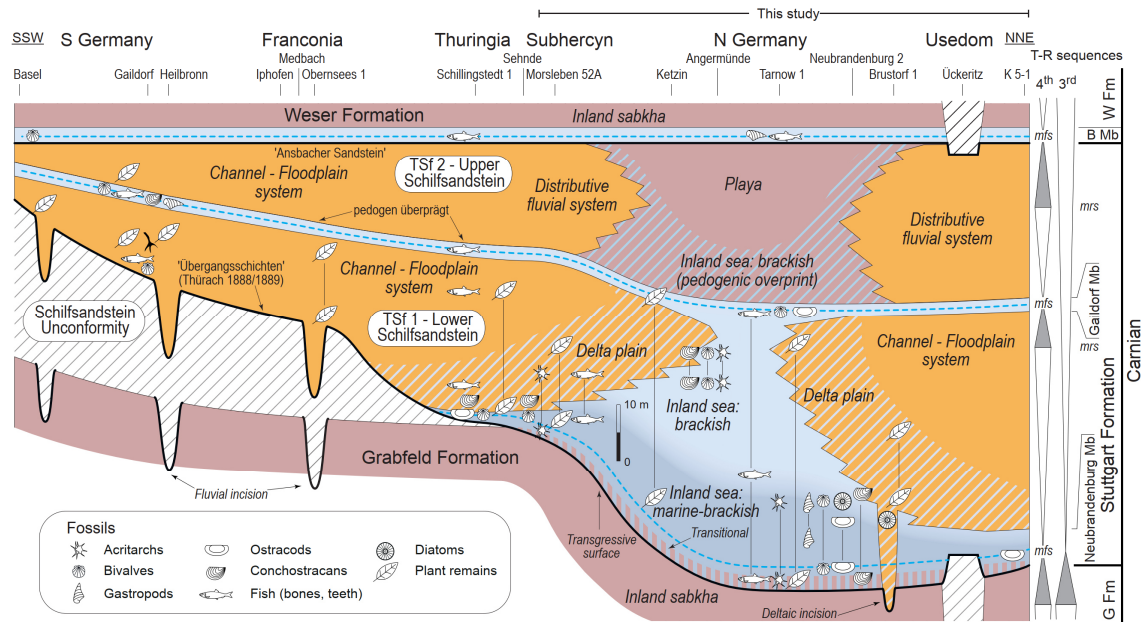


Fig. 2.5: Sequence stratigraphic scheme linking discontinuous successions of South Germany to continuous successions of North Germany. Outcrops Basel and Gaidorf: Etzold & Bläsi (2000), Etzold pers. comm.; outcrops Heilbronn and Iphofen: Bachmann & Wild (1976) and this work; Obernsees 1 and Medbach wells: this work; Schillingstedt 1 well: Kozur (1970b) and this work; outcrop Sehnde: Beutler et al. (1996) and this work; Morsleben 52A and Ketzin wells: Franz et al. (2014) and this work; Angermünde well: Kahlert et al. (1970); Tarnow 1, Neubrandenburg 2, Brustorf 1 and Ückeritz wells: Kozur (1970c), Franz et al. (2014) and this work; K 5-1 well: unpublished core report.

## 2.5 Subsurface facies mapping

### 2.5.1 Sea-level control

According to the principle control of mid-Carnian circum-Tethyan eustatic cycles on the CEB (Franz et al. 2014), the Stuttgart Formation can be described in terms of two transgressive-regressive cycles (Fig. 2.5). The first cycles started with the pre-Schilfsandstein transgression resulting in the formation of a large inland sea and the deposition of up to 20 thick predominantly shaly successions of the Neubrandenburg Member (Franz et al. 2014, 2018c). In particular, the lower part of the member is characterised by marine-brackish fauna with bivalves, ostracods, gastropods, acritarchs and other fossils (see Kozur & Bachmann 2010, Franz et al. 2014). Following the maximum extension of the inland sea, the regressive phase enabled the

successive basinwards-progradation of fluvio-deltaic environments identified to the Lower Schilfsandstein Member. The regression finalised in a brackish remnant sea covering only central parts of the NGB, final outbuilding of independent fluvio-deltaic systems and their partial pedogenic overprint (Fig. 2.6).

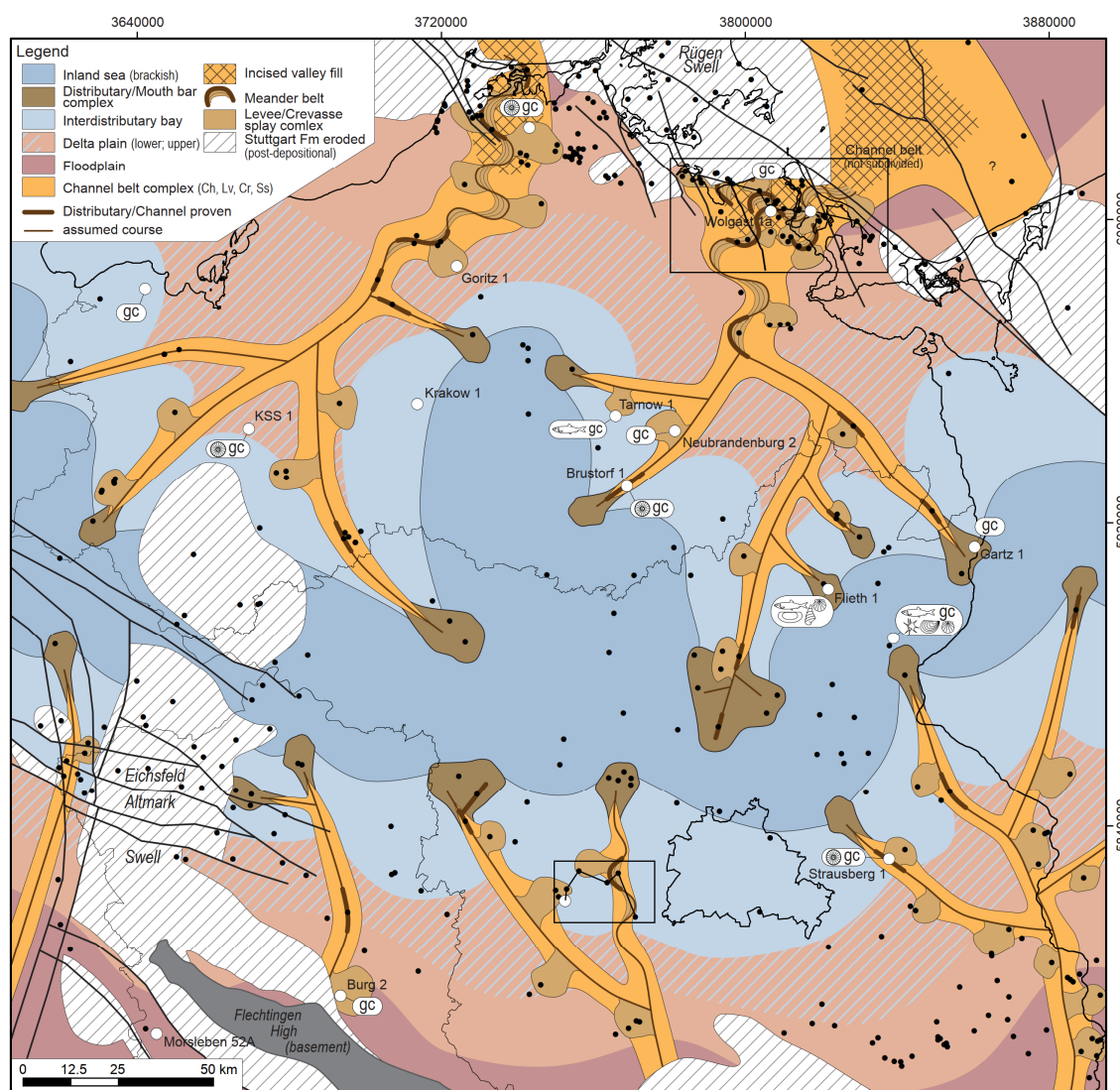


Fig. 2.6: Subsurface facies map of the Lower Schilfsandstein Member.

The second cycle started with the intra-Schilfsandstein transgression which again resulted in formation of an inland sea and deposition of the up to 5 m thick shaly Gaidorf Member (Lang 1909). The sparse occurrence of brackish-marine fauna with bivalves, gastropods and acritarchs were reported from several localities in South Germany as well as in the NGB (see Etzold & Schweizer 2005, Kozur & Bachmann 2010, Franz et al. 2014). Following deposition, the Gaidorf Member was

modified by pedogenesis and/or erosion following deposition in places, such as Thuringia or even South Germany. Compared with its precursor transgression, the intra-Schilfsandstein transgression was less pronounced and thus, the regressive phase enabled the rather rapid progradation of fan-like fluvial systems towards the centre of the NGB where these fluvial systems terminated. For the maximum regression stage, the centre of the NGB was occupied by a large inland playa which was possibly subject to terminal ingressions. The fluvial systems of the Upper Schilfsandstein Member resembled the drainage system of the Lower Schilfsandstein as they prograded from surrounding margins towards the basin centre (Fig. 2.7).

The deposition of the Stuttgart Formation was terminated by the post-Schilfsandstein transgression which resulted in an inland sea and deposition of the up to 10 m thick dolomitic, evaporitic and shaly Beaumont Member (Alberti 1834, Thürach 1888-89). A brackish-marine fauna with bivalves, ostracods, acritarchs and others forms occurs sparse in the NGB (Franz et al. 2014) but more frequently in South Germany (see Etzold & Schweizer 2005).

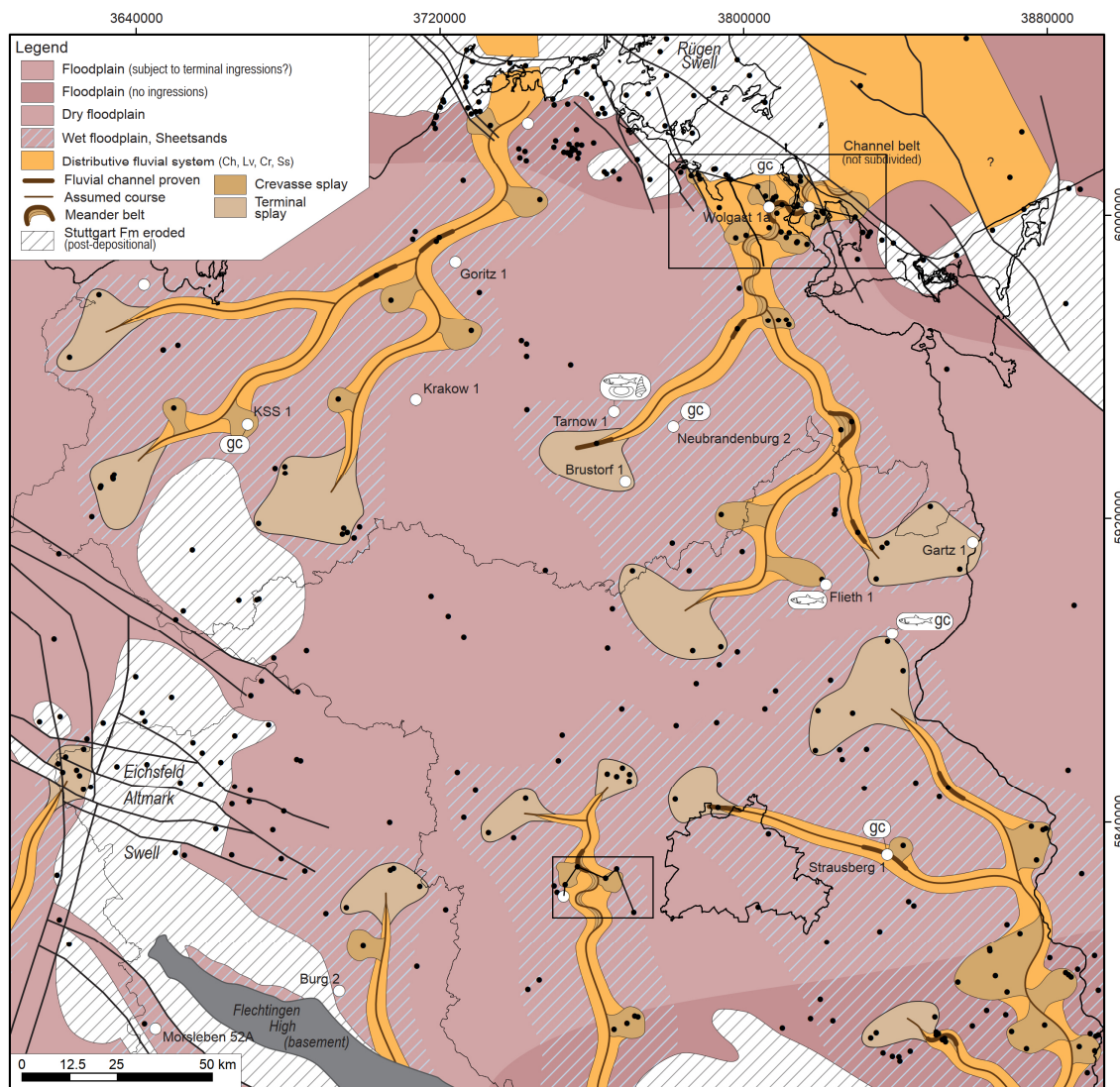


Fig. 2.7: Subsurface facies map of the Upper Schilfsandstein Member.

## 2.5.2 Morphology

Before and after the deposition of the Stuttgart Formation, basin-internal highs and basin margins were uplifted in the Early Carnian and Early Norian resulting in erosion associated to the Schilfsandstein Unconformity and Early Cimmerian Unconformity (Beutler & Schüler 1978, Beutler in DSK 2005, Stollhofen et al. 2008). Some of the uplifted basin-internal highs, such as the Rügen Swell and Eichsfeld-Altmark Swell, modified the deposition of the Stuttgart Formation. During the deposition of the Lower and Upper Schilfsandstein Members, the Rügen Swell formed a morphological high and controlled routing systems which drained Scandinavian sources to the North. For Lower and Upper Schilfsandstein Members, channel belts bypassed the Rügen Swell to the East and West where they entered the NGB. The same refers to the Eichsfeld-

Altmark Swell which controlled routing systems draining Variscan sources to the South (Figs. 2.6 and 2.7).

### 2.5.3 Facies analysis

The facies analysis focussed on the Lower and Upper Schilfsandstein as potential hydrothermal reservoirs are limited to these members. From the total core recovery of about 770 m, nine primary and four secondary lithofacies types were identified (Table 2.1). The former are thought to represent primary physical modes of deposition, whereas the latter show modifications of primary bedding due to pedogenic processes. As these lithofacies types correspond to examples previously reported by Shukla et al. (2010) and Franz et al. (2014, 2015), they are not described in detail herein.

Table 2.1: Primary and secondary lithofacies types of the Lower and Upper Schilfsandstein members. Shaded: secondary pedogenic lithofacies types.

Lithofacies type	Interpretation	Reference
Matrix-supported pebbles – Gmg	Lag deposit, upper flow regime	Shukla et al. (2010)
Horizontal-laminated sandstone – Sh	Bedload of upper flow regime, high energy critical flow	Shukla et al. (2010) Franz et al. (2014)
Low-angle cross-bedded sandstone – Sl	Bedload of lower to upper flow regime, migrating 2D-3D bedforms, high energy critical flow	Franz et al. (2015)
Cross-bedded sandstone – Sx	Bedload of lower flow regime, migrating 2D-3D bedforms	Shukla et al. (2010)
Ripple cross-laminated siltstone-sandstone – Sr	Bedload of lower flow regime, migrating ripples	Shukla et al. (2010) Franz et al. (2014)
Laminated mudstone – MI	Settling of suspension load, stagnant water body; upper plane-bed of sheet flows; incipient pedogenic destratification, carbonate precipitation	Shukla et al. (2010) Franz et al. (2014)
Laminated claystone-siltstone – Cl	Settling of suspension load, stagnant water body	Franz et al. (2014)
Heterolithics – Het	Lenticular, flaser and wavy bedding: repeated fluctuation of sediment input and modulation by waves, storms and currents	Franz et al. (2014)
Inclined heterolithic strata – IHS	Delta foreset deposits	Shukla et al. (2010)
Massive siltstone-sandstone – Sm	2D-3D bedforms, pedogenic destratification	Franz et al. (2015)
Siltstone-sandstone with root traces – Fr	Rooting of pioneer vegetation	Franz et al. (2014)
Coal – C	Histic epipedon of peat soils, histosol	Franz et al. (2014)
Palaeosol – P	Incipient to mature vertisol, calcisol or gypsisol	Shukla et al. (2010) Franz et al. (2014)

#### 2.5.3.1 Facies associations the Lower Schilfsandstein

From the core recovery of the Lower Schilfsandstein Member, twelve facies associations could be recognised. Partly supplemented by biofacies, these were grouped into seven associations characterised by typical log motifs (electrofacies): 1) Distributary/Fluvial channel, 2) Levee/Crevasse splay complex, 3) Floodplain,

4) Delta plain wetlands, 5) Interdistributary bay, 6) Distributary/Mouth bar complex, and 7) Inland sea (Table 2.2). These associations are described and interpreted briefly.

#### 1) Distributary/Fluvial channel

This up to 18 m thick association of lithofacies is characterised by an overall fining upward succession. At its base a distributary channel is typically marked by an erosional base (see chapter 2.5.3.2) followed by cosets of cross-bedded sandstone lithofacies (Fig. 2.8A). Towards the top, cosets of low-angle cross-bedded to cross-bedded sandstone lithofacies and ripple cross-laminated sandstone lithofacies follow and the top is marked by a shift to heterolithic or laminated claystone-siltstone lithofacies. These sharp based fining upward successions, predominantly formed of cross-bedded lithofacies, are thought to represent lateral accretion elements of point bar successions (e.g. Allen 1963, 1965, Bridge & Tye 2000). The gamma-ray (GR) and spontaneous potential (SP) logs show a sudden decrease of gamma ray and spontaneous potential corresponding to the erosional base of the channel followed by smooth and typical block to bell shaped log responses (Fig. 2.9).

The fills of channels were cored in the Strausberg 1, Brustorf 1 and Wolgast 1 wells in which vertical associations of channel fills with deposits of levee/crevasse splay complexes and delta plain wetlands indicate the lateral shifting and avulsion of channels, respectively (e.g. Allen 1965, Willis 1989, Miall 1996).

Table 2.2: Lower Schilfsandstein lithofacies associations identified in cores with granulometric values calculated according to Folk & Ward (1957); see also Fig. 4.13. To enable subsurface mapping, these associations were merged into seven associations characterised by typical log motifs. The thickness and porosity and permeability values are given as median with the number of data in brackets.

	Facies associations identified in cores	Individual reservoirs			Facies associations mapped	Compound reservoirs				
		Granulometry				Type	Thickness	Hydraulics		
		Median	Sorting	Skewn.				Phi (%)	K (mD)	
Fluvio-deltaic system	Distal	Fluvio-deltaic channel (Ch-f)	2.6 (4)	0.9	0.34	(1) Fluvio-deltaic channel	Channel belt	26 m (24)	23.4 (21)	897 (5)
	Fluvial plain	Levee (Lv-f)	–	–	–	(2) Levee/Crevasse splay complex				
		Crevasse splay (Cr-f)	2.7 (27)	0.78	0.32					
		Sheetsand (Ss)	2.6 (25)	0.7	0.3	(3) Floodplain	–	–	–	–
		Floodplain (Fl)	–	–	–					
	Delta plain	Distributary channel (Ch-d)	2.6 (22)	0.7	0.33	(1) Distributary channel	Channel belt	23 m (81)	22.7 (66)	443 (23)
		Levee (Lv-d)	4.1 (1)	0.5	0.02	(2) Levee/Crevasse splay complex				
		Crevasse splay (Cr-d)	3.2 (35)	0.72	0.3					
		Wetland (Wl)	4.1 (20)	0.52	0.0	(4) Delta plain wetlands	–	–	–	–
		Interdistributary Bay (IB)	4.1 (3)	0.63	–0.12	(5) Interdistributary bay	–	–	–	–
Delta front	Distributary/Mouth bar complex	–	–	–	(6) Distributary/Mouth bar complex	–	–	–	–	
	Inland Sea	–	–	–	(7) Inland Sea	–	–	–	–	

## 2) Levee/Crevasse splay complex

In individual successions, such as the Wolgast 1 well, levee and crevasse splay deposits often occur in vertical association and therefore were merged into a levee/crevasse splay complex. Deposits of natural levees are formed of suspension load represented by laminated claystone-siltstone lithofacies and heterolithic lithofacies (e.g. Allen 1965, Coleman et al. 1964, Brierley et al. 1997). By contrast, crevasse splay deposits are formed of bedload represented by sandy lithofacies (e.g. Allen 1965, Coleman 1969, Bristow et al. 1999). Resulting from crevassing and erosion of the levee (Brierley 1996, Bristow et al. 1999), the base of a proximal crevasse splay deposit is marked up to 1 m thick beds of matrix-supported mud clasts (Fig. 2.8B). Upwards, up to 3 m thick sets of matrix-supported pebbles are followed by cross-bedded or low-angle cross-bedded sandstone lithofacies and horizontal-laminated sandstone or ripple cross-laminated siltstone-sandstone lithofacies. Vertically stacking of fining upwards sets may form up to 20 m thick successions of horizontal-laminated or ripple cross-laminated sandstones (Figs. 2.9 and 2.10). The upper parts of proximal crevasse splay deposits often show features of incipient pedogenesis such as mottling (Fig. 2.8C). Accordingly, crevasse splay deposits maybe subdivided into lower subaqueous and upper subaerial parts (Shukla et al. 2010). For proximal crevasse splay deposits, gamma-ray and spontaneous potential logs show smooth to serrate and block shaped responses, such as in the Lütow 3 well, and bell shaped responses for intermediate examples, such as in the Neubrandenburg 2 well (Figs. 2.9 and 2.10).

Distal crevasse splay deposits are up to 6 m thick and formed of stacked up to 2 m thick sets of low-angle cross-bedded sandstone lithofacies followed by bioturbated laminated claystone-siltstone lithofacies (Fig. 2.8E). The vertically stacking of a few sets may delineate an overall coarsening upward trend (Colemann & Prior 1982) illustrated by funnel shaped responses of gamma-ray and spontaneous potential logs such as in the Tarnow 1 well (Fig. 2.10). An example of a levee/crevasse splay complex was described by Ricken et al. (1998) from the Tübingen area (South Germany). There, the about 30 m thick succession of aggradational sandstone sheets is mainly composed of horizontal-laminated and ripple-cross-bedded sandstone lithofacies. The vertical aggradation, including amalgamation, and progradational transition towards fine-grained lithofacies corresponds well to examples described herein (Figs. 2.9 and 2.10).

Typically, levee/crevasse splay deposits are rich in plant remnants suggesting vegetated river banks. Distal crevasse splay deposits comprise abundant plant debris



---

at bedding surfaces, proximal crevasse splay deposit comprise also larger remnants such as logs and branches (Fig. 2.10).

### 3) Floodplain

The floodplain association merges sandy and shaly suspension load. Sandy lithofacies are represented by low-angle cross-bedded sandstone, cross-bedded sandstone, horizontal-laminated sandstone and ripple cross-laminated siltstone-sandstone lithofacies forming typical up to 2 m thick sheetsands. Shaly lithofacies are characterised by grey to variegated laminated mudstone lithofacies of floodplain fines and palaeosols. Typical examples, such as in the Morsleben 52A well, show associations of sheetsands and pedogenic floodplain fines. These fining upwards successions are up to 4 m thick and result from channel overtopping during flood stages and formation of subaerial flows (e.g. Miall 1996, Shukla et al. 2010). At the floodplain, the deposition of sandy bedforms in the early phase was followed by settling of suspension load in the late phase and pedogenic modification.

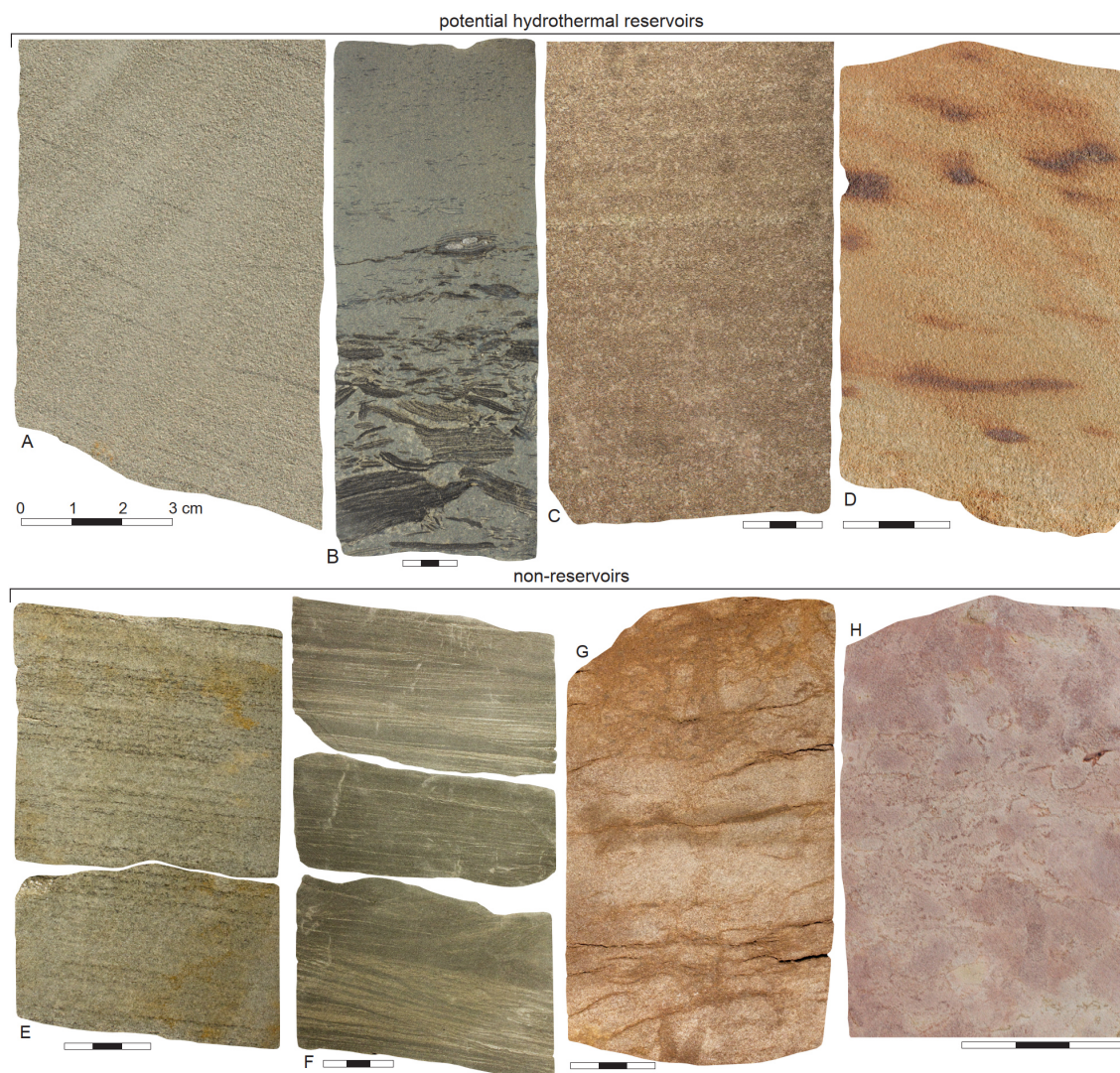


Fig. 2.8: Core examples of the Lower and Upper Schilfsandstein members. **Potential hydrothermal reservoirs:** (A) Strausberg 1/62, Lower Schilfsandstein, sample 6-15 (depth 791.95 m): cross-bedded sandstone (Sx) of a distributary channel fill (Ch-d); median: 3.3 (Phi), sorting: 0.74, skewness: 0.2, porosity (Archimedes method): 26.5 %, permeability (calculated from kf): 215 mD. (B) Neubrandenburg 2/85, Lower Schilfsandstein, sample 10-28 (depth 1549.3 m): normal gradation from matrix supported pebbles (Gmg; laminated to heterolithic mud clasts) to horizontal-laminated sandstone (Sh), lower subaquatic part of a proximal crevasse splay (Cr-d); sample 11-1 (depth 1549.1 m, not shown) immediately above sample 10-28: median 2.9 (Phi), sorting: 0.7, skewness: 0.47, porosity (He): 24.6 %, permeability (H<sub>2</sub>O): 350 mD. (C) Neubrandenburg 2/85, Lower Schilfsandstein, sample 11-9 (depth 1533.0 m): horizontal-laminated sandstone (Sh), upper subaquatic part of a proximal crevasse splay (Cr-d); median: 3.1 (Phi), sorting: 0.69, skewness: 0.3, porosity (He): 24.9 %, permeability (H<sub>2</sub>O): 227 mD. (D) KSS 1/66, Lower Schilfsandstein, sample 12-5 (depth 1270.0 m): low-angle cross-bedded sandstone (Sl), crevasse splay (Cr-d) with ferruginous impregnations; median: 3.3 (Phi), sorting: 0.76, skewness: 0.22, porosity (He): 30.8 %, permeability (H<sub>2</sub>O): 1516 mD. **Non-reservoirs:** (E) Tarnow 1/65, Lower Schilfsandstein, sample 11-28 (depth 1149.1 m): low-angle cross-bedded sandstone (Sl), lower subaquatic part of a distal crevasse splay (Cr-d) with abundant plant debris; median: 3.4 (Phi), sorting: 0.75, skewness: 0.28, porosity (He): 10.1 %, permeability (H<sub>2</sub>O): 3 mD; see also Fig. 2.16. (F) Tarnow 1/65, Lower Schilfsandstein, sample 11-31 (depth 1140.8 m): inclined heterolithic strata and laminated siltstone of an interdistributary bay fill (IB); median: 4.1 (Phi), sorting: 0.63, skewness: -0.13, porosity and permeability not measured. (G) Tarnow 1/65, Upper Schilfsandstein, sample 11-34 (depth 1111.15 m): bioturbated, ripple cross-laminated sandstone (Sr) of a distal sheetsand (Ss-f), pedogenic carbonate cementation; median: 3.4 (Phi), sorting: 0.79, skewness: 0.21, porosity (He): 9.7 %, permeability (H<sub>2</sub>O): 5 mD. (H) Strausberg 1/62, Upper Schilfsandstein, sample 6-21 (depth 744.0 m): massive sandstone (Sm), upper subaerial part of a fluvial crevasse splay (Cr), bedding completely superimposed due to bioturbation and pedogenic carbonate cementation; median: 3.5 (Phi), sorting: 0.82, skewness: 0.04, porosity (He): 9.7 %, permeability (H<sub>2</sub>O): 0 mD.

#### 4) Delta plain wetlands

In the KSS 1 well, the Lower Schilfsandstein Member is solely formed of this up to 20 m thick association of laminated claystone-siltstone, laminated mudstone, heterolithic and ripple cross-laminated siltstone-sandstone. In other wells, such as in the Brustorf 1 well, it occurs in vertical association with other lower delta plain facies associations (Figs. 2.9 and 2.10). The typical features are rooted horizons and coal seams suggesting repeated phases of suspension load input associated to high water stages followed by swamping and establishment of vegetation (e.g. Coleman & Prior 1984). The patterns of gamma-ray and spontaneous potential show smooth and serrate responses of logs; thick successions of laminated claystone-siltstone may result in an increase of gamma ray intensity.

#### 5) Interdistributary bay

The interdistributary bay facies association is characterised by dark grey to grey laminated claystone-siltstone, heterolithic and ripple cross-laminated siltstone-sandstone lithofacies; gently inclined heterolithic strata occurs subordinated (Fig. 2.8F). These lithofacies types form up to 30 m thick successions dominantly formed of suspension load (e.g. Coleman et al. 1964, Coleman & Prior 1984). Glaucony and fish remnants were recognised in the Klütz 1 and Tarnow 1 wells and may suggest a marine influence on this subaquatic lower delta plain environment. At the top, interdistributary bay fills may show transitions to the pedogenic floodplain. The patterns of gamma-ray and spontaneous potential logs are commonly serrated (Fig. 2.10).

#### 6) Distributary/Mouth bar complex

The distributary/mouth bar complex is mainly composed of laminated claystone-siltstone, heterolithic and ripple cross-laminated siltstone-sandstone lithofacies forming up to 1 m thick fining upward cosets. Vertically stacking of cosets contributes to an overall coarsening upwards trend of up to 10 m thick mouth bars (e.g. Fisher et al. 1969, Wright 1977, Olariu & Bhattacharya 2006). This coarsening upward trend is illustrated by funnel-like responses of gamma-ray and spontaneous potential logs. The subordinated occurrence of low-angle cross-bedded sandstone and cross-bedded sandstone lithofacies is considered to represent the fill of terminal distributary channels (e.g. Olariu & Bhattacharya 2006, Schomacker et al. 2010). In the Flieth 1 well, a marine-brackish fauna with bivalves, ostracods, gastropods and fish remnants was

recorded from below and in the lower progradational part of a mouth bar (Fig. 2.6; Kozur 1970a, Kannegieser & Kozur 1972).

#### 7) Inland Sea

The inland sea association is characterised by dark grey to grey laminated claystone-siltstone, laminated mudstone and heterolithic lithofacies. These lithofacies types form up to 40 m thick monotonous successions resulting from settling of buoyancy driven suspension load (Wright 1977). As the inland sea is located seawards to the deltaic environments reconstructed herein, it represents the classical prodelta in the sense of Fisher et al. (1969). According to the low variability in terms of lithofacies, the gamma-ray and spontaneous potential logs show smooth and serrate pattern. A marine-brackish fauna with bivalves, gastropods, ostracods, acritarchs, conchostracans and fish remnants was recorded in the Angermünde 1 and Flieth 1 wells (Fig. 2.6; Kahlert et al. 1970, Wehland 1970).

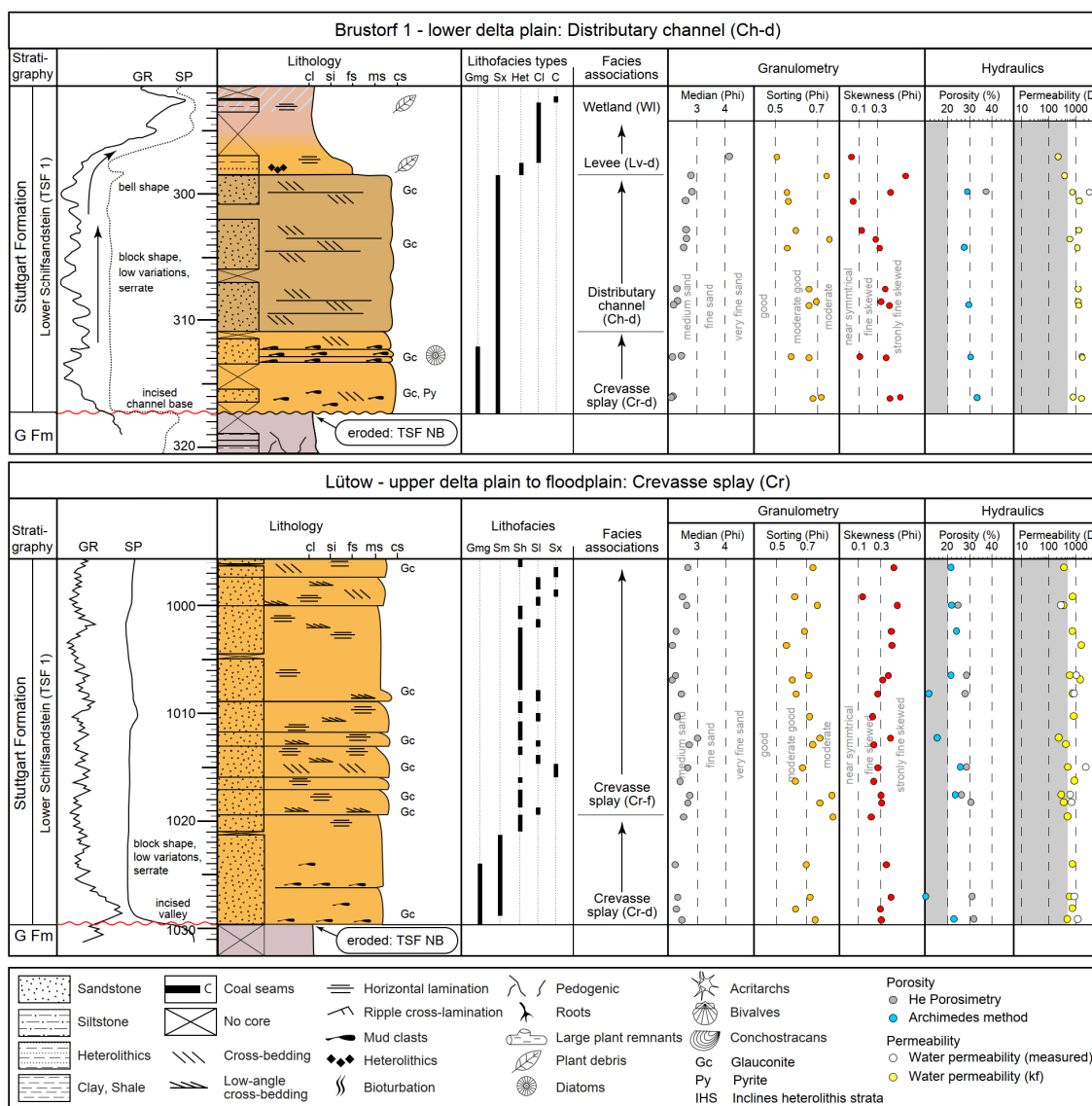


Fig. 2.9: Examples of Lower Schilfsandstein facies associations with granulometry and poroperm values; for colour code see Fig. 2.6.

### 2.5.3.2 The Lower Schilfsandstein fluvio-deltaic system

Following the pre-Schilfsandstein transgression, the inland sea successively diminished in size resulting in an elongated remnant sea covering the axial part of the North German Basin (Fig. 2.6). The regression triggered the basinwards-directed progradation of up to 60 m thick deltaic successions stretching from northern basin margins up to SW Mecklenburg and North Brandenburg and from southern basin margins up to the Altmark and the area around Berlin. From proximal to distal the net-thickness of sandstones incorporated into the deltaic successions successively decrease down to less than 10 m.

The subsurface facies map, illustrating late progradational phase and final outbuilding of deltas during the maximum regression, reveals several independent delta systems. These resemble the lobate high-constructive delta type of Fisher et al. (1969) in terms of morphology. The contemporaneous southwards-directed and northwards-directed progradation of deltas into the inland/remnant sea points to basinwards-directed drainage system of the Lower Schilfsandstein contrasting the exo-rheic drainage previously reconstructed by Beutler & Häusser (1982) and Beutler & Nitsch in DSK (2005).

The deltas of the Lower Schilfsandstein are characterised by distributive networks of channels with increasing bifurcation in downstream direction. Individual deltas are formed of up to four lobes, whereby each lobe was fed by an individual distributary channel. The distributary or fluvio-deltaic channel facies association was recognised in 31 wells with channel fill thicknesses ranging from 5 to 18 m (Fig. 2.11). In the Usedom, Darß and Ketzin areas, closely spaced wells enabled the mapping of lateral shifting channels and associated levee/crevasse splay complexes (Figs. 2.6 and 2.12). Only for these areas, meandering channel courses are shown in the subsurface facies map; elsewhere straight channel courses are shown.

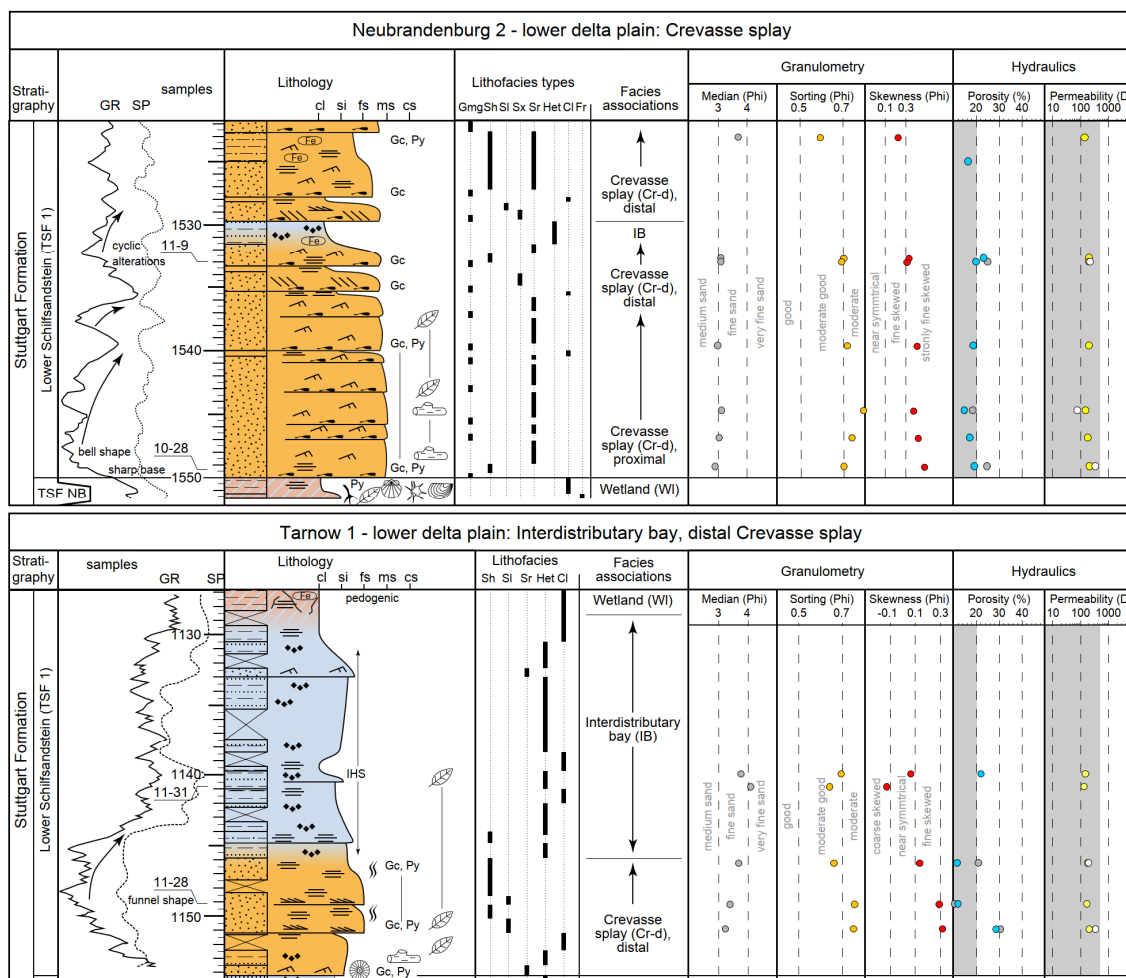


Fig. 2.10: Examples of Lower Schilfsandstein facies associations with granulometry and poroperm values; for colour code see Fig. 2.6, examples see Fig. 2.8, for legend see Fig. 2.9.

The high-constructive or regressive deltas of the Lower Schilfsandstein demonstrate the dominance of fluvial processes on delta formation (Fisher et al. 1969, Galloway 1975, Bhattacharya 2006). Abandonment and shifting of lobes in concert with crevassing and sheet flooding contributed to the formation of delta plains. The levee/crevasse splay association was recognised in 64 wells with thicknesses ranging from 5 to 27 m. Together with the distributary or fluvio-deltaic channel association, the levee/crevasse splay association forms sand-prone belts running across the delta plains which are summarised to channel belt complexes herein (Fig. 2.6). In downstream direction, the width of channel belt complexes decreases from almost 40 km at the proximal upper delta plain to about 14 km at the lower delta plain. The incision of channel belt complexes into delta plain and older deposits decrease in the same direction from about 50 m to about 15 m and less (Fig. 2.12, Appendix).

At distal fluvial plains and upper delta plains, the channel belt complexes are laterally associated to floodplains and wetlands which were subject to repeated changes from flooding to desiccation and partly pedogenic modification. In downstream direction, the channel belt complexes are flanked by partly vegetated wetlands and interdistributary bays at lower delta plains. At the distal end of delta lobes, distributary/mouth bar complexes are attached to the river mouths representing the delta front (Fig. 2.6).

Following its deposition, the fluvio-deltaic system of the Lower Schilfsandstein was flooded by the intra-Schilfsandstein transgression. Indications of transgressive reworking could not be observed.

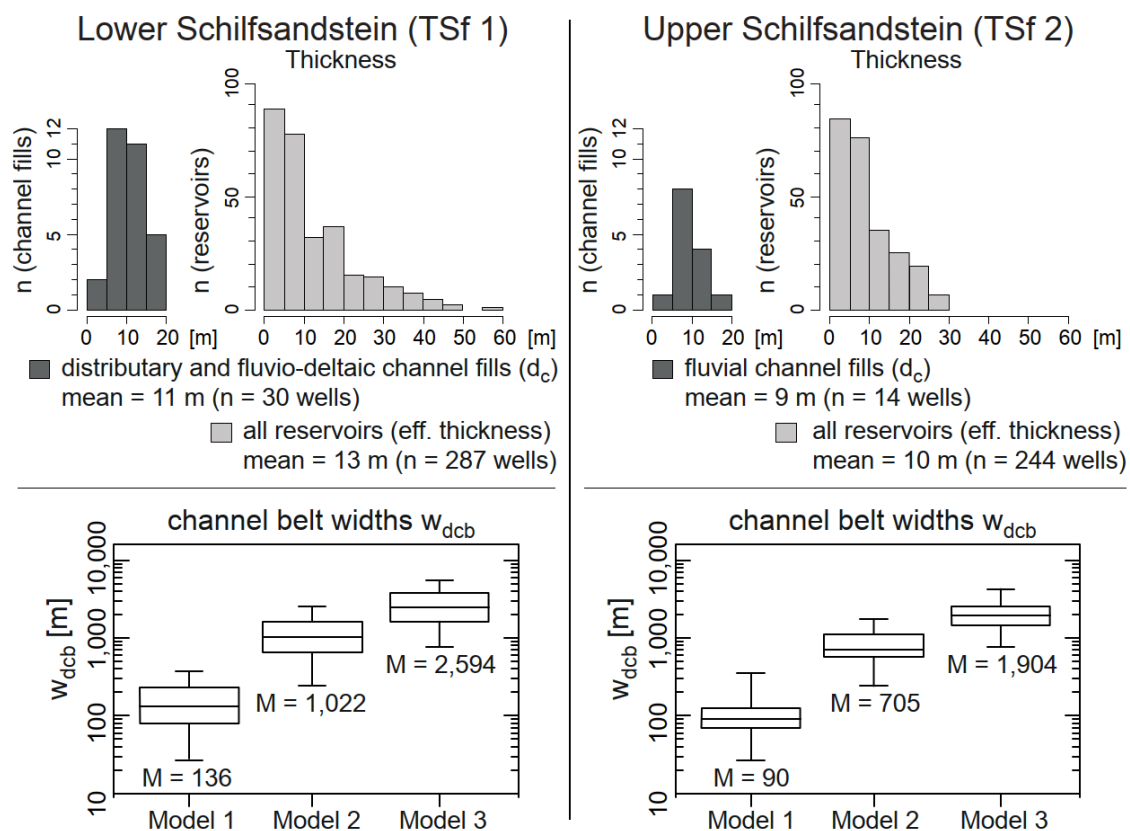


Fig. 2.11: Thickness distribution plots of distributary and fluvio-deltaic channel fills and effective reservoir thicknesses for the Lower and Upper Schilfsandstein. Based on channel fill thicknesses, the channel belt widths ( $w_{dcb}$ ) were calculated based on empirical formulas of Fielding & Crane (1987), Model 1:  $w_{dcb} = 0.95d_c^{2.07}$ ; Fielding & Crane (1987) and Miall (1996), Model 2:  $w_{dcb} = 12.1d_c^{1.85}$ ; Collinson (1978), Model 3:  $w_{dcb} = 64.6d_c^{1.54}$ .



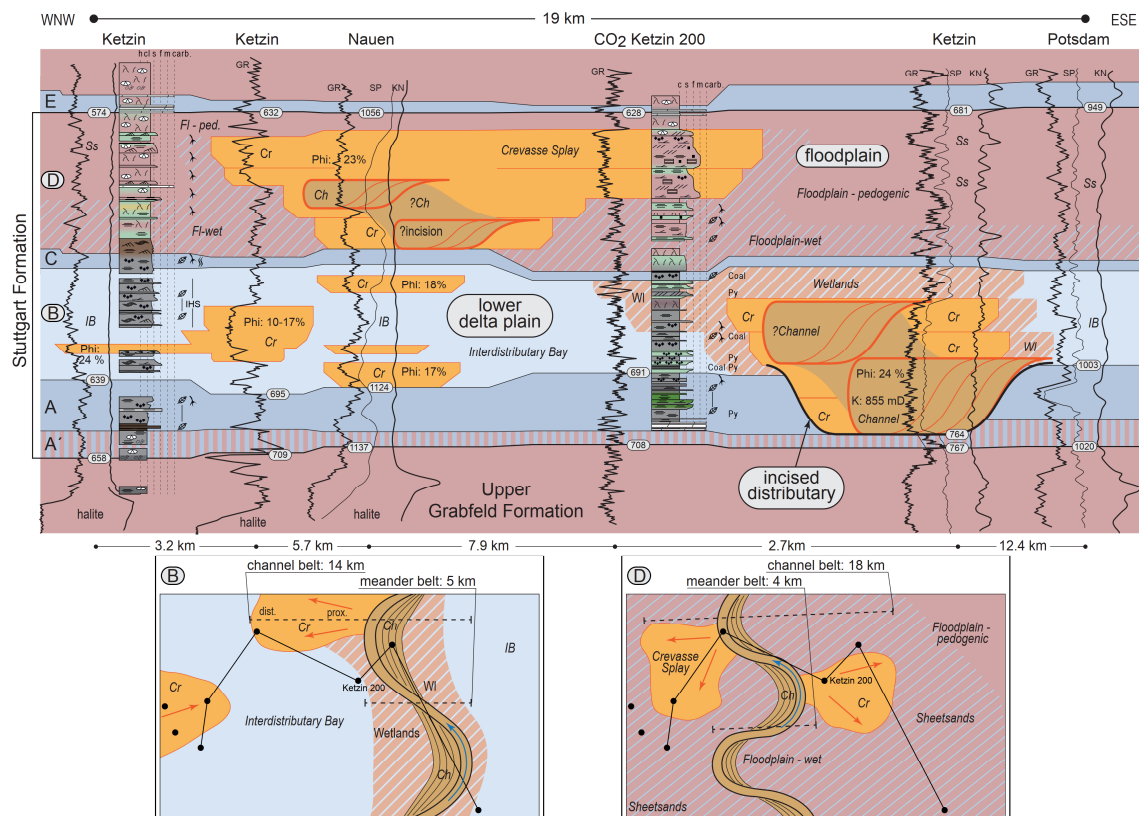


Fig. 2.12: Cross-section of the Ketzin area showing laterally shifting fluviodeltaic channels and lateral associated depositional environments. A = Neubrandenburg Member sensu Franz et al. (2014), A' = transitional interval km1/9 sensu Wehland (1968, 1970), B = Lower Schilfsandstein with detailed map (inlet), C = Gaildorf Member, D = Upper Schilfsandstein with detailed map (inlet), E = Beaumont Member (Weser Formation). Width I refers to the width of the meander belt, Width II refers to the width of the meander belt plus lateral associated crevasse splay. For legends see Figs. 2.6, 2.7 and 2.9.

### 2.5.3.3 Facies associations of the fluvial Upper Schilfsandstein

From the core recovery of the Upper Schilfsandstein, seven lithofacies associations could be recognised and are grouped into five associations characterised by typical log motifs (electrofacies): 1) Fluvial channel, 2) Levee/Crevasse splay complex, 3) Terminal splay 4) Wet floodplain, and 5) Dry floodplain (Table 2.3). These associations are described briefly.

#### 1) Fluvial channel and 2) Levee/Crevasse splay complex

These lithofacies associations, recognised for example in the Strausberg 1 and KSS 1 wells, resemble the features of Lower Schilfsandstein distributary channels and levee/crevasse splay complexes in terms of lithofacies and log responses (see chapter 2.5.3.1).

### 3) Terminal splays

In the Brustorf 1 and Gartz 1 wells, this association of lithofacies is recognised in form of up to 2 m thick fining upwards cosets. From base to top an ideal set is formed of low-angle cross-bedded sandstone, horizontal-laminated sandstone, ripple cross-laminated siltstone-sandstone and laminated mudstone lithofacies. The vertical association of lithofacies points to deposition by decelerating flows. Vertical stacking of sets results in up to 15 m thick predominantly sandy succession. Erosional reworking is indicated by mud clasts at the bases of individual cosets. Pedogenic modification resulted in incipient to complete destratification of the mudstone lithofacies at the top of cosets. Based on subsurface mapping, the facies association forms larger lobate or fan-like sandbodies at the distal ends of fluvial channels (Fig. 2.7). Due to this morphology and the vertical association of lithofacies, the facies association is considered terminal splays (Lang et al. 2004, Nichols & Fisher 2007).

Table 2.3: Upper Schilfsandstein lithofacies associations identified in cores with granulometric values calculated according to Folk & Ward (1957), see also Fig. 2.13. To enable subsurface mapping, these associations were merged into five associations characterised by typical log motifs. The thickness and porosity and permeability values are given as median with the number of data in brackets.

	Facies associations identified in cores	Individual reservoirs			Facies associations mapped	Compound reservoirs			
		Granulometry				Type	Thickness	Hydraulics	
		Median	Sorting	Skewness				Phi (%)	K (mD)
Distributive fluvial system	Fluvial channel (Ch)	2.6 (9)	0.86	0.38	(1) Fluvial channel	Channel belt	17 m (76)	24.0 (58)	546 (16)
	Levee (Lv)	–	–	–	(2) Levee/Crevasse splay complex				
	Crevasse splay (Cr)	3.3 (56)	0.66	0.24		–	–	–	–
	Terminal splay (Ts)				(3) Terminal splay	–	–	–	–
	Sheetsands (Ss)	3.1 (37)	0.68	0.24	(4) Wet Floodplain	–	–	–	–
	Wet floodplain (Fl-w)	4.0 (8)	0.57	-0.04		–	–	–	–
	Dry floodplain (Fl-d)	4.1 (6)	0.51	-0.02	(5) Dry floodplain	–	–	–	–

### 4) Wet and 5) Dry floodplain

The vertical association of sandy bedload and shaly suspension load is the typical feature of the wet and dry floodplain associations resulting from channel overtopping during flood stages and formation of subaerial flows (e.g. Miall 1996, Shukla et al. 2010). In the lower part, both associations may be formed of low-angle cross-bedded sandstone, cross-bedded sandstone, horizontal-laminated sandstone and ripple cross-laminated siltstone-sandstone lithofacies representing the bed load. In the upper part, representing the suspension load, the wet floodplain association is formed of grey heterolithic lithofacies and grey to variegated laminated mudstone lithofacies. Rooted horizons occurring in the latter lithofacies indicate vegetation following sheet flooding. Together with features of an incipient pedogenesis, predominantly wet floodplain environments, such as wetlands, are indicated as demonstrated by cores of

the Tarnow 1 well for example. In contrast to this, the suspension load deposited at the dry floodplain experienced intense modification due to pedogenic processes. As a consequence of mature palaeosols, e.g. vertisols, calcisols and gypsisols, the dry floodplain association of the Upper Schilfsandstein partly resembles the lithology of the Weser Formation as exemplified by the Morsleben 52A and Strausberg 1 wells.

#### 2.5.3.4 The Upper Schilfsandstein distributive fluvial system

In comparison with the pre-Schilfsandstein transgression, the intra-Schilfsandstein transgression resulted only in short-term flooding of the CEB. The pronounced transgression flooded the Lower Schilfsandstein fluvio-deltaic system and the following regression enabled the basinwards-directed progradation of fluvial channel-floodplain systems rejuvenating the basinwards-directed drainage of the Lower Schilfsandstein. These are recognised in form of progradational successions forming elongated to fan-shaped, up to 50 m thick sedimentary bodies of larger scale which were fed by distributive networks of fluvial channels (Fig. 2.7). In terms of morphology, the examples of the Upper Schilfsandstein may correspond to fluvial fans of Collinson (1996) or terminal fans of Kelly & Olsen (1993). But as the term fan is used for a wide range of alluvial to fluvial examples, the descriptive term distributive fluvial system (Nichols & Fisher 2007, Weissmann et al. 2010) seems to be more appropriate.

Each mapped distributive fluvial system was fed by an individual fluvial channel. The distributive pattern results from avulsion of channels and bifurcation at the downstream ends. In 14 wells, channel fills ranging from 5 to 14 m thickness could be recognised (Fig. 2.11). Closely spaced wells, for example in the Usedom and Ketzin areas, enabled the reconstruction of lateral shifting channels and associated levee/crevasse splay complexes (Figs. 2.7 and 2.12). In accordance to the Lower Schilfsandstein subsurface facies map, meandering channel courses are shown in the subsurface facies map; elsewhere straight channel courses are shown.

Crevasse and sheet flooding introduced sediments to floodplain environments laterally associated to channels. The levee/crevasse splay association was recognised in 58 wells with thicknesses ranging from 5 to 28 m. The fluvial channel and levee/crevasse splay facies associations formed sand-prone belts herein summarised to channel belt complexes (Fig. 2.7). Detailed mapping in the Usedom and Ketzin areas revealed widths of about 20 km for proximal to medial channel belts pointing to rather constant hydrological conditions for these parts of the distributive fluvial systems (Figs. 2.12 and 2.13). At the distal ends, channel belts terminate, probably resulting

from decreased discharge or channel capacities (Tooth 1999a, b), forming larger terminal splays due to unconfined flow (Lang et al. 2004).

The floodplain environments are characterised by increasing degrees of desiccation and pedogenesis with increasing distances to channels. Wetlands close to channels were temporally vegetated and experienced only incipient pedogenesis. By contrast, deposits of dry floodplains were subject to intense pedogenesis. Mature aridisols point to longer terms of desiccation and water loss through evaporation (Mack et al. 1993). From proximal to distal the net-thickness of sandstones incorporated into the distributive fluvial systems successively decrease down to less than 10 m.

The central parts of the NGB were not directly reached by distributive fluvial systems. Instead, floodwaters of terminal splays contributed to predominantly fine-grained suspension load deposits in the axial part of the basin. Repeated changes from flooding to desiccation and pedogenesis resulted in formation of mature palaeosols. If the axial part of the NGB was subject to terminal ingressions, as suggested by some fauna and glaucony, remains open.

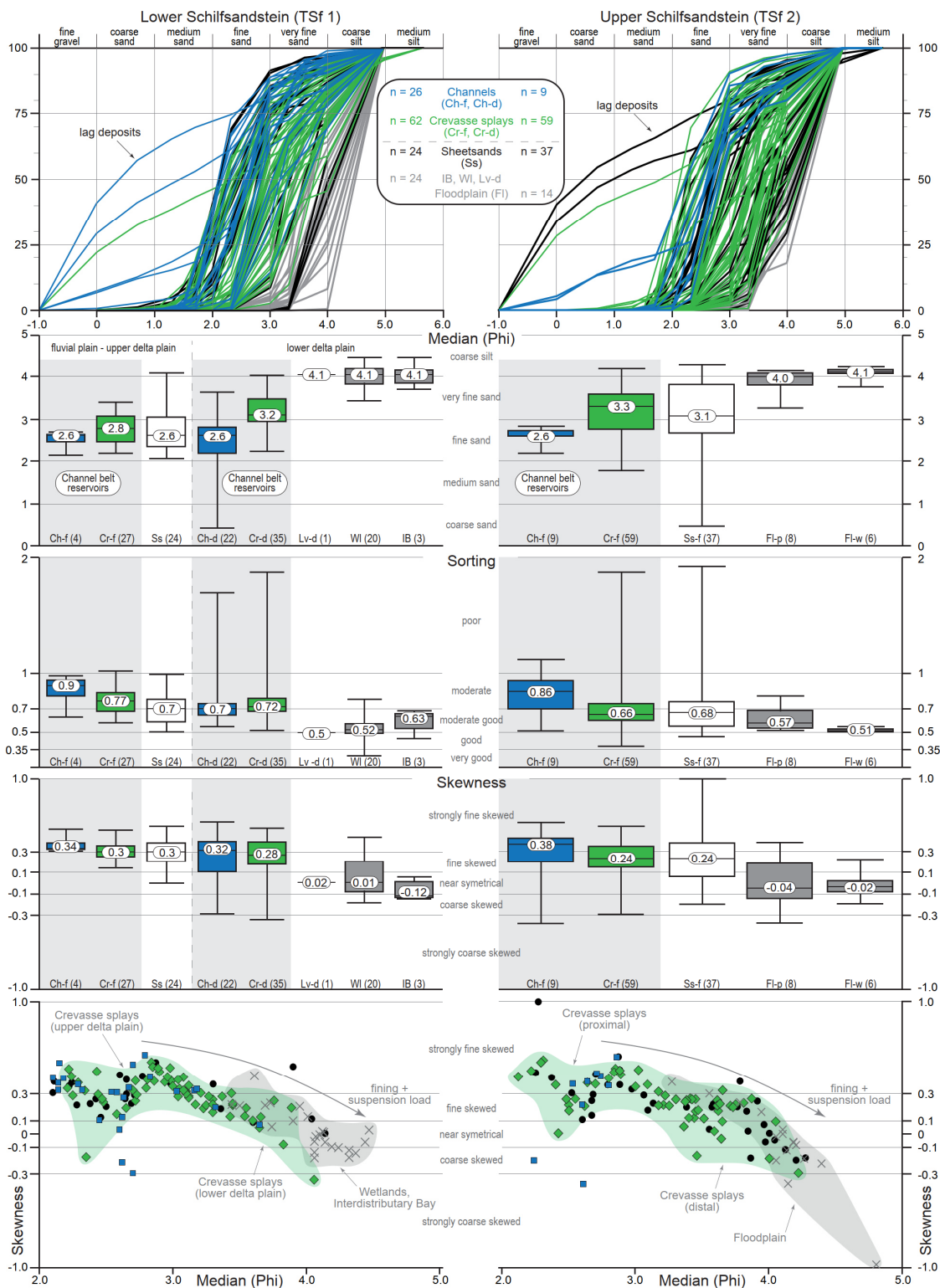


Fig. 2.13: Granulometry of the Lower Schilfsandstein Member (136 samples) and Upper Schilfsandstein Member (119 samples), grain size classes (Phi) according to Wentworth (1922), median (Phi), sorting and skewness according to Folk & Ward (1957). For the Lower Schilfsandstein, samples of upper delta plain and fluvial plain environments are shown together.

## 2.6 Reservoir quality

### 2.6.1 Granulometry

Detrital grains of the Lower and Upper Schilfsandstein Members are of low to moderate sphericity and subangular to subrounded grain shape in the sense of Wentworth (1922) pointing to a rather low textural maturity. This low textural maturity was recognised for samples from proximal parts as well as central part of the NGB and thus, a downstream trend towards a more accentuated roundness is not indicated.

The median grain sizes (Folk & Ward 1957) of 255 samples (18 wells) of both members range from 0.4 to 4.8 Phi (0.04 to 0.76 mm). According to the grain size classes of Wentworth (1922), two samples are classified coarse sand (0–1 Phi), three samples are medium sand (1–2 Phi), 108 samples are fine sand (2–3 Phi), 103 samples are very fine sand (3–4 Phi) and 39 samples are classified coarse silt (4–5 Phi). Thus, the majority of the samples are characterised fine to very fine sand.

On detail, grain size, sorting and skewness of sandstones are subject to noticeable changes which can be related to facies shifts and associated changes from bedload to suspension load processes. This is exemplified based on 137 samples of the Lower Schilfsandstein.

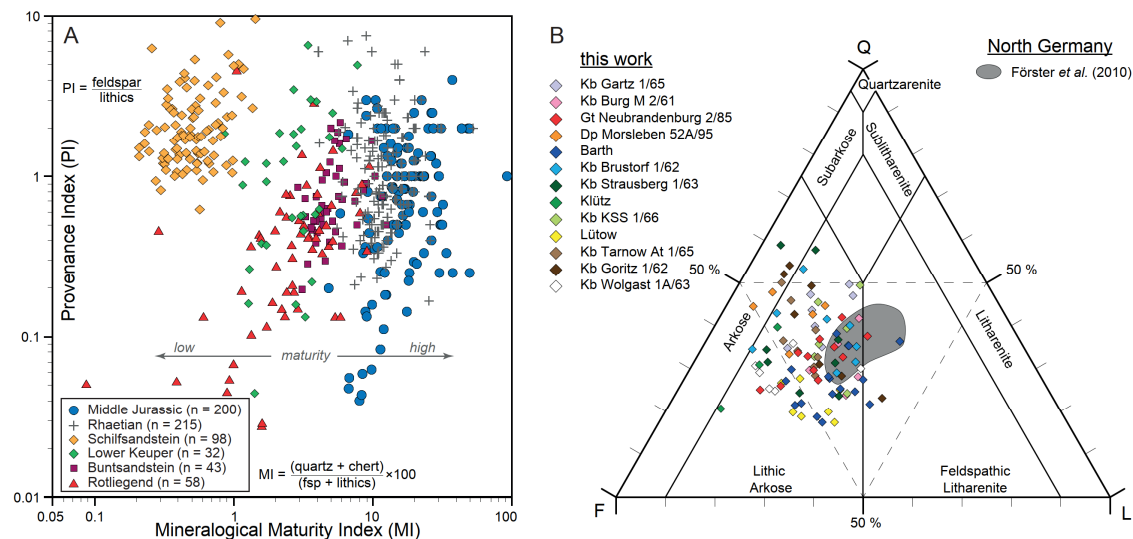


Fig. 2.14: Detrital mineralogy of reservoirs of the Stuttgart Formation (modified from Franz et al. 2018c). **(A)** Mineralogical Maturity Index vs. Provenance Index (Pettijohn 1957) of the Stuttgart Formation in comparison to Palaeozoic to Mesozoic sandstones of the North German Basin; samples of the Lower Keuper Erfurt Formation are from Häusser (1972). **(B)** Ternary plot (McBride 1963) of 98 samples investigated herein in comparison to examples previously published by Förster et al. (2010); Q = mono- and polycrystalline quartz and chert, F = feldspar, L = lithics (unstable rock fragments).

Sandy fills of distributary and fluvio-deltaic channels are both characterised by grain size medians of 2.6 Phi corresponding to 0.16 mm (Fig. 2.13). As already noted by Wurster (1964), a downstream trend towards finer grain sizes seems to be not indicated for the fills of the Lower Schilfsandstein channels, at least not by the data set detailed herein. The lower delta plain distributary channel fills (22 samples) are moderately to moderately-good sorted (median 0.7) and strongly fine skewed (median 0.32). The fill of a fluvio-deltaic channel (4 samples) is moderately sorted (median 0.9) and strongly fine skewed (median 0.34). Crevassing and sheetflooding introduced bed load and suspension load to floodplains and delta plains. Samples of floodplain to upper delta plain crevasse splays (27 samples) and sheetsands (25 samples) are fine grained with medians of 2.8 Phi (0.14 mm) and 2.6 Phi (0.16 mm), moderately sorted (0.77) and moderately-good sorted (0.7), and fine skewed (both 0.3). Samples of lower delta plain crevasse splays (35 samples) are very fine grained (median 3.2 Phi), moderately sorted (median 0.72) and fine skewed (median 0.28). These data may suggest, that crevassing at the lower delta plain was increasingly characterised by suspension load processes compared to crevassing at floodplains and upper delta plains (Fig. 2.13). Lateral to channel belts, formation of levee, wetland and interdistributary bay deposits was dominated by suspension load processes as indicated by fine grain sizes of 4.1 Phi (0.06 mm), moderate to good sorting (0.63–0.5) and coarse to near symmetrical skewness (-0.12–0.02).

The data set of the Upper Schilfsandstein (119 samples) enables the characterisation of channel fills (9 samples), crevasse splays (59 samples), sheetsands (37 samples) and floodplain fines (14 samples) by means of their granulometry. In accordance to the Lower Schilfsandstein, the lateral shift from bedload to suspension load appears to be the most significant process within the channel-floodplain system (Fig. 2.13).

### **2.6.2 Detrital mineralogy of sandstones**

The sandstones of the Lower and Upper Schilfsandstein Members are characterised by remarkable low compositional maturities. 98 samples of both members have mineralogical maturity indexes (Pettijohn 1957) of 0.2–1.4 and thus, vary significantly from older and younger sandstone of the NGB (Fig. 2.14A). According to McBride (1963), 6 samples are classified arkose, 87 are classified lithic arkose and 5 are classified feldspathic litharenites (Fig. 2.14B). In individual samples, feldspar has a range of 24.4–68.5 %, quartz has a range of 17.4–58.8 % and lithics have a range of 3.9–42.3 % of all detrital grains identified to feldspar, quartz and lithics. The feldspar

assemblage is dominantly composed of untwined and twined plagioclase; K-feldspar is less abundant. Monocrystalline quartz dominates the quartz assemblage followed by polycrystalline quartz and chert (Fig. 2.15). The majority of samples contain roughly equal parts of metamorphic and igneous lithoclasts followed by sedimentary lithoclasts, corresponding to the results of Förster et al. (2010). In a few samples of the Barth, Goritz and Morsleben wells, the assemblage of lithics is dominated by metamorphic rock fragments, mainly schists and gneisses, followed by igneous and sedimentary rock fragments.

Beside feldspar, quartz and lithics, the detrital fraction is characterised by subordinated occurrences of muscovite, biotite, glaucony, chlorite and heavy mineral grains. The fine-grained detrital fraction is represented by clayey or mixed carbonate-clastic matrixes which were recognised with an average abundance of 9.2 % within sandstones of crevasse splays and sheetsands (Fig. 2.8). The maximum abundance of 71.9 % matrix was noted within a sample of a floodplain sheetsand. In contrast to samples from overbank environments, samples of distributary and fluvio-deltaic channel fills are practically free of any matrix (Figs. 2.15 and 2.16).

The mineralogical composition of detrital grains, in particular the abundance of lithics, seems to be grain size-dependent. For the studied data set, the abundance of lithics increases with increasing grain sizes. The lowered abundance of lithics for samples of coarse silt is balanced out by increased abundances of both, quartz and feldspar. Apart from grain size-dependent variations, the mineralogical composition proved to be remarkable stable within the NGB. Significant variations related to transport distances were neither observed for the Lower Schilfsandstein nor the Upper Schilfsandstein.



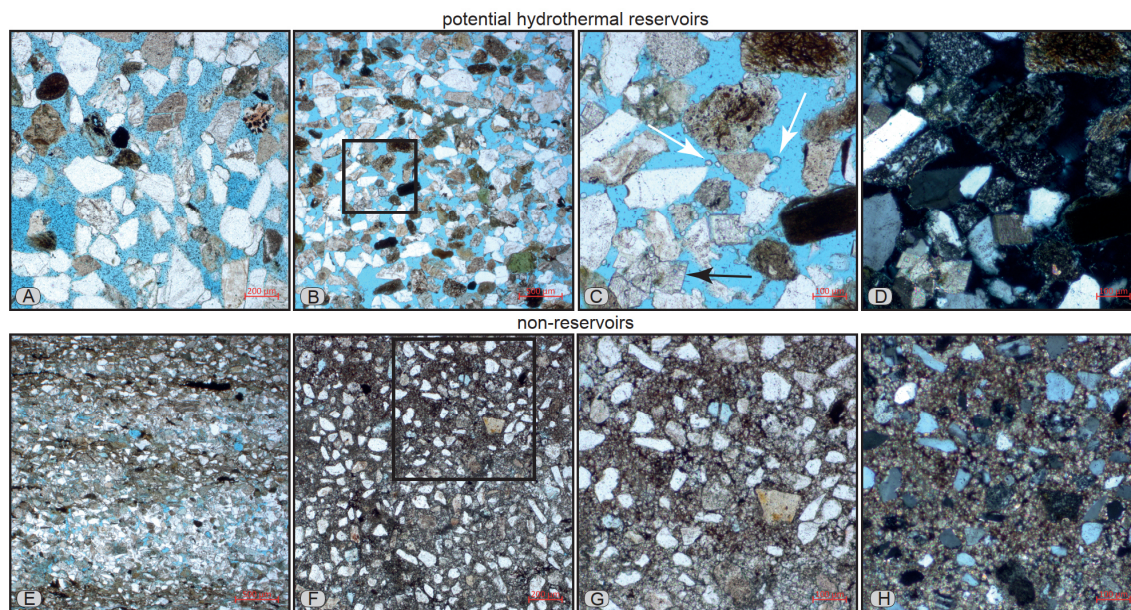


Fig. 2.15: Thin section examples. **Potential hydrothermal reservoirs:** (A) Brustorf 1/62, Lower Schilfsandstein, sample 11-11 (depth 312.9 m): cross-bedded fine-grained sandstone of a deltaic channel fill (Ch) showing floating grains, point contacts and open pore space (stained blue); median: 2.1 ( $\Phi$ ), sorting: 0.66, skewness: 0.39, porosity (Archimedes method): 30.2 %, permeability (calculated from  $k_f$ ): 1,682 mD; scale is 200  $\mu$ m, parallel nicols; see also Fig. 2.16. (B) Lütow well, Lower Schilfsandstein, sample 12-01 (depth 1,029.1 m): massive fine-grained sandstone of a proximal crevasse splay (Cr), note the low textural maturity and low compositional maturity with white to grey quartz and feldspar grains, brown to dark lithics and greenish glaucony, open pore space (stained blue), inlet shows C and D; median 2.4 ( $\Phi$ ), sorting: 0.75, skewness: 0.30, porosity ( $\Phi$ ): 32.0 %, permeability ( $H_2O$ ): 1,155 mD; scale is 500  $\mu$ m, parallel nicols. (C) As before, pore space shows only minor cementation with carbonate (black arrow) and small analcime crystals (white arrows); scale is 100  $\mu$ m, parallel nicols. (D) As before, scale is 100  $\mu$ m, crossed nicols. **Non-reservoirs:** (E) Tarnow 1/65, Lower Schilfsandstein, sample 11-30 (depth 1,139.9 m): matrix-rich laminated very fine-grained sandstone to siltstone (FI) of an interdistributary bay fill (IB); median: 3.7 ( $\Phi$ ), sorting: 0.69, skewness: 0.06, porosity (Archimedes method): 21.7 %, permeability (calculated from  $k_f$ ): 140 mD; scale is 500  $\mu$ m, parallel nicols; see also Fig. 2.16. (F) Strausberg 1/63, Upper Schilfsandstein, sample 6-21 (depth 744.0 m): matrix-rich, very fine-grained sandstone with floating detrital grains, pedogenic carbonate was re-crystallised during burial diagenesis resulting in neomorph fabric, see also Fig. 2.8H; inlet shows G and H; scale is 200  $\mu$ m, parallel nicols. (G) As before, scale is 100  $\mu$ m, parallel nicols. (H) As before, scale is 100  $\mu$ m, crossed nicols.

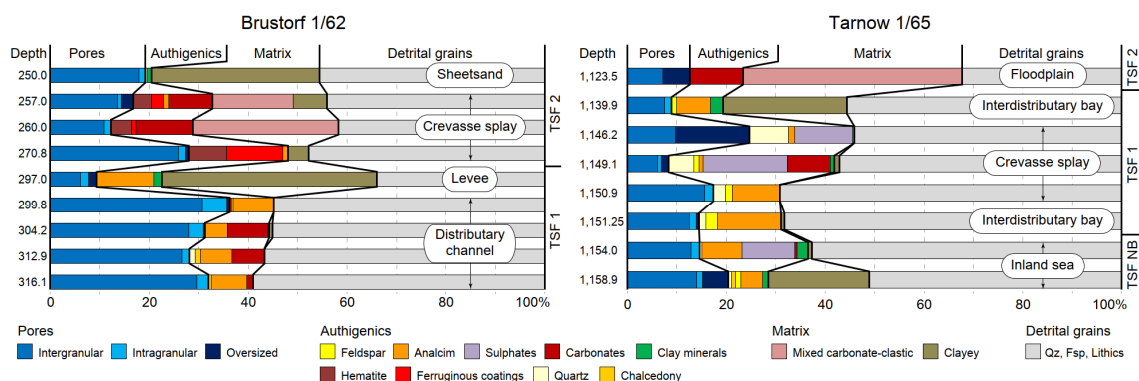


Fig. 2.16: Abundances of detrital grains, detrital matrix, authigenic minerals and pore space on the example of Brustorf 1 and Tarnow 1 wells.

### 2.6.3 Authigenic mineralogy of sandstones

Corrosion of detrital grains, authigenic overgrowth and cementation of open intergranular pore space evidences substantial modification of sandstones during burial diagenesis. Corrosion affected mainly feldspars ranging from apparently unaltered to almost completely corroded. Lithics and quartz grains were only subordinately affected by alteration processes. Authigenic quartz and feldspars occur as overgrows on detrital quartz and feldspar grains. Open pore space was subject to formation of small euhedral analcime crystals or poikilotopic patches as well as patches of calcite, dolomite, anhydrite and gypsum. Authigenic clay minerals are mainly represented by illite/smectite and chlorite and less abundant by kaolinite (Fig. 2.17).

Based on point counting analysis, the abundance of authigenic minerals ranges from 0.3 % to 45.1 %, the average abundance is 13.9 %. The wide range corresponds to samples apparently not affected by cementation and samples in which cementation resulted in the total reduction of pore space. But as authigenic cementation mainly occurred in the form of nests or isolated patches, the total reduction of the pore space represents the exception (Fig. 2.14).

Noteworthy is the low to intermediate grain packaging of samples from channel fills and crevasse splays resulting in partly high permeabilities. Point contacts and long-contacts predominate but also floating grains occur, whereas convex-concave contacts were only rarely observed (Figs. 2.15 and 2.17). For 53 samples the contact strength (Füchtbauer 1973) was estimated with a range of 1.4–2.8 and an average of 1.9. Considering the present maximum depth of up to 1250 m of investigated samples and maximum burial depth of up to 2500 m estimated by Hoth (1997) and Friberg (2001), the grain packaging seems to be not in agreement with the burial history of the Stuttgart Formation. This conflict is subject to an ongoing study focussing on the diagenesis of the Stuttgart Formation; detailed results will be published elsewhere. Preliminary results suggest the eo-diagenetic formation of cements supporting the grain fabric during burial which were later partly dissolved or replaced during a late diagenetic stage as already pointed out by Förster et al. (2010).

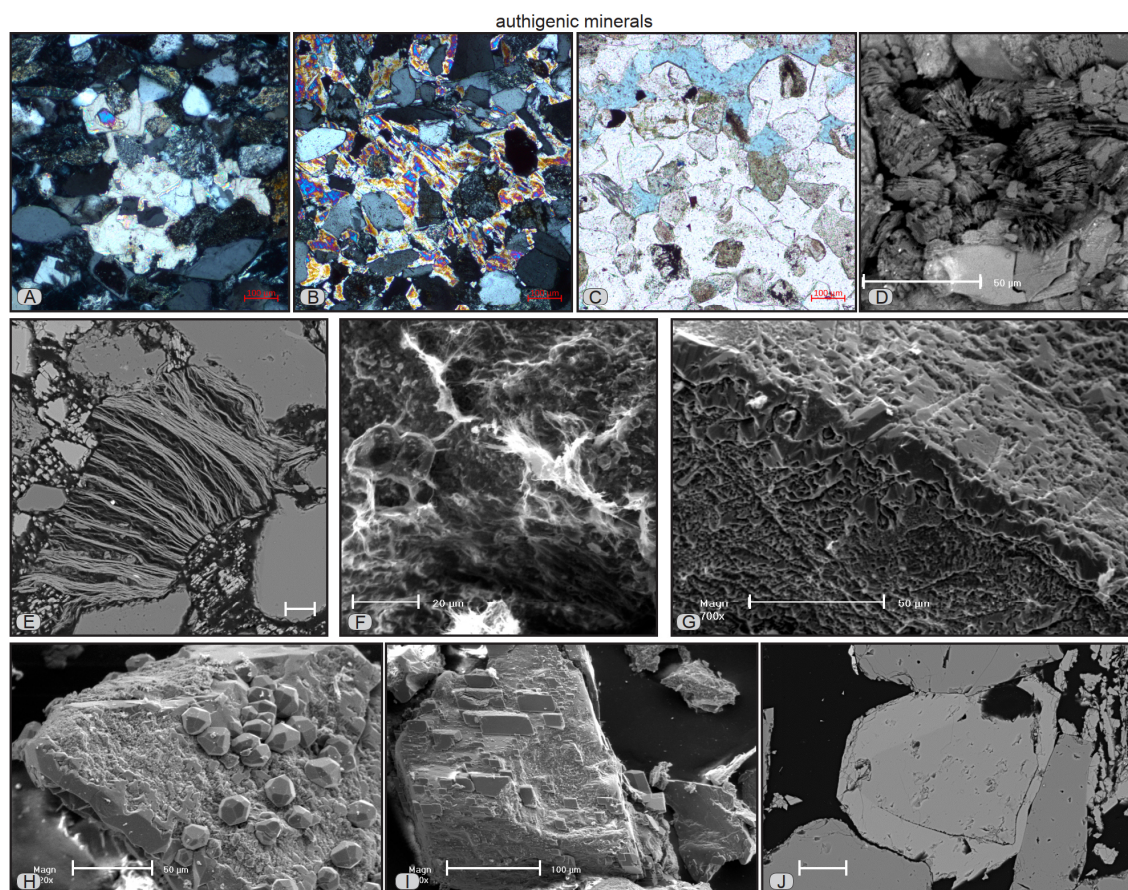


Fig. 2.17: Authigenic mineralogy. **(A)** Barth well, Lower Schilfsandstein, sample 11-1 (depth 776.2 m): horizontal-laminated sandstone (Sh) of a crevasse splay (Cr), local carbonate cementation of pore space; scale is 100  $\mu\text{m}$ ; crossed nicols. **(B)** Gartz 1/65, Upper Schilfsandstein, sample 12-16 (depth 1,313.65 m): ripple cross-bedded sandstone (Sr) of a crevasse splay (Cr), local anhydrite cementation of pore space; scale is 100  $\mu\text{m}$ ; crossed nicols. **(C)** Strausberg 1/63, Lower Schilfsandstein, sample 12-1 (depth 787.3 m): horizontal-laminated sandstone (Sh) of a fluvio-deltaic channel fill (Ch), local analcime cementation of pore space; scale is 100  $\mu\text{m}$ ; parallel nicols. **(D)** Gartz 1/65, Upper Schilfsandstein, sample 12-17 (depth 1,312.7 m): kaolinite booklets filling pore space; scale is 50  $\mu\text{m}$ ; SEM. **(E)** Tarnow 1/65, Lower Schilfsandstein, sample 11-29 (depth 1,146.2 m): authigenic meshwork chlorite filling pore space; scale is 20  $\mu\text{m}$ ; SEM; see also Fig. 2.16. **(F)** Lütow well, Lower Schilfsandstein, sample 12-2 (depth 1,027.0 m): fibrous illite overgrowth on detrital grains and pore space filling meshwork illite; scale is 20  $\mu\text{m}$ ; SEM. **(G)** Lütow well, Lower Schilfsandstein, sample 12-5 (depth 1,014.93 m): quartz overgrowth on detrital grain; scale is 50  $\mu\text{m}$ ; SEM. **(H)** Brustorf 1/62, Lower Schilfsandstein, sample 11-12 (depth 316.1 m): idiomorph analcime crystals on detrital grain; scale is 50  $\mu\text{m}$ ; SEM; see also Fig. 2.16. **(I)** As (G): feldspar overgrowth on detrital feldspar grain; scale is 100  $\mu\text{m}$ , SEM. **(J)** Barth well, Lower Schilfsandstein, sample 11-8 (depth 768.0 m): K-feldspar overgrowth on detrital feldspar grain; scale is 40  $\mu\text{m}$ ; SEM-EDX.

#### 2.6.4 Porosity and permeability

Porosity measurements (helium porosity, Archimedes method) of 225 samples of the Lower and Upper Schilfsandstein have a range of 2.0–39.7 %. Of this sample set, 136 samples of channel belt reservoirs have a median of 24.0 % and 89 samples of overbank reservoirs have a median of 22.0 %. Permeability measurements (water permeability) of 68 samples resulted in a wide range of 0.3–4659 mD. 44 samples of this set were identified to channel belt reservoirs and 24 samples to overbank

reservoirs. The channel belt reservoir sample set has a median permeability of 517 mD, but only 22 of the 48 samples have permeabilities exceeding the 500 mD threshold required for hydrothermal reservoirs. The overbank reservoir sample set has a median of 250 mD, remarkably below this threshold. A positive correlation of porosity and permeability seems to be only indicated for the channel belt reservoir samples set (Fig. 2.18).

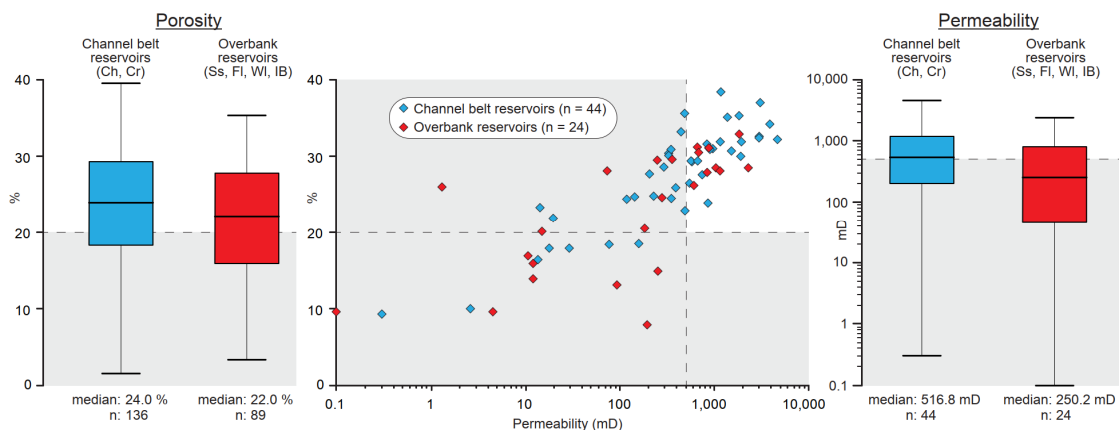


Fig. 2.18: Porosity and permeability of Lower and Upper Schilfsandstein reservoirs. Note the thresholds of 20 % and 500 mD required for hydrothermal reservoirs.

On detail, the hydraulic properties of Lower and Upper Schilfsandstein channel belt reservoirs show only negligible variations (Tabs. 2.2 and 2.3). Proximal examples of Lower Schilfsandstein channel belts are characterised by a porosity range of 8.0–39.7 % and a median porosity of 23.4 % (21 samples). The permeability ranges from 873 mD to 3868 mD with a median of 897 mD (5 samples). Distal examples are characterised by a porosity range of 6.0–38.5 % and a median porosity of 22.7 % (66 samples). The permeability has a wide range of 0.3–3058 mD with a median of 443 mD (23 samples). The Upper Schilfsandstein channel belt reservoirs have a porosity range of 2.0–39.7 % with a median of 24.0 % (58 samples). The permeability ranges from 14 mD to 4659 mD with a median of 546 mD (16 samples).

## 2.6.5 Reservoir quality mapping

Individual reservoirs of suitable quality may be present in any of the bedload dominated facies associations of the Lower and Upper Schilfsandstein. However, taking the minimum net-thickness of 20 m required for long-term operation of hydrothermal

reservoirs into account, only compound reservoir types formed of stacked individual reservoirs represent viable exploration targets (Tabs. 2.2 and 2.3).

Beside limitations concerning reservoir thicknesses, the potential of Lower and Upper Schilfsandstein reservoirs is further limited by the rather random distribution of high permeability values. Even though most of the permeability values exceeding the 500 mD threshold are recorded for reservoirs of the channel belt type, there are also a number of medium (250–500 mD) and low (<250 mD) permeability values recorded for this reservoir type, hampering a reliable reservoir prediction.

### **Lower Schilfsandstein**

From 295 wells investigated, 262 wells yielded sandstone reservoirs of up to 56 m net-thickness whereas in 33 wells no reservoir could be recognised. The mean net-thickness of sandstone reservoirs is 13 m for all wells investigated (Fig. 2.11). The required minimum net-thickness of 20 m was recorded in 62 wells resulting in about 21 % of all wells. The reservoir quality map shows that reservoirs exceeding 20 m net-thickness are related to channel belt complexes of the Lower Schilfsandstein (Fig. 2.19). There, sandstone reservoirs of the distributary or fluvio-deltaic channel and levee/crevasse splay facies associations form compound reservoirs of the channel belt type. This reservoir type is characterised by average net-thicknesses of 26 m at the distal fluvial plain and of 23 m at the delta plain (Table 2.2). Longer and connected, and thus predictable, occurrences of reservoirs exceeding 20 m thickness could only be recognised in the Usedom and Darß areas (Fig. 2.19). There, reservoirs of the channel belt type occur in an up to 38 km wide channel belt, considering the meander belt plus lateral associated crevasse splay complexes. Important to note, this is a maximum related to frequent lateral shifting and channel avulsion in the Usedom area (Appendix). Downstream the width of channel belts and thickness of reservoirs decrease. At delta plains, only isolated, and thus not predictable, occurrences of reservoirs exceeding 20 m thickness could be recognised. In the Ketzin area, mapped widths are about 5.5 km for the meander belt and about 14 km for the channel belt (Fig. 2.12). The medians of calculated meander belt widths range from 136 m to 2,594 m (Fig. 2.11). From the used empirical equations, only the equation presented by Collinson (1978) resulted in values of 770–5,538 m roughly matching the mapped meander belt width of the Ketzin area.

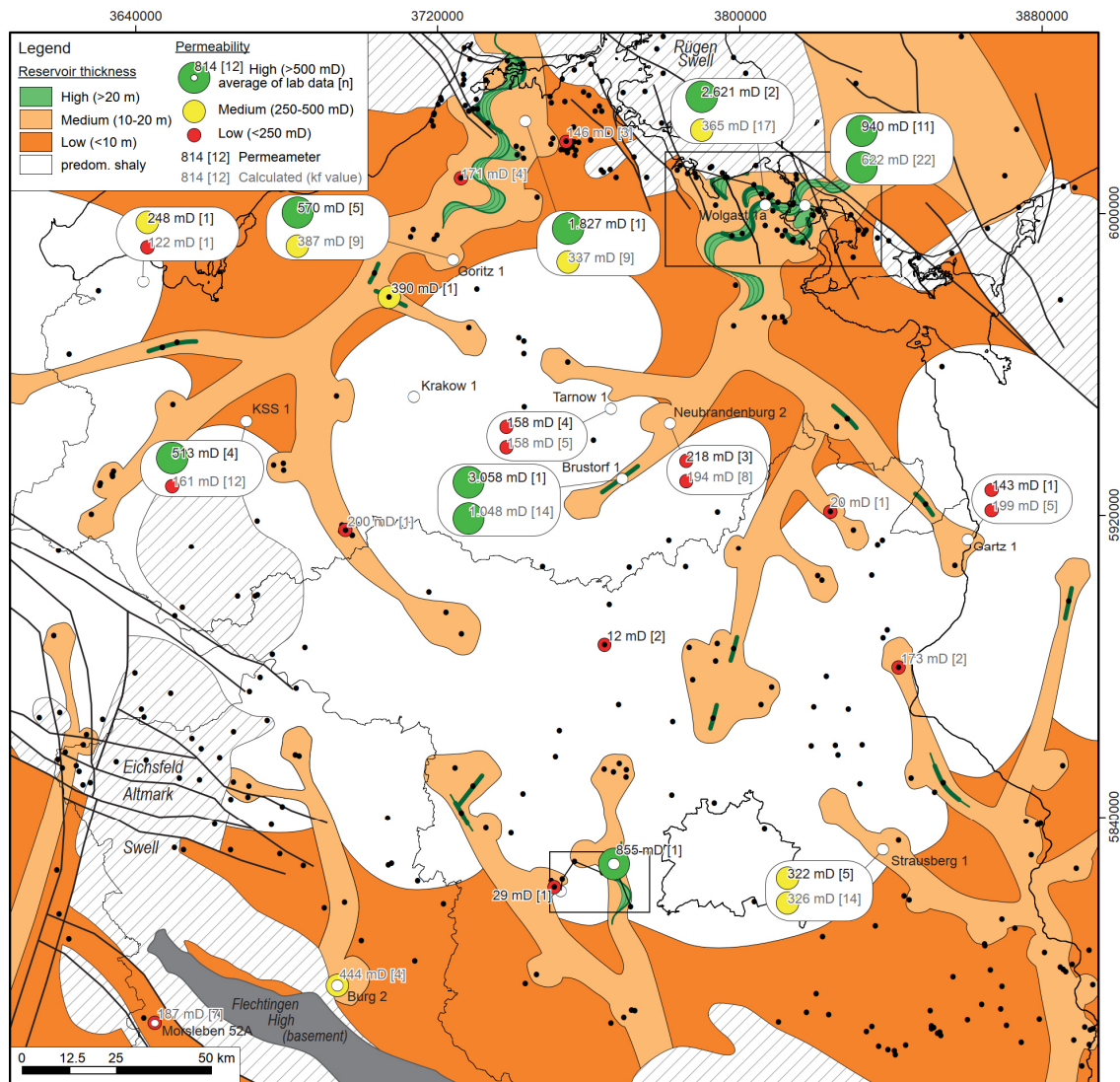


Fig. 2.19: Reservoir quality map of the Lower Schilfsandstein Member based on effective thicknesses and permeabilities of reservoirs.

### Upper Schilfsandstein

From 295 wells investigated, 148 wells yielded sandstone reservoirs of up to 28 m net-thickness whereas in 27 wells no reservoir could be recognised. Within 49 wells, the Upper Schilfsandstein was eroded due to post-depositional uplift. The mean net-thickness of sandstone reservoirs is 10 m for all wells investigated (Fig. 2.11). The required minimum net-thickness of 20 m was recorded in 34 wells resulting in about 12 % of all wells. In accordance to the Lower Schilfsandstein, reservoirs exceeding 20 m net-thickness are related to channel belt complexes of the Upper Schilfsandstein which are formed of fluvial channel and levee/crevasse splay facies associations. The associated channel belt reservoir type is characterised by an average net-thicknesses of 17 m (Table 2.3). Only in the Usedom area, a longer and connected occurrence of

reservoirs exceeding 20 m thickness could be recognised (Fig. 2.20). There, reservoirs of the channel belt type occur in an up to 19 km wide channel belt, considering the meander belt plus lateral associated crevasse splay complexes (Appendix). For the rest of the working area, only individual and isolated occurrences of reservoirs exceeding 20 m thickness could be observed, for example in the Ketzin area. In this area, the mapped widths are about 4 km for the meander belt and about 18 km for the channel belt (Fig. 2.12). The medians of calculated meander belt widths range from 90 m to 1,904 m (Fig. 2.11). With range of 770–4,182 m calculated meander belt width, only the equation presented by Collinson (1978) resulted in values roughly matching the mapped meander belt widths of the Ketzin area.

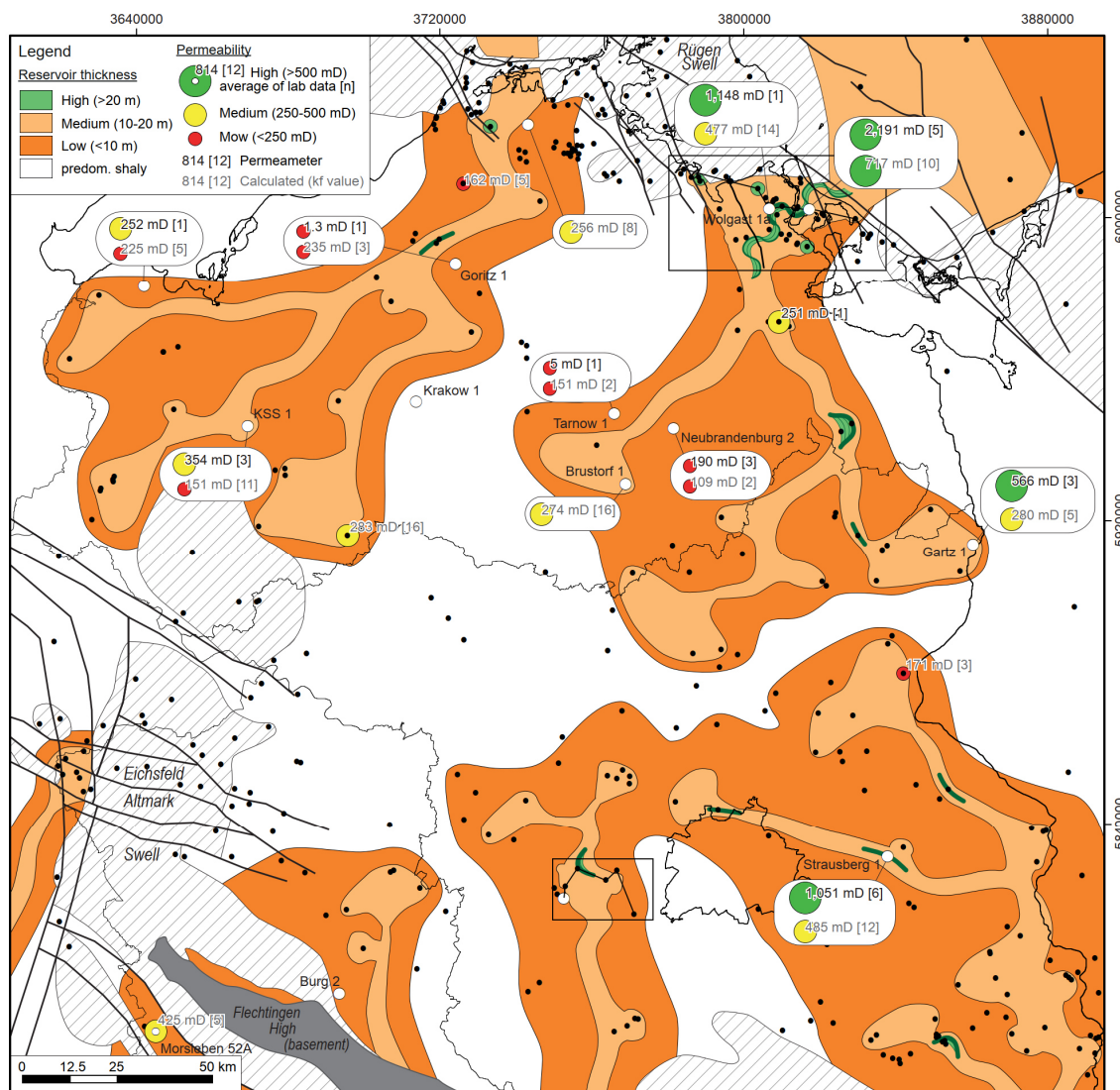


Fig. 2.20: Reservoir quality map of the Upper Schilfsandstein Member based on effective thicknesses and permeabilities of reservoirs.

## **2.7 Seismic exploration and mapping**

So far, conventional 2D seismic methods were employed for underexplored localities, mainly in order to get better constraints on the depth of important stratigraphic boundaries, such as the base Rhaetian. The following case studies describe how even conventional 2D seismic data could make significant contributions to target potential hydrothermal reservoir bodies, such as channel belts.

### **2.7.1 Example 1: Horn Graben (German North Sea)**

Seismic mapping of the Horn Graben area revealed up to 600 m deep incision of the Stuttgart Formation into the Grabfeld Formation. Three incised valleys could be mapped; two within the inner Horn Graben and one along the eastern flank (Fig. 2.21). In the German offshore, these valleys are up to 65 km long, up to 14 km wide and oriented parallel to the NE-SW oriented and elongated salt walls of the Horn Graben (Reinhold et al. 2008). Whereas the widths of the valley correspond well with herein described onshore examples, the incision rates of the valleys are strongly enhanced. This is due to syn-sedimentary salt tectonics, also witnessed by the strongly enhanced thicknesses of Triassic formations and the orientation of incised valleys parallel to salt walls (Best et al. 1993, Bachmann et al. 2010, Barnasch 2010).



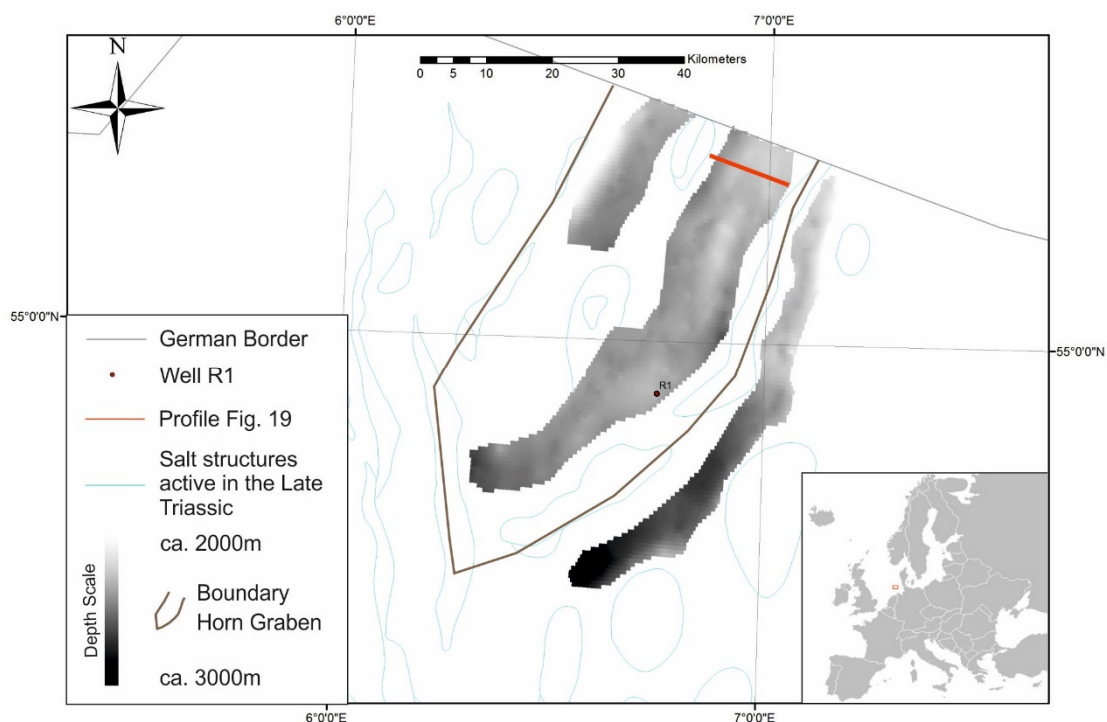


Fig. 2.21: Depth of the base Stuttgart Formation with mapped incised valleys in the Horn Graben area based on seismic data and the R1 well. Thickness and distribution of Triassic strata including the Stuttgart Formation were controlled by intense syn- and postdepositional salt tectonics.

The enhanced thicknesses of the Grabfeld and Stuttgart Formations in combination with the high-resolution seismic data enabled a more detailed reconstruction of valley morphologies compared to onshore examples. The terrace-like truncation surface between both formations points to repeated changes in river bed erosion due to variations in discharge and/or base-level. The lateral shift of channel-like geobodies results most likely from avulsion of lateral shifting fluviodeltaic channels (Fig. 2.22). As also indicated by the R-1 well, lateral shifting and avulsion of channels in concert with crevassing mainly contributed to the fill of incised valleys.

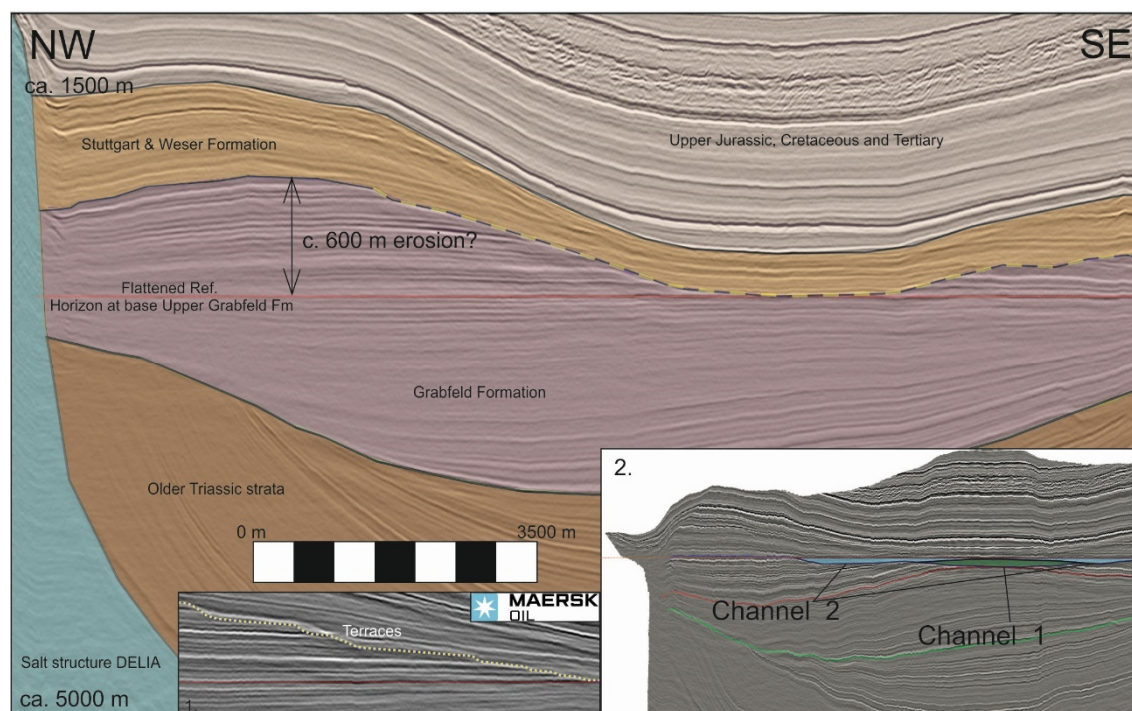


Fig. 2.22: Interpreted NW–SE seismic section in the Horn Graben, flattened at the base Upper Grabfeld Formation (red line). The yellow broken line indicates erosion at the base of the Stuttgart Formation. Inset 1 details the terrace-like truncation surface between the Grabfeld and Stuttgart formations. Inset 2 shows lateral shifting geobodies, most likely resulting from avulsion of lateral shifting fluvio-deltaic channels of the Lower Stuttgart Formation. The backstrip (violet line) of the top Stuttgart Formation (without considering decompaction) was kindly provided by Fabian Jähne-Klingberg (BGR).

## 2.7.2 Example 2: Wolin Block (Baltic Sea)

Seismic mapping of the German offshore around the Rügen Island in the context of the USO (Untergrundmodell Südliche Ostsee) research project (Deutschmann et al. 2018, Seidel et al. 2018) revealed two incised valleys located at the Wolin Block (Fig. 2.23). The western valley, located to the West of the North Jasmund Fault (NJF), is about 6 km wide and up to 100 m deep incised into the Grabfeld Formation and older strata (Fig. 2.24). In the seismic mapping area, this NW-SE trending valley widens and deepens in downstream direction where it seems to be associated to the valley mapped in the subsurface of the Usedom Island (Appendix). The eastern valley, located between the NJF and the Adler-Kamień Fault Zone (AKFZ), is about 8 km wide and up to 200 m incised. This valley probably continues via the Gryfice Block towards NW Poland, not subject to subsurface mapping herein (Figs. 2.6 and 2.7).

As suggested by offshore wells H 2-1, K 1-1 and K 5-1 located at the Wolin and Gryfice Blocks, the position and formation of valleys was at least partly controlled by pre- and syn-sedimentary tectonic movements. The Wolin Block, as a marginal part of the Rügen High, was uplifted prior to the deposition of the Stuttgart Formation and later

truncated due to fluvial incision. Corresponding to the onshore subsurface of West Pomerania (Appendix), gaps associated to pre-sedimentary uplift (Schilfsandstein Unconformity) were later partly superimposed by fluvial incision.

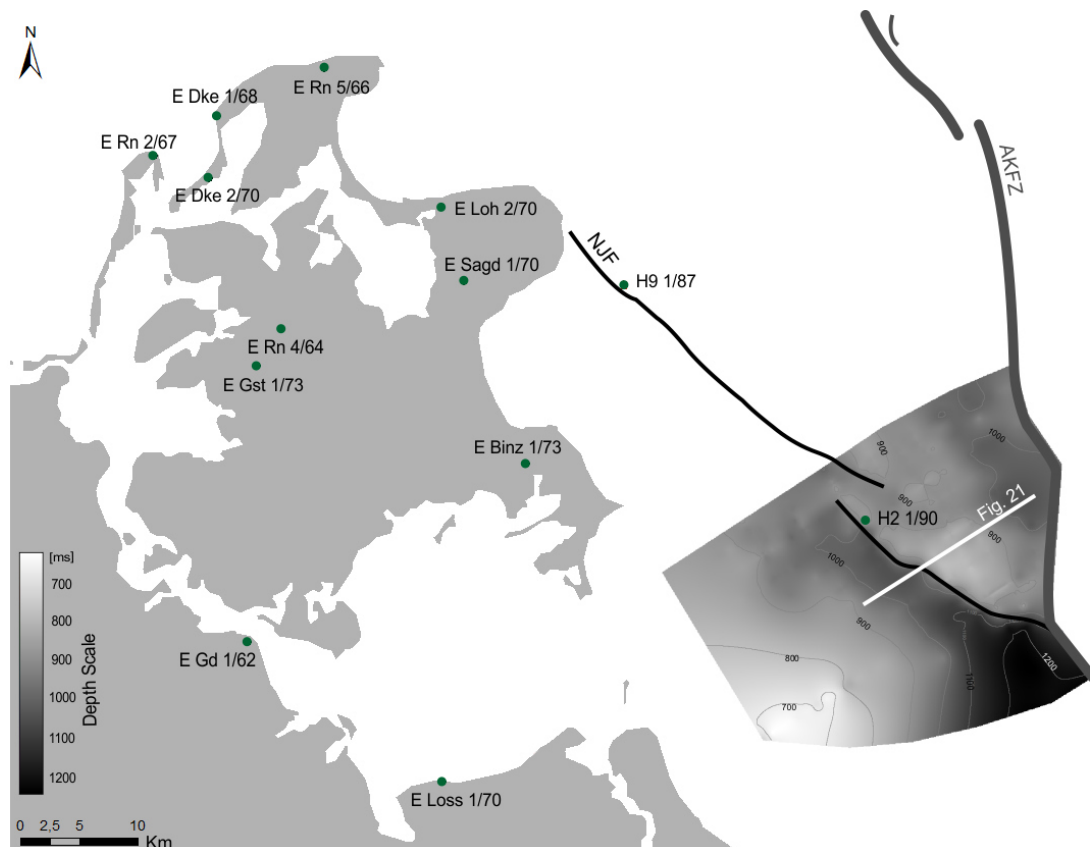


Fig. 2.23: Depth to base Stuttgart Formation in the offshore subsurface east of the Rügen Island based on seismic data and the H 2-1/90 well; AKFZ = Adler-Kamień Fault Zone, NJF = North Jasmund Fault (Seidel et al. 2018).

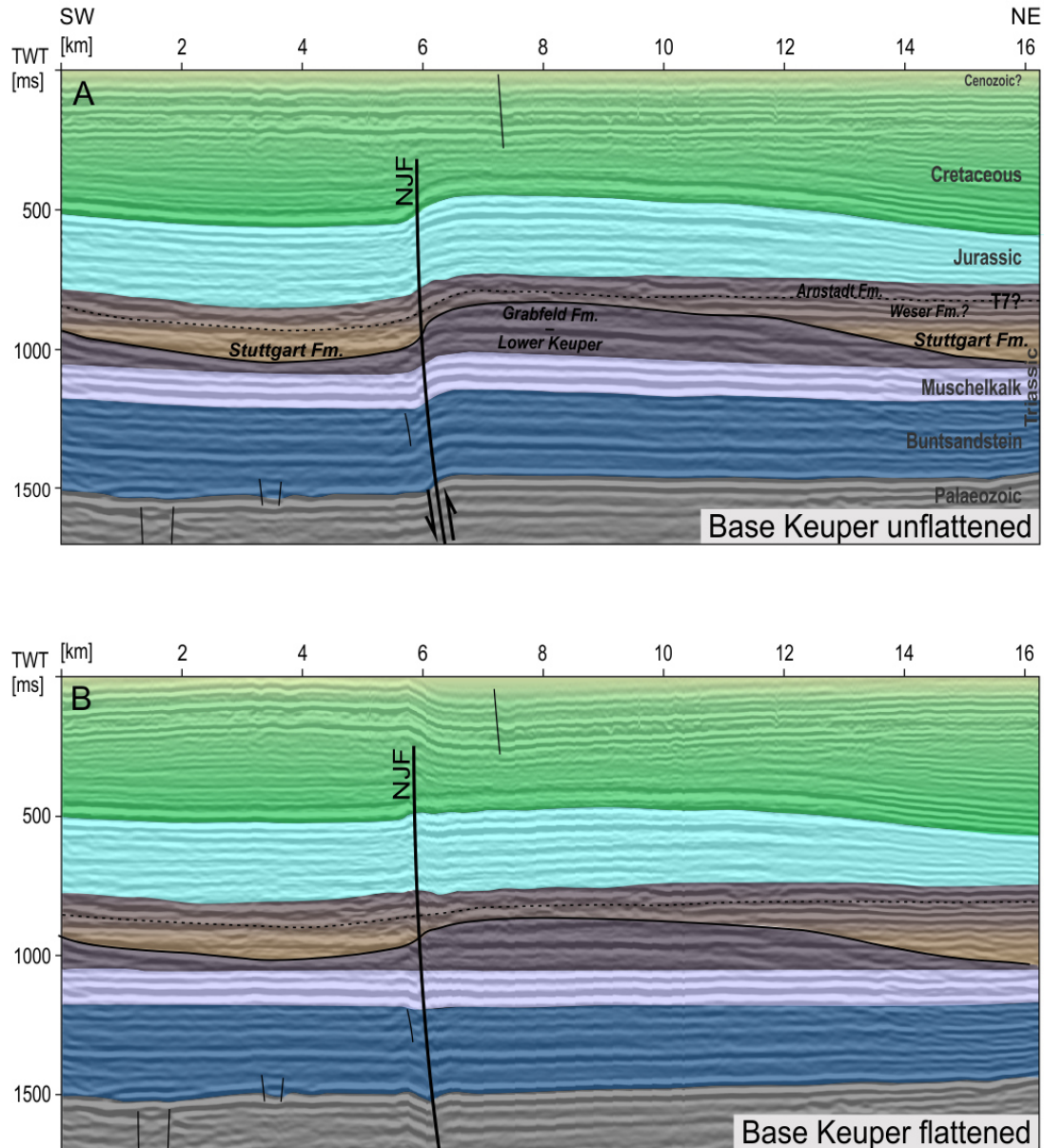


Fig. 2.24: Interpreted SW–NE seismic section (see Fig. 2.20). (A) Time-migrated and interpreted, T7 reflector corresponds to the base Arnstadt Formation. (B) As (A), flattened at base Keuper. NJF = North Jasmund Fault (Seidel et al. 2018).

## 2.8 Discussion

### 2.8.1 Controls on deposition and preservation of the Stuttgart Formation

Resulting from the complex history of the CEB, the deposition and present-day distribution of the Stuttgart Formation were primarily controlled by eustatic and tectonic processes and subordinately by climatic processes. In the Triassic and Jurassic, the general E–W and NE–SW extensional tectonic regime resulted in slow but continuous

subsidence rates of the epicontinental sag basin (Ziegler 1982, Bachmann & Grosse 1989, Kockel 2002, Kley et al. 2008). As part of peri-Tethyan lowlands, the epicontinental CEB was subject to repeated transgressions from Tethyan waters during the mid-Carnian, representing the main control on deposition of the Stuttgart Formation (Franz et al. 2014). Thickness pattern of the Neubrandenburg Member as well as the Lower and Upper Schilfsandstein Members show higher thicknesses in the WNW-ESE oriented axial part of the CEB, stretching from the Hamburg area to the North of Berlin, and decreasing thicknesses towards the North and South (Fig. 2.5, Franz et al. 2014, this work). This is in congruence with the subsidence centre of the CEB during the Triassic and Jurassic (Ziegler 1990, Stollhofen et al. 2008, Bachmann et al. 2010, Lott et al. 2010, Pharaoh et al. 2010). Accordingly, subsurface facies and thickness mapping of the Lower and Upper Schilfsandstein Members revealed fluvio-deltaic environments prograding from northern and southern margins towards this subsidence centre.

In concert with the rather short time-span of the Stuttgart Formation, the slow but continuous subsidence rates of the CEB resulted in limited thicknesses of reservoirs. As demonstrated herein, Lower and Upper Schilfsandstein hydrothermal reservoirs exceeding 20 m thickness are only locally distributed. Moreover, the present-day distribution of reservoirs may be limited by post-depositional tectonics due to the Norian Early Cimmerian Unconformity (ECU, Beutler & Schöler 1978), Cretaceous inversion and salt tectonics. Whereas the ECU was mainly responsible for erosion of the Stuttgart Formation (Figs. 2.6 and 2.7), Cretaceous inversion and salt tectonics were mainly responsible for uplift. Accordingly, the present-day depths of Schilfsandstein reservoirs range from 250 m to 2600 m in NE Germany. In particular depths above 1500 m will result in limited temperatures of hydrothermal reservoirs (Agemar et al. 2012). Beside limited depth, salt structures also have an influence on the fluid chemistry. With increasing depth, the amount of total dissolved solids increases by about 10 g per 100 m for Cretaceous to Keuper reservoir complexes (Wolfgramm et al. 2014). Reservoirs fluids influenced by Zechstein fluids due to mixing show increased salinities of up to 280 g/l TDS (Total Dissolved Solids, Fig. 2.25).

In comparison with upper Palaeozoic and Mesozoic sandstones of the CEB, the sandstones of the Lower and Upper Schilfsandstein Members are exceptional as they are characterised by very low mineralogical maturities (Fig. 2.14B; Förster et al. 2010, Franz et al. 2018c). Apart from the rather general discussion whether the Schilfsandstein represents a humid climate event (see Simms & Ruffell 1989; Visscher et al. 1994; Kozur & Bachmann 2010), the very low maturity – in particular, the high

content of feldspar and lithics – seems to be in conflict with a humid climate change proposed by Simms & Ruffell (1989) and others. Recently, Franz et al. (2018c) evaluated the detrital mineralogy, palaeosols and the macro- and palyno-flora of the Stuttgart Formation and proposed a model of sea-level controlled forcing of the epicontinental hydrological cycle. However, this needs further constraints as well as the rift shoulder uplift in the area of the Scandinavian Caledonides proposed by Kozur & Bachmann (2010).

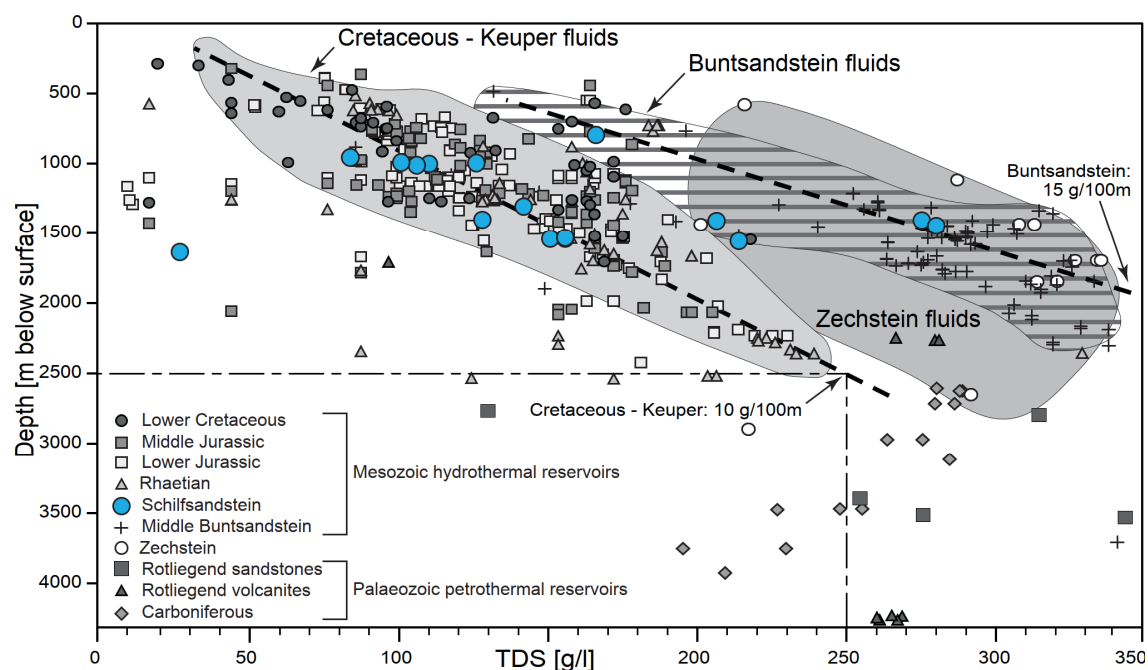


Fig. 2.25: Increasing depth results in increasing salinities of fluids; c. 550 fluid analyses of Mesozoic and Palaeozoic reservoirs (modified after Wolfgramm et al. 2014); fluids of Schilfsandstein reservoirs shown in blue (modified from Franz et al. 2018a).

## 2.8.2 Drainage pattern

The herein reconstructed basinwards-directed drainage pattern is based on subsurface facies mapping and further supported by downstream directed changes in channel capacity, as indicated by decreasing channel fill thicknesses, and increasing degree of bifurcation and avulsion of channels. From the Polish part of the Basin, Gajewska (1973) reported the progradation of fluvio-deltaic systems from northern and southern margins into a remnant sea covering the basin centre. Thus, the Lower Schilfsandstein remnant sea as reconstructed herein seems to have continued towards the East resulting in a basinwards-directed drainage pattern in the Northeast German and Polish parts of the basin.

However, this drainage pattern is in conflict to previous reconstructions. Based on the analysis of lithofacies and transport directions in South Germany, the Weserbergland and Thuringia, Wurster (1964), Kruck & Wolf (1975), Nürnberger (2010) and Shukla et al. (2010) reconstructed the N-S directed exo-rheic drainage of the Schilfsandstein. Likewise, Beutler & Häusser (1982), Beutler & Nitsch (2005) and Barnasch (2010) reconstructed the N-S directed drainage in the NGB based on subsurface mapping of lithologies and thickness of the Schilfsandstein.

Only preliminary provenance studies on detrital mica and zircons have been applied so far. Based on bulk K/Ar ages of white mica, Paul et al. (2008) proposed a Caledonian source of Schilfsandstein samples from Lower Saxony and Franconia (Bodenmühle). Interestingly, Hofmann et al. (2018) reported predominantly Variscan U-Pb ages of detrital zircons from outcrops Bodenmühle and Großmonra (Thuringia). These contradicting results of surface and subsurface mapping and preliminary provenance studies should be subject to a more detailed provenance study.

### **2.8.3 The Stuttgart Formation: a deep geothermal reservoir?**

Previous and recent reconnaissance studies have demonstrated the high potential of Mesozoic reservoir complexes, partly including the Stuttgart Formation (Katzung 1984, Diener et al. 1988-92, Beutler et al. 1993, Franz et al. 2015). The Rhaetian reservoirs operated at Waren and Neustadt-Glewe represent best practice examples of hydrothermal reservoir development. There, clean and highly mature sandstone reservoirs exceeding 20 m thickness and 500 mD permeability are successfully operated since decades (Franz et al. 2018a). Compared with these examples, the potential of the Stuttgart Formation appears rather limited due to lower effective thicknesses of reservoirs, low maturity of detrital grains, high amount of detrital matrix and authigenic minerals (see also Förster et al. 2010), and, resulting from this, high lateral variability of reservoir qualities. This contributes to considerable exploration risks of geothermal projects attempting to develop Schilfsandstein reservoirs. Apart from this, reservoirs exceeding 20 m effective thickness and 500 mD permeability could be proven for some regions and individual localities. There, for example in the Usedom area, the reservoirs of the Stuttgart Formation may be considered an alternative option if the development of Upper Keuper or Middle Jurassic reservoirs fails.

## 2.9 Concluding remarks

The herein presented set of basin-scale subsurface facies and reservoir quality maps of the Lower and Upper Schilfsandstein Members will contribute to an improved exploration of the Lower to Middle Keuper reservoir complex and evaluation of its geothermal potential. In addition to subsurface mapping of the Upper Keuper and Middle Jurassic reservoir complexes, the herein presented maps will help plan ongoing and future geothermal projects in North Germany. Geothermal projects will primarily attempt to develop high-quality Upper Keuper or Middle Jurassic reservoirs, representing key targets of geothermal exploration, but, if the development of these reservoirs fails, the Schilfsandstein reservoirs may represent an alternative option.

In the future, basin-scale subsurface maps should be substantiated by detailed mapping studies of Schilfsandstein reservoirs. Regional- to local-scale mapping studies will contribute to a further reduction of exploration risks and help to develop exploration strategies for individual localities combining well-based exploration with 3D seismic methods. The successful targeting of geobodies by means of 3D seismic campaigns will further contribute to a significant reduction in exploration risks and costs.

## Acknowledgment

The authors acknowledge funding by the Bundesministerium für Wirtschaft und Energie (grant numbers 0325285 and 0325920 to Matthias Franz and Markus Wolfgramm) BMWi. Karsten Obst, Juliane Brandes (LUNG Mecklenburg-Vorpommern), Michael Göthel (LBGR Brandenburg), Thomas Koch, Karl-Heinz Friedel (LAGB Sachsen-Anhalt), Lutz Katzschmann, Herrmann Huckriede (TLUG) and Heinz-Gerd Röhling (LBEG Niedersachsen) kindly provided access to well data and core material. Fabian Jähne-Klingberg (BGR) kindly provided backstripping data of the Horn Graben seismic data set. The authors acknowledge the permissions of Neptune Energy (Lingen, formerly Engie E&P) and Maersk Oil to publish data. SeisWare International Inc. kindly provided the software SeisWare™ with an educational software license. The reviews of Gerhard Bachmann (Universität Halle) and an anonymous reviewer as well as the editorial handling of Thorsten Agemar (LIAG Hannover) are gratefully acknowledged.



## References

- Agemar, T., Alten, J., Ganz, B., Kuder, J., Kühne, K., Schumacher, S. & Schulz, R. (2014): The Geothermal Information System for Germany - GeotIS – Zeitschrift der Deutschen Gesellschaft für Geowissenschaften, 165 (2), 129–144.
- Agemar, T., Schellschmidt, R., & Schulz, R. (2012): Subsurface temperature distribution in Germany. – *Geothermics* 44, 65–77.
- Alberti, F. v. (1834): Beitrag zu einer Monographie des Bunten Sandsteins, Muschelkalks und Keupers und die Verbindung dieser Gebilde zu einer Formation. 366 p., Tübingen (Cotta'sche Buchhandlung).
- Allen, J. R. L. (1963): The Classification of cross-stratified units, with notes on their origin. – *Sedimentology*, 2, 93–114.
- Allen, J. R. L. (1965): A review of the origin and characteristics of recent alluvial sediments. – *Sedimentology*, 5, 89–191.
- Bachmann, G. H. & Wild, H. (1976): Die Grenze Gipskeuper/Schilfsandstein bei Heilbronn/Neckar. – *Jahresberichte und Mitteilungen des Oberrheinischen geologischen Vereins*, 58: 137–152.
- Bachmann, G. H. & Grosse, S. (1989): Struktur und Entstehung des Norddeutschen Beckens – geologisch-geophysikalische Interpretation einer verbesserten Bouguer-Schwerekarte. – *Niedersächsische Akademie der Geowissenschaften Veröffentlichungen*, 2: 23–47.
- Bachmann, G.H. & Kozur, H. 2004. The Germanic Triassic: correlations with the international chronostratigraphic scale, numerical ages and Milankovitch cyclicity. – *Hallesches Jahrbuch für Geowissenschaften B* 26, 17–62.
- Bachmann, G.H., Geluk, M.C., Warrington, G., Becker-Roman, A., Beutler, G., Hagdorn, H., Hounslow, M.W., Nitsch, E., Röhling, H.-G., Simon, T. & Szulc, A., with contributions by Michiel Duser, M., Nielsen, L.H., Barnasch, J. & Franz, M. (2010): Triassic. In: Doornenbal, J.C. & Stevenson, A.G. (eds) *Petroleum Geological Atlas of the Southern Permian Basin Area*. Houten (EAGE Publications), 149–173.
- Baldschuhn, R., Binot, F., Fleig, S. & Kockel, F. (2001): Geotektonischer Atlas von Nordwestdeutschland und dem deutschen Nordsee-Sektor. – *Geologisches Jahrbuch*, A 153, 95 p.

- Bally, A. & Snelson, S. (1980): Realms of subsidence. In: Miall, A. D. (ed) Facts and principles of world petroleum occurrence. – Canadian Society of Petroleum Geologists Memoir, 6, 9–94.
- Barnasch, J. (2010): Der Keuper im Westteil des Zentraleuropäischen Beckens (Deutschland, Niederlande, England, Dänemark): diskontinuierliche Sedimentation, Litho-, Zyklo- und Sequenzstratigraphie. – Schriftenreihe der Deutschen Gesellschaft für Geowissenschaften 71, 170 p.
- Bhattacharya, J.P. (2006): Deltas. – In: Posamentier, H. & Walker, R. (eds) Facies Models Revisited. Society of Economic Petrologists and Mineralogists, Special Publication 84: 237–292.
- Best, G., Kockel, F. & Schoeneich, H. (1983): Geological history of the southern Horn Graben. – Geologie en Mijnbouw (Netherlands Journal of Geosciences), 62: 25–33.
- Beutler, G. (1976): Zur Ausbildung und Gliederung des Keupers in NE-Mecklenburg. – Jahrbuch für Geologie, 7/8: 119–126.
- Beutler, G. (1995): Quantifizierung der altkimmerischen Bewegungen in Nordwestdeutschland. – Berichte der Bundesanstalt für Geologie und Rohstoffe, Nr. 113087, 147 p.; Hannover [unpublished].
- Beutler, G. & Häusser, I. (1982): Über den Schilfsandstein der DDR. – Zeitschrift für Geologische Wissenschaften, 10: 511–525.
- Beutler, G. & Schüler, F. (1978): Über altkimmerische Bewegungen im Norden der DDR und ihre regionale Bedeutung (Fortschrittsbericht). – Zeitschrift für geologische Wissenschaften, 6, 403–420.
- Beutler, G., Röhling, H.G., Schulz, R. & Werner, K.H. (1994): Regionale Untersuchungen von geothermischen Reserven und Ressourcen in Nordwestdeutschland. – Endbericht, Archivnummer 111 758; Hannover (GGA).
- Beutler, G., Heunisch, C., Luppold, F.W., Rettig, B. & Röhling, H.G. (1996): Muschelkalk, Keuper und Lias am Mittellandkanal bei Sehnde (Niedersachsen) und die regionale Stellung des Keupers. – Geologisches Jahrbuch, A 145: 67–197.
- Bridge, J. S. & Tye, R. S. (2000): Interpreting the Dimensions of Ancient Fluvial Channel Bars, Channels, and Channel Belts from Wireline-Logs and Cores. – American Association of Petroleum Geologists, 84 (8): 1205–1228.
- Brierley, G. J., Ferguson, R. J. & Woolfe, K. J. (1997): What is a fluvial levee? – Sedimentary Geology, 114, 1–9.

- Bristow, C. S., Skelly, R. L. & Ethridge, F. G. (1999): Crevasse splays from the rapidly aggrading, sand-bed, braided Niobrara River, Nebraska: effect of base-level rise. – *Sedimentology*, 46, 1029–1047.
- Brown, L.F. & Fisher, W.L. (1971): V. Delta systems in other Basins: Triassic of the German Basin. - In: Fisher, W.L., Brown, L.F., Scott, A.J. & McGowen, J.H. (eds): *Delta systems in the exploration for oil and gas. A research colloquium.* Bureau of Economic Geology University of Texas: 70.
- Coleman, J. M. (1969): Brahmaputra River: channel processes and sedimentation. – *Sedimentary Geology*, 3, 129–239.
- Coleman, J. M., Gagliano, S. M. & Webb, J. E. (1964): Minor sedimentary structures in a prograding distributary. – *Marine Geology*, 1, 240–258.
- Coleman, J. & Prior, D. (1982): Deltaic environments. – In: Scholle, P. & Spearing, D. (eds) *Sandstone Depositional Environments.* American Association of Petroleum Geologists Memoirs, 31: 139–178.
- Collinson, J. (1978): Vertical sequence and sand body shape in alluvial sequences. – In: *Fluvial Sedimentology* (Ed. A.D. Miall), Canadian Society of Petroleum Geologists, Memoir 5: 577–586.
- Collinson, J.D. (1996): Alluvial sediments. – In: Reading, H.G. (Ed.) *Sedimentary Environments: Processes, Facies, Stratigraphy*, 3<sup>rd</sup> ed. Blackwell Science, Oxford, 37–82.
- DSK (Deutsche Stratigraphische Kommission, Ed.) (2005): *Stratigraphie von Deutschland, IV: Keuper.* Courier Forschungsinstitut Senckenberg 253, 296 p.
- Deutschmann, A., Meschede, M. & Obst, K. (2018): Fault system evolution in the Baltic Sea area west of Rügen, NE Germany. – In Kilhams, B., Kukla, P.A., Mazur, S., McKie, T., Mijnlief, H. & van Ojik, K. (eds): *Mesozoic Resource Potential in the Southern Permian Basin.* Geological Society, London, Special Publications, 469, DOI.org/10.1144/SP469.24 [in press].
- Diener, I, Wormbs, J. et al. (1988-92): *Abschlußberichte Geothermische Ressourcen im Nordteil der DDR 1:200.000.* – Zentrales Geologisches Institut Berlin.
- Dittrich, D. (1989): Der Schilfsandstein als synsedimentär-tektonisch geprägtes Sediment - eine Umdeutung bisheriger Befunde. – *Zeitschrift der deutschen geologischen Gesellschaft*, 140: 143–168.

- Dockter, J. & Schubert, J. (2005): Der Keuper in Thüringen und im thüringischen Grabfeld. – In: DSK (Deutsche Stratigraphische Kommission) (ed): Stratigraphie von Deutschland IV – Keuper. – Courier Forschungsinstitut Senckenberg, 253: 192–202.
- Duchrow, H. (1984): Der Keuper im Osnabrücker Bergland. – In: Klasen, H. (Ed.) Geologie des Osnabrücker Berglandes. Naturwissenschaftliches Museum Osnabrück, 221–333.
- Emmert, U. (1965): Ist der Schilfsandstein des Mittleren Keupers eine Flußablagerung. – *Geologica Bavarica*, 55: 146–168.
- Etzold, A. & Bläsi, H.-R. (2000): Exkursionsführer, Jahrestreffen der AG-Keuper 20.-23.07. 2000 in Waldshut-Tiengen [unpublished].
- Etzold, A. & Schweizer, V. (2005): Der Keuper in Baden-Württemberg. – In: DSK (Deutsche Stratigraphische Kommission) (Hrsg.): Stratigraphie von Deutschland IV – Keuper. Courier Forschungsinstitut Senckenberg, 253: 214–258.
- Feldrappe, H., Obst, K. & Wolfgramm, M. (2008): Die mesozoischen Aquifere des Norddeutschen Beckens und ihr Potential für die geothermische Nutzung. – *Zeitschrift für geologische Wissenschaften*, 36 (4-5): 199–222.
- Fielding, C. & Crane, R. (1987): An application of statistical modelling to the prediction of hydrocarbon recovery factors in fluvial reservoir sequences. – In: Ethridge, F., Flores, R. & Harvey, M. (eds) Recent developments in fluvial sedimentology. Society of Economic Paleontologists and Mineralogists, Special Publication 39: 321–327.
- Fisher, W. L., Brown, L. F., Scott, A. J. & McGowen, J. H. (Eds.) (1969): Delta Systems in the Exploration for Oil and Gas. Bureau of Economic Geology, The University of Texas at Austin, Texas.
- Förster, A., Schöner, R., Förster, H.J., Norden, B., Blaschke, A.W., Luckert, J., Beutler, G., Gaupp, R. & Rhede, D. (2010): Reservoir characterization of a CO<sub>2</sub> storage aquifer. The Upper Triassic Stuttgart Formation in the Northeast German Basin. – *Marine and Petroleum Geology*, 27 (10): 2156–2172.
- Folk, R.L. & Ward, W.C. (1957): Brazos River bar: a study in the significance of grain size parameters. – *Journal of Sedimentary Petrology* 27, 3–26.
- Franz, M. (2008): Litho- und Leitflächenstratigraphie, Chronostratigraphie, Zylo- und Sequenzstratigraphie des Keupers im östlichen Zentraleuropäischen Becken (Deutschland, Polen) und Dänischen Becken (Dänemark, Schweden). (Ph.D. Thesis) Martin-Luther-Universität Halle-Wittenberg, Germany, (<http://sundoc.bibliothek.uni-halle.de/diss-online/08/09H048/index.htm>).

- Franz, M., Nowak, K., Berner, U., Heunisch, K., Bandel, K., Röhling, H.-G. & Wolfgramm, M. (2014): Eustatic control on epicontinental basins: the example of the Stuttgart Formation in the Central European Basin (Middle Keuper, Late Triassic). – *Global and Planetary Change*, 122: 305–329.
- Franz, M., Wolfgramm, M., Barth, G., Nowak, K., Zimmermann, J., Budach, I. & Thorwart, K. (2015): Verbundprojekt: Identifikation hydraulisch geeigneter Bereiche innerhalb der mesozoischen Sandsteinaquifere in Norddeutschland. Forschungsvorhaben, Dokumentation, Schlussbericht. TU Bergakademie Freiberg, 317 S.
- Franz, M., Barth, G., Zimmermann, J., Budach, I., Nowak, N. & Wolfgramm, M. (2018a): Deep geothermal resources of the North German Basin: exploration examples of Mesozoic hydrothermal reservoirs. – In: Kilhams, B., Kukla, P. A., Mazur, S., Mckie, T., Mijnlief, H. F. & van Ojik, K. (Hrsg.). *Mesozoic Resource Potential in the Southern Permian Basin*. Geological Society, London, Special Publications, 469: 193–222, DOI.org/10.1144/SP469.11
- Franz, M., Bachmann, G. H., Barnasch, J., Heunisch, C. & Röhling, H.-G. (2018b): Der Keuper in der Stratigraphischen Tabelle von Deutschland 2016 – kontinuierliche Sedimentation in der norddeutschen Beckenfazies (Variante B). *Zeitschrift der Deutschen Gesellschaft für Geowissenschaften*, 169 (2): 203–224.
- Franz, M., Kustatscher, E., Heunisch, C., Niegel, S. & Röhling, H.-G. (2018c): The Schilfsandstein and its flora – arguments for a humid mid-Carnian episode? – *Journal of the Geological Society of London* [accepted manuscript].
- Freudenberger, W. (2005): Der Keuper in Franken und der Oberpfalz (Bayern). – In: DSK (Deutsche Stratigraphische Kommission) (Hrsg.): *Stratigraphie von Deutschland IV – Keuper*. – Courier Forschungsinstitut Senckenberg, 253: 203–213.
- Friberg, L. J. (2001): Untersuchungen zur Temperatur- und Absenkungsgeschichte sowie zur Bildung und Migration von Methan und molekularem Stickstoff im Nordostdeutschen Becken. *Berichte Forschungszentrum Jülich*, 3914.
- Füchtbauer, H. (1973): Zur Diagenese fluviatiler Sandsteine. – *Geologische Rundschau*, 63: 904–925.
- Gajewska, I. (1973): Charakterystyka osadów piskowca trzciniowego na Niziu Polskim. – *Kwartalnik geologiczny* 17, 507–515.

- Galloway, W. (1975): Process framework for describing the morphological and stratigraphic evolution of deltaic depositional systems. – In: Broussard, M. (ed) *Deltas*. Houston Geological Society, 87–98.
- Gast, R., Pasternack, M., Piske, J. & Rasch, H.-J. (1998): Das Rotliegend im Nordostdeutschen Raum: Regionale Übersicht, Stratigraphie, Fazies und Diagenese. – *Geologisches Jahrbuch*, A149: 59–79.
- Haunschild, H. & Ott, W.-D., mit Beiträgen von Hagdorn, H., Simon, T., Schwarz, H.-U. & Riesch, H. (1982): Profilbeschreibung, Stratigraphie und Paläogeographie der Forschungsbohrung Dinkelsbühl 1001. – *Geologica Bavarica*, 83: 5–55.
- Häusser, I. (1972): Zur sedimentpetrographischen Analyse der Sandsteinfolgen des Unteren und Mittleren Keupers im Nordteil der DDR. PhD Thesis, Bergakademie Freiberg, 111 p. [unpublished].
- Häusser, I. & Kurze, M. (1975): Sedimentationsbedingungen und Schwermineralführung im Mesozoikum des Nordteils der DDR. – *Zeitschrift für geologische Wissenschaften*, 3: 1317–1332.
- Heling, D. (1979): Zur Faziesanalyse des Schilfsandsteins. – *Jahresberichte und Mitteilungen oberrheinischer geologischer Verein*, Neue Folge 74: 191–213.
- Heunisch, C. (1999): Die Bedeutung der Palynologie für Biostratigraphie und Fazies in der Germanischen Trias. – In: Hauschke, N., Wilde, V. (Eds.), *Trias: eine ganz andere Welt*. Pfeil-Verlag, München, pp. 13–21.
- Hofmann, M., Voigt, T., Bittner, L., Gärtner, A., Zieger, J. & Linnemann, U. (2018): Reworked Middle Jurassic sandstones as a marker for Upper Cretaceous basin inversion in Central Europe —a case study for the U–Pb detrital zircon record of the Upper Cretaceous Schmilka section and their implication for the sedimentary cover of the Lausitz Block (Saxony, Germany). – *International Journal of Earth Sciences*, 107 (3): 913–932.
- Hoth, P. (1997): Fazies und Diagenese von Präperm-Sedimenten der Geotraverse Harz - Rügen. – *Schriftenreihe für Geowissenschaften*, 4, 139 p.
- Jung, R., Röhling, S., Ochmann, N., Rogge, S., Schellschmidt, R., Schulz, R. & Thielmann, T. (2002): Abschätzung des Technischen Potenzials der geothermischen Stromerzeugung und der geothermischen Kraft-Wärmekopplung (KWK) in Deutschland. – Gutachten im Auftrag des Deutschen Bundestag, Bundesanstalt für Geowissenschaften und Rohstoffe, Hannover 2002.

- Kabus, F., Lenz, G., Wolfgramm, M., Hoffmann, F. & Kellner, T. (2003): Studie zu den Möglichkeiten der Stromerzeugung aus hydrothermalen Geothermie in Mecklenburg-Vorpommern. GTN-Bericht 4383, 148 p.
- Kahlert, N., Schulz, E. & Weyer, D. (1970): Paläontologischer Kurzbericht zur Bohrung Angermünde 1/68 – Schilfsandstein. Bericht Nr. ZGI 53/70 [unpublished].
- Kannegieser, E. & Kozur, H. W. (1972): Zur Mikropaläontologie des Schilfsandsteins (Karn). – *Geologie*, 21 (2): 185–215.
- Katzung, G. (Hrsg.) (1984): *Geothermie-Atlas der Deutschen Demokratischen Republik*. – Zentrales Geologisches Institut Berlin, 27 p.
- Katzung, G. (2004): Geothermie. In: Katzung, G. (Hrsg.) *Geologie von Mecklenburg-Vorpommern*. E. Schweizerbart'sche Verlagsbuchhandlung (Nägele u. Obermiller), Stuttgart, Germany, 444–451.
- Katzung, G., Diener, I. & Kühn, P. (1992): Temperaturverteilung im Untergrund Ostdeutschlands und für die Nutzung der geothermischen Ressourcen in Betracht kommenden Aquifere. – *Braunkohle*, 1992: 27–32.
- Kelly, S.B. & Olsen, H. (1993): Terminal fans – a review with reference to Devonian examples. – *Sedimentary Geology*, 85: 339–374.
- Kley, J., Franzke, H.J., Jähne, F., Krawczyk, C., Lohr, T., Reicherter, K., Scheck-Wenderoth, M., Sippel, J., Tanner, D., van Gent, H. & the SPP 1135 Structural Geology Group. (2008): Strain and stress. – In: Littke, R., Bayer, U., Gajewski, D. & Nelskamp, S. (eds) *Dynamics of complex intracontinental basins: the Central European Basin System*, Springer, Berlin, pp 97–124.
- Kockel, F. (2002): Rifting processes in NW-Germany and the German North Sea sector. – *Netherlands Journal of Geosciences*, 81: 149–158.
- Köppen, A. (1997): Faziesentwicklung in der frühen Obertrias Mitteleuropas – ein sequenzstratigraphischer Vergleich. – *Gaea Heidelbergensis* 2, 233 p.
- Kozur, H. W. (1970a): Mikropaläontologische Bearbeitung der Bohrung Flieth 1/64. – Bericht, Sektion Geowissenschaften Bergakademie Freiberg, 8 p.; Freiberg [unpublished].
- Kozur, H. W. (1970b): Mikropaläontologische Bearbeitung der Bohrung Schillingstedt. – Zwischenbericht, Sektion Geowissenschaften Bergakademie Freiberg, 5 p.; Freiberg [unpublished].

- Kozur, H. W. (1970c): Mikropaläontologische Bearbeitung der Bohrung Tarnow 1/65. – Bericht, Sektion Geowissenschaften Bergakademie Freiberg, 6 p.; Freiberg [unpublished].
- Kozur, H. W. & Bachmann, G. H. (2010): The Middle Carnian Wet Intermezzo of the Stuttgart Formation (Schilfsandstein), Germanic Basin. – *Palaeogeography, Palaeoclimatology, Palaeoecology*, 290: 107–119.
- Kozur, H.W. & Weems, R.E. (2010): The biostratigraphic importance of conchostracans in the continental Triassic of the northern hemisphere. – In: Lucas, S. G. (ed.): *The Triassic Timescale*. Geological Society of London, Special Publication, 334: 315–417.
- Kruck, W. & Wolf, F. (1975): Ergebnisse einer Fazieskartierung im Schilfsandstein des Weserberglandes. – *Mitt. Geol.-Paläont. Inst. Univ. Hamburg*, 44: 417–421.
- Lang, R. (1909): Der mittlere Keuper im südlichen Württemberg. – *Jahreshefte des Vereins für Vaterländische Naturkunde Württemberg*, 65: 77–131.
- Lang, S.C., Payenberg, T.H.D., Reilly, M.R.W., Hicks, T., Benson, J., Kassin, J. (2004): Modern analogues for dryland sandy fluvial-lacustrine deltas and terminal splay reservoirs. – *Australian Petroleum Production & Exploration Association Journal*, 2004: 329–356.
- Mack, G.H., James, W.C. & Monger, H.C. (1993): Classification of paleosols. – *Geological Society of America Bulletin*, 105: 129–136.
- McBride, E.F. (1963): A classification of common sandstones. – *Journal of Sediment Petrology*, 33: 664–669.
- Miall, A. D. (1996): *The geology of fluvial deposits: sedimentary facies, basin analysis, and petroleum geology*, 582 p.; Springer.
- Miller, C.S., Peterse, F., da Silva, A.-C., Baranyi, V., Reichart, G.J. & Kürschner, W. (2017): Astronomical age constraints and extinction mechanisms of the Late Triassic Carnian crisis. – *Scientific Reports*, 2557.
- Nichols, G.J. & Fisher, J.A. (2007): Processes, facies and architecture of fluvial distributary system deposits. – *Sedimentary Geology*, 195: 75–90.
- Nöldeke, W. & Schwab, G. (1977): Zur tektonischen Entwicklung des Tafeldeckgebirges der Norddeutsch - Polnischen Senke unter besonderer Berücksichtigung des Nordteils der DDR. – *Zeitschrift für Angewandte Geologie*, 23 (8): 369–379.



- Nürnberg, T. (2010): Fazies und Genese der Stuttgart-Formation (Schilfsandstein) im Thüringer Becken und Thüringer Grabfeld. – Diplomarbeit Friedrich-Schiller-Universität Jena, 92 S.
- Olariu, C. & Bhattacharya, J. P. (2006): Terminal distributary channels and delta front architecture of river-dominated delta systems. – *Journal of Sedimentary Research*, 76 (1–2), 212–233.
- Paul, J., Wemmer, K., Ahrendt, H. (2008): Provenance of siliciclastic sediments (Permian–Jurassic) in the Central European Basin. – *Zeitschrift der Deutschen Gesellschaft für Geowissenschaften*, 159: 641–650.
- Pettijohn, F.J. 1957. *Sedimentary rocks*. Harper & Brothers, New York, 718 pp.
- Pharaoh, T.C., Dusar, M., Geluk, M.C., Kockel, F., Krawczyk, C.M., Krzywiec, P., Scheck-Wenderoth, M., Thybo, H., Vejbaek, O.V. & Van Wees, J.D. (2010): Tectonic evolution. – In: Doornenbal, J.C. & Stevenson, A.G. (eds) *Petroleum Geological Atlas of the Southern Permian Basin Area*. EAGE Publications b.v. (Houten): 25–57.
- Reinhold, K., Krull, P. & Kockel, F. (2008): Salzstrukturen Norddeutschlands, Geologische Karte 1:500 000. Bundesanstalt für Geowissenschaften und Rohstoffe.
- Ricken, W., Aigner, T. & Jacobsen, B. (1998): Levee-crevasse deposits from the German Schilfsandstein. – *Neues Jahrbuch für Geologie und Paläontologie Abhandlungen*, 1998: 77–94.
- Rockel, W., Hoth, P. & Seibt, P. (1997): Charakteristik und Aufschluss geothermaler Speicher. – *Geowissenschaften*, 15 (8): 244–252.
- Scholle, T. (1992): Genese und Diagenese des Rhät + Hettang/Untersinemur im Nordosten Deutschlands – ein Beitrag zur Nutzung geothermischer Energie. Dissertation, Ernst-Moritz Arndt-Universität Greifswald, 111 p.
- Schomacker, E. R., Kjemperud, A. V., Nystuen, J. P. & Jahren, J. S. (2010): Recognition and significance of sharp-based mouth-bar deposits in the Eocene Green River Formation, Uinta Basin, Utah. – *Sedimentology*, 57: 1069–1087.
- Schröder, B. (1977): Unterer Keuper und Schilfsandstein im germanischen Trias-Randbecken. – *Zentralblatt für Geologie und Paläontologie*, Teil I, 1976: 1030–1056.
- Schulz, R. & Röhling, H.-G. (2000): Geothermische Ressourcen in Nordwestdeutschland. – *Zeitschrift für Angewandte Geologie*, 46 (3): 122–129.

- Schwab, G. (1985): Palaomobilität der Norddeutsch-Polnischen Senke. – Dissertation, Akademie der Wissenschaften der DDR.
- Seidel, E., Meschede, M. & Obst, K. (2018): The Wiek Fault System east of Rügen Island: origin, tectonic phases and its relationship to the Trans-European Suture Zone. – In: Kilhams, B., Kukla, P. A., Mazur, S., Mckie, T., Mijnlieff, H. F. & van Ojik, K. (eds) Mesozoic Resource Potential in the Southern Permian Basin. Geological Society, London, Special Publications 469, DOI.org/10.1144/SP469.10 [in press].
- Shukla, U.K., Bachmann, G.H. & Singh, I.B. (2010): Facies architecture of the Stuttgart Formation (Schilfsandstein, Upper Triassic), central Germany, and its comparison with modern Ganga system, India. – *Palaeogeography, Palaeoclimatology, Palaeoecology*, 297: 110–128.
- Simms, M.J. & Ruffell, A.H. (1989): Synchronicity of climate change and extinctions in the Late Triassic. – *Geology*, 17: 265–268.
- Stollhofen, H., Bachmann, G., Barnash, J., Bayer, U., Beutler, G., Franz, M., Kästner, M., Legler, B., Mutterlose, J. & Radies, D. (2008): Upper Rotliegend to Early Cretaceous basin development. – In: Littke, R., Bayer, U., Gajewski, D. & Nelskamp, S. (eds.) *Dynamics of Complex Sedimentary Basins. The Example of the Central European Basin System*, Springer, pp. 181–210.
- Thürach, H. (1888-89): Übersicht über die Gliederung des Keupers im nördlichen Franken im Vergleich zu den benachbarten Gegenden. – *Geognostische Jahreshefte* 1, 75–162. *Geognostische Jahreshefte* 2, 1–90.
- Tooth, S. (1999a): Floodouts in Central Australia. – In: Miller, A.J., Gupta, A. (Eds.), *Varieties of Fluvial Form*. Wiley and Sons, London, pp. 219–247.
- Tooth, S. (1999b): Downstream changes in floodplain character on the Northern Plains of arid central Australia. – In: Smith, N.D., Rogers, J. (Eds.), *Fluvial Sedimentology VI. Special Publication of the International Association of Sedimentologists*, 28: 93–112.
- Visscher, H., Van Houte, M., Brugman, W.A. & Poort, P.R. (1994): Rejection of a Carnian (Late Triassic) ‘pluvial event’ in Europe. – *Review of Palaeobotany and Palynology*, 83: 217–226.
- Wehland, H. (1968): Zur Stratigraphie und Ausbildung des Oberen Muschelkalkes, des Keupers und des Jura im Nordosten der DDR. – *Freiberger Forschungsheft C* 248 [unveröff.].

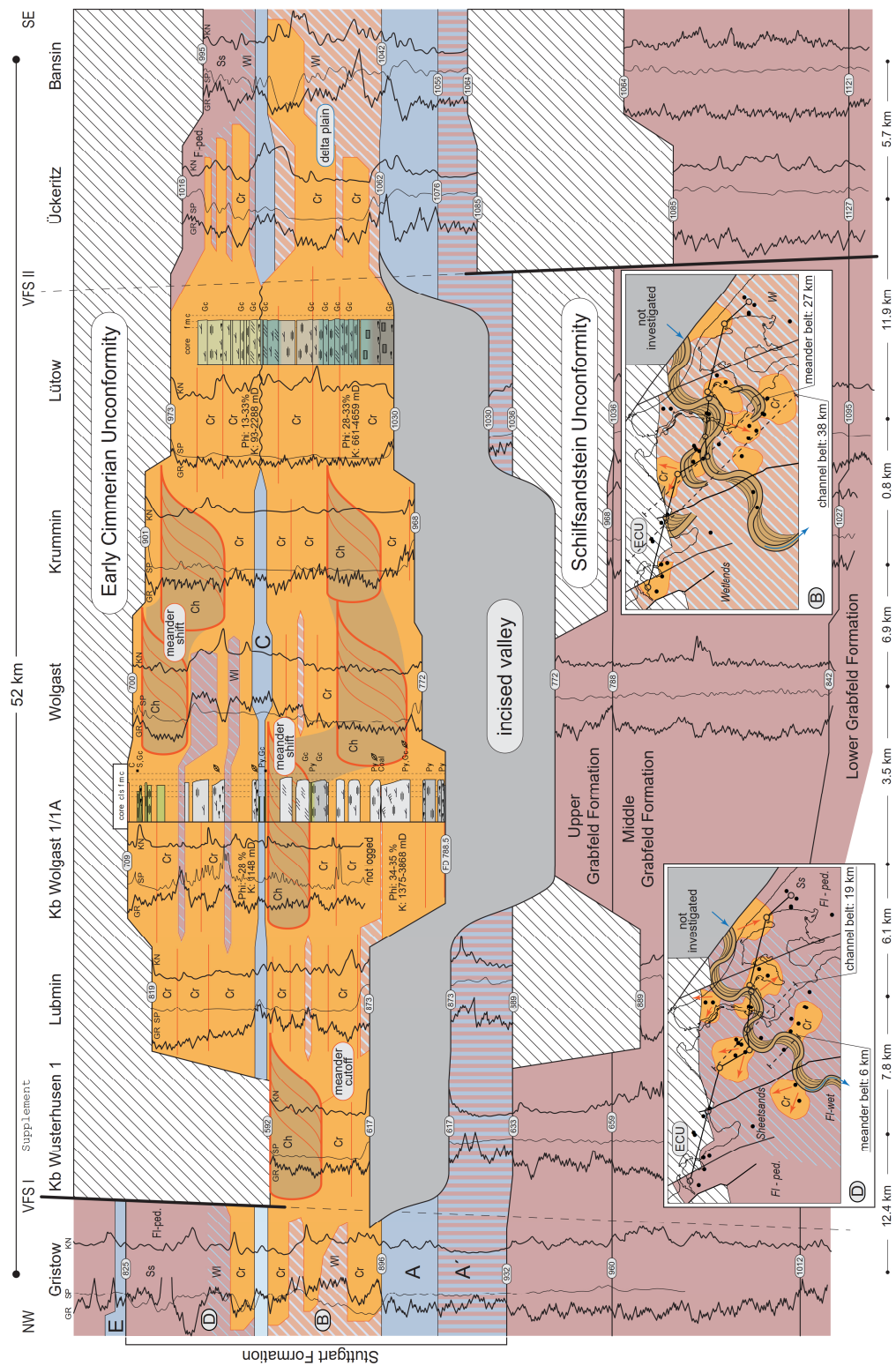
- Wehland, H. (1970): Kurzbericht über die Kartierungsbohrung Tarnow 1. Bericht Zentrales Geologisches Institut, Nr. RGEE 121/70, 27 p.; Berlin [unveröff.].
- Weissmann, G.S., Hartley, A.J., Nichols, G.J., Scuderi, L.A., Olson, M., Buehler, H. & Banteah, R. (2010): Fluvial form in modern continental sedimentary basins: Distributive fluvial systems. – *Geology*, 38 (1): 39–42.
- Wentworth, C. (1922): A scale of grade and class terms for clastic sediments. – *Journal of Geology*, 30: 377–392.
- Willis, B. J. (1989): Palaeochannel reconstruction from point bar deposits: a three-dimensional perspective. – *Sedimentology*, 36: 757–766.
- Wolfgramm, M. (2005): Fluidentwicklung und Diagenese im Norddeutschen Becken – Petrographie, Mikrothermometrie und Geochemie stabiler Isotope. – *Hallesches Jahrbuch, B, Beiheft 20*, 143 p.
- Wolfgramm, M., Franz, M. & Agemar, T. (2014): Explorationsstrategie tiefer geothermischer Ressourcen am Beispiel des Norddeutschen Beckens. – In: Bauer, M., Freeden, W., Jacobi, H. & Neu, T. (eds) *Handbuch Tiefe Geothermie*. Springer, Berlin, 463–505.
- Wormbs, J., Diener, I. & Pasternak, G. (1988): Geothermische Ressourcen im Nordteil der DDR (I). – Bericht, Zentrales Geologisches Institut Berlin.
- Wright, D. L. (1977): Sediment transport and deposition at river mouths: a synthesis. – *Geological Society of America Bulletin*, 88: 857–868.
- Wurster, P. (1964): Geologie des Schilfsandsteins. – *Mitteilungen des Geologischen Staatsinstituts Hamburg*, 33: 1–140.
- Wurster, P. (1972): Entgegnung auf Lincks neue Deutung der Geologie des Schilfsandsteins. – *Jahreshefte geologisches Landesamt Baden-Württemberg*, 14: 53–67.
- Zhang, Y., Li, M., Ogg, J., Montgomery, P., Huang, C., Chen, Z.-Q., Shi, Z., Enos, P. & Lehrmann, D.J. (2015): Cycle-calibrated magnetostratigraphy of the middle Carnian from South China: Implications for Late Triassic time scale and termination of the Yangtze Platform. – *Palaeogeography, Palaeoclimatology, Palaeoecology* 436, 135–166.
- Ziegler, P. A. (1982): *Geological Atlas of Western and Central Europe*. – The Hague: Shell International Petroleum Maatschappij, Elsevier, Amsterdam, 130 p.

Ziegler, P. A. (1990): Geological Atlas of Western and Central Europe. – Shell International Petroleum, Den Haag, 239 p.

Zimmermann, J. (2015): The Lower and Middle Jurassic System in the North German Basin: sequence stratigraphy, depositional environments and basin evolution. – Dissertation, TU Bergakademie Freiberg.

Zimmerman, J., Franz, M., Schaller, A., Wolfgramm, M. (2017): The Toarcian-Bajocian deltaic system in the North German Basin: subsurface mapping of ancient deltas – morphology, evolution and recent analogue. – *Sedimentology*, 65: 897–930.

## A Appendix



Cross-section of the Usedom area showing channel belts of the Lower and Upper Schilfsandstein. Phases of faulting and uplift prior and post-cursor to the deposition of the Stuttgart Formation resulted in the Western Pomeranian Fault System (WPFS) and erosion associated to the Schilfsandstein Unconformity and Early Cimmerian Unconformity (Beutler & Schüler 1978, Stollhofen et al. 2008, Franz et al. 2018b). Fluvio-deltaic incision and layer-cake architecture of marine-brackish and fluvio-deltaic strata was triggered and controlled by sea-level fluctuations. Stuttgart Formation: A – Neubrandenburg Member sensu Franz et al. (2014), A' – transitional interval km<sub>1</sub>/9 sensu (Wehland 1968, 1970), B – Lower Schilfsandstein, C – Gaildorf Member, D – Upper Schilfsandstein, Weser Formation: E – Beaumont Member.

## Chapter III

### 3 Depositional and diagenetic controls on porosity evolution in sandstone reservoirs of the Stuttgart Formation (North German Basin)

Accepted Publication: Niegel, S., Franz, M., 2023. Depositional and Diagenetic Controls on Porosity Evolution in Sandstone Reservoirs of the Stuttgart Formation (North German Basin). *Marine and Petroleum Geology*, 106157. <https://doi.org/10.1016/j.marpetgeo.2023.106157>

**Authors' edited topics:** This publication was equally conceptualized and written by Sebastian Niegel and Matthias Franz. The microscopic analyses (transmitted light microscopy, CL, SEM-EDX) of the detrital and authigenic minerals, the bulk rock chemistry, and the identification of the paragenetic sequences as well as the evaluation of the granulometric data of the investigated samples were realised by Sebastian Niegel. Matthias Franz worked on the discussion and made important corrections.

**Supplementary Data:** Supplementary data for this article can be found online at <https://doi.org/10.1016/j.marpetgeo.2023.106157>.

## Abstract

The Mesozoic succession of the North German Basin comprises permeable sandstones operated by 'conventional' open doublet systems for geothermal heat production. The high permeability, exceeding 6 Darcy at individual localities, is the result of undercompacted grain fabrics, low abundance of authigenic minerals and large secondary porosity volumes. The discrepancy of undercompacted grain fabrics and porosity volumes of >20 % at depth of up to 2,500 m gave rise to a basin-scale study, in which classical petrographic methods were employed to reconstruct the diagenesis of sandstones on the example of the Stuttgart Formation (Schilfsandstein, Late Triassic). Associated to the deposition of sandstones in distinct fluvio-deltaic environments, four diagenetic pathways are indicated by systematic variations of detrital and authigenic assemblages. These four pathways are herein introduced as Delta Channel, Delta Plain, Fluvial Channel, and Floodplain Diagenesis Types. In response to the history of the North German Basin, high permeabilities of sandstones of the Delta Channel and Fluvial Channel Diagenesis Types are related to the subsequent control of depositional and diagenetic regimes on porosity evolution. Pervasive eogenetic calcite cementations contributed to preservation of pre-burial intergranular volumes and effectively prevented the mechanical compaction of grain fabrics during late Triassic–late Jurassic burial diagenesis. The uplift from deep to shallow burial depth, associated to latest Jurassic–Cenozoic structural differentiation and inversion of the North German Basin, triggered substantial dissolution processes that mainly affected carbonate cementations. This opened pores and contributed to the evolution of secondary porosity, in particular in sandstones of the Delta Channel and Fluvial Channel Diagenesis Types. Moderate post-inversion reburial rates resulted only in negligible mechanical compaction and reduction of secondary porosity. The improved knowledge of diagenetic pathways, herein exemplified by sandstones of the Stuttgart Formation, will significantly contribute to improved predictions of Mesozoic hydrothermal reservoir in the North German Basin.

## 3.1 Introduction

The Mesozoic succession of the North German Basin (NGB) comprises highly porous and permeable sandstones, which are exploited for geothermal heat production since the 1980s (e.g., Katzung, 1984; Visser and Heedrik, 1987; Diener et al., 1988–1992; Beutler et al., 1994; Erlström et al., 2018; Weibel et al., 2020). Related to the high transmissivity of these hydrothermal reservoirs, development examples in Denmark,

Netherlands, North Germany, and South Sweden employ 'conventional' open doublet systems to produce geothermal energy for district heating and other use (overviews in Rockel et al., 1997; Mahler and Magtengaard, 2010; Erlström et al., 2018; Mijnlief, 2020).

The experience in operating open doublet systems in North Germany contributed to a deep knowledge concerning development, maintenance, and operation routine of hydrothermal reservoirs. Accordingly, successful developments require a minimum reservoir quality of  $>10$  Dm transmissivity and  $>50 \text{ m}^3 (\text{h} \times \text{MPa})^{-1}$  productivity index (e.g., Rockel et al. 1997). Previous exploration campaigns have targeted Mesozoic sandstones with transmissivities ranging from 10 Dm to more than 300 Dm in burial depth of up to 2,500 m (Katzung, 1984; Diener et al., 1988–1992; Wolfgramm et al., 2008; Franz and Wolfgramm, 2019). These high transmissivities are related to undercompacted grain fabrics, secondary porosity and low abundances of authigenic minerals (e.g., Scholle, 1992; Wolfgramm et al., 2008; Franz et al., 2015, 2018a); apparently a paradox considering the burial depth and related temperatures of up to 100 °C (Agemar et al., 2012; Wolfgramm et al. 2014).

In analogy to Rotliegend reservoir studies (e.g., Glennie et al., 1978; Hancock, 1978, Gaupp et al., 1993), the migration, accumulation, and possible alteration of hydrocarbons was the main objective of previous studies on the diagenesis of Mesozoic sandstones (e.g. Füchtbauer, 1967, 1973; Burley, 1986; Gaupp, 1991; Lippmann, 2012). But since the utilisation of unproductive Mesozoic reservoirs for geothermal energy production and CO<sub>2</sub> sequestration became an option, diagenesis studies increasingly focused on potential hydrothermal reservoirs or storage aquifers (e.g., Fine, 1986; Friis, 1987; Scholle, 1992; Baumgarten, 2010; Förster et al., 2010; Wolfgramm et al., 2008; Weibel et al., 2017).

Despite this considerable progress, the paradox of low mechanical compaction and open pore space at depth where mesogenetic processes usually result in intense cementation are not well understood. This gave rise to study the sandstone diagenesis on the example of the Stuttgart Formation (Schilfsandstein), which is characterised by repeated marine–terrestrial facies shifts and geographically wide-spread occurrence in the Central European Basin System (e.g., Kozur and Bachmann, 2010; Franz et al., 2014, 2018b; Zhang et al., 2020). This makes the Stuttgart Formation an ideal example to investigate the subsequent control of depositional and diagenetic regimes on sandstone diagenesis. The results of this basin-wide study reveal the impact of eo- and telogenetic stages on the hydraulic quality of sandstone reservoirs and thus, make a significant contribution to improved reservoir predictions.



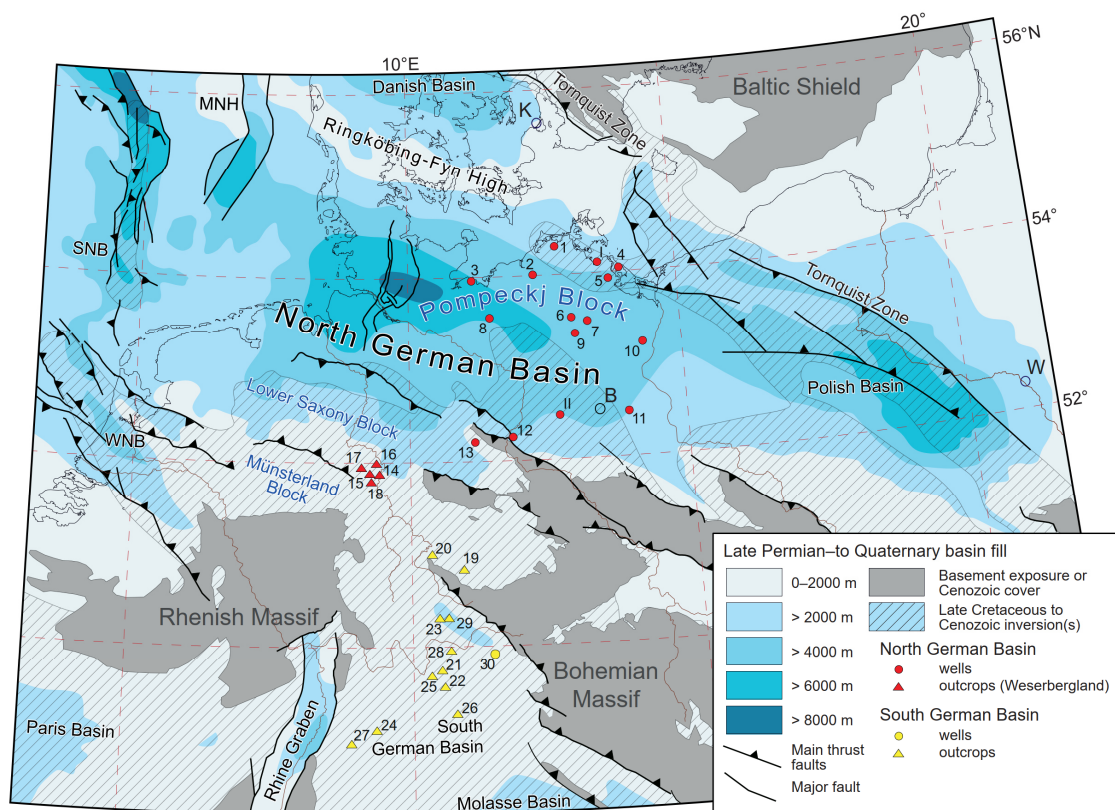


Fig. 3.1: Central European Basin System with subbasins, major fault systems and basement exposures, MNH – Mid North Sea High, SNB – South North Sea Basin, WNB – West Netherlands Basin; modified after Kley and Voigt (2008). Thickness of the Later Permian–Quaternary basin fill according to Ziegler (1990). North Germany: 1 – Kb Barth 6a/65, 2 – Kb Goritz 1/62, 3 – E Klütz 1/65, 4 – E Lütow 3/66, 5 – Kb Wolgast 1/1A/63, 6 – Kb Tarnow 1/65, 7 – Gt Neubrandenburg 2/85, 8 – Kb KSS 1/66, 9 – Kb Brustorf 1/62, 10 – Kb Gartz 1/65, 11 – Kb Strausberg 1/63, 12 – Kb Burg 2/61, 13 – Dp Morsleben 52a/95; localities referred to as in the text: I – Loissin 1/70, II – Ketzin storage site (several wells). Weserbergland: 14 – Birkenberg-Polle, 15 – Wiehenberg, 16 – Amelgatzen, 17 – Barntrop, 18 – Osterhagen. Thuringia: 19 – Drei Gleichen area (Arnstadt); 20 – Am Hohnert (Eisenach). South Germany: 21 – Abtswind, 22 – Eulenberg, 23 – Eyershausen, 24 – Heilbronn, 25 – Iphofen, 26 – Lichtenau, 27 – Maulbronn, 28 – Sand am Main, 29 – Trappstadt, 30 – Obersees 1.

## 3.2 Geological setting

### 3.2.1 The Central European Basin System

The Central European Basin System (CEBS) is a large epicontinental sag basin (cf. Bally and Snelson, 1980), which is composed of several subbasins, for example the North German Basin (Bachmann and Grosse, 1989; Ziegler, 1990; Gast et al., 1998). Following the Variscan Orogeny, the Central European Basin formed in the Late Carboniferous and has been active up to recent times. During the about 320 myr long basin history, a thick volcano-sedimentary basin fill accumulated with a depocentre in the western part of the North German Basin, where the sedimentary succession of the Upper Rotliegend–Quaternary partly exceeds a thickness of 8000 m (Fig. 3.1; Bachmann and Grosse 1989).

The long and complex basin history comprises phases of high subsidence alternating with phases of lowered subsidence and phases of uplift or exhumation (Nöldeke and Schwab, 1977; Schwab, 1985; Kley et al., 2008; Scheck-Wenderoth et al., 2008; Bachmann et al., 2010). Three main stages were recognized: (1) basin initiation from c. 320 Ma to 265 Ma, (2) basin fill from c. 265 Ma to 150 Ma, and (3) basin differentiation/inversion from c. 150 Ma to present (Nöldeke and Schwab, 1977; Schwab, 1985, Franz et al., 2018a).

The herein investigated Stuttgart Formation (Keuper Group, Upper Triassic) was deposited during the basin fill stage, in which W–E directed transtensional and extensional tectonic regimes contributed to continuous subsidence (e.g., Ziegler, 1982; Kley et al., 2008). In particular, the early phase of the basin fill stage was characterised by high subsidence rates resulting in the accumulation of 2500–4000 m thick Rotliegend–Buntsandstein deposits (Fig. 3.2). In Triassic and Jurassic times, subsidence successively diminished leading to low subsidence rates in the late phase of the basin fill stage. The change to basin differentiation and inversion was triggered by atlantic rifting and the collision of the African and European plates resulting in repeated uplift and exhumation of larger parts of the CEBS (e.g. Ziegler, 1990; Kley and Voigt, 2008). Consequently, the present-day burial depth of the Stuttgart Formation in the North German Basin result from continuous subsidence during the basin fill stage followed by subsequent uplift phases, in particular in Cretaceous–Tertiary times (Fig. 3.2; Jaritz, 1969, 1980; Stollhofen et al., 2008; Voigt et al., 2008; Bruns et al., 2013; Sośnicka and Lüders, 2020; Voigt et al., 2021). In the South German Basin, intense uplift during the basin differentiation/inversion stage resulted in exhumation of Triassic strata forming geographically wide-spread surface exposures (e.g. Voigt et al., 2010; Beyer, 2015; von Eynatten et al., 2021).

At individual localities in North Germany, the present-day burial depth of the Stuttgart Formation was further influenced by the mobilisation of Rotliegend and Zechstein salts, which started in the Early Triassic and attained maxima in Late Triassic–Middle Jurassic and Late Cretaceous–Tertiary intervals (Jaritz, 1974, 1987). Resulting salt structures differ strongly in the North German Basin. Large salt plugs with structural amplitudes of up to 8 km evolved in the western part (e.g. Trusheim, 1960; Jaritz, 1974; Baldschuhn et al., 2001), whereas low amplitude salt pillows predominate in the eastern part (e.g. Meinhold and Reinhardt, 1967; Kossow et al., 2000; Reinhold et al. 2008).

The recent geothermal gradients of the North German Basin are subject to pronounced regional variations corresponding to differences in the thickness and structure of the

basin fill. Resulting from heat flow values of 50–90 mW m<sup>-2</sup> (average 70 mW m<sup>-2</sup>; Lotz, 2004; Wolfgramm et al., 2014) average geothermal gradients vary from 33 K per km depth (Katzung, 2004) to 45–50 K per km depth (Hoth, 1997). Local geothermal gradients of up to 90 K per km depth are related to salt structures (Ziegenhardt et al., 1980; Hoth, 1997; Katzung, 2004).

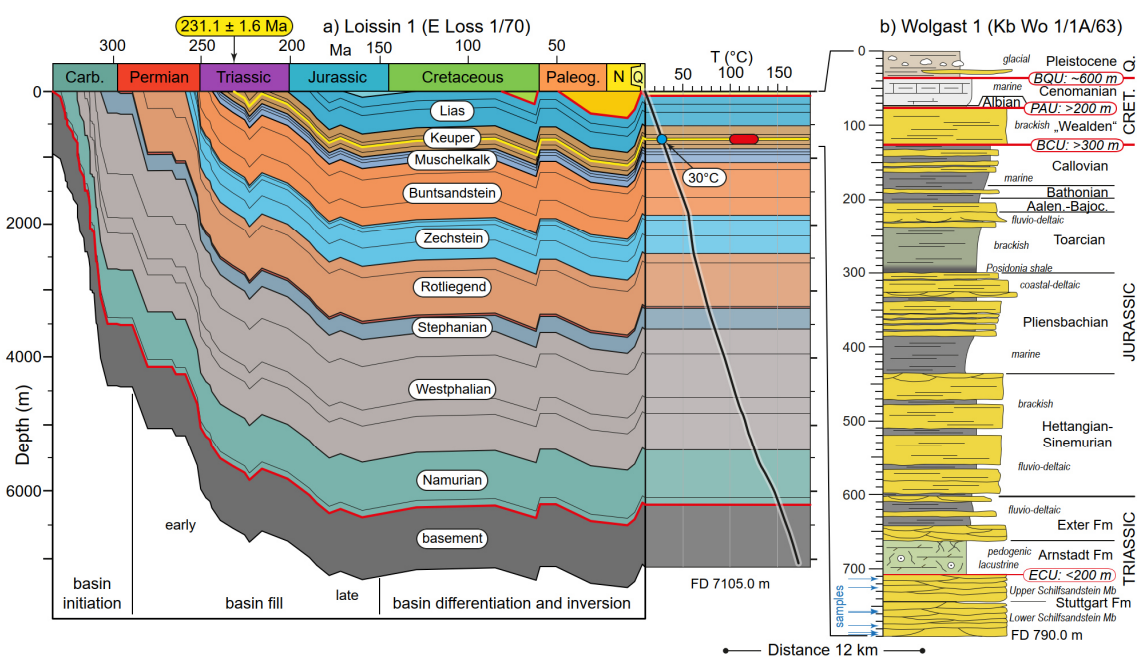


Fig. 3.2: Basin history and geothermal gradient of the eastern Pompeckj Block exemplified by the well Loissin 1 (a), modified from Friberg (2001), maximum depositional age of the Stuttgart Formation from Zeh et al. (2021). The burial history modelling of Friberg (2001) resulted in a maximum burial depth of Paleozoic–Mesozoic strata corresponding to present-day burial depths. However, the >75 °C offset between the 30 °C fluid temperature (blue dot) of the Stuttgart Formation at 650 m depth and the maximum burial temperature of 105–124 °C (red bar), estimated from temperature-dependent diagenetic processes, calls for a revised burial history. b) Post-depositional basin history of the Stuttgart Fm on the example of the well Wolgast 1/1A. The cored upper Triassic–Quaternary succession witnesses repeated phases of uplift and erosion, which have resulted in regional and basin-scale unconformities; ECU – Early Cimmerian Unconformity, BCU – Base-Cretaceous Unconformity, PAU – Pre-Albian Unconformity, BQU – Base-Quaternary Unconformity. For well locations see Fig. 3.1.

### 3.2.2 The Stuttgart Formation

The Stuttgart Formation, traditionally referred to as Schilfsandstein, is a prominent shaly–sandy interval in the otherwise shaly–evaporitic Middle Keuper Subgroup (e.g. Beutler in DSK, 2005). The Stuttgart Formation occurs wide-spread in the Central European Basin, but the thickness varies considerably from an average thickness of 60–70 m in North Germany (Fig. 3.2; Beutler, 1976; Beutler and Häusser 1982;) to 15–50 m in Thuringia (Dockter and Schubert, 2005) and 3–40 m in South Germany (Etzold and Schweizer, 2005; Freudenberger, 2005). The base of the Stuttgart Formation is defined at the base of the Neubrandenburg Member and the top at the base of the

Beaumont Member, the basal member of the Weser Formation (Fig. 3.3; e.g. Beutler in DSK 2005; Franz et al. 2014). The deposition of the Stuttgart Formation was controlled by pre-, intra- and post-Schilfsandstein transgressions resulting in the shaly to dolomitic Neubrandenburg, Gaildorf, and Beaumont Members (Franz et al., 2014). The Lower and Upper Schilfsandstein Members occur intercalated with these transgression horizons, representing the basinwards-directed progradation of fluvio-deltaic depositional environments (Fig. 3.3). Accordingly, both members are subject to substantial terrestrial–marine facies shifts from fluvio-deltaic sandstones to overbank, delta plain and prodelta shales. Sand-prone succession of fluvio-deltaic channel belts have a median porosity of 24.0 % and a median permeability of 517 mD according to Franz et al. (2018b). For detailed results on the Stuttgart Formation in North Germany, including facies maps, lithology examples and reservoir characterisation, the reader is referred to this contribution.

Bio-magnetostratigraphic correlations (Kozur and Bachmann, 2010; Zhang et al., 2020) and a new weighted average  $^{206}\text{U}/^{238}\text{Pb}$  age of  $231.1 \pm 1.6$  Ma (Zeh et al., 2021) constrain the Stuttgart Formation to an approximately 1 myr long interval (see also Miller et al., 2017) ranging from the Tuvlian 1 to Tuvlian 2 substage of the Late Carnian (Fig. 3.3). This short-time span, in combination with the basin-wide occurrence, makes the Stuttgart Formation an ideal example to study the impact of depositional regimes on diagenetic pathways of sandstone reservoirs.

### **3.3 Working areas, data base and methods**

To reconstruct the control of depositional regimes on the diagenesis of the Stuttgart Formation, sandstones deposited in terrestrial fluvial, fluvio-deltaic, and brackish-marine environments were investigated in a basin-scale study (Figs. 2.1 and 2.3). As a consequence of the complex history of the North German Basin, the present day burial depth of the Stuttgart Formation varies considerably from 200 m in the eastern part to more than 5,000 m in the western part (Baldschuhn et al., 2001; Feldrappe et al., 2008). In the axial part of the NGB, stretching from the German North Sea Sector to the North of Berlin, burial depths of the Stuttgart Formation range from 2,500 m in NE Germany to more than 5,000 m in NW Germany. Unfortunately, no core material was available from this part of the basin. The wells investigated herein are located to the North and South of the basin axis and available core material was recovered from depth of 200–1,550 m below surface. Accordingly, reservoir temperatures are in the range of 20–65 °C and fluid salinities are in the range of 25–280 g/l (TDS; Franz et

al., 2018b). The outcrops visited in southern parts of the CEBS are located in geographically wide-spread surface exposures of the Keuper Group, a result of uplift and exhumation during the basin differentiation and inversion stage.

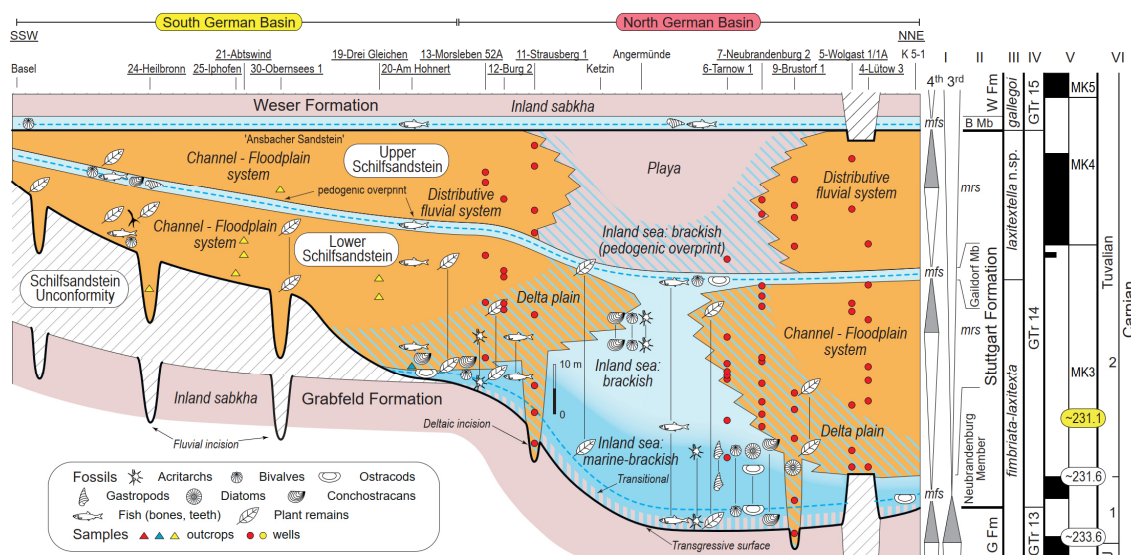


Fig. 3.3: Generalised N–S cross-section summarising large-scale architecture, depositional environments and stratigraphic control of the Stuttgart Formation, modified from Franz et al. (2018b) and Zeh et al. (2021). For position of wells and outcrops see Fig. 3.1; B Mb – Beaumont Member, G Fm – Grabfeld Formation, W Fm – Weser Formation, I – third- and fourth-order sequences, II – lithostratigraphy (Franz et al., 2014), III – conchostracan biostratigraphy (Kozur and Bachmann, 2010; Geyer and Kelber, 2018), IV – palynostratigraphy (Heunisch, 1999), V – magnetostratigraphy (reinterpreted from Zhang et al., 2020), VI – correlation with the Carnian stage and substages, yellow box: maximum depositional age of Zeh et al. (2021), white boxes: ages inferred from Zhang et al. (2020).

From available wells in Northeast Germany, 13 wells with complete core recovery of the fluvial, fluvio-deltaic and brackish-marine Stuttgart Formation were selected (Fig. 3.1). These cores were measured in detail, lithostratigraphically classified (see Beutler in DSK, 2005; Franz et al., 2014) and sampled for further investigations. The terrestrial fluvial Stuttgart Formation was visited and sampled in outcrops of the Weserbergland (5 localities), representing the southern margin of the NGB, and South Germany and Thuringia (12). Many of the herein investigated sites are classical Schilfsandstein localities described previously by Wurster (1964), Kruck and Wolf (1975), Bachmann and Wild (1976), Schröder (1977), Stets and Wurster (1977), Duchrow (1984), Visscher et al. (1994), Bachmann and Brunner (2002), Gehrman and Aigner (2002), Shukla and Bachmann (2007), Barnasch (2010), Franz et al. (2014, 2019), and others.

From the investigated wells and outcrops, a set of 120 samples was compiled from North Germany (102 samples), from Weserbergland (5), and from South Germany and

Thuringia (13). To investigate textural relationships between detrital and authigenic minerals, and to estimate the degree of compaction, 120 standard thin sections (~25 µm thickness, blue epoxy resin impregnated) were examined. Transmitted light microscopy was applied to qualify and quantify modal compositions and pore space by means of counting c. 300 points per thin section. To evaluate transport processes, sorting and roundness of detrital grains were determined using standard charts of Tucker (1985). The contact strength according to Füchtbauer (1988) and intergranular volumes (IGV) according to Houseknecht (1987) and Ehrenberg (1989) were calculated using (Formula 1) and (Formula 2), respectively.

$$\text{Contact strength} = \frac{(a + 2b + 3c + 4d)}{(a + b + c + d)} \quad (1)$$

Grain contact types: a – point, b – long, c – concav-convex, d – sutured

$$\text{Intergranular volume (IGV)} = \text{intergranular porosity} + \text{cement} \quad (2)$$

The results of microscopic analysis are presented in Tables 3.1–3.3 and in a supplementary file (Supplement).

To evaluate grain size dependency of the detrital composition, i.e. feldspar grains and lithics, grain-size analyses of 96 core samples from North Germany were re-evaluated. The 92 samples represent a subset of 255 samples for which Franz et al. (2018b) presented grain-size analyses. For sample preparation the reader is referred to this contribution; here we report the grain size classes (Phi and mm) according to Wentworth (1922) and statistical measures according to Folk and Ward (1957).

Scanning electron microscopy (SEM) and cathodoluminescence microscopy (CL) were applied to 28 thin sections of samples from North Germany to determine chemical compositions of detrital and authigenic minerals and evaluate cement and dissolution textures. For scanning electron microscopy, a SEM-EDX Zeiss-Evo MA 10 equipped with a tungsten filament and an EDAX element (resolution 3 nm at 30 kV) was used at the Geological Institute of the University of Greifswald. For cathodoluminescence microscopy, a high-power HC3-LM- Simon-Neuser CL microscope (Neuser et al., 1995) with a coupled Peltier-cooled Kappa PS 40C-285 camera system equipped with an Olympus BH-2 microscope was used at the Geoscience Centre of the University of Göttingen. The electron gun with an electron beam diameter of ca. 4 mm was operated at a voltage of 14 keV under high vacuum (10<sup>-4</sup> bar) with a filament current of 0.18 mA.

To control the results of microscopy, conventional X-ray diffraction (XRD) analysis was applied to 26 bulk rock samples from North Germany (16 samples), the Weserbergland (5) and South Germany (5). Sample preparation and measurements were carried out at the Geological Institute of the University of Leipzig using an X-ray diffractometer “Rigaku MiniFlex” (Co-K $\alpha$  radiation at 30 kV and 15 mA) in a step scan mode from 3° to 80° 2  $\theta$  (0.02° 2  $\theta$  steps, measuring time 2 s) without internal standard. Identification of mineral phases was performed using PANalytical X’Pert Highscore Software (Version 2.2a) and the ICDD database.

### 3.4 Results

Based on granulometry, detrital mineralogy, compaction of grain fabrics, and paragenetic sequences of authigenic minerals, four types of sandstone diagenesis could be identified. Considering the depositional environments described in Franz et al. (2018b), these types are referred to as: **1) Delta Channel**, **2) Delta Plain**, **3) Fluvial Channel**, and **4) Floodplain Diagenesis Types (DT)**. These diagenesis types were recognised in terrestrial–marine sandstones of the Lower Schilfsandstein Member; in terrestrial sandstones of the Upper Schilfsandstein Member only the Fluvial Channel and Floodplain Diagenesis Types are present (Tabs. 3.1 and 3.2; Fig. 3.4).

Table 3.1: Overview on the modal composition (point counting) of sandstones of the Lower Schilfsandstein Member; values are given as minimum–maximum (median); lithofacies associations according to Franz et al. (2018b); Lv - levee, Fl - floodplain, Ch-f - fluvial channel, Cr-f - fluvial crevasse splay, Ss - sheetsand, Ch-d - distributary (deltaic) channel, Cr-d - deltaic crevasse splay, WI - wetland, IB - interdistributary bay, D/Mb complex - distributary/mouthbar complex, x - accessorially present.

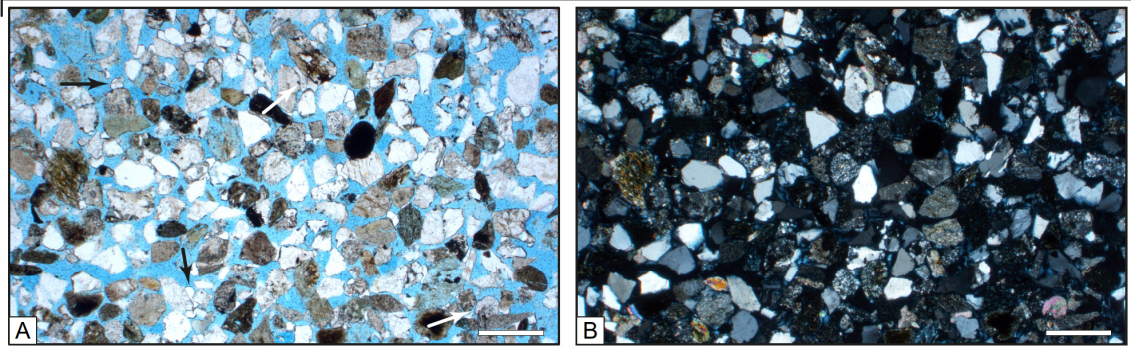
Lithofacies associations	Diagenesis types	Detritals						Authigenics						Compactional status					
		Feldspar	Quartz	Lithics	Matrix	Sum	Pyrite	Carbonate	Analcime	Sulphate	Fe-oxide/hydroxide	Quartz	Feldspar	Chlorite	Illite-Smectite	Kaolinite	Contact strength	Porosity	IGV
Fluvial plan	4 - Floodplain (n 3)	36.7-46.3 (38.9)	33.3-45.9 (42.6)	17.4-18.5 (18.4)	0-8.2 (<1)	16.7-33.0 (27.4)	--	--	0-1.4 (<1)	--	14.8-32.5 (25.0)	0-1.4 (<1)	--	--	x	--	1.6-2.4 (1.9)	9.1-26.8 (24.1)	35.6-47.8 (37.8)
	3 - Fluvial channel (n 21)	24.6-55.4 (42.5)	17.4-40.1 (28.9)	19.8-39.4 (31.3)	0-2.7 (<1)	<1-40.3 (8.6)	--	0-37.6 (1.3)	0-17.6 (<1)	0-3.0 (<1)	0-3.4 (1.9)	0-1.0 (<1)	0-1.5 (<1)	x	1.2-2.2 (1.7)	13.4-35.8 (26.3)	21.5-51.2 (34.6)		
	1 - Delta channel (n 27)	30.4-53.5 (40.5)	20.0-46.8 (32.3)	13.3-42.3 (26.1)	0-14.8 (<1)	6.7-34.7 (13.6)	x	0-16.5 (<1)	1-12.4 (5.9)	0-27.1 (<1)	0-11.0 (<1)	0-4.2 (<1)	0-7.2 (<1)	0-6.7 (<1)	x	1.3-2.2 (1.8)	0.5-36.5 (23.8)	24.9-42.9 (34.7)	
Delta plan	2 - Delta plain (n 13)	34.3-64.1 (42.6)	18.6-50.8 (34.4)	8.9-47.1 (20.0)	0-49.5 (19.2)	0-22.9 (13.2)	0-1.4 (<1)	x	0-16.8 (7.7)	0-3.9 (<1)	0-2.4 (<1)	0-4.3 (<1)	--	--	--	1.4-2.1 (1.7)	3.8-21.3 (14.5)	8.1-34.3 (29.1)	
	Lv	--	--	--	--	--	--	--	--	--	--	--	--	--	--	--	--	--	--
	WI	--	--	--	--	--	--	--	--	--	--	--	--	--	--	--	--	--	--
Delta front complex	not investigated	--	--	--	--	--	--	--	--	--	--	--	--	--	--	--	--	--	--
	D/Mb complex	--	--	--	--	--	--	--	--	--	--	--	--	--	--	--	--	--	--
Inland Sea	not investigated	--	--	--	--	--	--	--	--	--	--	--	--	--	--	--	--	--	--

Table 3.2: Overview on the modal composition (point counting) of sandstones of the Upper Schilfsandstein Member; values are given as minimum–maximum (median); lithofacies associations according to Franz et al. (2018b); TS - terminal splay, Fl-w - wet floodplain, Fl-d - dry floodplain.

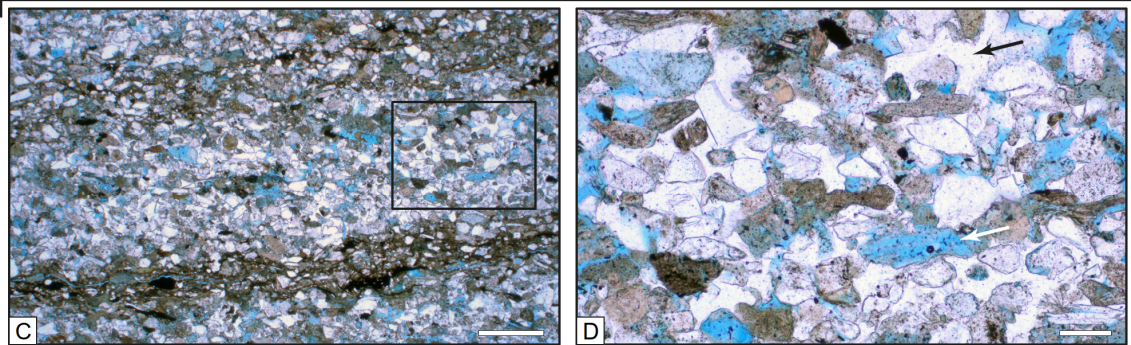
Lithofacies associations	Diagenesis types	Detritals						Authigenics						Compactional status					
		Feldspar	Quartz	Lithics	Matrix	Sum	Pyrite	Carbonate	Analcime	Sulphate	Fe-oxide/hydroxide	Quartz	Feldspar	Chlorite	Illite-Smectite	Kaolinite	Contact strength	Porosity	IGV
Distributive fluvial system	3 - Fluvial channel (n 22)	26.3-56.4 (42.1)	17.4-52.5 (34.1)	8.1-36.1 (22.0)	0-25.5 (<1)	2.9-29.1 (13.8)	x	0-18.5 (<1)	0-8.6 (1.9)	0-13.1 (<1)	0-12.9 (2.8)	0-1.9 (<1)	0-6.4 (<1)	0-2.4 (<1)	0-10.0 (1.2)	0-1.9 (<1)	1.2-2.3 (1.8)	8.2-40.0 (24.8)	26.6-39.4 (32.8)
	Ss (dis.)	28.6-58.3 (40.0)	25.0-58.8 (42.0)	3.9-32.8 (16.7)	0-71.9 (28.7)	0.3-25.6 (12.3)	--	0-10.9 (<1)	0-5.3 (<1)	0-4.3 (<1)	0-17.9 (6.1)	0-1.0 (<1)	0-2.4 (<1)	x	0-7.7 (<1)	x	1.3-2.2 (1.7)	0-28.0 (15.8)	2.9-39.1 (28.3)
	TS	--	--	--	--	--	--	--	--	--	--	--	--	--	--	--	--	--	--
Fl-w	not investigated	--	--	--	--	--	--	--	--	--	--	--	--	--	--	--	--	--	--
	Fl-d	--	--	--	--	--	--	--	--	--	--	--	--	--	--	--	--	--	--
Lv	not investigated	--	--	--	--	--	--	--	--	--	--	--	--	--	--	--	--	--	--



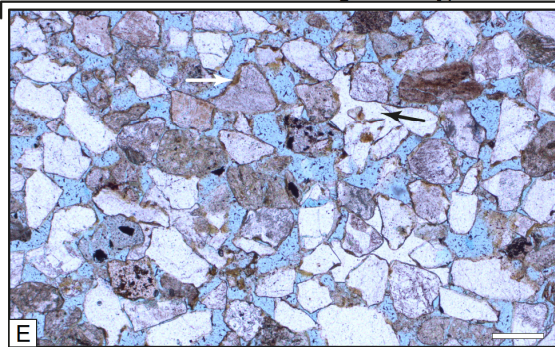
1 – Delta Channel Diagenesis Type



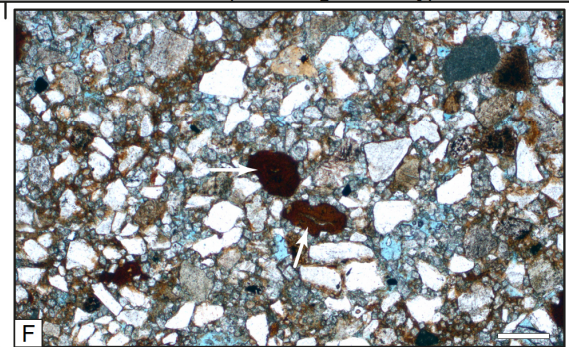
2 – Delta Plain Diagenesis Type



3 – Fluvial Channel Diagenesis Type



4 – Floodplain Diagenesis Type



low contact strength (1.2)

intermediate contact strength (2.4)

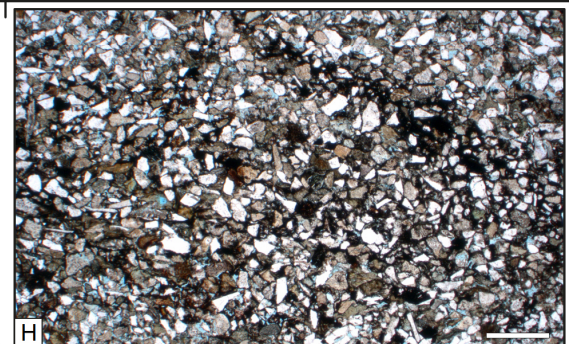
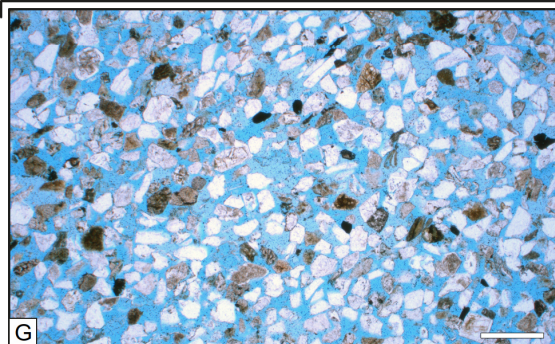


Fig. 3.4 (**facing page**): Thin section examples of the diagenesis types. **(A)** Fine-grained sandstone from a delta channel fill showing open pores space (stained blue) and only minor cementation with calcite (white arrows) and small analcime crystals (black arrows), Scale bar is 500  $\mu\text{m}$ , parallel nicols. Lower Schilfsandstein Mb, Brustorf 1 (sample 11-09). **(B)** As A, crossed nicols. **(C)** Laminated, matrix-rich, very fine-grained sandstone–siltstone from an interdistributary bay fill; inlet shows D. Scale bar is 500  $\mu\text{m}$ , parallel nicols. Lower Schilfsandstein Mb, Tarnow 1 (sample 11-30). **(D)** Inlet of C. White arrow shows dissolved detrital grains (intragranular pores), black arrow shows pore-filling analcime; scale bar is 100  $\mu\text{m}$ , parallel nicols. **(E)** Fine-grained sandstone from a fluvial channel fill with open pore space (stained light blue), small patches of poikilotopic analcime cement (black arrow) and tangential smectite-illite coatings (white arrow); note the low degree of roundness. Scale bar is 200  $\mu\text{m}$ , parallel nicols. Upper Schilfsandstein Mb, Strausberg 1 (sample 12-04). **(F)** Matrix-rich, very fine-grained sheetsand with small hematite nodules (white arrows); diagenetic recrystallisation of pedogenic carbonate resulted in neomorph fabric. Scale bar is 200  $\mu\text{m}$ , parallel nicols. Upper Schilfsandstein Mb, Strausberg 1 (sample 06-20). **(G)** High-porosity sandstone (40.0 %) of the Fluvial Channel DT. The under-compacted grain fabric (contact strength 1.2) and large intergranular porosity (IGV 36.2 %) result from eogenetic cementation, which effectively prevented burial mechanical compaction, and intense late-stage telogenetic dissolution processes. Scale bar is 500  $\mu\text{m}$ , parallel nicols. Upper Schilfsandstein Mb, Wolgast 1A well (sample 11-16). **(H)** Low-porosity sandstone (9.1 %) of the Floodplain DT. Abundant pedogenic Fe-oxide/hydroxide grain coats prevented eogenetic cementation and promoted burial mechanical compaction of the grain fabric (contact strength 2.4). Scale bar is 500  $\mu\text{m}$ , parallel nicols. Lower Schilfsandstein Mb, KSS 1 (sample 12-07).

---

### 3.4.1 Granulometry

The sandstones of the Stuttgart Formation (cores, North Germany) are characterised by low textural maturity resulting from poor to moderate sorting and low degree of roundness. Accordingly, detrital assemblages are dominated by very angular to subangular grains, subrounded to rounded grains are less frequent (Fig. 3.4).

#### 3.4.1.1 Lower Schilfsandstein Member

The grain sizes of sandstones of the Delta Channel Diagenesis Type (27 grain size analyses) range from 2.1 to 3.8 Phi (0.23–0.07 mm) with a median of 3.2 Phi (0.11 mm). According to Wentworth (1922), the sandstones are classified fine sand (2–3 Phi) and very fine sand (3–4 Phi). Sandstones of distributary channels and crevasse splays are good to moderately sorted (0.49 to 0.92 Phi, median 0.71 Phi) and near symmetrical to strongly fine skewed (-0.08 to 0.47, median 0.31), indicating a predominance of bedload processes.

Sandstones, siltstones and heterolithes of the Delta Plain Diagenesis Type (11 analyses) have a grain size range of 2.8–4.2 Phi (0.14–0.05 mm) with a median of 3.7 Phi (0.08 mm) representing very fine sand and coarse silt (4–5 Phi). The fine-grained deposits of levees, distal crevasse splays, wetlands and interdistributary bays are moderately to moderately good sorted (0.5 to 0.71 Phi, median 0.66 Phi) and coarse to strongly fine skewed (-0.18 to 0.54, median 0.1), indicating a mix of bedload and suspension load processes.

Sandstones of the Fluvial Channel Diagenesis Type (22 analyses) have a grain size range from 2.2 to 3.6 Phi (0.22–0.08 mm) with a median of 2.9 Phi (0.13 mm) and are classified fine sand and very fine sand according to Wentworth (1922). The sandstones are poorly to moderately good sorted (0.52 to 1.01 Phi, median 0.69 Phi) and near symmetrical to strongly fine skewed (0.09 to 0.54, median 0.34), indicating a predominance of bedload processes.

Only one grain size analysis of a sandstone of the Floodplain Diagenesis Type is available in the data set. This sample represents a sheetsand with a grain size of 3.6 Phi (0.08 mm), moderately good sorting (0.66), and fine skewed (0.1) grain size distribution (Fig. 3.5; Supplement).

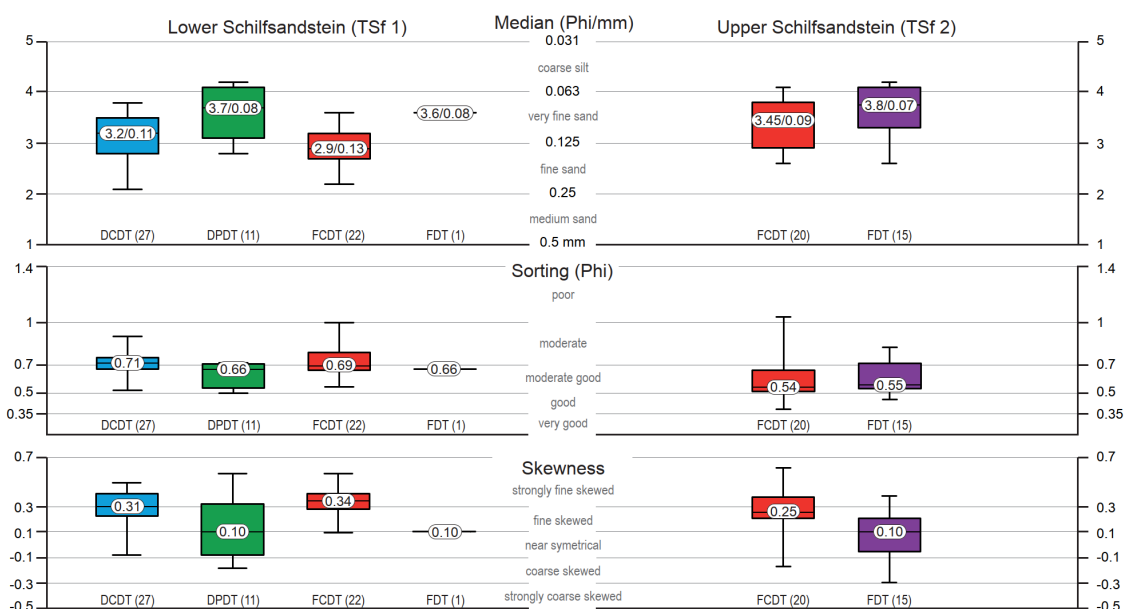


Fig. 3.5: Granulometric values for sandstones of fluvial and deltaic facies associations investigated herein. The 96 samples represent a subset of 255 samples investigated by Franz et al. (2018a). Grain size classes (Phi and mm) according to Wentworth (1922), median (Phi and mm), sorting (Phi) and skewness according to Folk and Ward (1957).

#### 3.4.1.2 Upper Schilfsandstein Member

The grain sizes of sandstones of the Fluvial Channel Diagenesis Type (20 analyses) range from 2.6 to 4.1 Phi (0.16–0.06 mm) with a median of 3.45 Phi (0.09 mm) and are classified fine sand (2–3 Phi), very fine sand (3–4 Phi) and coarse silt (4–5 Phi) according to Wentworth (1922). Sandstones and siltstones of fluvial channel fills and levee/crevasse splay complexes are poorly to moderately sorted (0.38 to 1.04 Phi, median 0.54 Phi) and coarse to strongly fine skewed (-0.16–0.58, median 0.25), indicating a predominance of bedload processes.

The shaly sandstones and siltstones of the Floodplain Diagenesis Type (15 analyses) have a grain-size range of 2.6–4.2 Phi (0.16–0.05 mm) with a median of 3.8 Phi (0.07 mm) and are classified fine sand, very fine sand and coarse silt. The predominantly fine-grained deposits of sheetsands, terminal splays, and wet and dry floodplains are moderately to good sorted (0.45 to 0.82 Phi, median 0.55 Phi) and coarse to strongly fine skewed (-0.29 to 0.39, median 0.1), indicating frequent changes of bedload and suspension load processes (Fig. 3.5; Supplement).

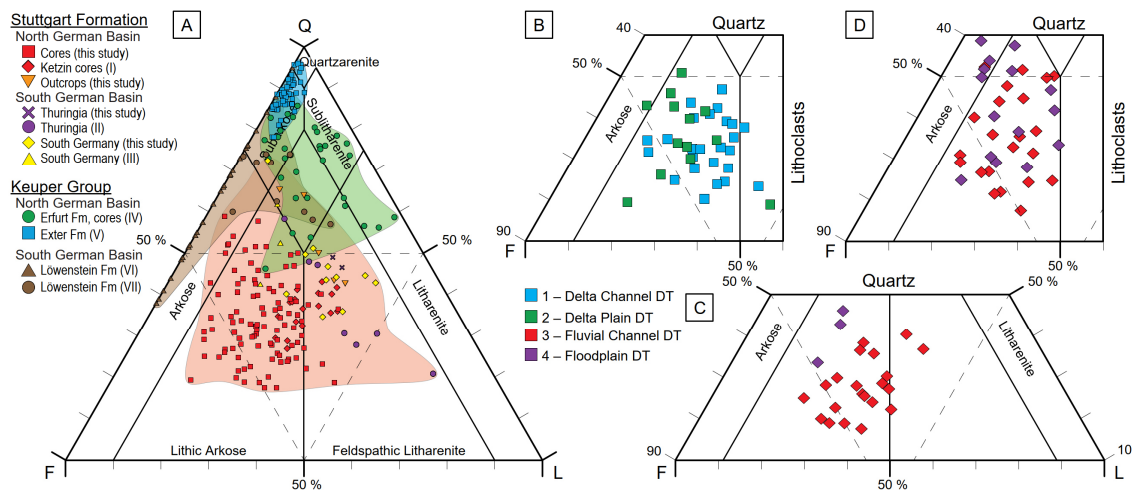


Fig. 3.6: Detrital mineralogy of the Stuttgart Formation. **(A)** Ternary plot (McBride, 1963) showing the 120 samples investigated in this study compared to previously published data of Keuper Group sandstones. In comparison to other sandstones of the Keuper Group, the compositional maturity of the Schilfsandstein is exceptional low. Q – mono- and polycrystalline quartz and chert, F – feldspar, L – lithics; I – Förster et al. (2010), II – Dockter et al. (1967), III – Helling (1965), IV – Häusser (1972), V – Franz and Barnasch (2021), VI – Helling (1963), VII – Kulke (1969); modified from Franz and Barnasch (2021). **(B–D)** Sandstones from North German cores identified to diagenesis types for the Lower Schilfsandstein Mb. (B and C) and Upper Schilfsandstein Mb. (D).

### 3.4.2 Detrital mineralogy

#### 3.4.2.1 Schilfsandstein cores

##### 3.4.2.1.1 Detrital grains (bedload)

The sandstones of the Stuttgart Formation are of low compositional maturity. Normalised to detrital feldspar, quartz and lithoclasts, the investigated sandstones are composed of 24.6–64.1 % feldspar (median 41.1 %), 17.4–58.8 % quartz (median 32.8 %) and 3.9–47.1 % lithoclasts (median 24.0 %) (Table 3.3). According to McBride (1963), the sandstones are classified lithic arkose, arkose and feldspathic litharenites (Fig. 3.6).

On detail, the abundances of detrital feldspar, quartz and lithoclasts are grain-size dependent. The abundance of lithoclasts ranges from 31.3 % (median) for sandstones of the Fluvial Channel Diagenesis Type (median grain size 2.9 Phi, 0.13 mm) to 16.7 % (median) for sandstone-siltstones and heterolithes of the Floodplain Diagenesis Type (median grain size 3.8 Phi, 0.07 mm). The lower quantity of lithics in sandstones of the Delta Plain and Floodplain Diagenesis Types is mainly balanced by higher quantity of quartz and feldspar grains (Tabs. 3.1 and 3.2; Fig. 3.6).

The feldspar assemblage is represented by K-feldspars orthoclase/microcline and sanidine and the plagioclases albite, oligoclase and andesine as indicated by CL and SEM-EDX microscopy and XRD analyses (Fig. 3.7). Optical microscopy suggests a dominance of K-feldspar outweighing plagioclase (Supplement). The appearance of detrital feldspar grains varies from apparently unaltered to strongly altered, illitised or completely dissolved (Fig. 3.8). Unaltered and optically clear feldspar grains are more abundant in sandstones of the Delta Channel and Fluvial Channel Diagenesis Types.

The quartz assemblage is dominantly composed of monocrystalline quartz, followed by polycrystalline quartz followed by chert. Monocrystalline quartz grains showing blue and red luminescence under CL microscope are considered of magmatic origin, whereas polycrystalline quartz grains showing brown luminescence are considered of metamorphic origin. In XRD analysis of bulk rock samples, quartz was identified by the main peak at  $\sim 26.6^\circ$  2 Theta (Fig. 3.7).

The lithoclast assemblage is dominated by fragments of metamorphic rocks (19.0–71.4 %, median 48.5 %) and magmatic rocks (20.0–76.2 %, median 46.4 %) outweighing sedimentary rock fragments (0–20.9 %, median 5.1 %). The average ratio of metamorphic and magmatic rock fragments ( $L_{\text{meta}}:L_{\text{mag}}$ ) is 1.2 (all samples). By means of transmitted light microscopy, phyllites, slates, schists, gneisses and quartzites could be identified based on structural characteristics, such as foliation. The assemblage of magmatic lithics is dominated by fragments of felsic volcanic rocks followed by mafic volcanic rocks followed by plutonic rocks (Supplement). Volcanic rock fragments have typical porphyritic, intersertal or pilotaxitic fabrics of phenocrysts floating in fine-grained greenish to dark groundmass. Feldspar laths in glassy volcanic lithoclasts have a Na-rich composition (Ca/Na ratio 0.19). Plutonic rock fragments are mainly represented by granites; but prominent microperthitic, micrographic and myrmekitic textures were only rarely observed. Sedimentary rock fragments are mainly represented by shales and less abundant by mudclasts, sandstone lithoclasts, and carbonate lithoclast. Based on the optical appearance in thin sections, diagenetic alteration of lithoclasts was less intense in sandstones of the Fluvial Channel

Diagenesis Type but more intense in sandstones of the Delta Channel and Delta Plain Diagenesis Types.

Accessory detritals are muscovite, biotite, glauconite, chlorite, heavy mineral grains (e.g. rutile, zircon, ilmenite) and plant remains. Mica flakes, partially bent or ruptured, are often chloritised representing diagenetic overprint.

Residual volcanic detritus and diagenetic alteration products of tephra are special components of the Schilfsandstein. The accessory occurrences of embayed angular quartz grains, idiomorphic K-feldspar grains, and idiomorphic zircon grains are related to syn-sedimentary tephra fall out followed by reworking and dispersal within an active river system (Zeh et al., 2021). Reworking of tephra beds resulted in formation of rip-up clasts, which are sporadically preserved. As a consequence of diagenetic degradation, these clasts were altered and partially to completely transformed to analcime (Fig. 3.9). But in most cases, the ubiquitous presence of analcime points to reworking and dispersal of unconsolidated tephra followed by the multistage transformation of labile volcanic detritus during burial diagenesis (see chapter 3.4.4).

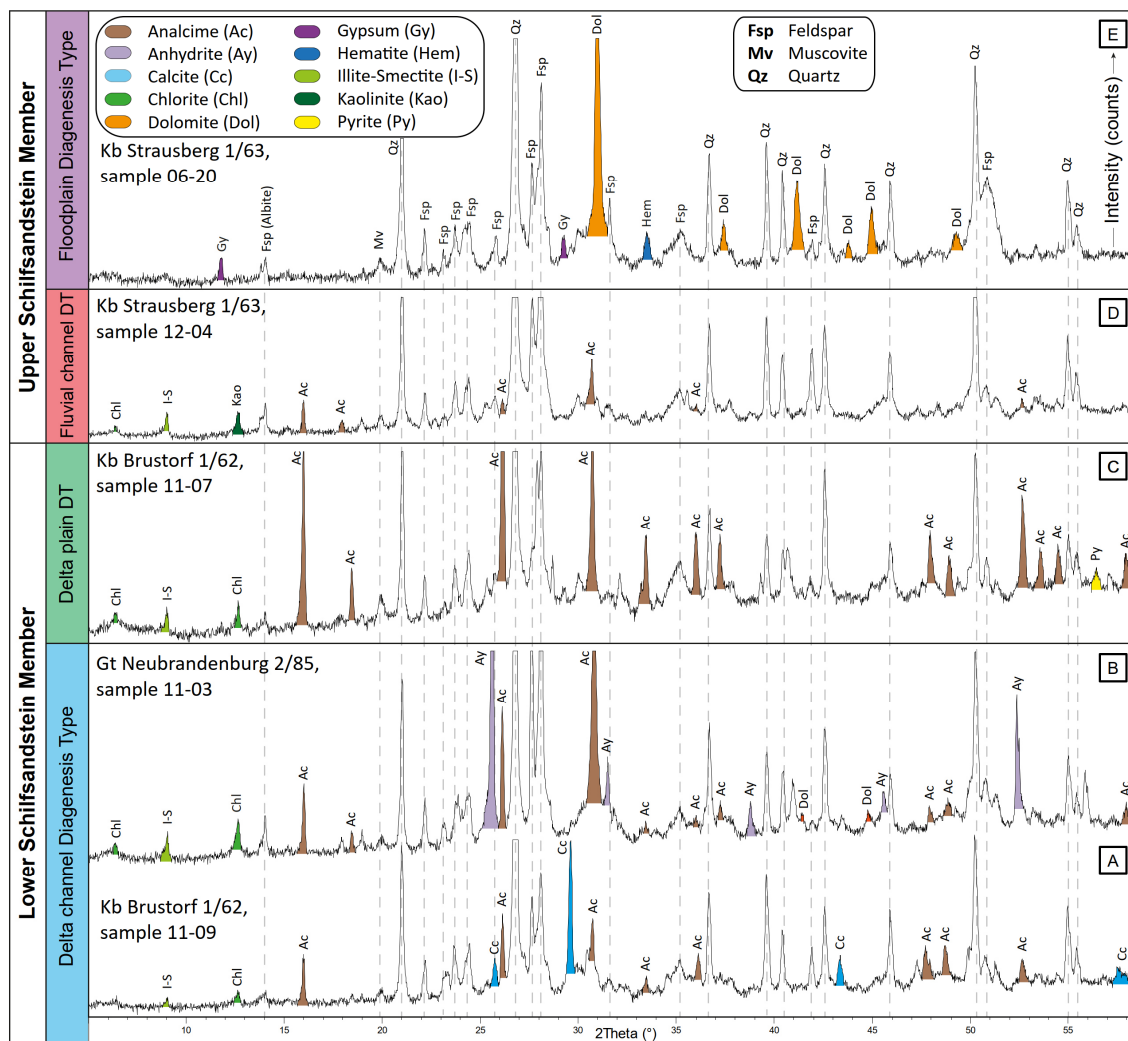


Fig. 3.7: X-ray diffraction pattern of the four diagenesis types (bulk rock samples), typical authigenic minerals are highlighted; peaks with flattened tips were cut off.

#### 3.4.2.1.2 Matrix (Suspension load)

Matrix is represented by clayey to silty and/or mixed carbonate-clastic sediment; occasionally disassembled and altered mud clasts appear as pseudomatrix. Based on point counting of thin sections, the volumetric abundance of matrix is subject to strong variations among the diagenesis types. According to grain size analyses, the bedload dominated sandstones of the Fluvial Channel and Delta Channel Diagenesis Types are characterised by low matrix volumes of <1 % (median). Higher matrix volumes of up to 29.7 % (median) of sandstone-siltstones and heterolithes of the Delta Plain and Floodplain Diagenesis Types result from increasing suspension load processes at deltaic and fluvial overbank environments (Fig. 3.4; Franz et al., 2018b). As shown by XRD analyses, the mainly greenish matrix of deltaic sandstones as well as the reddish matrix of fluvial sandstones are composed of illite-smectite mixed-layer clays identified

by the typical  $\sim 8.9^\circ$   $2\theta$  peak (Fig. 3.7). A diagenetic impregnation of clayey matrix with carbonate cement was observed within siltstone–sandstones of the Delta Plain and Floodplain diagenesis types (Fig. 3.8).

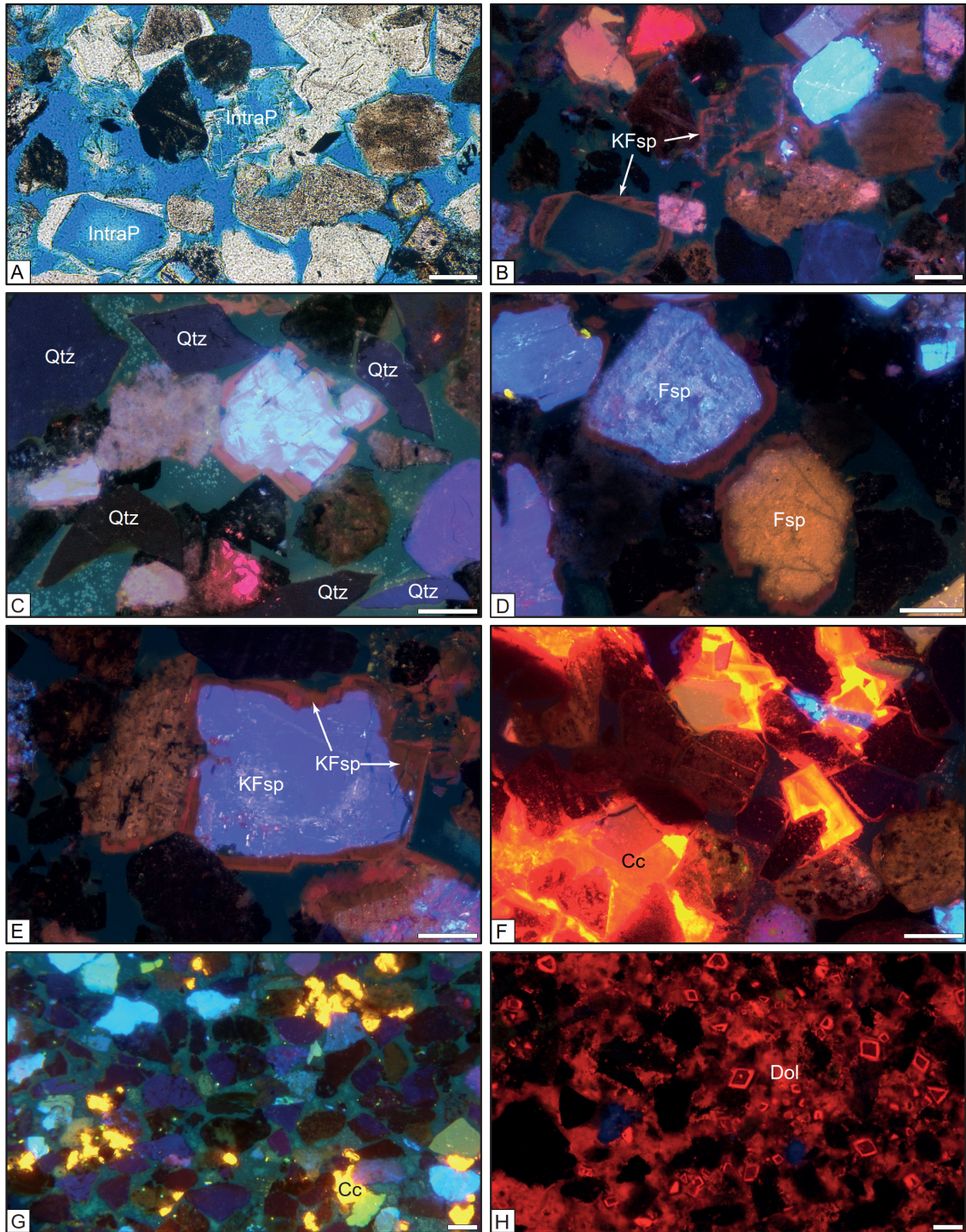
#### 3.4.2.2 Schilfsandstein outcrops

In terms of modal composition, sandstones from southern and northern parts of the basin differ notably (see Table 3.3). According to the higher abundance of quartz and lithoclasts, these sandstones mainly represent feldspathic litharenites and lithic subarkoses (Fig. 3.6). The quartz assemblage is dominated by monocrystalline quartz, followed by polycrystalline quartz followed by chert (Supplement). The assemblage of lithics is dominated by metamorphic rock fragments, followed by magmatic rock fragments and sedimentary rock fragments. The average ratio of metamorphic and magmatic rock fragments ( $L_{\text{meta}}:L_{\text{mag}}$ ) is 1.7 (all samples). The feldspar assemblage is dominated by K-feldspar outweighing plagioclase. The abundance of matrix varies from <1 to 5.7 %.

---

Fig. 3.8 (*facing page*): Cathodoluminescence microscopy examples of detrital and authigenic mineralogy. **(A)** Low contact strength and large open pore space (stained blue), Fluvial Channel DT. Note, abundant authigenic overgrowth and differential dissolution of feldspar grains resulting in intragranular porosity (IntraP); scale is 100  $\mu\text{m}$ , Wolgast 1A (sample 11-03), parallel nicols. **(B)** CL image of (A) with K-feldspar overgrowth showing dull reddish luminescence; scale is 100  $\mu\text{m}$ . **(C)** First cycle sand grains with very angular detrital quartz grains showing dark blue luminescence and angular feldspar grains showing light blue luminescence, Fluvial Channel DT; scale is 100  $\mu\text{m}$ , Wolgast 1A (sample 11-11). **(D)** Second cycle sand grains with subrounded to rounded feldspar grains showing blueish and brownish luminescence; scale is 100  $\mu\text{m}$ , Wolgast 1A (sample 11-11). **(E)** Large detrital K-feldspar grain (KFsp) showing blue luminescence and K-feldspar overgrowth showing dull reddish luminescence, Fluvial Channel DT; scale is 100  $\mu\text{m}$ , Wolgast 1A (sample 11-08). **(F)** Altered feldspar grains showing dull reddish luminescence and pore-filling authigenic calcite (Cc) showing bright to dark orange luminescence, Fluvial Channel DT; scale is 100  $\mu\text{m}$ , Strausberg 1 (sample 12-07). **(G)** Detrital K-feldspar (blue luminescence), plagioclase (yellowish green, pink to purple), altered feldspar and lithoclasts (brown), quartz (non-luminescent) and residual authigenic calcite (Cc, bright orange luminescence), Delta Channel DT; scale is 250  $\mu\text{m}$ , Brustorf 1 (sample 11-09). **(H)** Detrital matrix with authigenic dolomite (dark red luminescence) and idiomorphic dolomite rhombs showing growth bands, Floodplain DT; scale is 500  $\mu\text{m}$ , Tarnow 1 (sample 11-33).





### 3.4.3 Compaction, intergranular volume and porosity

#### 3.4.3.1 Schilfsandstein cores

##### 3.4.3.1.1 Compaction and contact strength

The mechanical compaction of the investigated sandstones is remarkably low. The grain fabrics are dominated by point contacts, whereas long-contacts and convex-concave contacts are present in low abundance (Fig. 3.4). Nevertheless, bending and breakage of mica, and rare occurrences of brittle deformation of detrital grains and the formation of pseudomatrix by ductile deformation of clayey lithoclasts attest mechanical compaction. Chemical compaction was of subordinated importance as sutured contacts and stylolites were only rarely observed.

The qualitative and quantitative analyses of grain contacts resulted in values of contact strength (Füchtbauer 1988) ranging from 1.2 to 2.4 (median 1.8) for all samples (Table 3.3). Despite considerable variations between individual samples, the median values of contact strengths show no systematic variation between the diagenesis types (Tabs. 3.1 and 3.2).

##### 3.4.3.1.2 Intergranular volume

Intergranular volumes calculated according to Houseknecht (1987) and Ehrenberg (1989) range from 2.9 to 51.2 % (median 32.4 %) for all samples (Table 3.3). For the Lower Schilfsandstein Member, high intergranular volumes were noted for the Floodplain Diagenesis Type (median 37.8 %), Delta Channel Diagenesis Type (median 34.7 %) and Fluvial Channel Diagenesis Type (median 34.6 %). Remarkable are sandstones with high intergranular volumes of more than 40 % corresponding to assumed initial porosities (Atkins and McBride, 1992). Slightly lowered intergranular volumes of 29.1 % (median) were noted for the Delta Plain Diagenesis Type (Table 3.1). Comparable values were recorded for the Upper Schilfsandstein Member with median intergranular volumes of 32.8 % for the Fluvial Channel Diagenesis Type and 28.3 % for the Floodplain Diagenesis Type (Table 3.2).

The high intergranular volumes and low contact strength of sandstones of the Fluvial Channel and Delta Channel Diagenesis Types indicate a cementation-controlled diagenesis during which early cementation supported the grain fabric and prevented significant mechanical compaction (Figs. 3.10 and 3.11). Calculated after Ehrenberg (1989), 1–96 % of the original porosity of these sandstones was destroyed

by cementation but only 0–65 % by mechanical compaction (Fig. 3.11). The medium intergranular volumes of sandstone-siltstones of the Delta plain and Floodplain diagenesis types indicate a rather mechanical compaction-controlled diagenesis during which 3–94 % of the original porosity was destroyed by mechanical compaction but only 0.5–62 % by cementation.

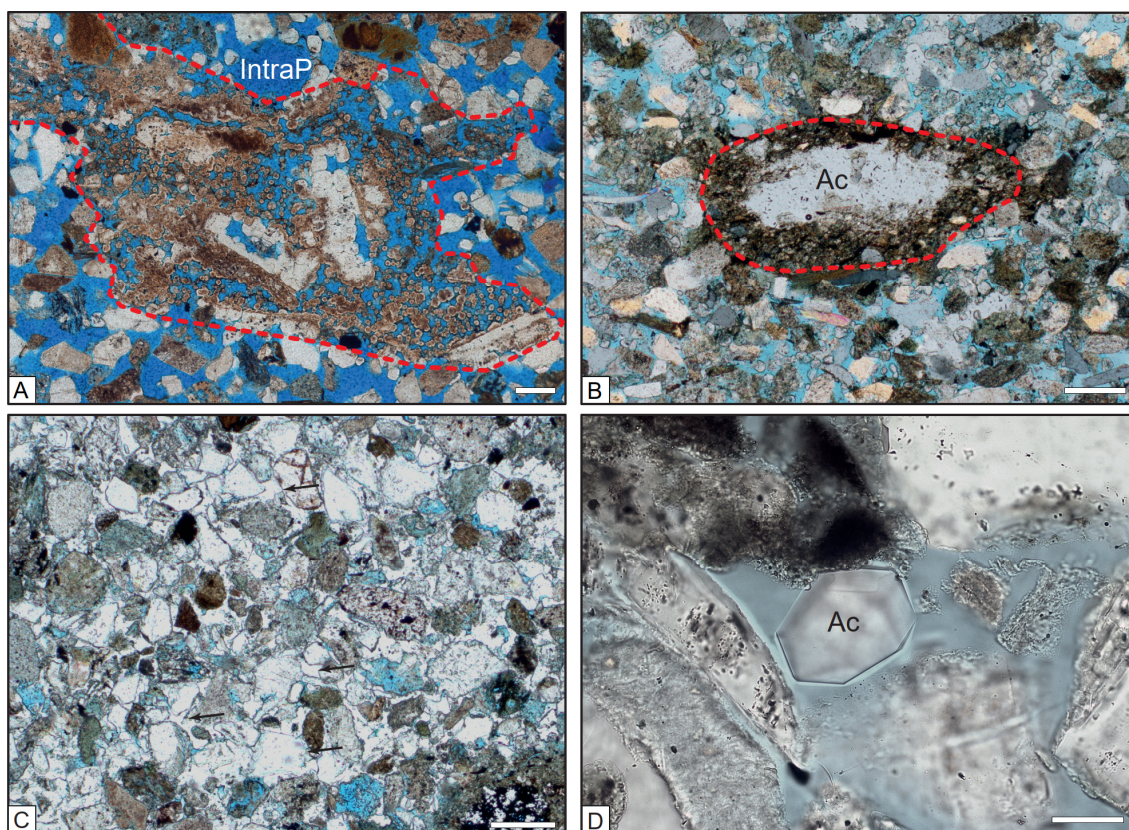


Fig. 3.9: Diagenetic degradation of volcanic detritus. **(A)** Larger tephra clast completely replaced by idiomorphic analcime crystals. The dashed line refers to the approximate outline of the former clast, Delta Channel DT. Late-stage dissolution contributed to inter- and intragranular porosity (IntraP, epoxy resin stained blue); scale bar is 200 µm. Brustorf 1A (sample 11-09), parallel nicols. **(B)** Residual tephra clast (dashed line) partly replaced by blocky analcime (Ac), Delta Plain DT; scale bar is 200 µm. Tarnow 1 (sample 11-26), circular polarisation. **(C)** Intense pore-filling analcime cementation (arrows), probably resulting from degradation of dispersed volcanic detritus, Delta Plain DT. The late-stage dissolution of detrital grains resulted in intragranular porosity (epoxy resin stained blue); scale bar is 200 µm. Brustorf 1A (sample 11-07), parallel nicols. **(D)** Idiomorphic analcime crystal typical for Delta Channel and Fluvial Channel DT's; scale bar is 50 µm. Strausberg 1 (sample 12-01), parallel nicols.

#### 3.4.3.1.3 Porosity

Considering all samples, the total porosity of 0–40.0 % (median 22.9 %) is mainly formed of intergranular pores (median 86.2 %), whereas intragranular pores (median 8.9 %) and oversized pores (median 3.6 %) are less abundant. High values of total porosity, partially exceeding 30 % in individual, are typical for sandstones of the Delta Channel and Fluvial Channel Diagenesis Types of the Lower and Upper

Schilfsandstein Members. Systematically lowered values of total porosity were noted for sandstones and sandstone-siltstones of the Delta Plain and Floodplain Diagenesis Types (Tabs. 3.1 and 3.2).

As shown by thin section microscopy, large volumes of total porosity are related to intense dissolution processes during mesogenetic and telogenetic stages (see chapter 3.4.4). Accordingly, intergranular pores result from complete dissolution of authigenic cementation and intragranular pores are the result of corrosion and dissolution of detrital feldspar grains and volcanic rock fragments. The formation of oversized pores, most abundant in sandstones of the Fluvial Channel Diagenesis Type, seems to be either attributed to dissolution of oversized clasts, probably reworked tephra, or dissolution of detrital grains and neighbouring authigenic cementation.

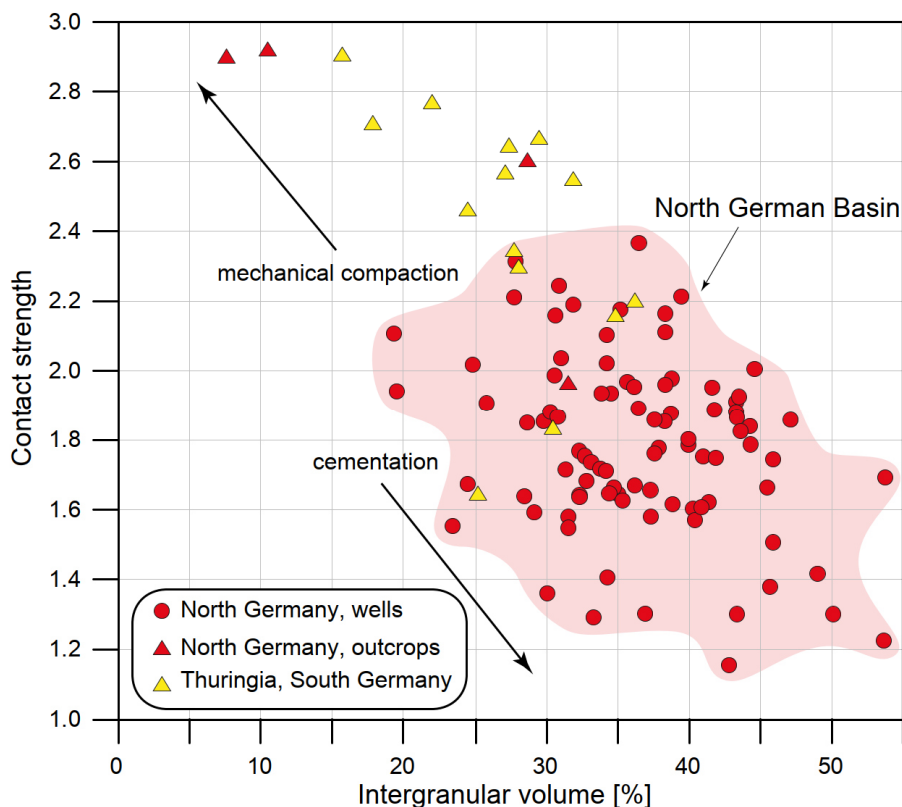


Fig. 3.10: Contrasting cementation- vs. mechanical compaction-controlled sandstone diagenesis resulted in noticeable differences of contact strength (Füchtbauer, 1988) and intergranular volume (Houseknecht, 1987; Ehrenberg, 1989).

### 3.4.3.2 Schilfsandstein outcrops

#### 3.4.3.2.1 Compaction and contact strength

The grain fabric of sandstones is dominated by long-contacts followed by convex-concave contacts. Point contacts and sutured contacts occur less frequently. With a contact strength (Füchtbauer 1988) ranging from 1.7 to 2.9 (median 2.6), the mechanical compaction is remarkably higher compared to sandstones from North Germany (Fig. 3.10, Table 3.3).

Table 3.3: Summarised petrographic data of the Schilfsandstein; values are given as minimum–maximum (median). Note the higher values of contact strength and associated lower values of intergranular pore volume (IGV) and porosity for samples from South Germany, Thuringia and Weserbergland compared to samples from North Germany.

Locality	Detritals				Authigenics	Compactional status		
	Feldspar	Quartz	Lithics	Matrix	all Authigenics	Contact strength	Porosity	IGV
North Germany	24.6–64.1 (41.1)	17.4–58.8 (32.8)	3.9–47.1 (24.0)	0–71.9 (1.0)	0–40.3 (13.1)	1.2–2.4 (1.8)	0–40.0 (22.9)	2.9–51.2 (32.4)
Weserbergland	18.0–22.4 (21.9)	42.7–65.3 (50.0)	12.2–37.3 (28.1)	0.5–23.6 (2.8)	6.2–26.3 (10.7)	2.0–2.9 (2.8)	1.4–20.9 (2.9)	6.6–28.6 (22.6)
Thuringia	18.8–19.5 (19.1)	56.5–49.0 (47.8)	31.5–34.7 (33.1)	0–2.4 (1.2)	10.0–27.1 (18.6)	2.6–2.8 (2.7)	0–12.0 (6.0)	22.0–27.1 (24.6)
South Germany	13.5–33.6 (22.5)	34.6–72.4 (44.2)	6.2–43.6 (32.9)	0–5.7 (1.0)	3.8–24.9 (13.0)	1.7–2.7 (2.4)	2.9–24.3 (14.8)	17.8–32.9 (26.8)

#### 3.4.3.2.2 Intergranular volume

The intergranular volume (Houseknecht, 1987; Ehrenberg, 1989) ranges from 6.6 to 32.9 % (Table 3.3). Considering that these samples mainly represent the Fluvial Channel Diagenesis Type, the intergranular volumes are considerably reduced compared to sandstones of the same diagenesis type from North Germany (see chapter 3.4.3.1). The high to medium contact strength and low to medium intergranular volumes point to a rather mechanical compaction-controlled diagenesis (Fig. 3.10). Calculated after Ehrenberg (1989), 26–88 % of the initial porosity was lost due to mechanical compaction but only 11–57 % of the initial porosity was lost due to cementation (Fig. 3.11).

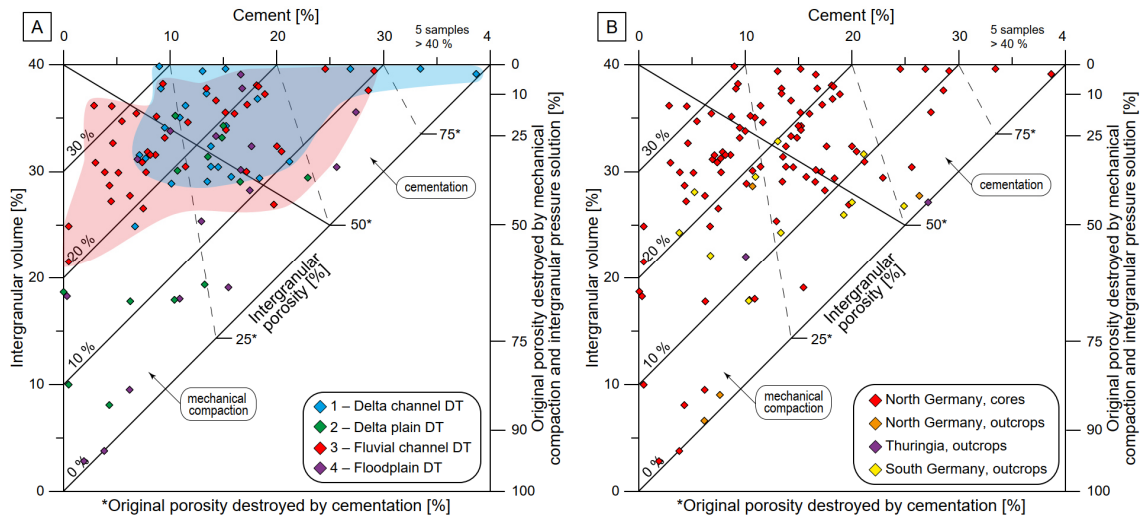


Fig. 3.11: Intergranular and cement volumes (Houseknecht, 1987; Ehrenberg, 1989). (A) Intergranular and cement volumes of samples from the North German Basin (Pompeckj Block) related to the four diagenesis types. (B) Intergranular and cement volumes of all samples.

### 3.4.3.2.3 Porosity

The total porosity of all samples ranges from 0 to 22.9 %. Intergranular pores account for 79.5 % (median of all samples) of the total porosity followed by intragranular pores with 15.6 % (median) and oversized pores with <1 % (median). Despite considerable variations, the median porosity values ranging from 2.9 % (Weserbergland) to 14.8 % (South Germany) are generally reduced compared to North Germany (Table 3.3).

## 3.4.4 Authigenic mineralogy

### 3.4.4.1 Schilfsandstein cores

The four diagenesis types of the Schilfsandstein are characterised by typical paragenetic sequences of authigenic minerals. The abundance of authigenic minerals derived from modal analyses varies from 0 to 40.3 % (median 13.1 %) for all investigated samples. Accordingly, the abundance of authigenics ranges from 8.6 % (median) for the Fluvial Channel Diagenesis Type to 27.4 % (median) for the Floodplain Diagenesis Type (Lower Schilfsandstein Mb; Table 3.1).

#### 1) Delta Channel Diagenesis Type

The paragenetic sequence typically includes pyrite, carbonate, feldspar, quartz, analcime and chlorite, which were subsequently formed in eo- to mesogenetic

regimes (Fig. 3.12). Modal analyses revealed an abundance of authigenic minerals of 13.6 % (median) and a porosity of 23.8 % (median), resulting from late-stage dissolution processes (Table 3.1).

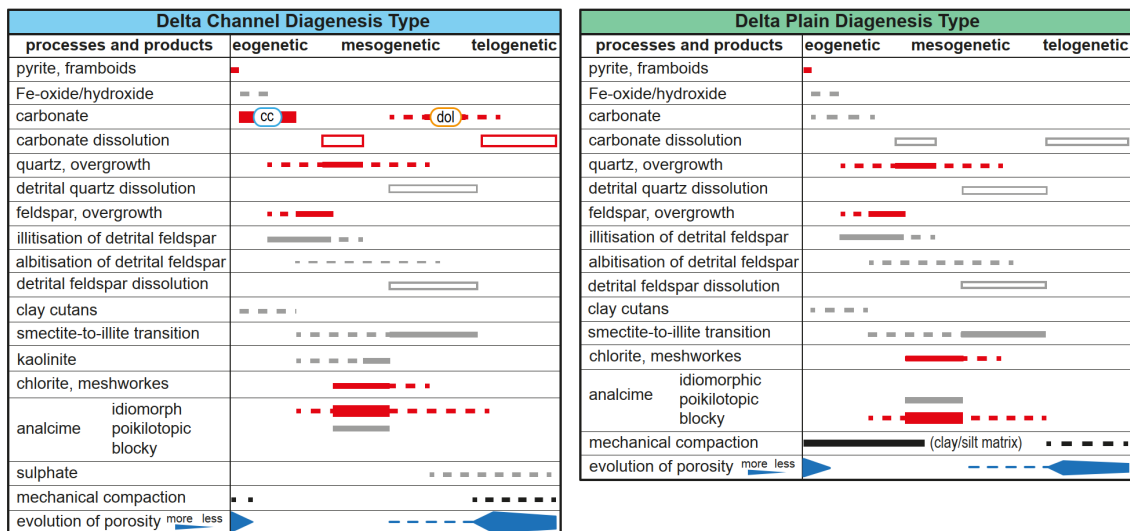


Fig. 3.12: Schematic paragenetic sequences of diagenetic processes and products of Delta Channel and Delta Plain DT's (Lower Schilfsandstein Mb, North Germany), for legend see Fig. 3.15.

Pyrite framboids of up to 2–10  $\mu\text{m}$  size represent the first authigenic phase formed synsedimentary or eogenetically (Figs. 3.12 and 3.13). Although framboidal pyrite is ubiquitously present, the volumetric abundance remains low compared to other authigenic minerals (Table 3.1, Supplement). In some localities, pyrite co-occurs with eogenetic illite-smectite cutans and Fe-oxides/hydroxides grain coats (Supplement). Accordingly, these grain coats are practically absent in most samples, but attain maxima of 6.7 % (illite-smectite) and 11.0 % (Fe-oxides/hydroxides) in individual samples (Table 3.1).

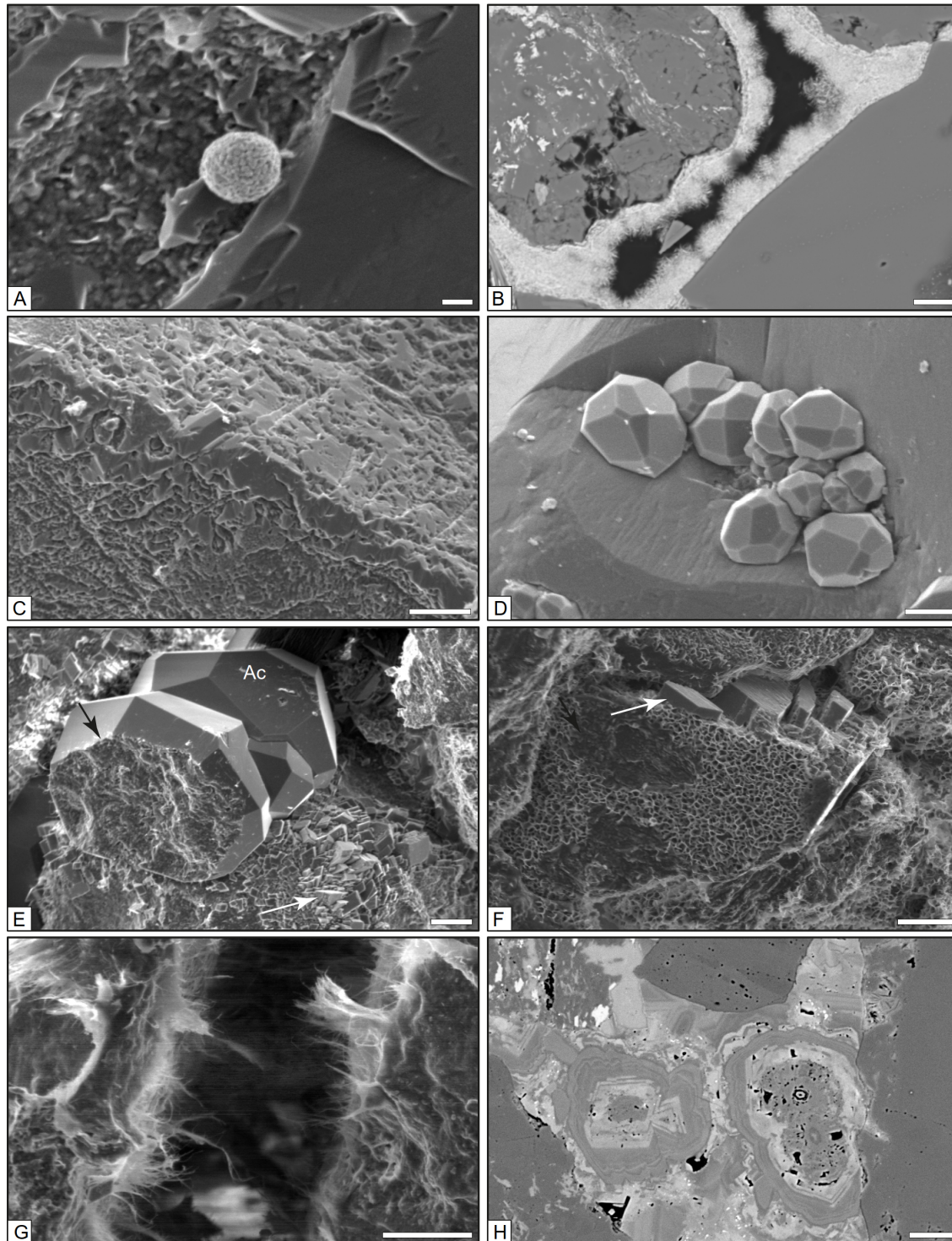


Fig. 3.13: Scanning electron microscopy examples of authigenic mineralogy. **(A)** Eogenetic pyrite (framboidal), Delta Channel DT; scale bar is 4  $\mu\text{m}$ , Brustorf 1 (sample 11-09). **(B)** Eogenetic Fe-oxide coatings on detrital grains, Delta Plain DT; scale bar is 10  $\mu\text{m}$ , Neubrandenburg 2 (sample 11-10). **(C)** Eogenetic quartz overgrowth, Fluvial Channel DT; scale bar is 20  $\mu\text{m}$ , Lütow 3 (sample 12-05). **(D)** Idiomorphic analcime crystals (mesogenetic), Delta Channel DT; scale bar is 20  $\mu\text{m}$ , Brustorf 1 (sample 11-12). **(E)** Mesogenetic succession of authigenic illite (black arrow) partially coating idiomorphic analcime (Ac), and small dolomite rhombs (white arrow) covering illite, Fluvial Channel DT; scale bar is 20  $\mu\text{m}$ , Lütow 3 (sample 12-05). **(F)** Mesogenetic succession of ordered illite-smectite grain coats (boxwork texture) overgrown by dolomite rhombs, Fluvial Channel DT; scale bar is 20  $\mu\text{m}$ , Burg 2 (sample 12-10). **(G)** Fibrous illite growing into open pore, Delta Channel DT; scale bar is 10  $\mu\text{m}$ , Lütow 3 (sample 12-02). **(H)** Late-stage dolomitization, ferroan dolomite with growth bands (chemical zonation), of early-stage pore-filling carbonate including concentric vadoids (pedogenic), Fluvial Channel DT; scale bar is 20  $\mu\text{m}$ , Wolgast 1A (sample 11-11).



Eogenetic quartz and feldspar overgrowth are present in low abundances ranging from 0 to 4.2 % (median <1 %) for authigenic quartz and from 0 to 1.4 % (median <1 %) for authigenic feldspar. Syntaxial quartz overgrowths of 2–20  $\mu\text{m}$  thickness are limited to monocrystalline quartz grains (Fig. 3.13). In a few cases, the boundaries between grains and overgrowths are marked by traces of fluid inclusions of c. 1  $\mu\text{m}$  size. Transmitted light, SEM-EDX and CL microscopic analyses revealed K-feldspar overgrowths on feldspar grains and rarely albitised feldspars. K-feldspar overgrowths have a nearly end-member composition and show chemical zoning recognised by dull brown and dark red luminescence (Fig. 3.8).

Carbonate authigenesis is represented by eogenetic calcite and mesogenetic dolomite with a cumulative abundance of 0–16.5 % (median <1 %). Eogenetic calcite occurs as pore-filling and blocky cement covering detrital grains and grain overgrowths. The eogenesis of calcite is indicated by the low contact strength of detrital grains and the large intergranular volumes occupied by calcite cement. Only in a few examples, eogenetic calcite enclosed broken feldspar grains, pointing to minor mechanical compaction processes prior to calcite formation (Fig. 3.14). Occasionally, calcite cement replaced detrital feldspar grains. Under CL microscope, calcite shows extensive bright orange to dark orange luminescence (Fig. 3.8). In XRD analyses of bulk rock samples, calcite was recognised by its typical  $\sim 29.5^\circ$  2 Theta peak (Fig. 3.7). Eogenetic calcite was partly transformed to dolomite in the mesogenetic regime. Up to 75  $\mu\text{m}$  large dolomite rhombs were observed as pore fillings, growing directly on detrital grains and/or authigenic analcime, and as replacements of dissolved feldspar grains and chlorite meshworks. Intense late-stage dissolution of pore-filling calcite/dolomite is indicated by residual poikilotopic calcite/dolomite observed in open pores and pore throats (Figs. 3.4, 3.8 and 3.14).

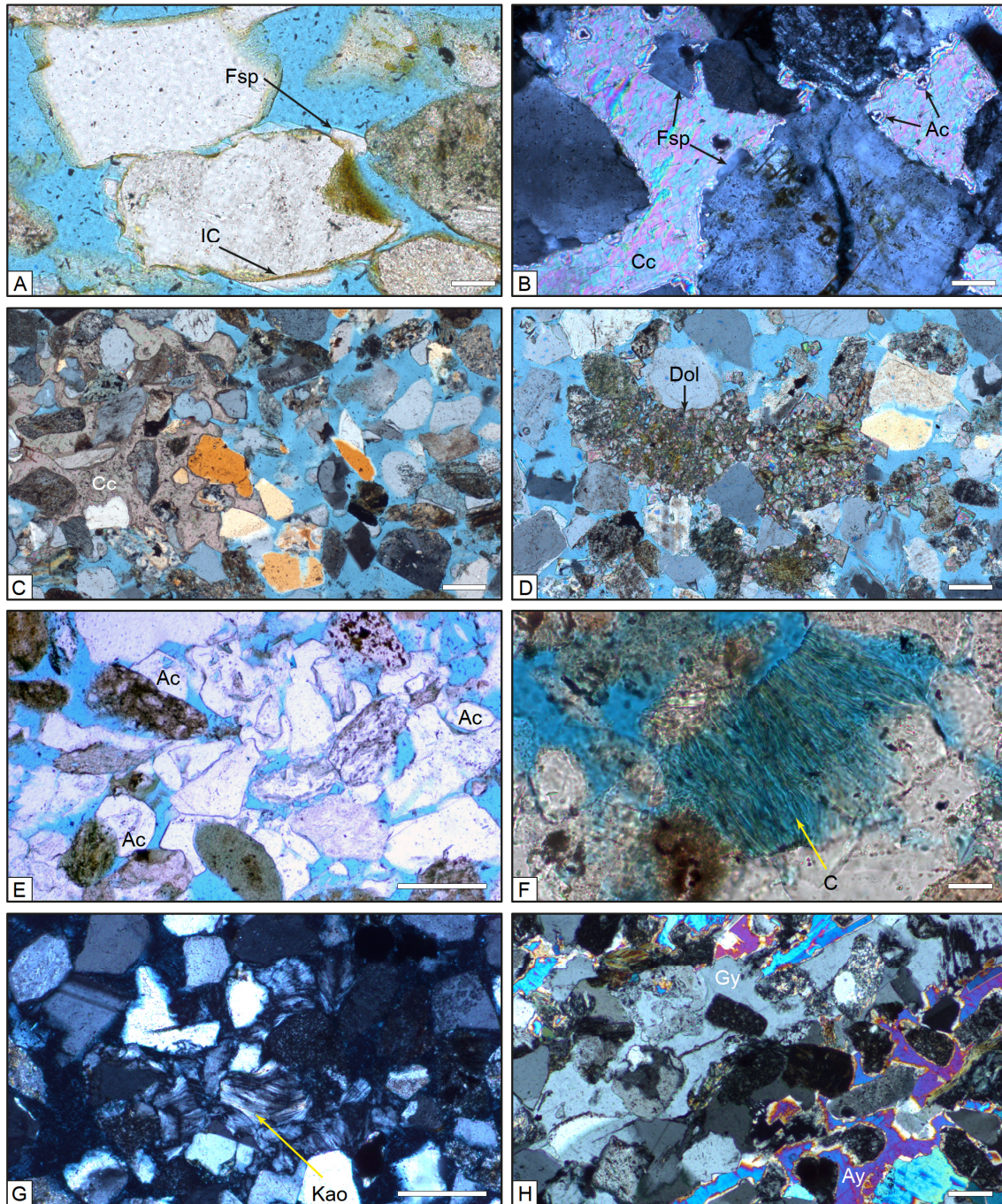


Fig. 3.14: Transmitted-light microscopy examples of detrital and authigenic mineralogy. **(A)** Eogenetic illite-smectite coating (IC) followed by feldspar overgrowth (Fsp), note grain embayment filled pre-depositionally by pedogenic clay and Fe-oxide, Fluvial Channel DT; scale bar is 50  $\mu\text{m}$ . Lütow 3 (sample 12-12), parallel nicols. **(B)** Eogenetic feldspar overgrowth (Fsp) and pore-filling calcite (Cc) followed by mesogenetic analcime locally replacing calcite, Delta Channel DT; scale bar is 50  $\mu\text{m}$ . Lütow 3 (sample 12-01), crossed nicols. **(C)** Residual pore-filling calcite (Cc), supporting the grain fabric, and intergranular porosity (epoxy resin stained blue) resulting from partial telogenetic dissolution of calcite, Delta Channel DT; scale bar is 200  $\mu\text{m}$ . Brustorf 1 (sample 11-11), circular polarisation. **(D)** Residual mesogenetic pore-filling dolomite and intergranular porosity, Fluvial channel DT; scale bar is 200  $\mu\text{m}$ . Wolgast 1A (sample 11-08), circular polarisation. **(E)** Mesogenetic analcime (Ac) and intergranular porosity (epoxy resin stained blue) resulting from late-stage dissolution of authigenic cementation, most probably calcite, Fluvial Channel DT; scale bar is 100  $\mu\text{m}$ . Lütow 3 (sample 12-03), parallel nicols. **(F)** Chloritised mica (biotite) flake (C), Delta Plain DT; scale bar is 20  $\mu\text{m}$ . Klütz 1 (sample 12-01), parallel nicols. **(G)** Mesogenetic pore-filling kaolinite booklets (Kao), Fluvial Channel DT; scale bar is 200  $\mu\text{m}$ . Wolgast 1A (sample 11-16), crossed nicols. **(H)** Mesogenetic pore-filling anhydrite (Ay) and gypsum (Gy) cement, Delta Channel DT; scale bar is 100  $\mu\text{m}$ . Neubrandenburg 2 (sample 11-02), crossed nicols.

Authigenic analcime, accounting for 1.0–12.4 % (median 5.9 %) of the modal composition, occurs as 10–150 µm large euhedral crystals and poikilotopic patches (Figs. 3.4 and 3.13). SEM-EDX analyses revealed the composition:  $\text{Na}_{0.52-0.87}(\text{Al}_{0.73-0.97}\text{Si}_2)\text{O}_6 \cdot \text{H}_2\text{O}$  (normalised to silicon) with an average Si/Al ratio of 2.37. In XRD analyses of bulk rock samples, analcime was identified by its main reflection at  $\sim 26.1^\circ$  2 Theta (Fig. 3.7). The authigenesis of poikilotopic analcime predated grain dissolution as shown by open intragranular pores enclosed by analcime cement. In contrast, the authigenesis of euhedral analcime crystals, partly occupying intragranular pores, also postdated grain dissolution (Fig. 3.12).

Authigenic clay minerals, mainly of the chlorite group, are present with an abundance of up to 7.2 % (median <1 %). Chlorite was observed as pore filling meshworks, grain coats and fan-like aggregates (Fig. 3.14). SEM-EDX analyses of chlorite meshworks revealed chamosite, the Fe endmember of the chlorite group. The composition  $(\text{Fe}^{2+}, \text{Mg}, \text{Fe}^{3+})_5\text{Al}(\text{Si}_3\text{Al})\text{O}_{10}(\text{OH}, \text{O})_8$  is characterised by 20 weight% Fe and a Mg/Al ratio of 0.70. In XRD analyses of bulk rock samples, chlorite shows typical peaks at  $6.3^\circ$  and  $\sim 12.7^\circ$  2 Theta (Fig. 3.7). Authigenic chlorite, postdating eogenetic quartz and feldspar overgrowths, is often overgrown by late-stage analcime, carbonate and sulphate. Other authigenic clay minerals, such as illite-smectite, sericite, illite and kaolinite, were only subordinately observed, for example as grain coats or as replacement of detrital feldspar grains and lithoclasts.

Sulphate cement was only observed in some samples from wells located at or close to salt structures, in which sulphate is present with abundances from 0 to 27.1 % (median <0.1 %). Therefore, sulphate is not considered as typical authigenic cementation of the Delta Channel Diagenesis Type. By means of XRD analyses of bulk rock samples, anhydrite was detected based on the typical peak at  $\sim 25.5^\circ$  2 Theta (Fig. 3.7). However, also gypsum occurred in examined thin sections (Fig. 3.14), whereas barite was only sporadically observed. As sulphate, where present, occurs pore-filling and covers any other authigenic mineral, the authigenesis of sulphate was obviously related to late-stage circulations of Zechstein fluids.

## 2) Delta Plain Diagenesis Type

The typical authigenic minerals of this diagenesis type are pyrite, quartz, K-feldspar, chlorite, and analcime, which were formed in eo- to mesogenetic regimes (Fig. 3.12). Typical and subordinated authigenic minerals account for 13.2 % (median) of the

modal composition. Moderate late-stage dissolution processes contributed to a median porosity of 14.5 % (Table 3.1).

Irregularly distributed pyrite framboids of 2–10  $\mu\text{m}$  size represent the earliest formed authigenic phase. For most of the samples, the quantity of pyrite is below 1 %; an individual sample yielded a maximum abundance of 1.4 % (Supplement). In XRD analyses of bulk rock samples, pyrite was identified by the 1.63 Å major peak at  $\sim 56.3^\circ$  2 Theta (Fig. 3.7). In individual samples, grain coats of sub- $\mu\text{m}$ - to  $\mu\text{m}$ -thick Fe-oxides/hydroxides co-occur with eogenetic pyrite framboids (Table 3.1, Supplement).

In analogy to the Delta Channel Diagenesis Type, early-stage carbonate authigenesis contributed to pore-filling cementation, which were then subject to late-stage dissolution as indicated by residual carbonate cements observed in individual pore throats. Accordingly, carbonate cement attains an abundance of <1% in individual samples, but is absent in most of the samples investigated.

Eogenetic overgrowth on detrital grains were noted with abundances of 0–3.9 % (median <1 %) for quartz and 0–2.4 % (median <1 %) for K-feldspar. The albitisation of plagioclase grains in eo- and mesogenetic stages was more intense within sandstones of the Delta Plain Diagenesis Type than within sandstones of the other diagenesis types. The authigenic albite has an end-member composition of  $\text{NaCaAlSi}_3\text{O}_8$  with Ca/Na ratios of 0.01–0.06.

In thin sections, pore-filling chlorite meshworks are present with 0–4.8 % (median <1 %) of the modal composition. Additional XRD analyses identified chlorite with major peaks at  $6.3^\circ$  and  $12.6^\circ$  2 Theta, and illite-smectite mixed-layer clay minerals with a peak at  $8.9^\circ$  2 Theta (Fig. 3.7). However, only chlorite could be identified in thin sections.

With an abundance of up to 16.8 % (median 7.7 %), analcime is the most frequent authigenic mineral. Blocky, pore-filling analcime covers early diagenetic grain overgrowths and mesogenetic chlorite (Fig. 3.4). In XRD analyses, analcime was identified by typical peaks at  $16.0^\circ$  2 Theta,  $26.2^\circ$  2 Theta, and  $30.1^\circ$  2 Theta (Fig. 3.7). The extensive analcime cementation seems to be related to intense dissolution of labile detrital grains, such as feldspar, and reworked tephra fragments (Figs. 3.4 and 3.9).

### 3) Fluvial Channel Diagenesis Type

The typical eo- to mesogenetic sequence includes Fe-oxides/hydroxides, carbonate, K-feldspar, illite-smectite, and analcime, which attain variable abundances in the Lower and Upper Schilfsandstein Members (Fig. 3.15). Intense late-stage dissolution processes resulted in high median porosity values of 26.8 % in the Lower Schilfsandstein Mb and of 24.8 % in the Upper Schilfsandstein Mb. Authigenic minerals account for 8.6 % in sandstones of the Lower Schilfsandstein Member and 13.8 % in sandstones of the Upper Schilfsandstein Member (Tabs. 3.1 and 3.2).

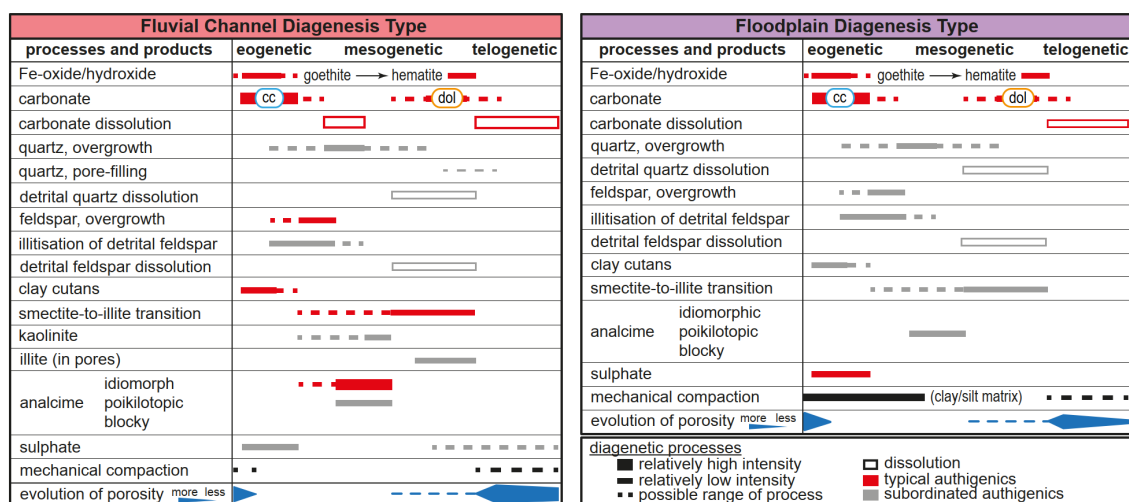


Fig. 3.15: Schematic paragenetic sequences of diagenetic processes and products reconstructed for the Fluvial Channel DT of the Lower and Upper Schilfsandstein and Floodplain DT of the Upper Schilfsandstein.

Fe-oxides/hydroxides occur as sub- $\mu\text{m}$ - to  $\mu\text{m}$ -thick brownish to opaque grain coats, and as pore-filling cement patches and concretions (Figs. 3.4 and 3.13). The quantity ranges from 0 to 3.0 % (median <1 %) in the Lower Schilfsandstein Member and from 0 to 12.9 % (median 2.8 %) in the Upper Schilfsandstein Member. SEM-EDX analyses attest high Fe and low Ti contents of grain coats resulting in a Ti/Fe ratio of 0.01. In few cases, ferrous grain coats replaced detrital feldspar grains and lithoclasts.

Carbonate is present as eogenetic calcite and mesogenetic dolomite with cumulative abundances of 0–37.6 % (median 1.3 %) in the Lower Schilfsandstein Member and 0–18.5 % (median <1 %) in the Upper Schilfsandstein Member (Tabs. 3.1 and 3.2). Blocky, pore-filling calcite covers detrital grains and Fe-oxide/hydroxide coatings. At a few localities, early stage calcite includes concentric vadoids (up to 100  $\mu\text{m}$  diameter) attesting to pedogenic carbonate precipitation (Fig. 3.13). Eogenetic calcite typically shows zoned dark orange to bright orange luminescence pointing to chemical zonation

(Fig. 3.8). Mesogenetic dolomite is present as pore-filling cementation and idiomorphic rhombs, due to transformation of eogenetic calcite, and euhedral rhombs (Fig. 3.13). As dolomite rhombs cover detrital grains, iron-bearing coatings, analcime, and authigenic illite, the formation of dolomite postdates mesogenetic analcime and illite authigenesis (Figs. 3.13 and 3.15). Sparitic, pore-filling ferroan dolomite is non-luminescent and characterised by chemical zonation related to variable Mg/Fe ratios ranging from 0.17–1.44 as revealed by SEM-EDX analyses (Fig. 3.13).

Authigenic sulphate is accessorially present in sandstones of the Lower Schilfsandstein Member and attains a quantity of 0–13.1 % (median <1 %) in sandstones of the Upper Schilfsandstein Member (Tabs. 3.1 and 3.2). Contemporaneously and/or subsequently to eogenetic calcite, patches of poikilotopic sulphate cement, visible as small nodules in hand specimen, were formed by pedogenic processes. A second stage of sulphate authigenesis, limited to localities at or close to salt structures, resulted in pore-filling anhydrite and gypsum and less frequently barite. SEM-EDX analyses of barite revealed 7.6 % strontium and Sr/Ba ratios of 0.15. These mesogenetic sulphates are enclosing all other authigenic minerals and cements.

Diagenetic feldspar either encloses detrital feldspar grains or Fe-oxide/hydroxide coatings and thus, postdates eogenetic grain coats. SEM-EDX analyses of feldspar grains and overgrowth revealed detrital plagioclase with Ca/Na ratios of 0.00–0.63 (Albite to Andesine) covered by K-feldspar overgrowth of Orthoclase/Microcline with constant K/Al ratios of 1.22–1.29. In addition, authigenic feldspar is further represented by albite partly replacing detrital anorthite grains. In SEM-EDX analyses, detrital anorthite has Ca/Na ratios of 0.83–1.00 and authigenic albite has Ca/Na ratios of 0.01–0.06. The cumulative abundances of authigenic feldspar is 0–9.4 % (median 1.9 %) in the Lower Schilfsandstein Member and 0–6.4 % (median <1 %) in the Upper Schilfsandstein Member (Tabs. 3.1 and 3.2).

Quartz authigenesis in the eogenetic regime contributed to overgrowth on detrital quartz grains, whereas authigenesis in the mesogenetic regime resulted in pore-filling quartz cement (Fig. 3.12). The cumulative abundances of both types are low, ranging from 0 % to 1.4 % (median <1 %) in the Lower Schilfsandstein Member and from 0 % to 1.9 % (median <1 %) in the Upper Schilfsandstein Member.

Authigenic clay minerals are represented by illite-smectite grain coats and pore-filling kaolinite and illite. Illite-smectite grain coats are present in low quantities of 0–1.5 % (median <1 %) in the Lower Schilfsandstein Member and 0–10.0 % (median 1.2 %) in the Upper Schilfsandstein Member. These up to 5 µm thick tangential grain coats of

ordered illite-smectite mixed-layer clay minerals show the typical boxwork texture and are considered the mesogenetic transformation of precursor detrital clay cutans (Fig. 3.13). The formation of pore-filling kaolinite booklets seems to be associated to corrosion of K-feldspar. Despite the low quantity of 0–1.9 % (median <1 %) in the modal composition of sandstones of the Upper Schilfsandstein Member, kaolinite could be identified based on the 7.17 Å peak at 12.7° 2 Theta (Fig. 3.7). Based on SEM analysis, late stage fibrous illite could be observed in pores covering detrital grains and authigenic minerals, such as mesogenetic analcime crystals (Fig. 3.13).

Authigenic analcime is present with variable abundances of 0–17.6 % (median <1 %) in the Lower Schilfsandstein Member and 0–8.6 % (median 1.9 %) in the Upper Schilfsandstein. Up to 15 µm large euhedral analcime crystals formed directly on detrital grains or Fe-oxide/hydroxide coatings and larger poikilotopic analcime patches (>>100 µm) filled open pores enclosing previously formed authigenics. SEM-EDX analyses point to the following chemical composition  $\text{Na}_{0.65-0.82}(\text{Si}_2\text{Al}_{0.72-0.90})\text{O}_6 \cdot \text{H}_2\text{O}$  with an average Si/Al of 2.35. As shown by open intragranular pores enclosed by poikilotopic analcime cement, the authigenesis of analcime predated the corrosion of detrital feldspar grains (Fig. 3.4).

#### 4) Floodplain Diagenesis Type

The typical authigenic minerals are Fe-oxide/hydroxide grain coatings, which are ubiquitously present in the investigated samples. Carbonate, sulphate and illite-smectite are of subordinated importance. Thus, the paragenetic sequence of the Floodplain Diagenesis Type resembles much of the Fluvial Channel Diagenesis Type. Noticeable differences are the presence of a mixed carbonate-clastic matrix, and the low quantities of illite-smectite coatings and authigenic analcime in samples of the Floodplain Diagenesis Type (Fig. 3.15). Typical and subordinated authigenic minerals account for 27.4 % (median) of the modal composition of sandstones of the Lower Schilfsandstein Member and 12.3 % (median) for sandstones of the Upper Schilfsandstein Member (Table 3.2). Late-stage dissolution processes contributed to median porosities of 24.1 % for sandstones of the Lower Schilfsandstein Member and 15.8 % for sandstones of the Upper Schilfsandstein Member.

Brownish, sub-µm- to µm-thick grain coats of Fe-oxides/hydroxides attain abundances of 14.8–32.5 % (median 25.0 %) in the Lower Schilfsandstein Member and 0–17.9 % (median 6.1 %) in the Upper Schilfsandstein Member. In XRD analyses of bulk rock samples, hematite was recognised by the 2.69 Å main peak at ~33.3° 2 Theta,

whereas goethite could not be detected (Fig. 3.7). Up to 5  $\mu\text{m}$  thick coats of tangential illite-smectite are accessorially present in the Lower Schilfsandstein Member and occur in low quantities of 0–7.7 % (median <1 %) in the Upper Schilfsandstein Member. The same refers to authigenic chlorite and kaolinite, which occur accessorially in sandstones of the Upper Schilfsandstein Member (Table 3.2).

Authigenic carbonate was recognised as early diagenetic calcite and late diagenetic non-ferroan to ferroan dolomite in samples of the Upper Schilfsandstein only. The cumulative abundance ranges from 0 to 10.9 % (median <1 %). In thin sections, pedogenic nodules occur as blocky, pore-filling calcite patches covering illite-smectite and/or Fe-oxide/hydroxide grain coats. Later, calcite cement was partly to completely replaced by blocky, pore-filling dolomite and idiomorphic dolomite rhombs. Under CL, dolomite show growth bands varying from dark red luminescence to non-luminescent (Fig. 3.8). SEM-EDX analyses revealed Mg/Ca ratios changing from 0.62 in the core to 0.4 in growth bands. The presence of dolomite was further verified by means of XRD analyses (Fig. 3.7).

Although pedogenic sulfate nodules are frequently present in succession of floodplain fines, only low quantities of 0–13.1 % (median <1%) of authigenic sulphate could be observed in sheetsands of the Upper Schilfsandstein Member (Table 3.2). The eogenetic formation of authigenic sulphate is indicated by low contact strength of the grain fabric around pore-filling cement patches. In XRD analyses of bulk rock samples, gypsum could be identified by typical peaks at  $\sim 11.9^\circ$  2 Theta and  $\sim 29.2^\circ$  2 Theta (Fig. 3.7).

Eogenetic quartz and feldspar overgrowths are generally present in low quantities. Quartz overgrowth attain maximum abundances of 1.4 % in the Lower Schilfsandstein Member and 1 % in the Upper Schilfsandstein Member. Feldspar overgrowths were only recognised in samples of the Upper Schilfsandstein Member with an abundance of 0–2.4 % (median <1 %).

Authigenic analcime is present with maximum abundances 1.4 % in the Lower Schilfsandstein Member and 5.3 % in the Upper Schilfsandstein. In samples of the latter, larger poikilotopic analcime patches enclosed previously formed authigenics attesting to a precipitation in the mesogenetic stage.



#### 3.4.4.2 Schilfsandstein outcrops

Despite larger distances between the outcrops areas, the investigated fluvial sandstones are characterised by the same paragenetic sequence of Fe-oxides/hydroxides, illite-smectite, feldspar, quartz, and chlorite (Supplement). Although authigenic analcime is lacking, the paragenetic sequence resembles much of the Fluvial Channel Diagenesis Type. Late-stage dissolution contributed to variable median porosity values ranging from 2.9 to 14.8 % and abundances of authigenic minerals ranging from 10.7 % to 13.0 % (Table 3.3).

Considering all samples, eogenetic Fe-oxide/hydroxide grain coats are present with abundances of 0–14.8 % (median <1 %) and illite-smectite grain coats are present with abundances of 0–22.5 % (median 1.0 %). As the next authigenic phase, feldspar overgrowths, covering detrital grains and Fe-oxide/hydroxide grain coats, account for 0–3.3 % (median <1 %) of the modal composition. Authigenic quartz was observed as eogenetic syntaxial overgrowth and as mesogenetic pore-filling cement. The cumulative abundance of authigenic quartz ranges from 0 % to 13.3 % (median 4.8 %) of the modal composition. Authigenic chlorite is mainly present as 10–80 µm-thick coatings (radial and tangential habit) covering detrital grains and illite-smectite coatings, whereas pore-filling chlorite meshworks are present in low quantities. The abundance of authigenic chlorite ranges from 0 to 16.7 % (median <1 %) of the modal composition. In individual samples, authigenic kaolinite booklets, euhedral dolomite rhombs and anhydrite cement could be identified accessorially.

### 3.5 Discussion

#### 3.5.1 Diagenesis of the Stuttgart Formation

The herein described types of sandstone diagenesis attest to the subsequent control of depositional and diagenetic regimes (Figs. 2.12 and 2.15). Accordingly, paragenetic sequences of authigenic minerals and evolution of porosity are mainly a function of detrital assemblages, pore-water chemistry and basin history (Fig. 3.16).

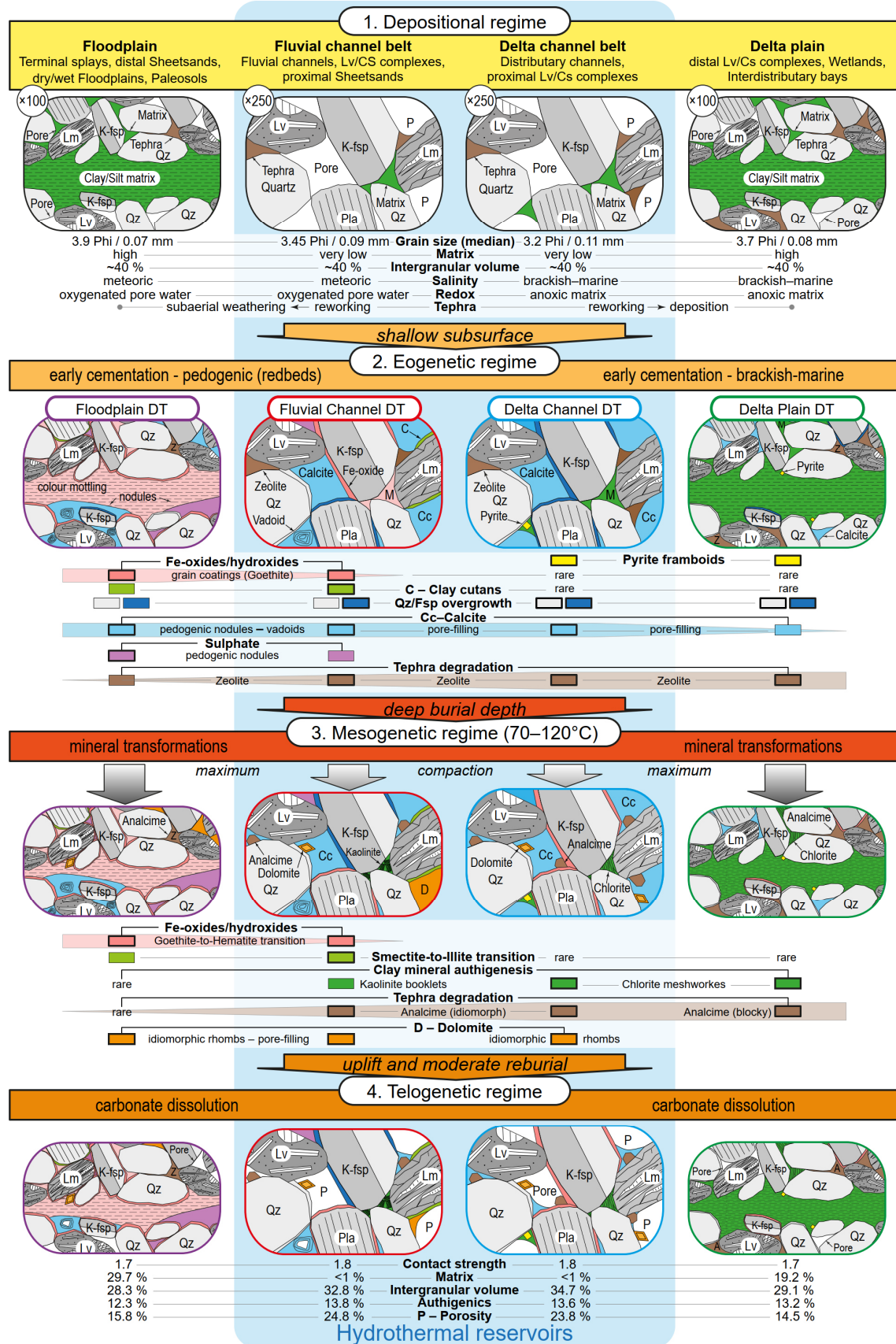


Fig. 3.16: Generalised scheme summarising the main diagenetic processes of herein proposed diagenesis types. Numbers refer to median values of the Lower Schilfsandstein Member (Delta Channel and Delta Plain DT's) and the Upper Schilfsandstein Member (Fluvial Channel and Floodplain DT's) shown in Tabs. 3.1 and 3.2; Lv/CS complex - levee/crevasse splay complex.

### 3.5.1.1 Depositional regime

The depositional regime is considered the sum of pre-depositional processes and specific conditions within depositional environments (e.g. Burley et al., 1985; Hiatt and Kyser, 2000; Lima and De Ros, 2002; Worden and Burley, 2003; Abouessa and Morad, 2009; Hammer et al., 2010; Morad et al., 2010; Bjørlykke, 2014; Khalifa and Morad, 2015; Saïag et al., 2016; Lan et al., 2016). A detailed evaluation of pre-depositional processes is beyond the scope of this contribution, but some conclusions can be drawn from the low compositional and textural maturity of the detrital assemblage. Comparing lithic arkoses and feldspathic litharenites of the Stuttgart Formation (see Fig. 3.6) with older Triassic sandstones, mainly representing lithic subarkoses to quartzarenites (e.g. Häusser and Kurze, 1975; Scholle, 1992; Solms and Röhling, 2001; Franz et al., 2018b; Zimmermann et al., 2018), the abundance of feldspar and lithic grains attest to basement erosion in source areas. This is in agreement with the late Triassic exhumation of the southern Baltic Shield (Triassic peneplain) described by Japsen et al. (2016). An increased volume of first-cycle sand in the detrital assemblage is further evidenced by the abundance of angular grains, in particular quartz grains, and the unaltered appearance of many detrital feldspar grains and lithics.

Previous facies analysis of Beutler and Häusser (1982), Förster et al. (2010), Franz et al., (2018b) revealed four depositional environments – fluvial channel belts, floodplains, delta channel belts, and interdistributary bays/wetlands – characterised by distinct detrital assemblages (Fig. 3.5, Tabs. 3.1 and 3.2). The typical formation waters of these environments – oxidising meteoric vs. reducing brackish-marine – were then crucial for diagenetic pathways, in particular during the eogenetic stage (e. g., Burley et al., 1985; Weibel, 1998; Weibel et al., 2017).

As special component, the detrital assemblages yielded volcanic detritus. In addition to euhedral zircon (see Zeh et al., 2021), the presence of diagenetically altered tephra clasts provides further evidence of ash-fall-out into the Schilfsandstein river system. As tephra is highly susceptible to diagenetic alteration (Hay, 1966, 1978; Hay and Sheppard, 2001; Weibel et al., 2019), the incomplete degradation of tephra clasts, present in a few samples only, remains an exception (Fig. 3.9).

### 3.5.1.2 Eogenetic regime

The eogenetic sequence of the Delta Channel and Delta Plain Diagenesis Types, including pyrite, carbonate cement, and quartz and feldspar overgrowth, corresponds

to the typical eogenesis of marine sandstones (summarised in Burley et al., 1985). Representing the first authigenic mineral, pyrite is either of syn-sedimentary (Skei, 1988) or early diagenetic origin (Berner, 1970; Friis, 1987). The formation of pyrite is related to the presence of decomposable organic matter, dissolved sulphate, and reactive iron (Berner, 1984; Raiswell, 1982; Weibel, 1998). Increasing alkalinity during alteration of organic matter (Berner, 1981; Curtis, 1987) favoured pre-burial calcite authigenesis, a common process of marine eogenesis (Burley et al., 1985; Fine, 1986; Friis, 1987; Morad, 1998; Morad et al., 2000). The migration of increasingly alkaline pore fluids contributed to intense pore-filling precipitation of calcite, in particular in sandstones of the Delta Channel Diagenesis Type. The precipitation of calcite pre- and postdated the formation of clay cutans (smectite), and overgrowths of quartz and feldspar on detrital grains (Figs. 3.12 and 3.16). As a consequence of the general progradational architecture of the Lower Schilfsandstein Member, resulting from regressive trends of the inland sea (Franz et al., 2014), parts of the deltaic system were subsequently subaerially exposed and pedogenetically modified (Fig. 3.3; Franz et al., 2018b). In vertical successions, this facies shift is resulted in an upward change from marine eogenesis to a mix of marine and terrestrial eogenesis. This may explain the co-occurrence of pyrite and Fe-oxides/hydroxides in individual localities.

The eogenesis of the Fluvial Channel and Floodplain Diagenesis types was controlled by pedogenic processes. The presence of oxygenated, meteoric pore water and leaching/illuviation of clay minerals resulted in Fe-oxide/hydroxide coatings, most probably goethite, (see Weibel, 1999) and clay cutans covering detrital grains. Accordingly, the early-stage sequence of both diagenesis types corresponds to the typical eogenesis of terrestrial red-bed successions (e.g., Glennie et al., 1978; Walker et al., 1978; Burley et al., 1985; Gaupp, 1996; Leveille et al., 1997; Weibel, 1998; Lippmann, 2012). The vertical displacement of Fe-oxides/hydroxides and clay minerals (leaching), and the precipitation of carbonate/sulphate nodules corresponds to mature palaeosols described from the floodplains of the Schilfsandstein river system (e.g. Nitsch, 2005; Franz et al., 2019). The early pedogenic development obviously limited the subsequent migration of pore fluids and partly inhibited the formation of quartz and feldspar overgrowth (Fig. 3.15). The presence of quartz and feldspar overgrowth in less pedogenically modified sandstones of the Fluvial Channel Diagenesis Type is related to the migration of pore waters during the eogenetic stage (see also Heling, 1965; Füchtbauer, 1973).

### 3.5.1.3 Mesogenetic regime

With increasing burial temperature, the detrital matrix, clay cutans, and pore-filling cementation were subject to typical mesogenetic transformations. Important processes were the goethite-to-hematite transformation of Fe-oxide/hydroxide coatings (e.g. Weibel, 1999) and the transformation of detrital clay cutans, probably smectite or random smectite-illite, to ordered illite-smectite mixed-layer minerals, also observed by Förster et al. (2010). The breakdown of smectite, resulting in the release of iron, magnesium and sodium, triggered further modifications (e.g. Burley et al., 1985; McKinley et al., 2003). Liberated iron most probably contributed to the formation of chlorite observed as pore-filling meshworks, grain coats and fan-like aggregates in sandstone of the Delta Channel and Delta Plain Diagenesis Types. The partial conversion of pore-filling eogenetic calcite to dolomite was possibly triggered by magnesium released from smectite breakdown or from intruding near-marine formation waters. The stepwise thermal degradation of volcanic ash, which started in the eogenetic regime (see Hay, 1966, 1978; Hay and Sheppard, 2001; Weibel et al., 2019), finally led to the precipitation of analcime in the mesogenetic regime, which is volumetrically abundant in brackish-marine sandstones of the Delta Channel and Delta Plain Diagenesis Types. This seems to be in accordance to Hay (1966), who related the formation of analcime to marine formation water. Analcime is less abundant to rare in distal fluvial sandstones of the North German Basin and absent in proximal fluvial sandstones of the South German Basin (Tabs. 3.1 and 3.2; Supplement). This may be related to the presence of meteoric formation water responsible for the eogenetic degradation of volcanic detritus to montmorillonite (Hay, 1966). Later, montmorillonite was most probably transformed to illite, a typical temperature-related dehydration process of the mesogenetic regime (e.g., De Segonzac, 1970; Perry and Hower, 1970; Dypvik, 1983; see also discussion in Zeh et al., 2021).

Alteration and corrosion mainly affected feldspar grains and some types of volcanic rock fragments. Typical processes are the albitisation of detrital plagioclase, most abundant in sandstones of the Delta Plain Diagenesis Type, and partial to complete corrosion of individual feldspar grains, present in sandstones of all diagenesis types. In particular, the complete dissolution of individual feldspar grains contributed to secondary intragranular pores, which are most abundant in sandstones of the Delta Channel and Fluvial Channel Diagenesis Types. As these alteration processes were not limited to distinct types of the feldspar assemblage, the different appearance of feldspar grains – fresh to completely dissolved – is related to mixing of first and second cycle feldspar grains. In particular feldspar grains from recycled sediment are expected

to be more labile to diagenetic alteration than those of first cycle sands (Milliken et al., 1989; Krainer and Spötl, 1989; Johnsson and Meade, 1990; Nesbitt et al., 1997). The formation of oversized pores due to dissolution of grains and neighbouring cement further contributed to secondary porosity.

The undercompacted grain fabric of sandstone of the Fluvial Channel and Delta Channel Diagenesis Types in cores from North Germany attest to cementation-controlled diagenetic pathways (Houseknecht, 1987; Ehrenberg, 1989), during which pervasive early-stage calcite cementation effectively prevented the grain fabric from significant burial mechanical compaction (Fig. 3.16). Consequently, higher contact strength of sandstones of the Fluvial Channel Diagenesis Type in South Germany, Thuringia and Weserbergland may be attributed to incomplete eogenetic cementation resulting in a more mechanical compaction-controlled diagenetic pathway (Table 3.3).

#### 3.5.1.4 Telogenetic regime

The successive modification of sandstones in eo- and mesogenetic regimes correspond to the prograde diagenesis of the Stuttgart Formation published previously (Heling, 1965; Füchtbauer, 1973; Heling and Beyer, 1992; Förster et al., 2010). However, the fluid temperatures of the Stuttgart Formation, ranging from 20 to 65 °C within investigated wells from North Germany, are insufficient to explain the above described temperature-dependent mesogenetic processes. These mineral transformations constrain the burial maximum to a temperature of at least 105 °C (see chapter 3.5.2). The considerable offset between present-day fluid temperature and maximum burial temperature is herein related to the basin differentiation and inversion stage (e.g. Jaritz, 1969; Nöldeke and Schwab, 1977; Ziegler, 1990), during which the Stuttgart Formation was uplifted to shallower burial depth in the North German Basin and exhumed in the South German Basin.

Associated to uplift and exhumation, changes of temperature, pressure and pore fluid chemistry triggered retrograde diagenetic processes, in particular the dissolution of eo- to mesogenetic pore-filling cementations. These dissolution processes, which contributed to the evolution of secondary porosity, were most effective in sandstones of the Delta Channel and Fluvial Channel Diagenesis Types with median values of total porosity of 23.8 % and 26.3 %, respectively (Tabs. 3.1 and 3.2). These values, derived from modal analysis of thin sections, correspond to a median porosity of 24.0 % obtained from helium porosity measurements of sand-prone succession of fluvio-deltaic channels Franz et al. (2018b). As sandstones of the Delta Plain and Floodplain

Diagenesis Types were less affected by dissolution, large intergranular volumes and connectivity of pores seem to be important prerequisites for both, pervasive early-stage cementation and effective late-stage dissolution.

In the outcrop areas, the exhumation of the Keuper Group resulted in infiltration of meteoric waters. Dissolution processes effected mainly the detrital assemblage of the Stuttgart Formation as suggested by a higher median value of intragranular porosity of 15.6 % (of the total porosity) in samples from South Germany (see chapter 3.4.3). The authigenic assemblage was apparently not affected by enhanced dissolution in near-surface regimes as shown by comparable median abundances of authigenics in sandstones from North and South Germany (Table 3.3).

### **3.5.2 Constraints on burial and uplift history**

Temperature-related diagenetic processes, evident in core and outcrop samples of the Stuttgart Formation, resulted in modification of eogenetic minerals and alteration of detrital grains. Some of these transformation reactions give indications on maximum burial temperatures and, combined with the retrograde diagenetic pathway (telogenesis), provide some constraints on the Mesozoic–Cenozoic burial and uplift history of the CEBS (Fig. 3.17).

#### **3.5.2.1 Maximum burial temperature and depth**

As a consequence of continuously increasing burial depth, the Stuttgart Formation was exposed to temperatures  $>70$  °C, the lower limit of the mesogenetic stage (Khalifa and Morad, 2012; Hesse and Gaupp, 2021). Temperatures of  $>70$  °C are in particular indicated by the presence of mesogenetic illite-smectite, hematite, analcime and dolomite, the typical paragenetic succession of the Fluvial Channel and Floodplain Diagenesis Types (Fig. 3.16).

Authigenic chlorite is considered the transformation product of detrital biotite (Heling, 1965; Füchtbauer, 1974; Luo et al., 2009), but also kaolinite and smectite could be precursor minerals (Gould et al., 2010; Dowey et al., 2012). In addition, the neof ormation of chlorite is related to alteration of volcanic detritus (Anjos et al., 2000; Berger et al., 2009), to fluid systems of volcanic rocks (Brecht, 1999; Wolfgramm, 2005), and to the formation of analcime (Shifa et al., 2016). Apart from precursor minerals, the authigenesis of chlorite in sandstones is associated to temperatures between 70 °C and more than 100 °C (Glasmann et al., 1989; Ehrenberg and

Nadeau 1989; Weibel, 1999; Ma et al., 2018). However, the availability of liberated potassium may lower this temperature range to 47–68 °C (Weibel, 1999; McKinley et al., 2003).

The stepwise conversion of detrital smectite via random smectite-illite mixed-layers to ordered illite-smectite mixed-layers at threshold temperatures of 47 °C and 74 °C was reported by Weibel (1999). According to Chang et al. (1986) and Boles and Franks (1979), the ordering of illite-smectite mixed layers occurs in somewhat higher temperature ranges of 90–115 °C and 100–200 °C, respectively.

Although analcime may form in marine and non-marine depositional environments (e.g. Ross, 1928; Coombs, 1965; Goodwin and Surdam, 1967; English, 2001; Do Campo et al., 2007), its authigenesis in sediments is almost exclusively associated to the diagenetic degradation of volcanic detritus, in particular volcanic glass (e.g. Hay, 1966; Hurst and Irwin, 1982; Hay and Sheppard, 2001). For the sodic volcanic system, increasing burial temperatures result in the stepwise transformation of volcanic glass via clinoptilolite and analcime to albite (Iijima, 1988; Ogiwara and Iijima, 1990; Noh and Boles, 1993; Hay and Sheppard, 2001; Weibel et al., 2019). Accordingly, analcime is formed above 80–86 °C and stable up to 120–124 °C temperature (Weibel et al., 2019). However, the potential of the analcime geothermometer (Saha, 1961; Coombs and Whetten, 1967; Iijima, 1988; Weibel et al., 2019) is challenged by autoclave experiments, in which authigenic analcime attained a lower stability limit of 200 °C (Schmidt et al., 2017) and an upper stability limit of c. 600 °C (Liou, 1971).

The albitisation of detrital feldspar grains is a dissolution-precipitation process (e.g. Saigal et al., 1988), which is known to occur in temperature ranges of 65–120 °C (Aagard et al., 1990) and 75–100 °C, respectively (Morad, 1986; Morad et al., 1990). Sufficient amounts of sodium may have been sourced from highly saline pore waters and/or from the transformation of smectite to illite at similar temperatures (Morad et al., 2000). Further sodium was probably liberated from the thermal degradation of volcanic glass.

The formation of non-ferroan dolomite at the expense of eogenetic calcite is a typical mesogenetic process (e.g. Scotchman and Johnes, 1990; Weibel, 1998; Lin et al., 2022). Magnesium and iron species, liberated from smectite breakdown, may have contributed to the precipitation of ferroan dolomites showing typical chemical zonation (Ziegler, 2006). The precipitation of ferroan dolomite is related to temperature ranges of



50–140 °C (Mansurbeg et al., 2008), 80–140 °C (Khalifa and Morad, 2012) and 100–125 °C, respectively (McNeil et al., 1995).

The presence of hematite in sandstones of the Fluvial Channel and Floodplain Diagenesis Types, goethite is absent (Kasina et al., 2017; this study) or only subordinately present (Förster et al., 2010), indicates the conversion of eogenetic goethite coatings to mesogenetic hematite (e.g. Walker, 1976; Weibel, 1999). Weibel (1999) proposed a burial temperature of >105 °C for samples of the Triassic Skagerrak Formation, in which all goethite has been converted to hematite.

Accepting the temperature ranges proposed by Weibel (1999), Boles and Franks (1979), McNeil et al. (1995), and Weibel et al. (2019), the paragenetic succession of illite-smectite, hematite, analcime and dolomite constrains the maximum burial temperature of the Stuttgart Formation to 105–120 °C. This temperature range translates to a maximum burial depth of 2,100–2,500 m for the Stuttgart Formation considering a palaeogeothermal gradient of c. 40 K/km (see Wolfgramm and Schmidt-Mumm, 2001; Japsen et al., 2007; Duschl et al., 2016) and 20 °C palaeosurface temperature (see discussion in Lippmann, 2012). The estimated burial maximum of about 2,500 m corresponds to the present-day burial depth of 2,500–2,800 m of the Stuttgart Formation in the axial part of the eastern NGB (Hoth et al., 1993). The shallower present day burial depth of 200–1,550 m in wells located to the North and South of the basin axis are herein related to substantial uplift and erosion during the basin differentiation and inversion stage.

The maximum burial temperature of the Stuttgart Formation of 105–120 °C is largely in agreement with published thermal maturity and thermochronological data of Lower–Middle Keuper. Bachmann et al. (2002), Rodon and Littke (2005) and Beyer (2015) reported vitrinite reflectance (VRr) values of 0.6–1.4 % for South Germany, 0.44–1.21 % for NW Germany (excluding grabens and troughs) and 0.53–1.24 % for Thuringia. These values were related to burial temperatures of 70–100 °C (Rodon and Littke, 2005; Beyer, 2015), which corresponds roughly to burial history modelling based on apatite fission track data of Lower–Middle Keuper sandstones from Thuringia (von Eynatten et al., 2021). The comparable thermal maturity of Keuper strata point to balanced subsidence pattern in larger parts of the CEBS during the late basin fill stage, followed by uplift in the northern CEBS and uplift/exhumation of Triassic strata in southern parts of the CEBS.

### 3.5.2.2 Uplift and reburial

The disconformable contact of Lower Cretaceous strata to older Mesozoic strata, represents a prominent bounding surface within the younger Mesozoic succession of the North German Basin (Fig. 3.2; Jaritz, 1969; Nöldeke and Schwab, 1977; Ziegler, 1990). Previous reconstructions point to geographically wide-spread erosion in the latest Jurassic–early Cretaceous interval with 700–2,900 m of strata missing (e.g. Jaritz, 1969, 1980; John, 1975; Kossow and Krawczyk, 2002; Schnabel et al., 2021). Accordingly, burial history modelling indicate a Late Jurassic burial maximum followed by erosion of c. 700 m of strata (Rodon and Littke, 2005). Locally, more than 3,000 m of strata were eroded at the western Pompeckj Block (Bruns et al., 2013).

The scenario of a Late Jurassic burial maximum followed by latest Jurassic–early Cretaceous uplift is compatible to the stratigraphic successions of herein investigated wells (Fig. 3.2). Disregarding wells located at or close to salt structures, the present-day burial depth of the Stuttgart Formation of 1,000–1,550 m points to an uplift of 550–1,500 m, which is in the range of previous reconstructions (e.g. Jaritz, 1969; John, 1975; Kossow and Krawczyk, 2002; Schnabel et al., 2021, Rodon and Littke, 2005; Bruns et al., 2013). However, the herein suggested quantification and timing of the burial maximum needs to be constrained by additional thermal maturity data and burial history modelling (Fig. 3.17).

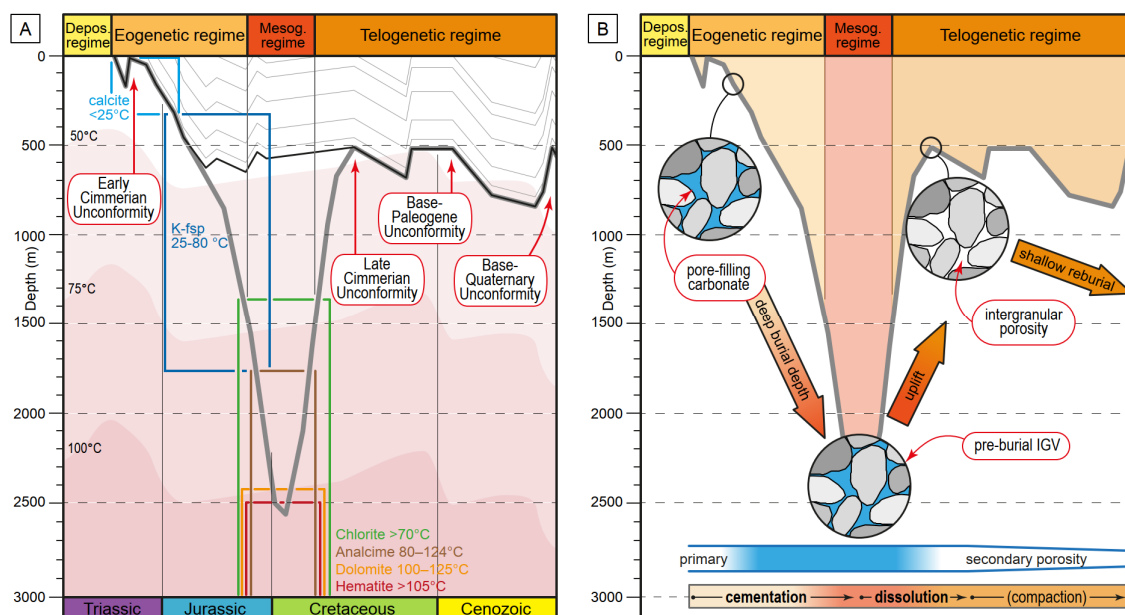


Fig. 3.17: Schematic burial and diagenetic history of the Schilfsandstein in NE Germany. **(A)** Burial and temperature history of the well Loissin 1 after Friberg (2001) and paragenetic succession of authigenic minerals of the Fluvial Channel DT, see also Fig. 3.2. Temperature-dependant authigenic minerals, i.e. observed in the Wolgast 1a well (12 km distance to Loissin 1), indicate at least 105 °C maximum burial temperature corresponding to a maximum burial depth of c. 2,500 m (bold grey line). However, temperature history modelling of Friberg (2001) resulted in c. 50 °C maximum burial temperature (thin black and grey lines) only. **(B)** Simplified diagenetic pathways, during which pore-filling eogenetic carbonate cementation contributed to the stabilisation of the grain fabric in the mesogenetic stage. The following uplift to shallow burial depth triggered dissolution of carbonate cements in the telogenetic regime resulting in large volumes of secondary porosity; IGV – intergranular volume.

The Cretaceous–Cenozoic basin history was characterised by increasing differentiation of the North German Basin (Jaritz, 1969; Nöldeke and Schwab, 1977; Ziegler, 1990). In the eastern North German Basin, moderate thicknesses of the discontinuous Late Cretaceous–Cenozoic succession of up to c. 700 m resulted in shallow to moderate reburial of the Stuttgart Formation (Fig. 3.2). Apart from minor mechanical compaction of the grain fabric, the sandstones of the Stuttgart Formation did not undergo a second prograde diagenesis in this part of the basin (Fig. 3.17). In contrast, thicknesses of Late Cretaceous–Cenozoic of up to 2,500 m in the western part of the basin resulted in deep reburial of pre-Cretaceous strata. Consequently, the second prograde diagenesis resulted in mechanical compaction of grain fabrics, late-stage authigenesis of sulphate, quartz, and halite in sandstones of the Keuper Group (e.g. Heling, 1965; Füchtbauer, 1973; Baermann et al., 2000; Wagner et al., 2005).

### 3.6 Conclusions

The herein proposed types of sandstone diagenesis provide further constraints on the control of depositional environments on paragenetic sequences of authigenic minerals.

As demonstrated herein, fluvio-deltaic depositional environments of the Stuttgart Formation had direct impact on the eogenetic succession of authigenic minerals. Of particular importance for hydrothermal reservoirs are pervasive early-stage cementations, which prevented grain fabrics from mechanical compaction during burial diagenesis. The preservation of pre-burial intergranular volumes is an important prerequisite for the late-stage evolution of large secondary porosity. This is further emphasised by herein reported cases of incomplete early-stage cementation, which resulted in irreversible mechanical compaction of grain fabrics during burial diagenesis. Consequently, the late-stage secondary porosity volumes are significantly reduced. As the successful development of hydrothermal reservoirs requires reliable predictions of permeable sandstones, the herein proposed diagenesis types will make a significant contribution, in particular when combined with available subsurface facies mappings.

The herein proposed model of cementation-controlled burial diagenesis, followed by dissolution-controlled retrograde diagenesis (uplift) and low to moderate reburial corresponds to the Mesozoic–Cenozoic evolution of larger parts of the North German Basin. Thus, the diagenesis model can be applied to predictions of other reservoirs, i.e. Rhaetian reservoirs, within the Mesozoic succession of the North German Basin. The application to other subbasins of the Central European Basin System, such as the Lower Saxony Basin, is limited due to significant differences in the latest Jurassic–Cenozoic basin history.

## **Acknowledgement**

The authors acknowledge funding by the Federal Ministry for Economic Affairs and Climate Action (BMWK, grant numbers 0325920 and 03EE4011D). The Geological State Surveys of Bayern, Brandenburg, Mecklenburg-Vorpommern, Niedersachsen, and Sachsen-Anhalt kindly provided access to core repositories. The support of Graciela M. Sosa, Alfons M. van den Kerkhof, and Volker Karius (University of Göttingen), Christian Buse (Geothermie Neubrandenburg GmbH), Kerstin Nowak (Halle), and Werner Ehrmann (University of Leipzig) with Cathodoluminescence, XRD and SEM-EDX analyses is gratefully acknowledged. The authors acknowledge guidance of Gerhard H. Bachmann (University of Halle-Wittenberg) and Jens Barnasch (K+S Kassel) to outcrops in South Germany and Weserbergland, valuable discussions with Markus Wolfgramm (Schwerin), the constructive review of Reinhard Gaupp (University of Jena) and the editorial handling of Salvatore Critelli (University of Calabria).

## References

- Aagaard, P., Egeberg, P.K., Saigal, G.C., Morad, S., Bjørlykke, K., 1990. Diagenetic albitization of detrital K-feldspars in Jurassic, Lower Cretaceous and Tertiary reservoir rocks from offshore Norway, II. Formation water chemistry and kinetic considerations. *Journal of Sedimentary Petrology* 60, 575–581. <https://doi.org/10.1306/212F91EC-2B24-11D7-8648000102C1865D>.
- Abouessa, A., Morad, A., 2009. An integrated study of diagenesis and depositional facies in tidal sandstones: Hawaz Formation (middle Ordovician), Murzuq Basin, Libya. *Journal of Petroleum Geology* 32(1), 39–65. <https://doi.org/10.1111/j.1747-5457.2009.00434.x>.
- Agemar, T., Schellschmidt, R., Schulz, R., 2012. Subsurface Temperature Distribution of Germany. *Geothermics*, 44, 65–77. <https://doi.org/10.1016/j.geothermics.2012.07.002>.
- Anjos, S.M.C., De Ros, L.F., de Souza, R.S., de Assis Silva, C.M., Sombra, C.L., 2000. Depositional and diagenetic controls on the reservoir quality of Lower Cretaceous Pendencia sandstones, Potiguar rift basin. *Braz. AAPG Bull.* 84, 1719–1742. <https://doi.org/10.1306/8626C375-173B-11D7-8645000102C1865D>.
- Atkins, J.E., McBride, E.F., 1992. Porosity and packing of Holocene river, dune, and beach sands: *AAPG Bulletin*, v. 76, 339–355. <https://doi.org/10.1306/BDFF87F4-1718-11D7-8645000102C1865D>.
- Bachmann, G.H., Brunner, H., 2002. Nordwürttemberg. Stuttgart, Heilbronn und weitere Umgebung. *Samml. Geol. Führer*, 90, 403 pp., Berlin (Borntraeger).
- Bachmann, G.H., Hiltmann, W., Lerche, I., 2002. Inkohlung des Unteren Keupers in Südwestdeutschland. *Neues Jahrbuch für Geologie und Paläontologie, Abhandlungen* 226, 271–288. <https://doi.org/10.1127/njgpa/226/2002/271>.
- Bachmann, G.H., Geluk, M.C., Warrington, G., Becker-Roman, A., Beutler, G., Hagdorn, H., Hounslow, M.W., Nitsch, E., Röhling, H.-G., Simon, T., Szulc, A., with contributions by Duser, M., Nielsen, L.H., Barnasch, J., Franz, M. (2010): Triassic. In: Doornenbal, J.C., Stevenson, A.G. (Eds.), *Petroleum Geological Atlas of the Southern Permian Basin Area*, Houten (EAGE Publ.), pp. 149–173.
- Bachmann, G.H., Grosse, S., 1989. Struktur und Entstehung des Norddeutschen Beckens – geologisch-geophysikalische Interpretation einer verbesserten Bouguer-Schwerkarte. – *Niedersächsische Akademie der Geowissenschaften Veröffentlichungen* 2, 23–47.

- Bachmann, G.H., Wild, H., 1976. Die Grenze Gipskeuper/Schilfsandstein bei Heilbronn/Neckar. – Jber. Mitt. Oberrhein. Geol. Ver., 58: 137–152.
- Baermann, A., Kröger, J., Taug, R., Wüstenhagen, K., Zarth, M., 2000. Anhydritzemente im Rhätsandstein Hamburgs – Morphologie und Strukturen. Zeitschrift für angewandte Geologie 46, 2–7.
- Baldschuhn, R., Binot, F., Fleig, S., Kockel, F., 2001. Geotektonischer Atlas von NW Deutschland und dem deutschen Nordsee-Sektor. Geologisches Jahrbuch Reihe A, 153, Hannover.
- Bally, A., Snelson, S., 1980. Realms of subsidence, in: Miall, A.D. (Ed.), Facts and Principles of World Petroleum Occurrence. Canadian Society of Petroleum Geologists, Memoirs, 6, pp. 9–94.
- Barnasch, J., 2010. Der Keuper im Westteil des Zentraleuropäischen Beckens (Deutschland, Niederlande, England, Dänemark): diskontinuierliche Sedimentation, Litho-, Zyklo- und Sequenzstratigraphie. Schriftenreihe der Deutschen Gesellschaft für Geowissenschaften, 7–169. <https://doi.org/10.1127/sdgg/71/2010/7>.
- Baumgarten, H., 2010. Die Wealden-Sandsteine als Reinjektionshorizont in der Bohrung Groß-Buchholz GT-1: Gesteinsphysikalische und sedimentpetrographische Charakterisierung (Doctoral dissertation, Diplomarbeit, Leibniz-Universität Hannover).
- Berger, A., Gier, S., Krois, P., 2009. Porosity-preserving chlorite cements in shallow-marine volcanoclastic sandstones: evidence from Cretaceous sandstones of the Sawan gas field. Pak. AAPG Bull. 93, 595–615. <https://doi.org/10.1306/01300908096>.
- Berner, R.A., 1970. Sedimentary pyrite formation. American Journal of Science 268, 1–23. <https://doi.org/10.2475/ajs.268.1.1>.
- Berner, R.A., 1981. Authigenic mineral formation resulting from organic matter decomposition in modern sediments. Fortschritte der Mineralogie 59, 117–135.
- Berner, R.A., 1984. Sedimentary pyrite formation. An update: Geochimica et Cosmochimica Acta 48, 605–615. [https://doi.org/10.1016/0016-7037\(84\)90089-9](https://doi.org/10.1016/0016-7037(84)90089-9).
- Beutler, G., 1976. Zur Ausbildung und Gliederung des Keupers in NE-Mecklenburg. – Jb. Geol., 7/8, 119–126.
- Beutler, G., Häusser, I., 1982. Über den Schilfsandstein der DDR. Zeitschrift für Geologische Wissenschaften 10(4), 511–525.

- Beutler, G., Röhling, H.G., Schulz, R., Werner, K.H., 1994. Regionale Untersuchungen von geothermischen Reserven und Ressourcen in Nordwestdeutschland. – Endbericht, Archivnr. 111 758; Hannover (GGA).
- Beyer, D., 2015. Evolution of reservoir properties in the Lower Triassic aquifer sandstones of the Thuringian Syncline in Central Germany (Doctoral dissertation).
- Bjørlykke, K., 2014. Relationships between depositional environments, burial history and rock properties. Some principal aspects of diagenetic process in sedimentary basins. *Sedimentary Geology* 301, 1–14. <https://doi.org/10.1016/j.sedgeo.2013.12.002>.
- Boles, J.R., Franks, S.G., 1979. Clay diagenesis in Wilcox sandstones of Southwest Texas; implications of smectite diagenesis on sandstone cementation. *Journal of Sedimentary Research*, 49(1), 55–70.
- Brecht, G.A., 1999. Authigene Phyllosilikate in permokarbonen SiO<sub>2</sub>-reichen Vulkaniten Ostdeutschlands. *Berliner geowiss. Abh.* A201, 1–181.
- Bruns, B., di Primio, R., Berner, U., Littke, R., 2013. Petroleum system evolution in the inverted Lower Saxony Basin, northwest Germany: a 3D basin modeling study. *Geofluids* 13, 246–271. <http://dx.doi.org/10.1111/gfl.12016>.
- Burley S.D., 1986. The development and destruction of porosity within Upper Jurassic reservoir sandstones of the Piper and Tartan Fields, Outer Moray Firth, North Sea. *Clay Min* 21, 649–694. <https://doi.org/10.1180/claymin.1986.021.4.14>.
- Burley, S.D., Kantorowicz, J.D., Waugh, B., 1985. Clastic diagenesis, in: Brenchley, P., Williams, B.P.B. (Eds.), *Sedimentology: Recent and Applied Aspects*, Spec. Publ. Geol. Soc. London 18, pp. 189–226.
- Chang, H.K., Mackenzie, F.T., Schoonmaker, J., 1986. Comparisons between the diagenesis of dioctahedral and trioctahedral smectite, Brazilian offshore basins. *Clays and Clay Minerals*, 34(4), 407–423. <https://doi.org/10.1346/CCMN.1986.0340408>.
- Coombs, D.S., 1965. Sedimentary analcime rocks and sodium-rich gneisses. *Mineralogical Magazine* 34, 144–158. <https://doi.org/10.1180/minmag.1965.034.268.12>.
- Coombs, D.S., Whetten, J.T., 1967. Composition of analcime from sedimentary and burial metamorphic rocks. *Geol. Soc. America Bull.* 78, 269–82. [https://doi.org/10.1130/0016-7606\(1967\)78\[269:COAFSA\]2.0.CO;2](https://doi.org/10.1130/0016-7606(1967)78[269:COAFSA]2.0.CO;2).

- Curtis, C.D., 1987. Mineralogical consequences of organic matter degradation in sediments: inorganic/organic diagenesis, in: Leggett, J.K., Zuffa, G.G., (Eds.), *Marine Clastic Sedimentology*. Graham and Trotman, London, pp. 108–123.
- Diener, I., Pasternak, G., Rustizka, I., Stollberg, K., Tessin, R., Wormbs, J., Katzung, G., 1988: Geothermische Ressourcen im Nordteil der DDR (I) – Blatt Neuruppin. – ZGI Berlin.
- Diener, I., Pasternak, G., Stollberg, K., Tesch, M., Tessin, R., Toleikis, R., Wormbs, J., 1990a: Geothermische Ressourcen im Nordteil der DDR (II) – Blatt Eberswalde/Bad Freienwalde. – ZGI Berlin.
- Diener, I., Pasternak, G., Stollberg, K., Tesch, M., Tessin, R., Toleikis, R., Wormbs, J., 1990b: Geothermische Perspektivitätsbewertung für die Geothermienutzung in NE-Deutschland – Blatt Berlin/Frankfurt O. – UWG mbH Berlin.
- Diener, I., Pasternak, G., Stollberg, K., 1991: Geologische Grundlagen für die Geothermienutzung in Nordost-Deutschland – Blatt Magdeburg/Brandenburg. – UWG mbH Berlin.
- Diener, I., Wormbs, J., Rustizka, I., Pasternak, G., Toleikis, R., Tessin, R., Trottnner, D., Wunderlich, H., 1989: Geothermische Ressourcen im N-Teil der DDR (I) – Blatt Schwerin/Bad Doberan. – ZGI Berlin.
- Diener, I., Wormbs, J., Pasternak, G., Stollberg, K., Tesch, M., Tessin, R., 1992a: Geologische Grundlagen zur Geothermienutzung in Nordost-Deutschland – Blatt Rostock/Stralsund. – UWG mbH Berlin.
- Diener, I., Wormbs, J., Pasternak, G., Stollberg, K., Tesch, M., Tessin, R., Toleikis, R., 1992b: Geologische Grundlagen für die Geothermienutzung in Nordost-Deutschland (Kartenwerk) – Blatt Salzwedel. – UWG mbH Berlin.
- Diener, I., Tesch, M., Pasternak, G., 1992c: Geologische Grundlagen für die Geothermienutzung in Nordost-Deutschland – Blatt Finsterwalde/Cottbus. – UWG mbH Berlin.
- Do Campo, M., del Papa, C., Jiménez-Millán, J., Nieto, F., 2007. Clay mineral assemblages and analcime formation in a Palaeogene fluvial–lacustrine sequence (Maíz Gordo Formation Palaeogene) from northwestern Argentina. *Sediment. Geol.* 201, 56–74. <https://doi.org/10.1016/j.sedgeo.2007.04.007>.
- Dockter, J., Langbein, R., Seidel, G., 1967. Keuper in Thüringen. Abschlussbericht (unpublished).



- Dockter, J., Schubert, J., 2005. Der Keuper in Thüringen und im thüringischen Grabfeld. – In: DSK – Deutsche Stratigraphische Kommission (Ed.), Stratigraphie von Deutschland, IV. Keuper. Courier Forschungsinstitut Senckenberg, 253, pp. 192–202.
- Dowey, P.J., Hodgson, D.M., Worden, R.H., 2012. Pre-requisites, processes, and prediction of chlorite grain coatings in petroleum reservoirs: a review of subsurface examples. *Marine Petroleum Geology* 32, 63–75. <https://doi.org/10.1016/j.marpetgeo.2011.11.007>.
- DSK (Deutsche Stratigraphische Kommission) (Ed.), 2005. Stratigraphie von Deutschland, IV: Keuper. Courier Forschungsinstitut Senckenberg 253.
- Duchrow, H., 1984. Der Keuper im Osnabrücker Bergland, in: Klasen, H. (Ed.), Geologie des Osnabrücker Berglandes. Naturwiss. Mus. Osnabrück, pp. 221–333.
- Duschl, F., Van den Kerkhof, A.M., Sosa, G., Leiss, B., Wiegand, B., Vollbrecht, A., Sauter, M., 2016. Fluid inclusion and microfabric studies on Zechstein carbonates (Ca<sup>2</sup>) and related fracture mineralizations – New insights on gas migration in the Lower Saxony Basin (Germany). *Marine and Petroleum Geology* 77, 300–322. <http://dx.doi.org/10.1016/j.marpetgeo.2016.06.020>.
- Dypvik, H., 1983. Clay mineral Transformations in Tertiary and Mesozoic Sediments from North Sea. *Bull. Am. Ass. Petrol. Geol.* 67, 160–165. <https://doi.org/10.1306/03B5ACDC-16D1-11D7-8645000102C1865D>.
- Ehrenberg, S.N., 1989. Assessing the relative importance of compaction processes and cementation to reduction of porosity in sandstones: discussion; compaction and porosity evolution of Pliocene sandstones, Ventura Basin, California: discussion. *American Association of Petroleum Geologists Bulletin* 73, 1274–1276. <https://doi.org/10.1306/44B4AA1E-170A-11D7-8645000102C1865D>.
- Ehrenberg, S.N., Nadeau, P.H., 1989. Formation of diagenetic illite in sandstones of the Garn Formation, Haltenbanken area, mid-Norwegian continental shelf. *Clay Minerals* 24, 233–253. <https://doi.org/10.1180/claymin.1989.024.2.09>.
- English, P.M., 2001. Formation of analcime and moganite at Lake Lewis, central Australia: significance of groundwater evolution in diagenesis. *Sedimentary Geology* 143, 219–244. [https://doi.org/10.1016/S0037-0738\(01\)00063-X](https://doi.org/10.1016/S0037-0738(01)00063-X).
- Erlström, M., Boldreel, L.O., Lindström, S., Kristensen, L., Mathiesen, A., Andersen, M.S., Nielsen, L.H., 2018. Stratigraphy and geothermal assessment of Mesozoic sandstone reservoirs in the Øresund Basin—exemplified by well data and seismic

- profiles. *Bulletin of the Geological Society of Denmark*, 66, 123–149.  
<https://doi.org/10.37570/bgsd-2018-66-06>.
- Etzold, A., Schweizer, V., 2005. Der Keuper in Baden-Württemberg, in: DSK – Deutsche Stratigraphische Kommission (Ed.), *Stratigraphie von Deutschland*, IV. Keuper. – *Cour. Forschungsinst. Senckenb.*, 253: 214–258.
- Feldrappe, H., Obst, K., Wolfgramm, M., 2008. Die mesozoischen Aquifere des Norddeutschen Beckens und ihr Potential für die geothermische Nutzung. – *Zeitschrift für geologische Wissenschaften*, 36 (4–5), 199–222.
- Fine, S., 1986. The diagenesis of the Lower Triassic Bunter Sandstone Formation, Onshore Denmark. *Geol. Surv. Den., Ser. A*, 15.
- Folk, R.L., Ward, W.C., 1957. Brazos River bar: a study in the significance of grain size parameters. *Journal of Sedimentary Petrology* 27, 3–26.  
<http://dx.doi.org/10.1306/74D70646-2B21-11D7-8648000102C1865D>.
- Förster, A., Schöner, R., Förster, H.-J., Norden, B., Blaschke, A.-W., Luckert, J., Beutler, G., Gaupp, R., Rhede, D., 2010. Reservoir characterization of a CO<sub>2</sub> storage aquifer: The Upper Triassic Stuttgart Formation in the Northeast German Basin. *Marine and Petroleum Geology* 27, 2156–2172.  
<https://doi.org/10.1016/j.marpetgeo.2010.07.010>.
- Franz, M., Nowak, K., Berner, U., Heunisch, C., Bandel, K., Röhling, H.-G., Wolfgramm, M., 2014. Eustatic control on epicontinental basins: the example of the Stuttgart Formation in the Central European Basin (Middle Keuper, Late Triassic). *Global and Planetary Change* 122, 305–329.  
<https://doi.org/10.1016/j.gloplacha.2014.07.010>.
- Franz, M., Wolfgramm, M., Barth, G., Nowak, K., Zimmermann, J., Budach, I., Thorwart, K., 2015. Verbundprojekt: Identifikation hydraulisch geeigneter Bereiche innerhalb der mesozoischen Sandsteinaquifere in Norddeutschland – Sandsteinfazies. Forschungsvorhaben, Dokumentation, Schlussbericht. TU Bergakademie Freiberg.
- Franz, M., Barth, G., Zimmermann, J., Budach, I., Nowak, N., Wolfgramm, M., 2018a. Deep geothermal resources of the North German Basin: exploration examples of Mesozoic hydrothermal reservoirs, in: Kilhams, B., Kukla, P.A., Mazur, S., Mckie, T., Mijnlief, H.F., van Ojik, K. (Eds.), *Mesozoic Resource Potential in the Southern Permian Basin*. *Geol. Soc. London, Spec. Publ.* 469, pp. 193–222.  
<https://doi.org/10.1144/SP469.11>.

- Franz, M., Nowak, K., Niegel, S., Seidel, E., Wolf, M., Wolfgramm, M., 2018b. Deep geothermal resources of the North German Basin: The hydrothermal reservoirs of the Stuttgart Formation (Schilfsandstein, Upper Triassic). *Zeitschrift der Deutschen Gesellschaft für Geowissenschaften* 169 (3) 353–387. <https://doi.org/10.1127/zdgg/2018/0164>.
- Franz, M., Kustatscher, E., Heunisch, C., Niegel, S., Röhling, H.-G., 2019. The Schilfsandstein and its flora – arguments for a humid mid-Carnian episode? *J. Geol. Soc. London* 176, 133–148. <https://doi.org/10.1144/jgs2018-053>.
- Franz, M., Wolfgramm, M., 2019. Geothermie Schwerin-Lankow – ein Leuchtturmprojekt im Norddeutschen Becken. *Geothermische Energie* 93, 10–13.
- Franz, M., Barnasch, J., 2021. Der Keuper im zentralen Germanischen Becken, in: Hauschke, N., Franz, M., Bachmann, G.H. (Eds.), *Trias – Aufbruch in das Erdmittelalter*, München: Pfeil, 83–108.
- Freudenberger, W., 2005. Der Keuper in Franken und der Oberpfalz (Bayern), in: DSK – Deutsche Stratigraphische Kommission (Ed.), *Stratigraphie von Deutschland, IV. Keuper*. *Cour. Forschungsinst. Senckenb.*, 253: 203–213.
- Friberg, L.J., 2001. Untersuchungen zur Temperatur- und Absenkungsgeschichte sowie zur Bildung und Migration von Methan und molekularem Stickstoff im Nordostdeutschen Becken. *Ber. Forschungszentrum Jülich* 3914, 1–248.
- Friis, H., 1987. Diagenesis of the Gassum formation Rhaetian-lower Jurassic, Danish Subbasin. *Danmarks Geologiske Undersøgelse Serie A*, 18, pp. 1–41. <https://doi.org/10.34194/seriea.v18.7037>.
- Füchtbauer, H., 1967. Influence of depositional environment on diagenesis of the Triassic Bunter sandstones. *Sedimentary Geology*, 1, 159–179.
- Füchtbauer, H., 1973. Zur Diagenese fluviatiler Sandsteine. *Geologische Rundschau* 63, 904–925.
- Füchtbauer, H., 1974. *Sediments and Sedimentary Rocks*, 1. Wiley, New York.
- Füchtbauer, H., 1988. *Sedimente und Sedimentgesteine*. E. Schweizerbart'sche Verlagsbuchhandlung, Stuttgart.
- Gast, R., Pasternack, M., Piske, J., Rasch, H.-J., 1998. Das Rotliegend im Nordostdeutschen Raum: Regionale Übersicht, Stratigraphie, Fazies und Diagenese. *Geologisches Jahrbuch*, A149, 59–80.

- Gaupp, R., 1991. Zur Fazies und Diagenese des Mittelrhät-Hauptsandsteins im Gasfeld Thönse. Das Gasfeld Thönse in Niedersachsen - ein Unikat, Niedersächsische Akademie der Geowissenschaften Veröffentlichungen 6, 34–55.
- Gaupp, R., 1996. Diagenesis types and their application in diagenesis mapping. Zentralblatt für Geologie und Paläontologie Teil I, 1994 (11/12), 1183–1199.
- Gaupp, R., Matter, A., Platt, J., Ramseyer, K., Walzebuck, J., 1993. Diagenesis and fluid evolution of deeply buried Permian (Rotliegende) Gas Reservoirs. AAPG, V77, 7, 1111–1128.
- Gehrmann, O., Aigner, T., 2002. Der Schilfsandstein (Obere Trias) bei Heilbronn (SW-Deutschland): Hinweise auf tidale Einflüsse. Neues Jb. Geol. Paläontol. Abh. 223, 377–403. <https://doi.org/10.1127/njgpa/223/2002/377>.
- Geyer, G., Kelber, K.-P., 2018. Spinicaudata („Conchostraca“, Crustacea) from the Middle Keuper (Upper Triassic) of the southern Germanic Basin, with a review of Carnian–Norian taxa and suggested biozones. Paläontol. Z. 92, 1–34. <https://doi.org/10.1007/s12542-017-0363-7>.
- Glasmann J.R., Lundegard P.D., Clark R.A., Penny B.K., Collins I.D., 1989. Geochemical evidence for the history of diagenesis and fluid migration: Brent Sandstones, Heather Field. North Sea. Clay Minerals 24, 255–284. <https://doi.org/10.1180/claymin.1989.024.2.10>.
- Glennie, K.W., Mudd, G.C., Nagtegaal, P.J.C., 1978. Depositional environment and diagenesis of Permian Rotliegendes sandstones in Leman Bank and Sole Pit areas of the U.K. Southern North Sea. Journal of the Geological Society, 135(1), 25–34. <https://doi.org/10.1144/gsjgs.135.1.0025>.
- Goodwin, J.H., Surdam, R.C., 1967. Zeolitization of tuffaceous rocks of the Green River Formation, Wyoming: Science 157, 307–308. <https://doi.org/10.1126/science.157.3786.307>.
- Gould, K., Pe-Piper, G., Piper, D.J.W., 2010. Relationship of diagenetic chlorite rims to depositional facies in Lower Cretaceous reservoir sandstones of the Scotian Basin. Sedimentology 57, 587–610. <https://doi.org/10.1111/j.1365-3091.2009.01106.x>.
- Hammer, E., Mørk, M., Naess, A., 2010. Facies controls on the diagenesis and compaction in fluvial-deltaic deposits. Marine and Petroleum Geology 27, 1737–1751. <https://doi.org/10.1016/j.marpetgeo.2009.11.002>.

- Hancock, N.J., 1978. Possible causes of Rotliegend sandstone diagenesis in northern West Germany. *Journal of the Geological Society*, 135(1), 35–40. <https://doi.org/10.1144/gsjgs.135.1.0035>.
- Häusser, I., 1972. Zur sedimentpetrographischen Analyse der Sandsteifolgen des Unteren und Mittleren Keupers im Nordteil der DDR. – Ph.D. thesis Bergakad. Freiberg, 111 p. [unpubl.].
- Häusser, I., Kurze, M., 1975. Sedimentationsbedingungen und Schwermineralführung im Mesozoikum des Nordteils der DDR. *Zeitschrift für Geologische Wissenschaften* 3, 1317–1332.
- Hay R.L., 1978. Zeolites in sedimentary rocks. *Sedimentology*. *Encyclopedia of Earth Science*. Springer, Berlin, Heidelberg. [https://doi.org/10.1007/3-540-31079-7\\_251](https://doi.org/10.1007/3-540-31079-7_251).
- Hay, R.L., 1966. Zeolites and zeolitic reactions in sedimentary rocks. *Geological Society of America Special Paper* 85, 1–130. <https://doi.org/10.1130/SPE85-p1>.
- Hay, R.L., Sheppard, R.A., 2001. Occurrence of zeolites in sedimentary rocks: An overview. *Reviews in mineralogy and geochemistry*, 45(1), 217–234. <https://doi.org/10.2138/rmg.2001.45.6>.
- Heling, D., 1963. Zur Petrographie des Stubensandsteins Petrographische Untersuchungen an einem Stubensandsteinprofil östlich Stuttgart. *Beiträge zur Mineralogie und Petrographie*, 9(3), 251–284. <https://doi.org/10.1007/BF02650154>.
- Heling, D., 1965. Zur Petrographie des Schilfsandsteins. *Beiträge zur Mineralogie und Petrographie* 11, 272–296. <https://doi.org/10.1007/BF01172137>.
- Heling, D., Beyer, M., 1992. Glaukonit im Schilfsandstein: Schlüssel zur kontroversen Faziesanalyse? *Jahresberichte und Mitteilungen des Oberrheinischen Geologischen Vereins, Neue Folge* 74, 191–213. <https://dx.doi.org/10.1127/jmogv/74/1992/191>.
- Hesse, R., Gaupp, R., 2021. *Diagenese klastischer Sedimente*. Springer Spektrum, Berlin, Heidelberg. <https://doi.org/10.1007/978-3-662-59685-2>.
- Heunisch, C., 1999. Die Bedeutung der Palynologie für Biostratigraphie und Fazies in der Germanischen Trias, in: Hauschke, N., Wilde, V. (Eds.), *Trias: eine ganz andere Welt*. Pfeil-Verlag, München, pp. 13–21.
- Hiatt, E.E., Kyser, T.K., 2000. Links between Depositional and Diagenetic Processes in Basin Analysis: Porosity and Permeability Evolution in Sedimentary Rocks, in: Kyser, K. (Ed.), *Fluids and Basin Evolution*, Chapter: 4, Mineralogical Association of Canada, pp. 63–92.

- Hoth, K., Rusbült, J., Zagora, K., Beer, H., Hartmann, O., 1993. Die tiefen Bohrungen im Zentralabschnitt der Mitteleuropäischen Senke – Dokumentation für den Zeitabschnitt 1962–1990. Schriftenreihe für Geowissenschaften 2, Gesellschaft für Geowissenschaften e. V. (i. G.), Berlin.
- Hoth, P., 1997. Fazies und Diagenese von Präperm-Sedimenten der Geotraverse Harz–Rügen. Schriftenr. Geowiss. 4.
- Houseknecht, D.W., 1987. Assessing the relative importance of compaction processes and cementation to reduction of porosity in sandstones. AAPG Bulletin 71, 633–642.
- Hurst, A., Irwin, H., 1982. Geological modelling of clay diagenesis in sandstones. Clay Minerals, 17, 5–22. <https://doi.org/10.1180/claymin.1982.017.1.03>.
- Iijima, A., 1988. Diagenetic transformation of minerals as exemplified by zeolites and silica minerals, in: Chilingarian, G.V., Wolf, K.H. (Eds.), *Diagenesis II, Developments in Sedimentology*. Elsevier Science Publishers, Amsterdam, pp. 147–211. [https://doi.org/10.1016/S0070-4571\(08\)70008-6](https://doi.org/10.1016/S0070-4571(08)70008-6).
- Japsen, P., Green, P.F., Nielsen, L.H., Rasmussen, E.S., Bidstrup, T., 2007. Mesozoic–Cenozoic exhumation events in the eastern North Sea Basin: a multi-disciplinary study based on palaeothermal, palaeoburial, stratigraphic and seismic data. Basin Research, 19, 451–490. <https://doi.org/10.1111/j.1365-2117.2007.00329.x>.
- Japsen, P., Green, P.F., Bonow, J.M., Erlström, M., 2016. Episodic burial and exhumation of the southern Baltic Shield: Epeirogenic uplifts during and after break-up of Pangea. Gondwana Research, 35, 357–377. <https://doi.org/10.1016/j.gr.2015.06.005>.
- Jaritz, W., 1969. Epirogenese in Nordwestdeutschland im höheren Jura und in der Unterkreide. Geologische Rundschau, 59(1), 114–124. <https://doi.org/10.1007/BF01824946>.
- Jaritz, W., 1974. Zur Entstehung der Salzstrukturen Nordwestdeutschlands [On the formation of salt structures in NW Germany]. Geologisches Jahrbuch, 10, 1–77.
- Jaritz, W., 1980. Einige Aspekte der Entwicklungsgeschichte der nordwestdeutschen Salzstöcke. Zeitschrift der deutschen geologischen Gesellschaft, 131, 387–408. <https://doi.org/10.1127/zdgg/131/1980/387>.
- Jaritz, W., 1987. The origin and development of salt structures in Northwest Germany, in: Lerche, I., O'Brien, J.J. (Eds.), *Dynamical Geology of Salt and Related Structures*. Academic Press, Orlando, FL, USA, pp. 479–493.

- John, H., 1975. Hebungs- und Senkungsvorgänge in Nordwestdeutschland. *Erdöl und Kohle*, 28, 273–277.
- Johnsson, M.J., Meade, R.H., 1990. Chemical weathering of fluvial sediments during alluvial storage; the Macuapanim Island point bar, Solimoes River, Brazil. *Journal of Sedimentary Research* 60 (6): 827–842. doi: <https://doi.org/10.1306/212F9296-2B24-11D7-8648000102C1865D>.
- Kasina M., Bock, S., Würdemann, H., Pudlo, D., Picard, A., Lichtschlag, A., März C., Wagenknecht, L., Wehrmann, L.M., Vogt, C., Ferdelman T.G., Meister, P., 2017. Mineralogical and geochemical analysis of Fe-phases in drill-cores from the Triassic Stuttgart Formation at Ketzin CO<sub>2</sub> storage site before CO<sub>2</sub> arrival. *Environmental Earth Sciences* 76 (161), 1–20. <https://doi.org/10.1007/s12665-017-6460-9>.
- Katzung, G., 1984. *Geothermie-Atlas der Deutschen Demokratischen Republik*. Zentrales Geologisches Institut Berlin.
- Katzung, G., 2004. Geothermie, in: Katzung, G. (Ed.), *Geologie von Mecklenburg-Vorpommern*. Schweizerbart'sche Verlagsbuchhandlung, Stuttgart, pp. 444–451.
- Khalifa, M., Morad, S., 2012. Impact of structural setting on diagenesis of fluvial and tidal sandstones: The Bahi Formation, Upper Cretaceous, NW Sirt Basin, North Central Libya. *Marine and Petroleum Geology* 38(1), 211–231. <https://doi.org/10.1016/j.marpetgeo.2011.05.006>.
- Khalifa, M.A., Morad, S., 2015. Impact of depositional facies on the distribution of diagenetic alterations in the Devonian shoreface sandstone reservoirs, Southern Ghadamis Basin, Libya. *Sedimentary Geology* 329, 62–80. <https://doi.org/10.1016/j.sedgeo.2015.09.003>.
- Kley, J., Franzke, H.J., Jähne, F., Krawczyk, C., Lohr, T., Reicherter, K., Scheck-Wenderoth, M., Sippel, J., Tanner, D., van Gent, H., the SPP 1135 Structural Geology Group, 2008. Strain and stress, in: Littke, R., Bayer, U., Gajewski, D., Nelskamp, S. (Eds.), *Dynamics of complex intracontinental basins: the Central European Basin System*. Springer, Berlin, pp. 97–124.
- Kley, J., Voigt, T., 2008. Late Cretaceous intraplate thrusting in central Europe: effect of Africa–Iberia–Europe convergence, not Alpine collision. *Geology*, 36, 839–842. <https://doi.org/10.1130/G24930A.1>.
- Kossow, D., Krawczyk, C., McCann, T., Strecker, M., Negendank, J. F., 2000. Style and evolution of salt pillows and related structures in the northern part of the

- Northeast German Basin. *International Journal of earth sciences*, 89(3), 652–664. <http://dx.doi.org/10.1007/s005310000116>.
- Kossow, D., Krawczyk, C., 2002. Structure and quantification of processes controlling the evolution of the inverted NE-German Basin. *Marine and Petroleum Geology* 19, 601–618. [http://dx.doi.org/10.1016/S0264-8172\(02\)00032-6](http://dx.doi.org/10.1016/S0264-8172(02)00032-6).
- Kozur, H.W., Bachmann, G.H., 2010. The Middle Carnian Wet Intermezzo of the Stuttgart Formation (Schilfsandstein), Germanic Basin. *Palaeogeography, Palaeoclimatology, Palaeoecology* 290, 107–119. <https://doi.org/10.1016/j.palaeo.2009.11.004>.
- Krainer, K., Spötl, C., 1989. Detrital and authigenic feldspars in Permian and early Triassic sandstones, Eastern Alps (Austria). *Sediment. Geol.* 62, 59–77. [https://doi.org/10.1016/0037-0738\(89\)90101-2](https://doi.org/10.1016/0037-0738(89)90101-2).
- Kruck, W., Wolf, F., 1975. Ergebnisse einer Fazieskartierung im Schilfsandstein des Weserberglandes. – *Mitt. Geol.-Paläont. Inst. Univ. Hamburg*, 44: 417–421.
- Kulke, H., 1969. Petrographie und Diagenese des Stubensandsteines (mittlerer Keuper) aus Tiefbohrungen im Raum Memmingen (Bayern). *Contr. Mineral. and Petrol.*, 20, 135–163. <https://doi.org/10.1007/BF00399628>.
- Lan, C., Yang, M., Zhang, Y., 2016. Impact of sequence stratigraphy, depositional facies and diagenesis on reservoir quality: A case study on the Pennsylvanian Taiyuan sandstones, northeastern Ordos Basin, China. *Marine and Petroleum Geology* 69, 216–230. <https://doi.org/10.1016/j.marpetgeo.2015.09.009>.
- Leveille, G.P., Knipe, R., More, C., Ellis, D., Dudley, G., Jones, G., Fisher, Q.J., Allinson, G., 1997. Compartmentalization of Rotliegendes gas reservoirs by sealing faults, Jupiter Fields area, southern North Sea, in: Ziegler, K., Turner, P., Daines, S.R. (Eds.), *Petroleum Geology of the Southern North Sea: Future Potential*, Geological Society of London, Special Publications, 123(1), pp. 87–104.
- Lima, R.D., De Ros, L.F., 2002. The role of depositional setting and diagenesis on the reservoir quality of Devonian sandstones from the Solimões Basin, Brazilian Amazonia. *Marine and Petroleum Geology* 19, 1047–1071. [https://doi.org/10.1016/S0264-8172\(03\)00002-3](https://doi.org/10.1016/S0264-8172(03)00002-3).
- Lin, L., Yu, Y., Nan, H., Chen, H., 2022. Petrologic and geochemical characteristics of carbonate cements in the Upper Triassic Xujiache Formation tight gas sandstone, western Sichuan Basin, China. *AAPG Bulletin*, 106 (2): 461–490. <https://doi.org/10.1306/10042119129>.



- Liou, J.G., 1971. Analcime equilibria. *Lithos* 4, 389–402. [https://doi.org/10.1016/0024-4937\(71\)90122-8](https://doi.org/10.1016/0024-4937(71)90122-8).
- Lippmann, R., 2012. Diagenesis in Rotliegend, Triassic and Jurassic clastic hydrocarbon reservoirs of the Central Graben, North Sea. (Ph.D. Thesis) Friedrich-Schiller-Universität Jena, Germany.
- Lotz, B., 2004. Neubewertung des rezenten Wärmestroms im Nordostdeutschen Becken [Reevaluation of the recent heat flow in the North German Basin]. Scientific Technical Report STR 04/04.
- Luo, J.L., Morad, S., Salem, A., Ketzer, J.M., Lie, L., Guo, D.Y., Hlal, O., 2009. Impact of diagenesis on reservoir quality evolution in fluvial and lacustrine-deltaic sandstones: evidence from Jurassic and Triassic Sandstones from the Ordos Basin, China. *Journal of Petroleum Geology* 32, 79–102. <https://doi.org/10.1111/j.1747-5457.2009.00436.x>.
- Ma, P., Lin, C., Zhang, S., Dong, C., Zhao, Y., Dong, D., Shehzad, K., Awais, M., Guo, D., Mu, X., 2018. Diagenetic history and reservoir quality of tight sandstones: A case study from Shiqianfeng sandstones in upper Permian of Dongpu Depression, Bohai Bay Basin, eastern China. *Marine and Petroleum Geology* 89, 280–299. <https://doi.org/10.1016/j.marpetgeo.2017.09.029>.
- Mahler, A., Magtengaard, J., 2010. Country update report for Denmark. Proceedings World Geothermal Congress 2010, Bali, Indonesia, 25-29 April 2010.
- Mansurbeg, H., Morad, S., Salem, A., Marfil, R., El-Ghali, M.A.K., Nystuen, J.P., Caja, M.A., Amorosi, A., Garcia, D. La Iglesia, A., 2008. Diagenesis and reservoir quality evolution of palaeocene deep-water, marine sandstones, the Shetland-Faroes Basin, British continental shelf. *Marine and Petroleum Geology*, 25(6), 514–543. <https://doi.org/10.1016/j.marpetgeo.2007.07.012>.
- McBride, E.F., 1963. A classification of common sandstones. *Journal of Sediment Petrology* 33, 664–669. <https://doi.org/10.1306/74D70EE8-2B21-11D7-8648000102C1865D>.
- McKinley, J., Worden, R., Ruffell, A., 2003. Smectite in sandstones: a review of the controls on occurrence and behavior during diagenesis, in: Worden, R.H., Morad, S. (Eds.), *Clay Mineral Cements in Sandstones* (Special Publication 34 of the IAS). Blackwell Publishing Ltd, Malden, pp. 109–128. <https://doi.org/10.1002/9781444304336.ch5>.

- McNeil, B., Shaw, H.F., Rankin, A.H., 1995. Diagenesis of the Rotliegend Sandstones in the V-Fields, southern North Sea: a fluid inclusion study. Geological Society, London, Special Publications, 86(1), 125–139. <https://doi.org/10.1144/GSL.SP.1995.086.01.10>.
- Meinhold, R., Reinhardt, H.-G., 1967. Halokinese im Nordostdeutschen Tiefland. Berichte der deutschen Gesellschaft für geologische Wissenschaften, Abteilung A 12, 329–353.
- Mijnlieff, H. F., 2020. Introduction to the geothermal play and reservoir geology of the Netherlands. Netherlands Journal of Geosciences, 99, e2. <https://doi.org/10.1017/njg.2020.2>
- Milliken, K.L., McBride, E.F., Land, L.S., 1989. Numerical assessment of dissolution versus replacement in the subsurface destruction of detrital feldspars, Oligocene Frio Formation, South Texas. Journal of Sedimentary Petrology 59, 740–757. <https://doi.org/10.1306/212F9061-2B24-11D7-8648000102C1865D>.
- Miller, C.S., Peterse, F., da Silva, A.-C., Baranyi, V., Reichart, G.J., Kürschner, W., 2017. Astronomical age constraints and extinction mechanisms of the Late Triassic Carnian crisis. Scientific Reports, 7, No 2557: 1–7. <https://doi.org/10.1038/s41598-017-02817-7>.
- Morad, S., 1986. Albitization of K-feldspar grains in Proterozoic arkoses and greywackes from southern Sweden. Neues Jahrbuch für Mineralogie Mh 1986, 145–156.
- Morad, S., 1998. Carbonate cementation in sandstones: distribution patterns and geochemical evolution, in: Morad, S. (Ed.), Carbonate Cementation in Sandstones: Distribution Patterns and Geochemical Evolution (Special Publication 26 of the IAS). Blackwell Publishing Ltd, Oxford, UK, pp. 1–26.
- Morad, S., Al-Ramadan, K., Ketzer, J.M., De Ros, L.F., 2010. The impact of diagenesis on the heterogeneity of sandstone reservoirs: a review of the depositional facies and sequence stratigraphy. AAPG Bulletin 94, 1267–1309. <https://doi.org/10.1306/04211009178>.
- Morad, S., Bergan, M., Knarud, R., Nystuen, J. P., 1990. Albitization of detrital plagioclase in Triassic reservoir sandstones from the Snorre Field, Norwegian North Sea. Journal of Sedimentary Research 60 (3), 411–425.
- Morad, S.; Ketzer, J.M.; De Ros, L.F., 2000. Spatial and temporal distribution of diagenetic alterations in Spatial and temporal distribution of diagenetic alterations in

- siliciclastic rocks: implications for mass transfer in sedimentary basins. *Sedimentology* 47 (Millenium Reviews), 95–120. <https://doi.org/10.1046/j.1365-3091.2000.00007.x>.
- Nesbitt, H.W., Fedo, C.M., Young, G.M., 1997. Quartz and Feldspar Stability, Steady and Non-Steady State Weathering and Petrogenesis of Siliciclastic Sands and Muds. *Journal of Geology*, 105, 173–191. <https://doi.org/10.1086/515908>.
- Neuser, R.D., Bruhn, F., Götze, J., Habermann, D., Richter, D.K., 1995. Kathodolumineszenz: Methodik und Anwendung. *Zentralblatt für Geologie und Paläontologie Teil I*, H. 1/2, 287–306.
- Nitsch, E., 2005. Paläoböden im süddeutschen Keuper (Exkursion E am 31. März 2005). *Jahresberichte und Mitteilungen des Oberrheinischen Geologischen Vereins*, 87, 135–176. <https://doi.org/10.1127/jmogv/87/2005/135>.
- Noh, J.H., Boles, J.R., 1993. Origin of zeolite cements in the Miocene sandstones, North Tejon oil fields, California. *Journal of Sedimentary Research*, 63(2), 248–260.
- Nöldeke, W., Schwab, G., 1977. Zur tektonischen Entwicklung des Tafeldeckgebirges der Norddeutsch-Polnischen Senke unter besonderer Berücksichtigung des Nordteils der DDR. *Z. Angew. Geol.* 23 (8), 369–379.
- Ogihara, S., Iijima, A., 1990. Exceptionally K-rich clinoptilolite—heulandite group zeolites from three offshore boreholes off northern Japan. *European Journal of Mineralogy*, 819–826. <https://doi.org/10.1127/ejm/2/6/0819>.
- Perry, E. D., Hower, J., 1970. Burial diagenesis in Gulf Coast pelitic sediments. *Clays and Clay minerals* 18, 165–177.
- Raiswell, R., 1982. Pyrite texture, isotopic composition and the availability of iron. *American Journal of Science* 282, 1244–1263. <https://dx.doi.org/10.2475/ajs.282.8.1244>.
- Reinhold, K., Krull, P., Kockel, F., 2008. Salzstrukturen Norddeutschlands, Geologische Karte 1: 500.000. Berlin/Hannover (Bundesanst. Geowiss. Rohstoffe).
- Rockel, W., Hoth, P., Seibt, P., 1997. Charakteristik und Aufschluss geothermaler Speicher. *Geowissenschaften*, 15, 244–252.
- Rodon, S., Littke, R., 2005. Thermal maturity in the Central European Basin system (Schleswig-Holstein area): results of 1D basin modeling and new maturity maps. *International Journal of Earth Sciences*, 94(5), 815–833. <http://dx.doi.org/10.1007/s00531-005-0006-1>.

- Ross, C.S., 1928. Sedimentary analcite. *Am. Miner.* 13, 195–197.
- Saha, P., 1961. The system NaAlSiO<sub>4</sub> (nepheline)-NaAlSi<sub>3</sub>O<sub>8</sub> (albite)-H<sub>2</sub>O. *Am. Mineralogist* 46, 859–884.
- Saiag, J., Brigaud, B., Portier, É., Desaubliaux, G., Bucherie, A., Miska, S., Pagel, M., 2016. Sedimentological control on the diagenesis and reservoir quality of tidal sandstones of the upper Cape Hay formation (Permian, Bonaparte Basin, Australia). *Marine and Petroleum Geology* 77, 597–624. <https://doi.org/10.1016/j.marpetgeo.2016.07.002>.
- Saigal, G.C., Morad, S., Bjørlykke, K., Egeberg, P.K., Aagaard, P., 1988. Diagenetic albitization of detrital K-feldspar in Jurassic, Lower Cretaceous, and Tertiary clastic reservoir rocks from offshore Norway, I. textures and origin. *Journal of Sedimentary Petrology* 58 (6), 1003–1013. <https://doi.org/10.1306/212F8EE5-2B24-11D7-8648000102C1865D>.
- Scheck-Wenderoth, M., Krzywiec, P., Zühlke, R., Maystrenko, Y., Froitzheim, N., 2008. Permian to Cretaceous tectonics, in: McCann, T. (Ed.), *The Geology of Central Europe, Volume 2: Mesozoic and Cenozoic*. Geological Society, London, pp. 999–1031.
- Schmidt, R.B., Bucher, K., Drüppel, K., Stober, I., 2017. Experimental interaction of hydrothermal Na-Cl solution with fracture surfaces of geothermal reservoir sandstone of the Upper Rhine Graben. *Applied Geochemistry*, 81, 36–52. <http://dx.doi.org/10.1016/j.apgeochem.2017.03.010>.
- Schnabel, M., Noack, V., Ahlrichs, N., Hübscher, C., 2021. A comprehensive model of seismic velocities for the Bay of Mecklenburg (Baltic Sea) at the North German Basin margin: implications for basin development. *Geo-Marine Letters*, 41: 20, 1–12. <https://doi.org/10.1007/s00367-021-00692-w>.
- Scholle, T., 1992. *Genese und Diagenese des Rhät + Hettang/Untersinemur im Nordosten Deutschlands – Ein Beitrag zur Nutzung geothermischer Energie*. Diss. Univ. Greifswald.
- Schröder, B., 1977. Unterer Keuper und Schilfsandstein im germanischen Trias-Randbecken. – *Zbl. Geol. Paläont.*, T. 1, 1976: 1030–1056.
- Schwab, G., 1985. *Paläomobilität der Norddeutsch-Polnischen Senke*. Diss. Akad. Wiss. DDR [unpubl.].
- Scotchman, I.C., Johnes, L.H., 1990. Wave-Dominated Deltaic Reservoirs of the Brent Group, Northwest Hutton Field, North Sea, in: Barwis, J.H., McPherson, J.G.,

- Studlick, J.R.J. (Eds.), Sandstone Petroleum Reservoirs. Casebooks in Earth Sciences. Springer, New York, NY, pp. 227–261.
- Segonzac, G.D., 1970. The Transformation of Clay Minerals during Diagenesis and Low-Grade Metamorphism: A Review. *Sedimentology* 15, 281–346. <https://doi.org/10.1111/j.1365-3091.1970.tb02190.x>.
- Shifa, Z., Xiaomin, Z., Xin, L., Dong, W., Dongna, Z., 2016. Authigenic minerals and diagenetic evolution in altered volcanic materials and their impacts on hydrocarbon reservoirs: evidence from the lower Permian in the northwestern margin of Junggar Basin, China. *Arabian Journal of Geosciences*, 9(2), 1–19. <http://dx.doi.org/10.1007/s12517-015-2201-0>.
- Shukla, U.K., Bachmann, G.H., 2007. Estuarine sedimentation in the Stuttgart Formation (Carnian, Late Triassic), South Germany. *Neues Jahrbuch für Geologie und Paläontologie, Abhandlungen* 243, 305–323. <https://doi.org/10.1127/0077-7749/2007/0243-0305>.
- Skei J.M., 1988. Formation of framboidal iron sulfide in the water of a permanently anoxic fjord-Framvaren, South Norway. *Mar. Chem.* 23, 345–352. [https://doi.org/10.1016/0304-4203\(88\)90103-X](https://doi.org/10.1016/0304-4203(88)90103-X).
- Solms, M, Röhling, H.-G., 2001. Lithologische und petrographische Untersuchungen im höheren Unteren und Mittleren Buntsandstein der Bohrung Hämelerwald-Z1. Ber. Nieders. Landesamt Bodenforsch., 55 S., 1 CD; Hannover (unpublished report).
- Sośnicka, M., Lüders, V. (2020). Fluid inclusion evidence for low-temperature thermochemical sulfate reduction (TSR) of dry coal gas in Upper Permian carbonate reservoirs (Zechstein, Ca<sub>2</sub>) in the North German Basin. *Chemical Geology*, 534: 119453. <https://doi.org/10.1016/j.chemgeo.2019.119453>.
- Stets, J., Wurster, P., 1977. Der Lichtenauer Randstrom des Schilfsandstein-Deltas. *Z. dt. Geol. Ges.* 128, 99–120.
- Stollhofen, H., Bachmann, G., Barnash, J., Bayer, U., Beutler, G., Franz, M., Kästner, M., Legler, B., Mutterlose, J., Radies, D., 2008. Upper Rotliegend to Early Cretaceous basin development, in: Littke, R., Bayer, U., Gajewski, D., Nelskamp, S. (Eds.), Dynamics of complex sedimentary basins. The example of the Central European Basin System. Springer, Berlin, pp. 181–210.
- Trusheim, F., 1960. Mechanism of salt migration in northern Germany. *Association of Petroleum Geologists Bulletin*, 44(9), 1519–1540. <https://doi.org/10.1306/0bda61ca-16bd-11d7-8645000102c1865d>.

- Tucker, M.E., 1985. Einführung in die Sedimentpetrologie. Ferdinand Enke Verlag, Stuttgart.
- Visscher, H., Van Houte, M., Brugman, W.A., Poort, P.R., 1994. Rejection of a Carnian (Late Triassic) “pluvial event” in Europe. *Rev. Palaeobot. Palynol.*, 83: 217–226. [https://doi.org/10.1016/0034-6667\(94\)90070-1](https://doi.org/10.1016/0034-6667(94)90070-1).
- Visser, W.A., Heederik, J.P., 1987. Geothermal energy, in: Zonneveld, J.I.S., van Loon, A.J. (Eds.), *Seventy-five years of geology and mining in the Netherlands 1912–1987*. Royal Geological and Mining Society of the Netherlands (The Hague), pp. 243–258.
- Voigt, S., Wagreeich, M., Surlyk, F., Walaszczyk, I.U.D, Cech, S., Voigt, T., Wiese, F., Wilmsen, M., Niebuhr, B., Reich, M., Funk, H., Michalik, J., Jagt, J.W.M., Felder, P.J., Schulp, A.S., 2008. Cretaceous, in: McCann, T. (Ed.), *The Geology of Central Europe. Volume 2: Mesozoic and Cenozoic*. Geological Society, London, pp. 923–995.
- Voigt, T., Grobleben, J., Schöner, R., Gaupp, R., 2010. Die thermische Reife permokarboner Ablagerungen in Thüringen – Schlussfolgerungen für die Versenkungsgeschichte der Thüringer Mulde. *Beitr. Geol. Thür., N. F.*, 17, 83–100.
- Voigt, T., Kley, J., Voigt, S., 2021. Dawn and dusk of Late Cretaceous basin inversion in central Europe. *Solid Earth*, 12, 1443–1471. <https://doi.org/10.5194/se-12-1443-2021>.
- von Eynatten, H., Kley, J., Dunkl, I., Hoffmann, V.E., Simon, A., 2021. Late Cretaceous to Paleogene exhumation in central Europe – localized inversion vs. large-scale domal uplift. *Solid Earth*, 12, 935–958. <https://doi.org/10.5194/se-12-935-2021>.
- Wagner, R., Kühn, M., Meyn, V., Pape, H., Vath, U., Clauser, C., 2005. Numerical simulation of pore space clogging in geothermal reservoirs by precipitation of anhydrite. *International Journal of Rock Mechanics & Mining Sciences*, 42, 1070–1081. <https://doi.org/10.1016/j.ijrmms.2005.05.008>.
- Walker T.R., 1976. Diagenetic origin of continental red beds, in: Falke, H. (Ed.), *The Continental Permian in Central West, and South Europe*. Reidel Publishing Company, Dordrecht, The Netherlands, pp. 240–282.
- Walker T.R., Wauch, B., Crone, A.J., 1978. Diagenesis in first cycle desert alluvium of Cenozoic age, southwestern United States and northwestern Mexico. *Bulletin of the geological Society of America*, 89, 19–32. [https://doi.org/10.1130/0016-7606\(1978\)89%3C19:DIFDAO%3E2.0.CO;2](https://doi.org/10.1130/0016-7606(1978)89%3C19:DIFDAO%3E2.0.CO;2).

- Weibel, R., 1998. Diagenesis in oxidising and locally reducing conditions - an example from the Triassic Skagerrak Formation, Denmark. *Sedimentary Geology* 121, 259–276. [https://doi.org/10.1016/S0037-0738\(98\)00085-2](https://doi.org/10.1016/S0037-0738(98)00085-2).
- Weibel, R., 1999. Effects of burial on the clay assemblages in the Triassic Skagerrak Formation Denmark. *Clay Min.* 34, 619–635. <https://doi.org/10.1180/000985599546488>.
- Weibel, R., Olivarius, M., Kjøller, C., Kristensen, L., Hjuler, M.L., Friis, H., Nielsen, L.H., 2017. The influence of climate on early and burial diagenesis of Triassic and Jurassic sandstones from the Norwegian–Danish Basin. *The Depositional Record*, 3(1), 60–91. <https://doi.org/10.1002/dep2.27>.
- Weibel, R., Olivarius, M., Jakobsen, F.C., Whitehouse, M., Larsen, M., Midtgaard, H., Nielsen, K., 2019. Thermogenetic degradation of early zeolite cement: An important process for generating anomalously high porosity and permeability in deeply buried sandstone reservoirs?. *Marine and Petroleum Geology*, 103, 620–645. <https://doi.org/10.1016/j.marpetgeo.2019.02.006>.
- Weibel, R., Olivarius, M., Vosgerau, H., Mathiesen, A., Kristensen, L., Nielsen, C.M., Nielsen, L.H., 2020. Overview of potential geothermal reservoirs in Denmark. *Netherlands Journal of Geosciences*, 99, e3. <https://doi.org/10.1017/njg.2020.5>.
- Wentworth, C., 1922. A scale of grade and class terms for clastic sediments. *Journal of Geology* 30, 377–392.
- Wolfgramm, M., 2005. Fluidentwicklung und Diagenese im Norddeutschen Becken – Petrographie, Mikrothermometrie und Geochemie stabiler Isotope. *Hallesches Jb.*, B, Beiheft 20.
- Wolfgramm, M., Schmidt-Mumm, A., 2001. Die zeitliche Einordnung diagenetischer und hydrothermalen Fluidphasen im Nordostdeutschen Becken (NEDB). *Zbl. Geol. Paläont. Teil I*, 2001 (3/4), 237–256.
- Wolfgramm, M., Franz, M., Agemar, T., 2014. Explorationsstrategie tiefer geothermischer Ressourcen am Beispiel des Norddeutschen Beckens, in: Bauer, M., Freeden, W., Jacobi, H., Neu, T. (Eds.), *Handbuch Tiefe Geothermie*. Springer, Berlin, pp. 463–505.
- Wolfgramm, M., Rauppach, K., Seibt, P., 2008. Reservoir geological characterization of Mesozoic sandstones by petrophysical, mineralogical and geochemical data. *Z. geol. Wiss.* 36 (4/5), 249–265.

- Worden, R.H., Burley, S.D., 2003. Sandstone diagenesis: the evolution of sand to sandstone, in: Burley, S.D., Worden, R.H. (Eds.), *Sandstone Diagenesis*. (Special Publication 4 of the IAS). Blackwell Publishing Ltd., Oxford, UK, pp. 1–44.
- Wurster, P., 1964. *Geologie des Schilfsandsteins*. Mitteilungen des Geologischen Staatsinstituts Hamburg 33.
- Zeh, A., Franz, M., Obst, K., 2021. Zircon of Triassic Age in the Stuttgart Formation (Schilfsandstein)—Witness of Tephra Fallout in the Central European Basin and New Constraints on the Mid-Carnian Episode. *Frontiers in Earth Science* 9, 15 p. <https://doi.org/10.3389/feart.2021.778820>
- Zhang, Y., Ogg, J. G., Franz, M., Bachmann, G. H., Szurlies, M., Röhling, H.-G., Obst, K., Rolf, C., 2020. Carnian (Late Triassic) magnetostratigraphy from the Germanic Basin allowing global correlation of the Mid-Carnian Episode. *Earth and Planetary Science Letters*. <https://doi:10.1029/2019TC005874>.
- Ziegenhardt, W., Schön, M., Gilch, M., 1980. Einige Ergebnisse der strukturgeologischen Erkundung von Untergrundspeichern [Tectonic exploration of underground storage sites – some results]. *Zeitschrift für Angewandte Geologie*, 26, 165–171.
- Ziegler, K., 2006. Clay minerals of the Permian Rotliegend Group in the North Sea and adjacent areas. *Clay minerals* 41(1), 355–393. <https://doi.org/10.1180/0009855064110200>.
- Ziegler, P.A., 1982. Triassic rifts and facies patterns in Western and Central Europe. *Geol. Rd.* 71 (3), 747–772.
- Ziegler, P.A., 1990. *Geological Atlas of Western and Central Europe*. Shell International Petroleum Maatschapij BV, Den Haag.
- Zimmermann, J., Franz, M., Schaller, A., Wolfgramm, M., 2018. The Toarcian-Bajocian deltaic system in the North German Basin: subsurface mapping of ancient deltas – morphology, evolution and controls. *Sedimentology*, 65, 897–930.



## Chapter IV

### 4 From eo- to telogenesis in sandstone diagenesis: constraints from fluid inclusions, stable isotopes and U/Pb dating of authigenic cementations

This chapter contains data, which were generated during the project and will be published in the future. The used analyses were chosen in order to specify the process of diagenesis and the development of the North German Basin.

**Authors' edited topics:** This chapter was mainly conceptualized and written by Sebastian Niegel. Graciela Sosa and Alfons van den Kerkhof supported the cathodoluminescence. Graciela Sosa analysed the fluid inclusions, interpreted the data of microthermometry, and wrote the corresponding methodical part as well as the discussion. Benny Fischer handled the chemical preparation of the samples for sulfate analysis and described the corresponding methodical part. U/Pb datings of carbonate cementations were done by Armin Zeh and Aratz Beranoaguirre at the Karlsruhe Institute of Technology. The reactive transport modelling and its method were partially described by Ulrich Maier. Discussions and corrections were made by Matthias Franz and Markus Wolfgramm.

## **4.1 Introduction**

Niegel and Franz (2023; see chapter IV) indicate that containing authigenic minerals were formed at higher temperatures than the present depths of the Schilfsandstein in the North German Basin would suggest. This hypothesis is also in agreement with the postulated uplift identified by Friberg (2001).

This study addresses the analytical results of fluid inclusions, stable isotopes (C, O, S), carbonate dating and reactive transport modelling to accurately determine the burial history, maximum burial temperature and time of formation of authigenic minerals, and to characterise the palaeofluids in terms of origin, composition, formation conditions and age of diagenetic and hydrothermal pore waters.

## **4.2 Data set and methods**

### **4.2.1 Samples**

In order to characterise the burial diagenesis of the Stuttgart Formation in the North German Basin, microscopic methods (transmitted light, SEM-EDX, CL, fluid inclusions), stable isotopes (C, O, S), carbonate dating and reactive transport modelling were used. Samples of the Schilfsandstein Members were available from ten cored wells (40 samples, Table 4.1) in the North German Basin. These comprise the wells Barth 6a/65, Goritz 1/62, Lütow 3/66, Wolgast 1/1A/63, Tarnow 1/65, Neubrandenburg 2/85, KSS 1/66, Brustorf 1/62, Gartz 1/65 and Strausberg 1/63 (Fig. 3.1). These samples were already part of the study of Niegel and Franz (2023; chapter III) and were buried at depths between 201 and 1559 m.

Table 4.1: Analysed samples of the Schilfsandstein Members.

Well	Sample	Depth (m)	Stratigraphy	Stable isotopes		Fluid inclusions
				Carbon and Oxygen	Sulphur	
Kb Barth 6a/65	11-01	776,20	Lower Schilfsandstein Mb	1	--	--
	11-04	772,50		1		
	11-07	770,80		1		
	11-08	768,00		1		
Kb Brustorf 1/62	11-11	312,90	Upper Schilfsandstein Mb	1	--	--
	11-09	304,20	Upper Schilfsandstein Mb	1		
	11-02	260,00	Lower Schilfsandstein Mb	1		
	11-01	257,00		1		
Kb Gartz 1/65	12-21	1298,70	Upper Schilfsandstein Mb	--	1	--
	12-11	1340,00	Lower Schilfsandstein Mb	--	1	
Kb Goritz 1/62	12-03	242,00	Upper Schilfsandstein Mb	1	--	--
	12-04	236,00	Lower Schilfsandstein Mb	1		
	12-06	227,00		1		
	12-11	201,00		1		
Kb KSS 1/66	12-14	1252,30	Upper Schilfsandstein Mb	--	1	--
E Lütow 3/66	12-01	1029,10	Upper Schilfsandstein Mb	1	--	--
	12-05	1014,93		1		
	12-16	1012,20	Lower Schilfsandstein Mb	1		
	12-10	996,40		1		
	12-12	990,80		1		
Gt Neubrandenburg 2/85	11-03	1544,70	Lower Schilfsandstein Mb	1	1	--
	11-02	1546,85		1	1	
Kb Strausberg 1/63	12-07	763,80	Upper Schilfsandstein Mb	1	--	--
	06-21	744,00		1		
	06-15	791,95	Lower Schilfsandstein Mb	1		
	06-13	795,90		--		
Kb Tarnow 1/65	11-28	1149,10	Lower Schilfsandstein Mb	1	1	--
	11-29	1146,20		1	1	
	11-25	1154,00	Neubrandenburg Mb	--	1	
Kb Wolgast 1/1A/63	11-19	712,20	Upper Schilfsandstein Mb	1	--	--
	11-01	788,60	Lower Schilfsandstein Mb	1		--
	11-03	785,10		1		1
	11-05	777,00		--		1
	11-08	761,80		1		1
	11-11	754,50		1		1
	11-12	753,50		--		1

#### 4.2.2 SEM-EDX and CL

Selected thin sections were carbon-coated for scanning electron microscopy (SEM) and cathodoluminescence imaging (CL) for chemical compositions, internal structures and zoning in authigenic minerals.

The investigation of ten thin sections with scanning electron microscope equipped with energy dispersive X-ray spectroscope (Zeiss-Evo MA 10) was realised at the University of Greifswald. This device is equipped with a tungsten filament and an EDAX element and has a resolution of 3 nm at 30 kV.

Cathodoluminescence studies were carried out at the University of Göttingen using a hot cathode HC3-LM-Simon-Neuser CL microscope (Neuser et al., 1995) equipped with a Kappa DX 40C Peltier-cooled camera (resolution 1.5 mpix). Luminescence

colours are described according to their appearance under visual observation. The electron beam has a diameter of c. 4 mm, and the operating conditions under high vacuum (10–4 bar) were 14 kV acceleration voltage and a beam current of 0.18 mA, corresponding to 20–40  $\mu\text{A}/\text{mm}^2$  beam current density.

### 4.2.3 Microthermometry

Doubly polished wafers with a thickness of 50  $\mu\text{m}$  were prepared from mirrored cuttings of the samples used for cathodoluminescence analysis. Phase transitions in fluid inclusions in Fe-dolomite quartz were investigated at the University of Göttingen by using a LINKAM THMS 600 heating-freezing stage cooled with liquid nitrogen. The stage was calibrated by a set of synthetic fluid-inclusion standards. For temperatures around  $-56.6\text{ }^\circ\text{C}$  (the melting point of  $\text{CO}_2$ ) and around  $0\text{ }^\circ\text{C}$ , the accuracy is better than  $0.5\text{ }^\circ\text{C}$ , whereas for temperatures between 200 and  $600\text{ }^\circ\text{C}$ , the accuracy is better than  $5\text{ }^\circ\text{C}$ . Salinities were calculated from ice melting temperatures using the revised equations of Bodnar (2003) and Steele-MacInnis et al. (2011). An attached QICam camera system (resolution 1.4 mpx) was used to image the fluid inclusions.

### 4.2.4 Stable isotopes

#### 4.2.4.1 Carbon and oxygen isotopes

For the carbon and oxygen stable isotope measurements, 35 samples with at least 1 % authigenic calcite or dolomite of total sediment were selected, 27 samples of which have delivered useable values. Calcite was measured in samples of the wells Barth, Kb Brustorf 1/62, Kb Goritz 1/62, Kb Strausberg 1/63 and Kb Tarnow At 1/65. Furthermore, dolomite was analysed in samples of the wells Lütow, Gt Neubrandenburg 2/85, Kb Strausberg 1/63 and Kb Wolgast 1/1A/63. Twenty samples are originated from the Lower Schilfsandstein Member and seven samples from the Upper Schilfsandstein Member (see Table 4.2).

Powders of total rock samples were analysed in the stable isotope laboratory at the University of Göttingen. These samples were reacted with 100 % phosphoric acid (density  $> 1.95\text{ g}/\text{cm}^3$ ) at  $70\text{ }^\circ\text{C}$  using a Thermo Kiel VI carbonate preparation line coupled to a Finnigan Delta plus massspectrometer. The  $\delta^{13}\text{C}$  value is reported relative to V-PDB and the  $\delta^{18}\text{O}$  value is reported relative to V-SMOW. The precision of these values is better than  $\pm 0.05$  ( $1\ \sigma$ ), verified by replicate analysis of laboratory standards.

The measured  $\delta^{18}\text{O}$  values of dolomite were corrected by the formula according to Rosenbaum and Sheppard (1986). Based on the results of oxygen isotopes and microthermometry of authigenic carbonates, the isotopic composition of the paleofluids is calculated after Friedman and O'Neil (1977) for calcite and after Fritz and Smith (1970) for dolomite.

#### 4.2.4.2 Sulphur isotopes

Nine samples with at least 5 % authigenic sulphate in relation to the total sediment were selected for the measurement of stable sulphur isotopes. This comprises samples of the wells Gartz 1/65, KSS 1/66, Neubrandenburg 2/85, Tarnow 1/65 and Strausberg 1/63 (shown in Table 4.2). One sample originates from the Neubrandenburg Member, six samples come from the Lower Schilfsandstein Member and two samples from the Upper Schilfsandstein Member.

For the analysis, the anhydrite was chemically precipitated to barite. Therefore, the rock samples were grinded in an agate mortar to a very fine powder. From the grinded rock samples,  $2.50 \pm 0.05$  g of powder were used, 500 ml distilled water were added and mixed in an ultrasonic bath for 15 min. The solutions were filtered with a filter of 10  $\mu\text{m}$  pore size, and subsequently heated up to 70–75 °C. To the 500 ml solution 0.1 mol·l<sup>-1</sup> HCl (Merck KGaA, Darmstadt, Germany) were added until a pH of 3 (approx. 25 ml HCl). With an Eppendorf pipette 50 ml of 1 mol l<sup>-1</sup> BaCl<sub>2</sub> (Merck KGaA, Darmstadt, Germany) were added slowly. The resulting BaSO<sub>4</sub> precipitate was filtered (1  $\mu\text{m}$  pore size) and dried at 105 °C in a drying oven. All determinations are generally offered in duplicates.

ALS Global in Dublin measured these nine precipitates of barite by, using a MAT 253 Stable Isotope Ratio Mass Spectrometer coupled to a Costech ECS 4010 Elemental Analyzer. The  $\delta^{34}\text{S}$  values are reported relative to V-CDT with a precision of 0.2 ‰.

#### 4.2.5 U/Pb dating of carbonates

Two samples, dolomite (Kb Wolgast 1/1A/63, sample 11-03) and calcite (Kb Brustorf 1/62, sample 11-11) of the Lower Schilfsandstein Member, were analysed by the U/Pb method. U/Pb dates were acquired using laser ablation-inductively coupled plasma mass spectrometry (LA-ICPMS) at KIT (Karlsruhe Institute of Technology), applying a modified method of Gerdes and Zeh (2006, 2009). A Mass spectrometer

ELEMENT XR sector field ICP from Thermo Fischer was coupled to a EXCIMER laser EXITE (193 nm) from Teledyne Photonmachines and the laser spot-size was 85  $\mu\text{m}$ .

Preliminary U/Pb dating of dolomite and calcite has been done. Further measurements are planned to increase statistical certainty.

#### **4.2.6 Reactive transport modelling**

The multicomponent reactive transport code MIN3P (Mayer, 1999; Mayer et al., 2002; Bao et al., 2017; Maier et al., 2022) was developed to simulate equilibrium- and kinetic hydrochemical reactions in subsurface porous media. A generalised framework allows the user to define components, species and reaction networks of any desired complexity, which can include intra-aqueous reactions as well as heterogeneous reactions between phases. Of particular interest to the problem at hand are reactions including the aqueous and mineral phase, such as dissolution or precipitation of minerals. Equilibrium reactions considered are aqueous complexation, gas partitioning between phases, oxidation-reduction, ion exchange, and surface complexation. Mineral reactions generally use a kinetic formulation. This reactive scheme is combined with Darcy's or Richard's equation, respectively, for saturated or variably saturated water flow, and advective-dispersive transport in the aqueous phase. In this way, reactive transport in 1-D, 2-D or 3-D porous media and rock formations can be modelled.

Simulations were based on the thermodynamic database associated with MIN3P, which originates from the MINTQA2 code (Allison et al., 1991) and is continuously extended, comparable to other hydrochemical databases such as PHREEQC (Parkhurst and Appelo, 2013). The reaction framework has recently been updated with the computation of molar volumes of solutes which allows the alteration of chemical equilibria as a function of pressure changes in the deep geosphere (Maier et al., 2022).

Geochemical modelling was performed using the samples of the Stuttgart Formation in the Wolgast well as an example. The initial simplified mineral input is given on the averaged mineral composition (quartz: 24 %, albite: 20 %, muscovite: 6 %, pyrite: 1 %, K-feldspar: 9 %, initial porosity: 40 %) determined by the transmitted light microscopy of the Wolgast samples in Niegel and Franz (2023). Since the lithoclasts could not be directly integrated into the model, the chemical composition was estimated and the corresponding contents of quartz and feldspar were increased. The chemical composition of tephra according to Portnyagin et al. (2020) was integrated for the simulation of analcime.

As concentration input for the initial fluid composition, the chemistry of estuary water by Patel and Sahoo (2021) was implemented. In addition, data from sea water published by WHO 2005 and Parkhurst and Appelo (2013) were used.

MIN3P allows a linear heating, thus only the subsidence was modelled. The subsidence in the model is simulated with a duration of 86,1 million years and a formation temperature of 120 °C, representing the period from deposition to the postulated maximum burial depth in the Late Jurassic. The temperature represents the intersection of the calculated minimum formation temperatures of microthmerometry (c. 120 °C, Fig. 4.4) and the maximum formation temperatures for analcime given in Fig. 3.17 (124 °C). The hydrostatic pressure was estimated using the gradient 10 m/1 bar. The calculation of density based on the studies of Mao and Duan (2008).

Table 4.2: Isotopic data (C, O, S) of calcite, dolomite and sulphate of the Schilfsandstein Members.

Well	Sample	Depth [m]	Stratigraphy	Authigenic mineral	n	Stable isotopes				calculated temperatures after Friedman and O'Neil (1977) [°C]	$\delta^{34}\text{S}_{\text{VCDT}}$ [‰]	
						$\delta^{18}\text{O}_{\text{SNOW}}$ [‰]	$\delta^{18}\text{O}_{\text{PDB}}$ [‰] <sup>1)</sup>	$\delta^{13}\text{C}_{\text{PDB}}$ [‰]				
Kb Barth 6a/65	11-01	776,20	Lower Schilfsandstein Mb	calcite	4	23,32	-7,31	-6,09	50	-		
	11-04	772,50				21,72	-8,87	-7,05	59			
	11-07	770,80				21,22	-9,35	-6,88	63			
	11-08	768,00				21,68	-8,91	-6,94	60			
Kb Brustorf 1/62	11-01	257,00	Upper Schilfsandstein Mb	calcite	2	24,86	-5,82	-4,59	42	-		
	11-02	260,00				26,59	-4,14	-5,07	34			
	11-09	304,20	Lower Schilfsandstein Mb			20,46	-10,09	-7,72	68			
	11-11	312,90				20,72	-9,84	-7,30	66			
Kb Gartz 1/65	12-21	1298,70	Upper Schilfsandstein Mb	sulphate	1		--		12,5	-		
	12-11	1340,00	Lower Schilfsandstein Mb			1			15,8			
Kb Goritz 1/62	12-11	201,00	Upper Schilfsandstein Mb	calcite	3	25,16	-5,53	-1,45	40	-		
	12-03	242,00	Lower Schilfsandstein Mb			23,50	-7,14	-6,76	49			
	12-04	236,00	Lower Schilfsandstein Mb			24,26	-6,40	-3,83	45			
	12-06	227,00	Lower Schilfsandstein Mb			23,99	-6,66	-3,89	45			
Kb KSS 1/66	12-14	1252,30	Upper Schilfsandstein Mb	sulphate	1		--		13,8	-		
	12-10	996,40	Upper Schilfsandstein Mb			24,98	-4,53	-6,63	65			
	12-12	990,80	Upper Schilfsandstein Mb			25,51	-4,02	-6,02	60			
	12-01	1029,10	Lower Schilfsandstein Mb			25,40	-4,12	-5,77	62			
E Lütow 3/66	12-05	1014,93	Lower Schilfsandstein Mb	dolomite	3	25,28	-4,24	-5,98	62	-		
	12-16	1012,20				25,86	-3,68	-5,78	57			
	11-02	1546,85				20,18	-10,36	-5,78	70			
	11-03	1544,70				20,46	-10,09	-7,03	68			
Gl Neubrandenburg 2/85	11-03	1544,70	Lower Schilfsandstein Mb	sulphate	2		--		13,6	-		
	11-02	1546,85					--		12,4			
	12-07	763,80				20,28	-10,26	-8,07	69			
	06-21	744,00				29,10	-0,53	-4,70	42			
Kb Strausberg 1/63	06-15	791,95	Lower Schilfsandstein Mb	calcite	1	20,74	-9,82	-7,16	66	-		
	06-13	795,90				sulphate	1		--		16,7	
	11-28	1149,10					calcite	1	20,30		-10,24	-7,88
	11-29	1146,20				sulphate	2		--		13,7	
11-25	1154,00	Neubrandenburg Mb	1		--		13,0					
Kb Wolgast 1/1A/63	11-19	712,20	Lower Schilfsandstein Mb	dolomite	3	27,81	-1,78	-5,88	46	-		
	11-11	754,50				27,97	-1,63	-3,58	45			
	11-03	785,10				26,20	-3,35	-4,21	56			
	11-01	788,60				28,21	-1,40	-4,51	45			

<sup>1)</sup>  $\delta^{18}\text{O}_{\text{PDB}}$  converted in ‰



## 4.3 Results

### 4.3.1 Detrital mineralogy

According to Wentworth (1922), the 33 samples of the Lower and Upper Schilfsandstein Members are coarse sandy to coarse silty, depending on the lithofacies. They are dominantly fine-grained. The detrital fragments are characterised by sub-angular to sub-rounded grain shapes and low to moderate sphericities (*sensu* Tucker, 1985). Contacts between individual fragments prevail, but there are cemented zones too. Mechanically unstable components, such as detrital mica and altered rock fragments, are slightly deformed by compaction.

The samples reveal 18.8–58.8 % quartz, 24.4–56.3 % feldspar and 3.9–42.3 % lithoclasts of all detrital grains. Thus, the largest part of samples is classified as lithic arkose and subordinated as arkose and feldspathic litharenites (McBride, 1963). More details are given in Niegel and Franz (2023; see chapter III). These indicate low compositional maturities in accordance with Heling (1965), Dockter et al. (1967) and Förster et al. (2010).

The quartz assemblage corresponds predominantly monocrystalline grains outweighing polycrystalline grains and rare cherts. Dark blue to violet CL colours are common in quartz detrital fragments (Fig. 4.1), denoting a plutonic or high-grade metamorphic origin of the mineral. The feldspar assemblage is dominantly composed of K-feldspars outweighing plagioclase and rarely abundant microcline. Feldspar grains are mainly unaltered, but plagioclase is partially altered to sericite. The CL signal of feldspar is one to several magnitudes stronger than that of quartz. Alkali feldspar and plagioclase can often be distinguished by their CL properties: bright blue for K-feldspar and red to pink for plagioclase (Fig. 4.1). The assemblage of lithic fragments shows mainly metamorphic and felsic igneous rock fragments followed by a lower portion of mafic igneous and sedimentary rock fragments. Especially the igneous rock fragments are often strongly altered. Meta-sedimentary and sedimentary rocks are dominantly composed of variable amounts of mica and quartz. Felsic and mafic igneous rock fragments consist of quartz and feldspar, with muscovite/sericite, and chlorite.

Minor occurring detrital components are muscovite, biotite, glauconite, chlorite, heavy minerals (e.g. garnet, magnetite, amphibole, zircon, apatite, titanite) and plant remains.

The matrix fraction is dominated by clay minerals (smectite/illite) and only occasionally by a mixture of carbonate and clastic components. Chloritization of detrital biotite flakes is common.

example of the Schilfsandstein showing low degree of compaction

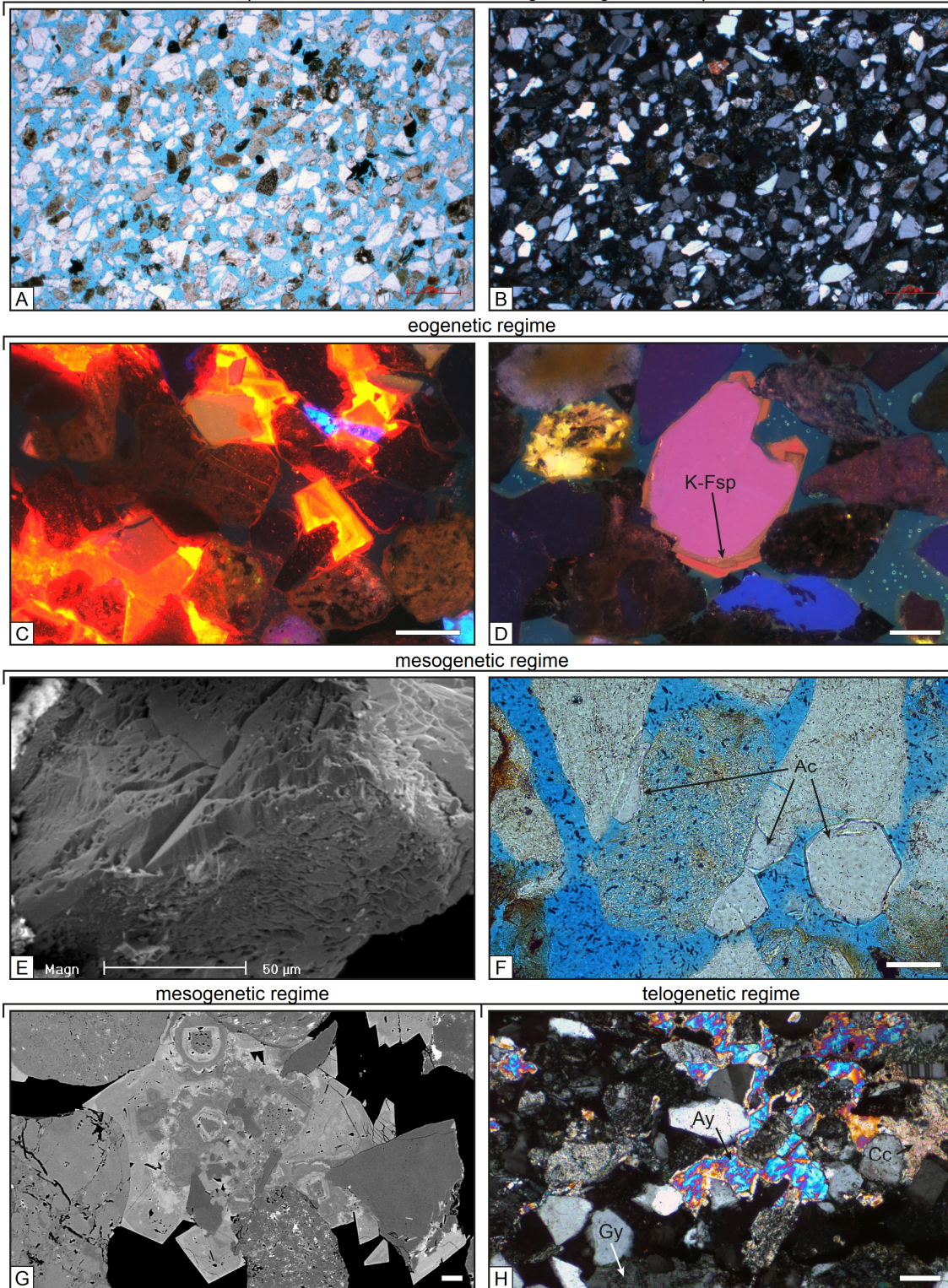


Fig. 4.1 (*facing page*): Thin section examples and authigenic mineralogy. **(A)** Kb Wolgast 1/1A/63, sample 11-16: fine-grained sandstone showing low degree of mechanical compaction and high porosity; scale is 500  $\mu\text{m}$ , parallel nicols. **(B)** As before; also showing no cementations; scale bar represents 500  $\mu\text{m}$ , crossed nicols. **(C)** Kb Strausberg 1/62, sample 12-07: CL image of pore-filling authigenic calcite showing bright to dark orange luminescence; scale is 100  $\mu\text{m}$ . **(D)** Kb Wolgast 1/1A/63, sample 11-11: CL image of detrital K-feldspar overgrown by a K-feldspar (K-Fsp) showing non to reddish CL colours; scale is 100  $\mu\text{m}$ . **(E)** Lütow, sample 12-05: Quartz overgrowth on detrital grain; scale is 50  $\mu\text{m}$ , SEM image. **(F)** Kb Brustorf 1/62, sample 11-11: Analcime crystals on detrital grain; scale bar is 100  $\mu\text{m}$ , parallel nicols. **(G)** Kb Wolgast 1/1A/63, sample 11-11: Fe-dolomite showing growth bands; scale is 20  $\mu\text{m}$ , SEM image. **(H)** Kb Tarnow At 1/65, sample 11-28: cementation with anhydrite (Ay), gypsum (Gy) and calcite (Cc); scale is 100  $\mu\text{m}$ , crossed nicols.

### 4.3.2 Compaction and contact strength, intergranular volume and porosity

The mechanical compaction of the investigated sandstones is low. This becomes evident by the grain fabrics, which are dominated by point contacts between detrital grains (Fig. 4.1). Partially, there are even floating grains. Long- and convex-concave contacts are less present, sutured contacts occur only rarely. The analysed grain contacts point to calculated values of contact strength (Füchtbauer, 1988) from 1.2 to 2.2 (median 1.7).

Based on the high percentage of point contacts, the grain fabric points to a low mechanical compaction of the sediments (Füchtbauer, 1988). Mechanical compaction is also confirmed by bending and breakage of mica. Brittle deformation of feldspar and the formation of pseudomatrix indicate a ductile deformation of clayey lithoclasts. Chemical compaction is indicated by concavo-convex and sutured contacts between detrital grains and rarely documented stylolites.

The primary porosity, represented by the intergranular volume, is between 2.9 and 51.2 % (median 34.9 %). This relatively high primary porosity reflects the comparatively low mechanical compaction. The secondary porosity, which presents the recent porosity, shows values from 0.5 to 31.6 % (median 15.5 %). More details are given in Niegel and Franz (2023; see chapter III).

### 4.3.3 Diagenesis and authigenic mineralogy

The Schilfsandstein samples have undergone significant diagenetic modification during burial. Diagenetic processes include mechanical and chemical compaction, and precipitation of different minerals. This comprises the growth of K-feldspar, abundant carbonates (calcite, dolomite and Fe-dolomite) and analcime, sulphates (gypsum, anhydrite and barite), quartz, Fe-oxides/hydroxides, clay minerals and pyrite occur in a subordinate manner (Fig. 4.1). The authigenic minerals correspond between c. 13.2 %

and 40.8 % of the total rock volume. Furthermore, dissolution of feldspar, alteration of lithic fragments, transformation from smectite to illite and chloritization of biotite characterize the diagenesis too. More details are given in Niegel and Franz (2023; see chapter III).

#### **4.3.4 Microthermometry**

Fluid inclusions have been studied in the Schilfsandstein samples collected from the well Wolgast 1/1A/63 (depth: 785.1–754.5 m). Fluid phase petrology considers the inclusion shape, size and phase volume fractions (Van den Kerkhof and Hein, 2001). The cement phases dolomite and quartz contain fluid inclusions, whereas microcline cement is free of fluid inclusions. The fluid inclusion properties are summarised in Table 4.3.

Typically, the inclusions in dolomite decorate growth zones or concentrate at the boundary between roundish dolomite nuclei and zoned blocky dolomite (Fig. 4.1) and can be regarded as primary origin. The fluid inclusions are aqueous in composition and mostly irregular with sizes between 1 and 4  $\mu\text{m}$  (rarely up to 7  $\mu\text{m}$ ; Fig. 4.3). At room temperature the fluid inclusions contain two phases (liquid and vapour) or sometimes only liquid (“all-liquid monophasic”, Fig. 4.2).

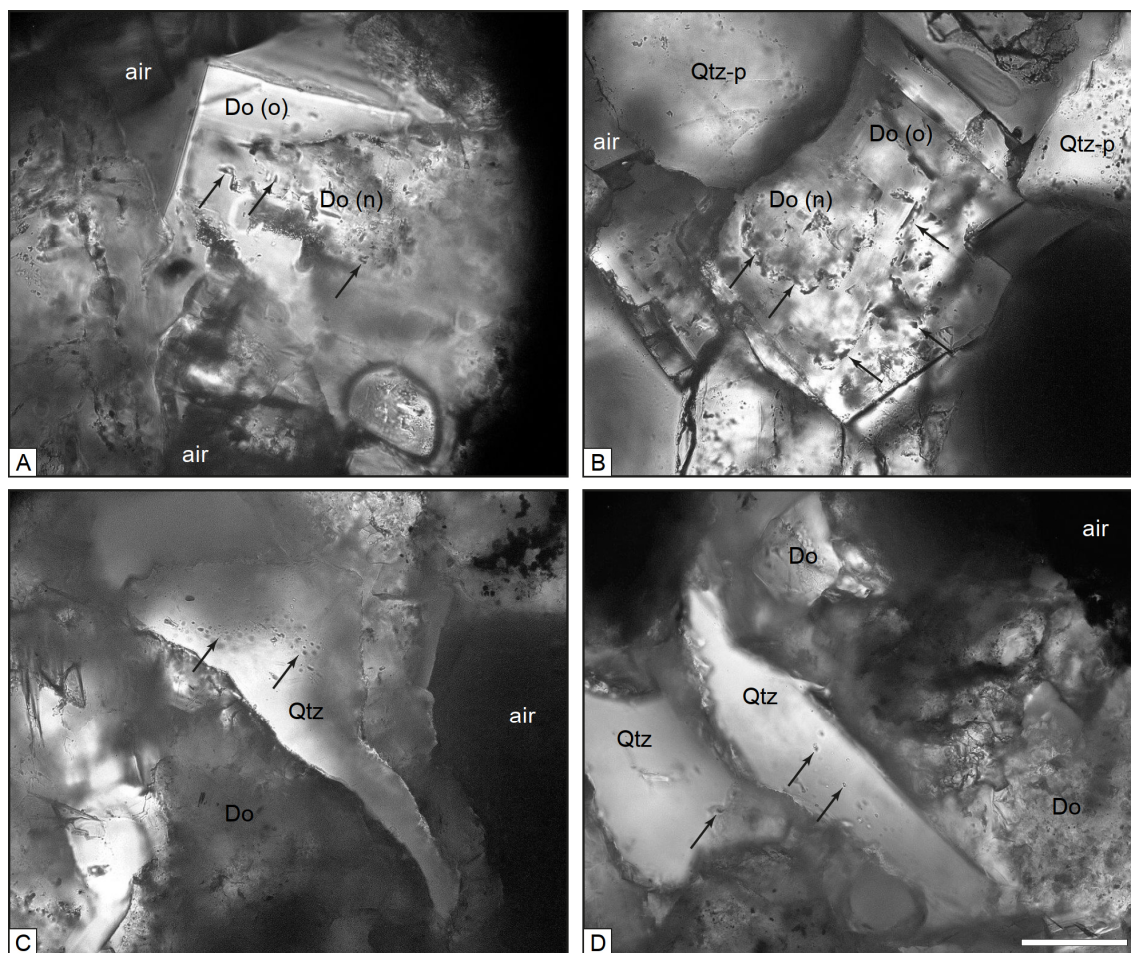


Fig. 4.2: Microphotographs illustrating fluid inclusion found in the samples. **(A)** Kb Wolgast 1/1A/63, sample 11-08: Fluid inclusions in dolomite (Do, n = nucleus, o = overgrowth) contain two phases or sometimes only liquid; for scale see Fig. D. **(B)** Kb Wolgast 1/1A/63, sample 11-11: Fluid inclusions in dolomite and quartz (Qtz, p = particle) contain two phases or sometimes only liquid; for scale see Fig. D. **(C)** Kb Wolgast 1/1A/63, sample 11-05: In quartz cement fluid inclusions typically formed clusters; for scale see Fig. D. **(D)** Kb Wolgast 1/1A/63, sample 11-05: Isolated fluid inclusions in quartz cement can also be referred to as primary; scale is 50  $\mu\text{m}$ .

In quartz cement, fluid inclusions typically form clusters or they are isolated and can also be referred to as primary. Their size is always small and mainly varies between 1 and 4  $\mu\text{m}$  (Figs. 4.2 and 4.3).

Microthermometry measurements revealed the temperatures of eutectic melting ( $T_e$ ), the melting of hydrohalite ( $T_{m, \text{HH}}$ ), final ice melting ( $T_{m, \text{ice}}$ ), and total homogenisation ( $T_{\text{ht}}$ ). In the smallest inclusions of 1–2  $\mu\text{m}$  only  $T_{\text{ht}}$  could be observed, but no melting.

Brine compositions for primary fluid inclusions in dolomite can be defined in the system  $\text{CaCl}_2\text{-NaCl-H}_2\text{O}$ . Their composition varies between c. 81–94 %  $\text{H}_2\text{O}$ , 5–15 %  $\text{CaCl}_2$  and 1–4 %  $\text{NaCl}$  (Fig. 4.3). Based on the melting behaviour fluid inclusions were distinguished with lower salinity (2–9 wt%  $\text{NaCl}$ -eq.), which occur in both dolomite and

quartz cement, and fluid inclusions with higher salinity (17–20 wt% NaCl-eq.), which are found only in dolomite (Fig. 4.3).

The fluid inclusions with lower salinity record ice melting between -1.1 and -3.9 °C, corresponding to 2–6 wt% NaCl. Due to the low salinity the eutectic temperature could be measured only incidentally and gave -22 °C, pointing to solutions with NaCl predominance.

The fluid inclusions of higher salinity in dolomite froze during cooling runs at temperatures below c. -70 °C. On subsequent warming eutectic melting ( $T_e$ ) could be recorded between -56 and -53 °C, pointing to  $\text{CaCl}_2$ -bearing solutions, besides NaCl. Subsequently, hydrohalite melting ( $T_{m, \text{HH}}$ ) was observed between -33.9 and -32.9 °C, followed by final ice melting ( $T_{m, \text{ice}}$ ) between -1.3 and -17.1 °C. Calculated total salinities (Bodnar, 1994) cluster in the ranges of 2-9 and 17–20 wt% NaCl-equivalent (Fig. 4.3). The  $\text{CaCl}_2$  content calculated from hydrohalite and ice melting temperatures (Steele-MacInnis et al., 2011) may be up to c. 15 wt% (Fig. 4.3).

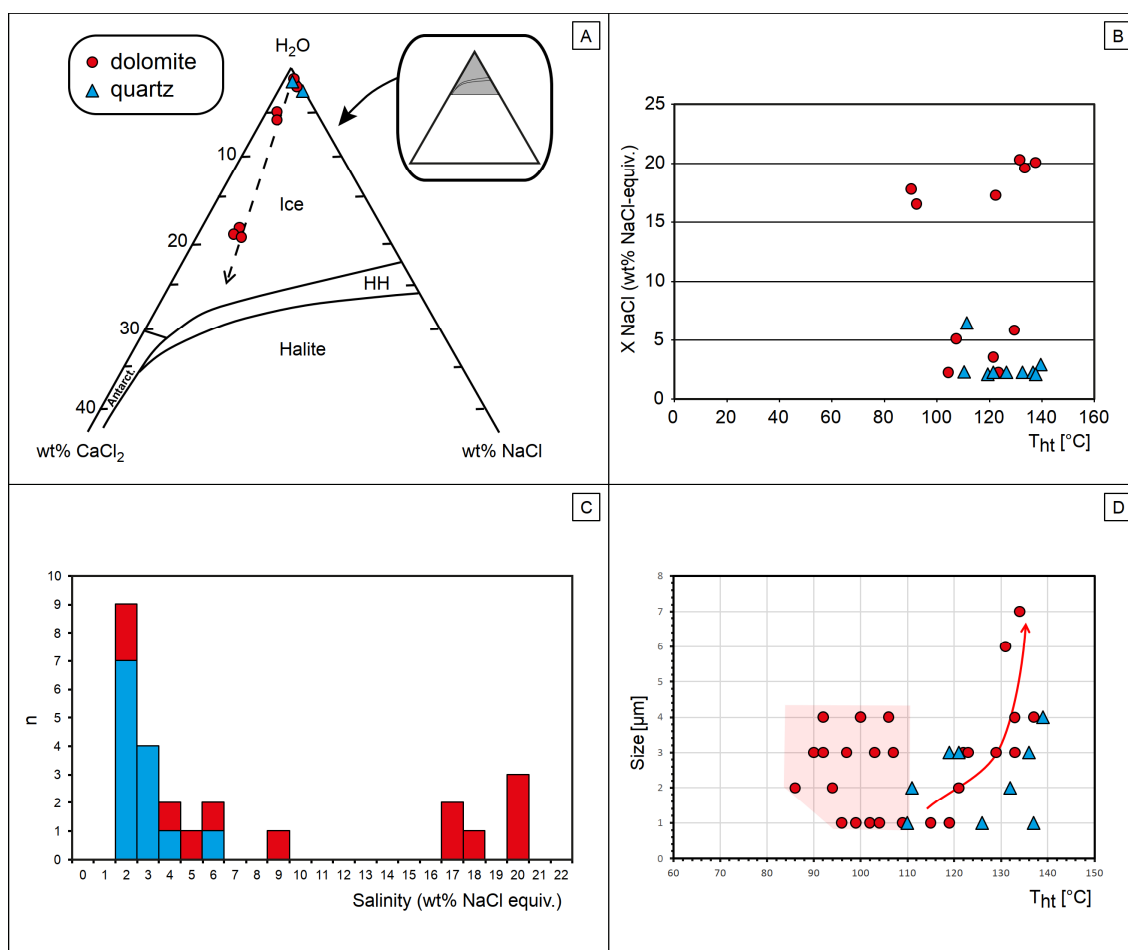


Fig. 4.3: Microthermometry. (A) The system  $\text{H}_2\text{O}-\text{CaCl}_2-\text{NaCl}$  showing the stability fields of ice, hydrohalite (HH), halite and antarcticite. The plotted bulk-salt concentrations are derived from hydrohalite and ice-melting temperatures. (B) Homogenisation temperature vs. NaCl (wt% NaCl-equivalent) of fluid inclusions. (C) Salinity (wt% NaCl equivalent) vs. counts (N) of fluid inclusions. (D) Homogenisation temperature vs. size of fluid inclusions.

Total homogenisation temperatures ( $T_{\text{ht}}$ ) of the fluid inclusions in dolomite are mostly in the range between 86 and 137 °C, with a frequency maximum at c. 120 °C. In quartz cement, homogenisation temperatures fall in the 110–139 °C range and overlap with the higher  $T_{\text{ht}}$  found for dolomite (Fig. 4.3). On the other hand, all-liquid inclusions were found also in the dolomite cement, which must represent lower formation temperatures.

The fluid-inclusion measurements are the base for isochore calculations (ISOC software; Bakker, 2003) to estimate the P-T conditions of fluid trapping. The paleo-geothermal gradient during the Mesozoic was estimated with c. 40 °C/km (Duschl et al., 2016). Fluid inclusions must have been trapped at the intersection of the isochores and the appropriate paleo-geothermal gradient.

It was found, that fluid inclusions in dolomite cement must be trapped at a burial depth of at least c. 2.4 km and c. 4.3 km at maximum, deriving from the calculated formation

temperatures between c. 120 and c. 190 °C (Fig. 4.4). Fluid inclusions in quartz must be trapped at a burial depth of at least c. 3.3 km and c. 4.5 km, deriving from the calculated formation temperatures between c. 150 and c. 200 °C (Fig. 4.4).

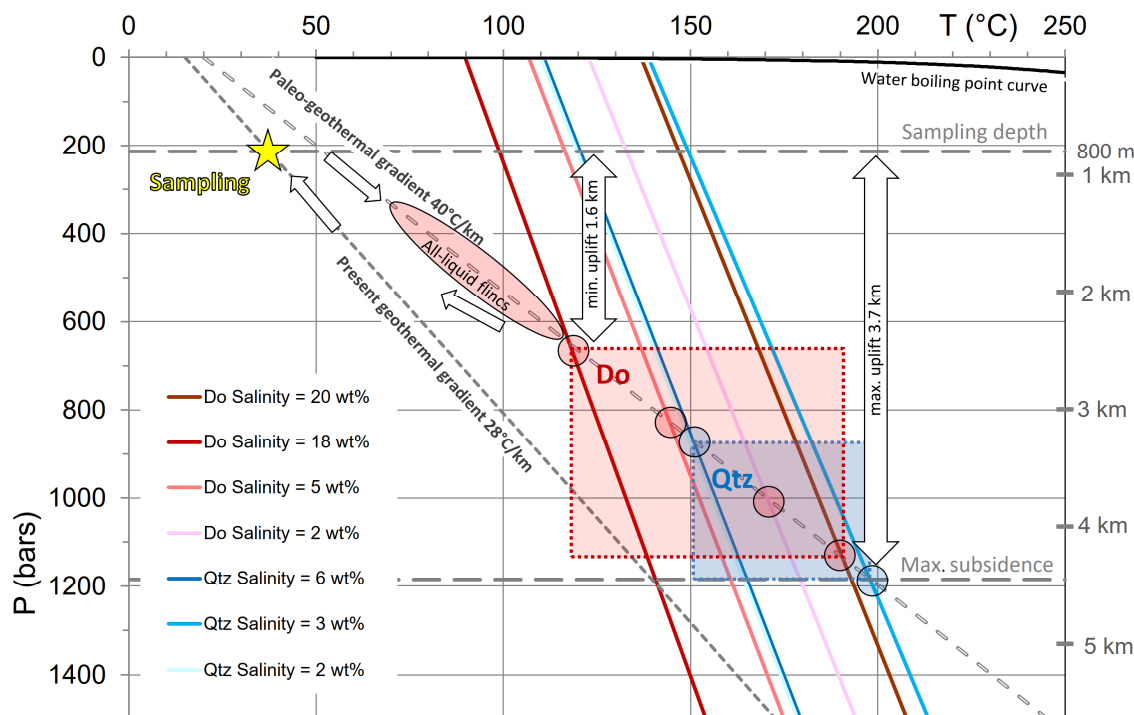


Fig. 4.4: Thermobarometric estimates for fluid inclusions in dolomite (Do) and quartz (Qtz) hosted by Schilfsandstein from the cored well Wolgast 1/1A/63, showing the range of trapping conditions. Depositional temperatures of c. 20 °C according Hornung et al. (2007). The results predict a possible uplift from c. 1.6 to 3.7 km for the Schilfsandstein.

### 4.3.5 Stable isotopes

#### 4.3.5.1 Carbon and oxygen isotopes

The stable isotopes ( $\delta^{18}\text{O}_{\text{SMOW}}$  and  $\delta^{13}\text{C}_{\text{PDB}}$ ) of calcitic and dolomitic cementations were measured from well samples. A summary of the isotope data is given in Table 4.2.

The  $\delta^{13}\text{C}_{\text{PDB}}$  values are similar in dolomite and calcite, but calcite has a larger range of values. Dolomite shows values between -6.63 and -3.58 ‰ and calcite between -8.07 and -1.45 ‰. In detail, the  $\delta^{13}\text{C}_{\text{PDB}}$  values of calcite range from -7.88 to -3.83 ‰ in the Lower Schilfsandstein Member (n = 13) and from -8.07 to -1.45 ‰ in the Upper Schilfsandstein Member (n = 4). The  $\delta^{13}\text{C}_{\text{PDB}}$  values of dolomite range from -5.98 to -3.58 ‰ in the Lower Schilfsandstein Member (n = 6) and from -6.63 to -4.70 ‰ in the Upper Schilfsandstein Member (n = 4). No significant trends are noticeable comparing the Schilfsandstein Members to each other.



Dolomite tendentially shows higher  $\delta^{18}\text{O}_{\text{SMOW}}$  values between 24.98 and 29.10 ‰ than calcite (values between 20.18 and 26.59 ‰). In detail, the  $\delta^{18}\text{O}_{\text{SMOW}}$  values of calcite range from 20.18 to 24.26 ‰ (in  $\delta^{18}\text{O}_{\text{PDB}}$ : -10.36 to -6.40 ‰) in the Lower Schilfsandstein Member (n = 13) and from 20.28 to 26.59 ‰ (in  $\delta^{18}\text{O}_{\text{PDB}}$ : -10.26 to -4.14 ‰) in the Upper Schilfsandstein Member (n = 4). The  $\delta^{18}\text{O}_{\text{SMOW}}$  values of dolomite range from 25.28 to 28.21 ‰ (in  $\delta^{18}\text{O}_{\text{PDB}}$ : -4.24 to -1.40 ‰) in the Lower Schilfsandstein Member (n = 6) and from 24.98 to 29.10 ‰ (in  $\delta^{18}\text{O}_{\text{PDB}}$ : -4.53 to -0.53 ‰) in the Upper Schilfsandstein Member (n = 4).

In the Lower Schilfsandstein Member the  $\delta^{18}\text{O}_{\text{SMOW}}$  values of dolomite are significantly higher than the  $\delta^{18}\text{O}_{\text{SMOW}}$  values of calcite. Likewise, the  $\delta^{18}\text{O}_{\text{SMOW}}$  values of dolomite also tend to be higher than the  $\delta^{18}\text{O}_{\text{SMOW}}$  values of calcite in the Upper Schilfsandstein Member.

Table 4.3: Properties of measured fluid inclusions in quartz and dolomite of the Schilfsandstein Members.

Well	Sample	Present sample depth [m]	Stratigraphy	Host authigenic mineral	Phases at Troom	FI Number	Type	vol. frac. H <sub>2</sub> O	Size [µm]	T <sub>0</sub> [°C]	T <sub>m, HI</sub> [°C]	T <sub>m, ice</sub> [°C]	Salinity		T <sub>H</sub> [°C]	LV	Composition					
													wt% NaCl	wt% CaCl <sub>2</sub>								
11-03	785,10	Lower Schilfsandstein Mb	dolomite	LV 1	primary	0.87	1 x 3															
				LV 2	primary	0.90	3 x 1															
				LV 3	primary	0.90	2 x 4															
				LV 4	primary	0.95	1 x 3	-53	-33,4	-3,1												
				LV 1	primary	0.97	1 x 3															
				LV 2	primary	0.90	2 x 4															
				LV 3	primary	0.97	2 x 2															
				LV 4	primary	0.90	1 x 4															
				LV 1	primary	0.95	4 x 6															
				LV 2	primary	0.95	2 x 4															
				LV 1	primary	0.97	2 x 3															
				LV 2	primary	0.97	1 x 1															
				LV 3	primary	0.97	1 x 1															
				LV 4	primary	0.97	2 x 2															
				LV 5	primary	0.95	3 x 4	-22														
LV 6	primary	0.95	1 x 1																			
LV 7	primary	0.97	1 x 3																			
LV 8	primary	0.97	1 x 3																			
LV 1	primary	0.95	1 x 2																			
LV 2	primary	0.95	1 x 3																			
LV 2	primary	0.97	2 x 2																			
LV 3	primary	0.95	1 x 1																			
LV 4	primary	0.97	1 x 3																			
LV 5	primary	0.97	1 x 1																			
LV 6	primary	0.97	1 x 1																			
LV 1	primary	0.90	1 x 3																			
LV 2	primary	0.95	1 x 1																			
LV 1	primary	0.95	1 x 4																			
LV 2	primary	0.97	1 x 1																			
LV 1	primary	0.95	4 x 6	-66																		
LV 2	primary	0.95	4 x 7																			
LV 3	primary	0.90	1 x 3																			
LV 4	primary	0.90	1 x 1																			
LV 5	primary	0.95	1 x 4																			
LV 1	primary	0.97	1 x 3																			
LV 1	primary	0.97	1 x 4																			
LV 1	primary	0.95	1 x 3																			
LV 1	primary	0.97	1 x 3																			
LV 2	primary	0.97	1 x 2																			
LV 3	primary	0.97	1 x 2																			
LV 1	primary	0.97	1 x 3																			
LV 2	primary	0.97	1 x 3																			
LV 1	primary	0.95	3 x 4																			
LV 1	primary	0.95	7 x 12																			
11-08	761,80	Lower Schilfsandstein Mb	dolomite																			
11-11	754,50	Lower Schilfsandstein Mb	dolomite	LV 1	primary	0.90	1 x 3															
				LV 2	primary	0.95	1 x 1															
				LV 1	primary	0.95	1 x 4															
				LV 2	primary	0.97	1 x 1															
				LV 1	primary	0.95	4 x 6	-66														
				LV 2	primary	0.95	4 x 7															
				LV 3	primary	0.90	1 x 3															
				LV 4	primary	0.90	1 x 1															
				LV 5	primary	0.95	1 x 4															
				LV 1	primary	0.97	1 x 3															
				LV 1	primary	0.97	1 x 4															
				LV 1	primary	0.95	1 x 3															
				LV 1	primary	0.97	1 x 3															
				LV 2	primary	0.97	1 x 2															
				LV 3	primary	0.97	1 x 2															
LV 1	primary	0.97	1 x 3																			
LV 1	primary	0.97	1 x 3																			
11-12	753,50	Lower Schilfsandstein Mb	dolomite																			

Isotope fraction curves showed in Fig. 4.5 are derived from Friedman and O'Neil (1977) for calcite and from Fritz and Smith (1970) for dolomite. These calculations enable to make evidences about paleofluids and formation temperatures. The Upper Triassic sea water had values of  $-0.12 \delta^{18}\text{O}_{\text{SMOW}}$  according to Rigo and Joachimski (2010).

Calcite showing  $\delta^{18}\text{O}_{\text{PDB}}$  values from  $-10.36$  to  $-4.14$  ‰, is inferred to precipitate from pore-water with temperatures from  $34$ – $70$  °C (Fig. 4.5). The analysed dolomite offering  $\delta^{18}\text{O}_{\text{PDB}}$  values between  $-4.53$  ‰ and  $-0.53$  ‰, is inferred to have precipitated at temperatures of  $42$ – $65$  °C (Fig. 4.5).

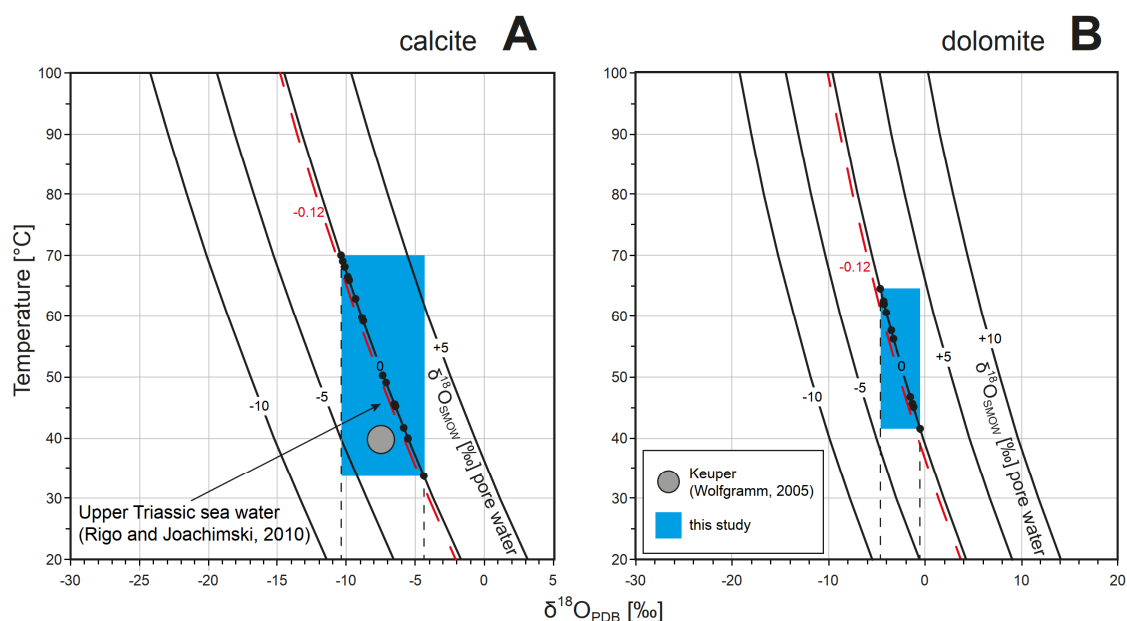


Fig. 4.5: Range of temperature and  $\delta^{18}\text{O}_{\text{SMOW}}$  values of pore-waters calculated from oxygen isotopes of: (A) calcite-cemented sandstone samples (isotope fractionation curve is derived from Friedman and O'Neil (1977). Calcite with  $\delta^{18}\text{O}_{\text{PDB}}$  values (-10.36 to -4.14 ‰) is inferred to precipitate from pore-water with temperatures from 34–70 °C. (B) Dolomite-cemented sandstone samples (isotopic fractionation curve is from Fritz and Smith (1970)). Dolomite with  $\delta^{18}\text{O}_{\text{PDB}}$  values (-4.53 to -0.53 ‰) is inferred to have precipitated at temperatures of 42–65 °C.

#### 4.3.5.2 Sulphur isotopes

The stable isotopes ( $\delta^{34}\text{S}_{\text{VCDT}}$ ) of authigenic anhydrite were measured as the chemical precipitated barite. A summary of the isotope data is given in Table 4.2.

The  $\delta^{34}\text{S}_{\text{VCDT}}$  values range from 12.5 to 16.7 ‰ in the Schilfsandstein Members (6 Delta Channel, 1 Fluvial Channel and 1 Floodplain Diagenesis Types; according to Niegel and Franz (2023)) and the Neubrandenburg Member has one measured value of 24.5 ‰. So, the Schilfsandstein Members show values lower than recent seawater and the Neubrandenburg Member higher than recent seawater. Six values (12.6 to 13.8 ‰) are lower and three values (15.8 to 24.5 ‰) are higher than the global trend of  $\delta^{34}\text{S}_{\text{VCDT}}$  values.

Within the Schilfsandstein Members, no trend in  $\delta^{34}\text{S}_{\text{VCDT}}$  values is noticeable. Only the value of the Neubrandenburg Member (24.5 ‰) seems to be an outlier.

#### 4.3.6 U/Pb dating of carbonates

The preliminary measured concordia ages are  $231.6 \pm 19.9 / 20.00$  Ma (24 documented ages, Fig. 4.6) for calcite cementation and  $101.7 \pm 54.2 / 54.2$  Ma

(33 documented ages, Fig. 4.7) for dolomite cementation. The U/Pb dating has shown 8 ages for dolomite and 7 ages for calcite, which are not within the isochrone and have therefore been excluded for the evaluation. The ages have mean squared weighted deviates (MSWD) of 1.51 (dolomite) and 2.86 (calcite). This indicates some scatter in the data that may be attributed to an analytical error, a slight open U-Pb system behavior in some domains, or no complete initial equilibration of the Pb isotopes (Rasbury and Cole, 2009). Because of these uncertainties, the results should be interpreted cautiously and further measurements should be done to increase statistical certainty.

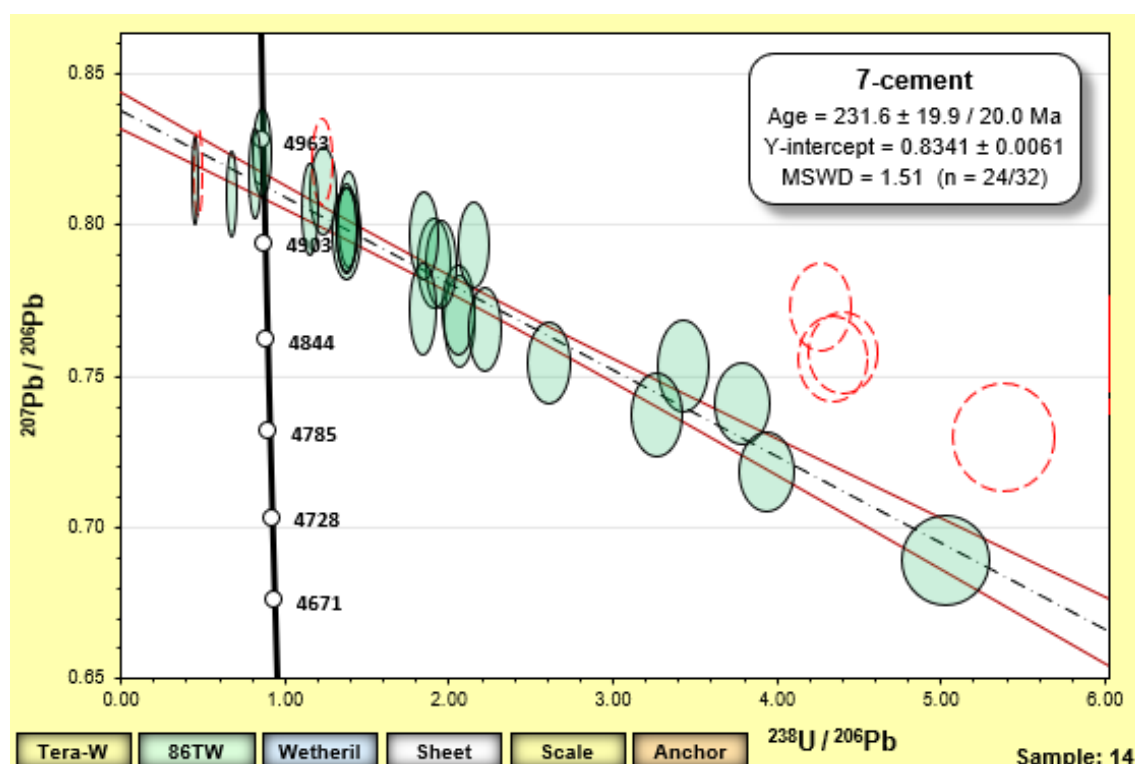


Fig. 4.6: Concordia diagram showing results of U/Pb dating of dolomite; sample 11-03 of Kb Wolgast 1/1A/63, Fluvial Channel Diagenesis Type (according to Niegel and Franz, 2023), Lower Schilfsandstein Member 24 ages (green circles) and 8 excluded ages due to analytical uncertainties (circles with red dashed lines).

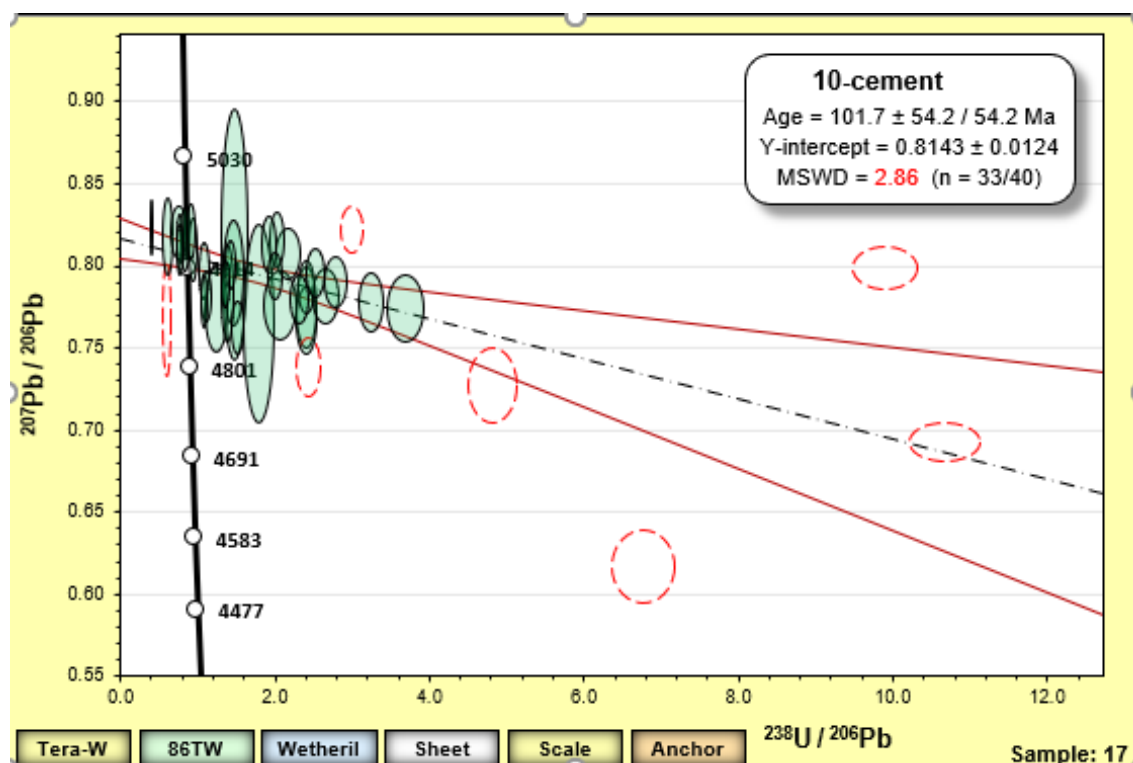


Fig. 4.7: Concordia diagram showing results of U/Pb dating of calcite; sample 11-11 of Kb Brustorf 1/62, Delta Channel Diagenesis Type (according to Niegel and Franz, 2023), Lower Schilfsandstein Member 33 ages (green circles) and 7 excluded ages due to analytical uncertainties (circles with red dashed lines).

#### 4.3.7 Reactive transport modelling

Modelling in a closed geochemical system without external influx of e.g. pore waters did not generate results (saturation indices) which represented the typical diagenetic sequences of the Schilfsandstein. So, we decided to focus only on authigenic analcime. Therefore, the model was adjusted to precipitate analcime (Fig. 4.8).

The simulation without tephra generated negative saturation indices during the whole time of heating. Thus, no analcime is precipitated. Adding tephra to the reactive transport modelling increases the saturation indices close to zero and higher. At the beginning of the simulation the saturation indices are positive and so analcime can be precipitated. After this peak during further heating the saturation indices decrease towards zero. Thus, analcime seems not to be stable at increasing temperatures.

The results of the reactive transport modelling (Fig. 4.8) show that detrital tephra deposits could be a possible component to form analcime in the Schilfsandstein.

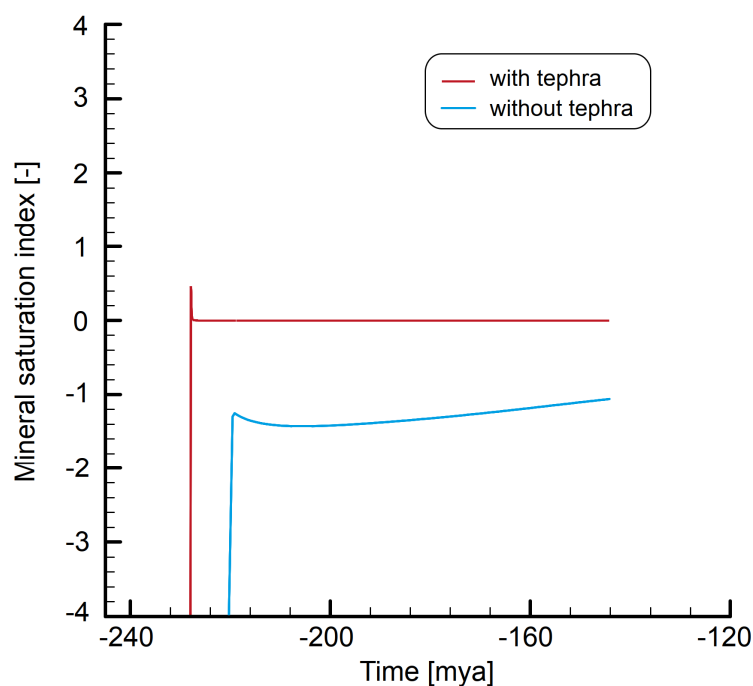


Fig. 4.8: Simulated saturation index of analcime with and without detrital tephra. The timescale, representing geological age, proceeds from depositional time to postulated maximal burial depth.

## 4.4 Discussion

### 4.4.1 Origin of authigenic carbonates and quartz

#### 4.4.1.1 Stable isotopes of calcite and dolomite

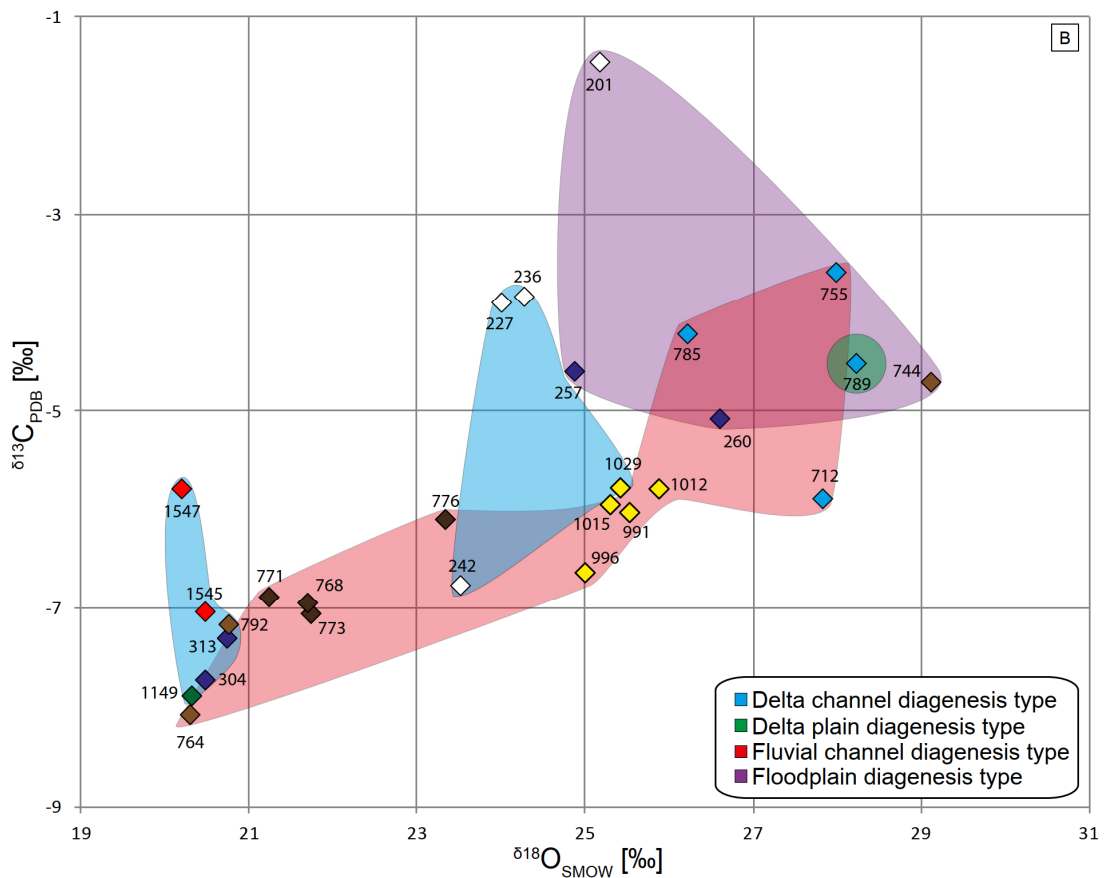
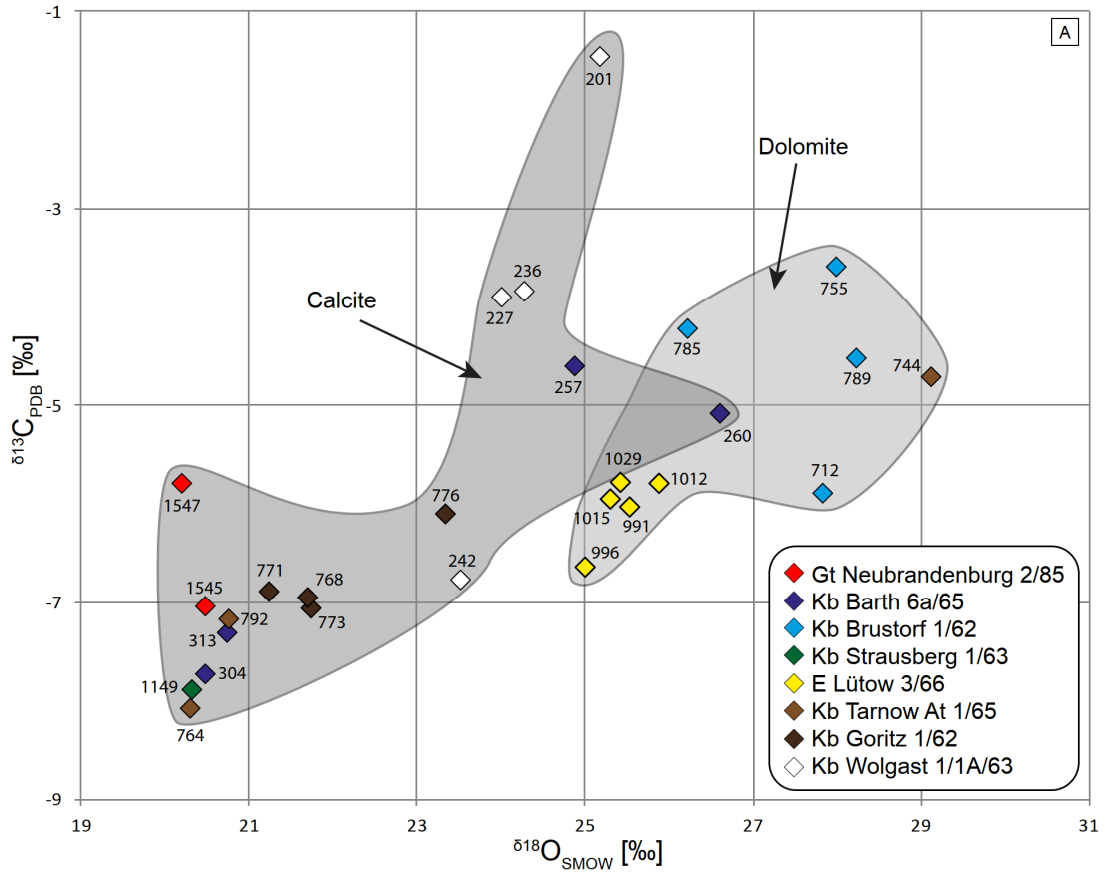
Dolomite and calcite, tendentially have decreasing values of  $\delta^{13}\text{C}_{\text{PDB}}$  with increasing present depths and thus increasing temperatures (Fig. 4.9). In general, negative  $\delta^{13}\text{C}_{\text{PDB}}$  signatures suggest that they originate from decarboxylation of organic matter and  $\text{Ca}^{2+}$  ions in formation water with the addition of  $\text{CO}_2$  (Cao et al., 2017). Furthermore, calcite and dolomite separately show a trend to lower  $\delta^{18}\text{O}_{\text{SMOW}}$  values in greater depths. These decreasing values are related to increasing temperatures and fluid-rock interactions during burial diagenesis (Cao et al., 2017), which is in accordance with the trend of greater depths at lower values.

Further, there seems to be a dependence of the depositional regime. So, the Delta Channel Diagenesis Type tend to lower  $\delta^{13}\text{C}_{\text{PDB}}$  and  $\delta^{18}\text{O}_{\text{SMOW}}$  values than the Delta Plain and Floodplain Diagenesis Types, representing the overbank facies (Fig. 4.9). The Fluvial Channel Diagenesis Type represents a wide value range and offers no significant trend.

The wells Tarnow At 1/65, Neubrandenburg 2/85 and Kb Brustorf 1/62 have nearly the same location in the North German Basin (Fig. 2.1). The carbonates in the Stuttgart Formation of these wells offer quite different  $\delta^{18}\text{O}_{\text{SMOW}}$  values and do not show a common trend to basinal and meteoric waters. Therefore, the location within the North German Basin, regarding to basin centre or marginal fault zones, can be excluded as reason for the fluid evolution. In general, the  $\delta^{13}\text{C}_{\text{PDB}}$  signatures are known from Rotliegend sediments (Platt, 1993; Sullivan et al., 1990; Rieken, 1988; Bath et al., 1987) or meteoric carbonates (Moore and Druckmann, 1981).

---

Fig. 4.9 (*acing page*): Correlation of  $\delta^{18}\text{O}_{\text{SMOW}}$  and  $\delta^{13}\text{C}_{\text{PDB}}$  values of calcite and dolomite in the Schilfsandstein Members from different locations. For location see Fig. 3.1. Values at the markers represent the present depths of samples in meter. (A) Clusters of dolomite and calcite. (B) Clusters of diagenesis types described by Niegel and Franz (2023).





The measured values of  $\delta^{18}\text{O}_{\text{SMOW}}$  can be used as geothermometer (Fig. 4.5). According to Hornung et al. (2007), temperatures of c. 20 °C were present in the Julian. So, the adjusted temperatures (14–50 °C), resulting from the Isotope fraction curve (Fig. 4.5), at a paleo-geothermal gradient of c. 40 °C/km (Duschl et al., 2016) represent depths of 350–1250 m. Therefore, either the calcite was formed in a depositional to eogenetic regime or during a second prograding diagenesis in the Albian to Cenomanian. The adjusted temperatures (22–45 °C) represent formation depths from 550–1125 m for dolomite. Thus, dolomite was formed in an eogenetic to mesogenetic regime (Fig. 4.10).

The results of the isotopic analysis (45–56°C) and fluid inclusions (up to 190 °C) of dolomite show different ranges of formation temperatures in the Wolgast well. In general, the direct method of fluid inclusion analyses is more precise than the isotopic analysis of carbonates in bulk rock samples. Inaccuracies relating to the indirect method of bulk rock analysis can result from recrystallised carbonates, which, therefore, would not be representative for the maximum formation temperature. Mixed signatures of different authigenic carbonates and/or carbonatic detrital grains can also lead to uncertainties.

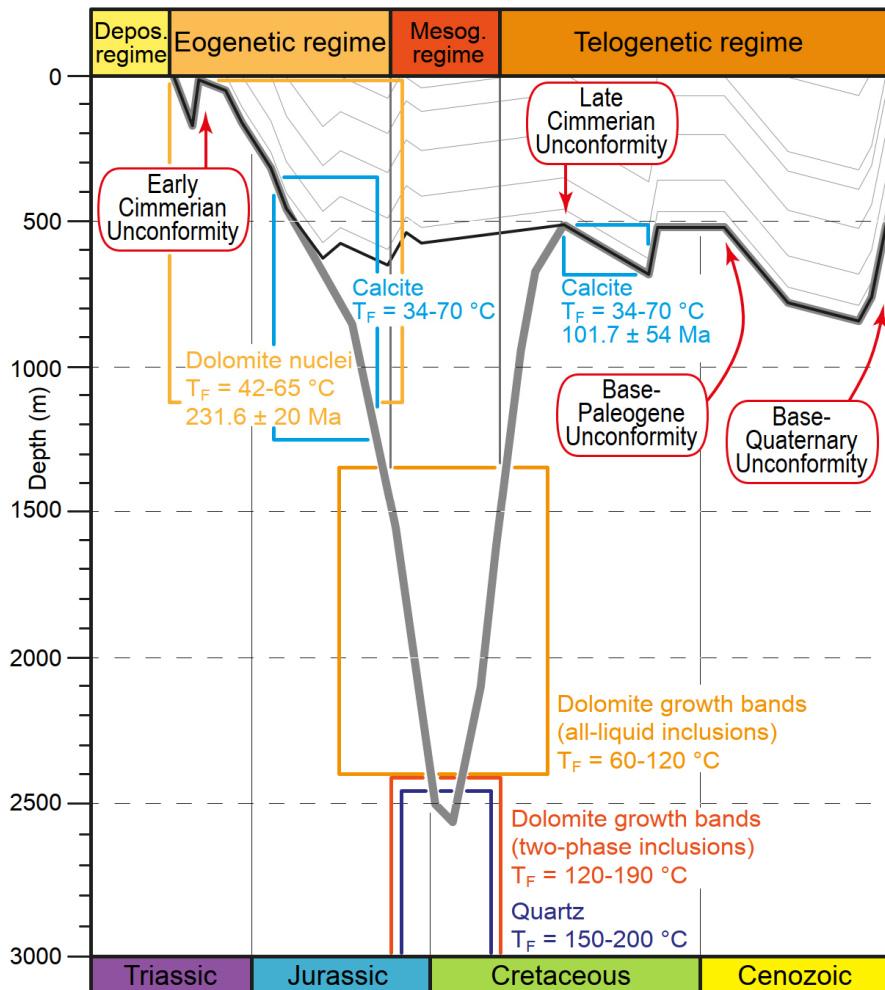


Fig. 4.10: Schematic burial and diagenetic history of the Schilfsandstein in NE Germany. Burial history of the well Loissin 1 after Friberg (2001). Time and depth of formation of the respective mineral phases investigated in this study are marked by coloured rectangles.  $T_F$  = formation temperature. Temperature-dependent authigenic minerals, i.e. observed in the Wolgast 1a well (12 km distance to Loissin 1), indicate a maximum burial depth of c. 2.500 m (bold grey line). However, temperature history modelling of Friberg (2001) resulted only in c. 50 °C maximum burial temperature (thin black and grey lines), modified after Niegel and Franz (2023).

#### 4.4.1.2 Microthermometry of dolomite and quartz

Thermobarometric estimates for fluid inclusions in ferroan dolomite and quartz hosted by Schilfsandstein from the cored well Wolgast 1/1A/63, show the range of trapping conditions (Fig. 4.4). Considering a sampling depth of c. 800 m suggests an uplift of c. 1.6 to maximal 3.7 km since Mesozoic times. As dolomite formed before the quartz cement, we assume that a part of the fluid inclusions in dolomite must have been trapped already at an early subsidence stage with formation temperatures probably between c. 60 and 120 °C (c. 1.3–2.4 km max. subsidence, Fig. 4.10). Based on the isotopic fractionation curve, the lowest temperatures agree approximately with the calculated temperatures (45–56 °C, Table 4.2) in the Schilfsandstein of the Wolgast

well, (Fritz and Smith, 1970; Fig. 4.5). We consider the all-liquid inclusions, which survived natural heating during ongoing subsidence are the earliest inclusions recorded in the samples. This interpretation assumes that necking down did not occur at a later stage of rock evolution. This assumption can be made here, as no textural evidence for necking down was found in the samples (e.g., Goldstein and Reynolds, 1994). Accordingly, the biphasic inclusions must have formed at least in part by stretching as a response to natural heating. This interpretation is supported by the observation that larger fluid inclusions (up to 7  $\mu\text{m}$ ) are found only in dolomite (Fig. 4.3), although the size of the inclusions in dolomite and quartz do normally not exceed 5  $\mu\text{m}$ . These larger inclusions correspond to the highest homogenisation temperatures. Therefore, we assume that fluid inclusions in dolomite with  $T_h > \text{c. } 110^\circ\text{C}$  correspond to stretched inclusions, which equilibrated during the overprint caused by natural heating of up to  $\text{c. } 200^\circ\text{C}$  (up to  $\text{c. } 4.5$  km max. subsidence; Fig. 4.10). Quartz cement was partly formed later than dolomite at temperatures between  $\text{c. } 150$  and  $200^\circ\text{C}$  ( $T_h$ :  $110$ – $140^\circ\text{C}$ ;  $\text{c. } 3.3$ – $4.5$  km max. subsidence). Considering the present depth of the Schilfsandstein between 785.1 and 754.5 m in the Wolgast well, however, a temperature of approx.  $50^\circ\text{C}$  has to be assumed, which leads to a discrepancy.

The wide spread of the salinity found for inclusions in the dolomite cement can be interpreted as mixture between early-diagenetic (low-salinity, NaCl-bearing) and late-diagenetic (high-salinity  $\text{CaCl}_2$ -rich) fluids (Fig. 4.3). The higher  $\text{CaCl}_2$ -contents can be explained by the increasing alteration/albitization of plagioclase in the arkose sandstone, which results in higher  $\text{Ca}^{2+}/\text{Na}^+$  ratios in solution. These compositions are characteristic for the deep fluids in the North German Basin (e.g., Wolfgramm, 2012). The absence of high-salinity  $\text{CaCl}_2$ -rich inclusions in the quartz cement suggests that the exchange between the pore fluids and fluid inclusions were more limited in quartz cement compared to dolomite.

#### 4.4.1.3 U/Pb dating of carbonates

In general, examples of U/Pb dating of carbonates are very rare. The carbonates presented here are the first examples from the Central European Basin to be analysed using this method.

The age of Fe-dolomite ( $231.6 \pm 19.9 / 20.00$  Ma, Fig. 4.6) coincides with a depositional age of  $231.1 \pm 1.6$  Ma (Zeh et al., 2021), representing eogenetic carbonate cementation. This is in agreement with the documented eogenetic carbonate cementation of Niegel and Franz (2023), which prevented the mechanical compaction

during burial diagenesis. However, Niegel and Franz (2023) described calcite as eogenetic grain fabric supporting cementation for this. A potential source for the dolomite is the overlying dolomitic Beaumont Member, from where fluids may have migrated into the Schilfsandstein. For this, the Beaumont Member must directly overlay the Schilfsandstein Member (e.g. in the Neubrandenburg well, Fig. 2.3). Another potential source could be the basal Arnstadt Formation (*Basisdolomit*), which has an erosive discordant contact with the underlying Stuttgart Formation in the Wolgast well, resulting from the Cimmerian Unconformity. The eogenetic dolomite is in contrast to the dolomite documented by Niegel and Franz (2023, see chapter III), which was classified as mesogenetic cementation. Remarkably, dolomite, offering two phases of formation with lower formation temperatures between c. 60 and 120 °C (all-liquid inclusions) and higher formation temperatures between c. 120 and 190 °C (two-phase inclusions) represents mesogenetic conditions (see chapter 4.4.1.2 and Fig. 4.10). The data of temperature ranges of Mansurbeg et al. (2008) with 50–140 °C, Khalifa and Morad (2012) with 80–140 °C and McNeil et al. (1995) with 100–125 °C support the mesogenetic precipitation of ferroan dolomite too.

The analysed Fe-dolomite in the Wolgast well shows growth bands (chemical zonation, Figs. 3.13H and 4.1G), possibly representing an ongoing cementation from eogenetic to mesogenetic regime during the basin evolution. This hypothesis is supported by the fluid inclusions, which demonstrate two phases of mesogenetic dolomite. Possibly, the U/Pb dating analysed the eogenetic dolomite nuclei and the microthermometric measurements document the fluid inclusions in the mesogenetic dolomite growth bands. This is consistent with the fact that fluid inclusions in dolomite typically decorate growth zones or are concentrated at the boundary between roundish dolomite nuclei and zoned blocky dolomite (see chapter 4.3.4). According to Goldstein and Reynolds (1994), two-phase inclusions can be expected above 50°C. Thus, a temperature of < 50°C can be assumed for the dolomite nuclei, which is consistent with the temperatures (45–56 °C) calculated by isotopic analysis of dolomite in the Wolgast well.

The age of calcite ( $101.7 \pm 54.2 / 54.2$  Ma, Fig. 4.7) corresponds to latest Albian age (102 Ma). This represents the late-stage uplift (telogenesis), following the burial maximum in the latest Jurassic maximum burial. The sediments of the Albian could be a potential source for the precipitated calcite in the Schilfsandstein Member. However, in the Wolgast well, there are more than c. 630 m between the Stuttgart Formation and the Albian, what seems to be too far for migration of pore fluids. Calcite dissolution during the uplift with subsequent recrystallization of calcite during the post-Albian

reburial could be another possible process. After that, a second retrograde diagenesis, presumably during the Upper Cretaceous/Tertiary, must have taken place, as today's Schilfsandstein shows opened pore space. This scenario would be in accordance with the burial history, showed in Fig. 3.17 and the analysed formation temperatures from 34 to 70 °C (see chapter 4.4.1.1).

#### 4.4.2 Origin of authigenic sulphates

Comparing the results of sulphur isotope analyses with data from the literature, the sulphates of the Schilfsandstein fit well into the global trend curve of sulphur (see Fig. 4.11). The sulphur isotopes in the range of 12.5 to 16.7 ‰ correspond to values between the marine deposited Zechstein sulphates and the Gipskeuper. The sulphur isotopes indicate that the sulphates were formed by a mixture of fluids, originating from the Late Permian (Zechstein) and Triassic (Fig. 4.11). Only the sample of the Neubrandenburg Member tends to originate more from Muschelkalk fluids.

The sulphur isotopes of the Schilfsandstein are lower than the sulphur isotopes of recent seawater. Early diagenetic sulfur isotope evolution is characterised by a prominent isotope fractionation associated with bacterial sulfate reduction, resulting in decreasing  $\delta^{34}\text{S}_{\text{VCDT}}$  values (Hesse and Gaupp, 2021). This is proven by the occurrence of typical pyrite framboids in the sandstones of the Stuttgart Formation.

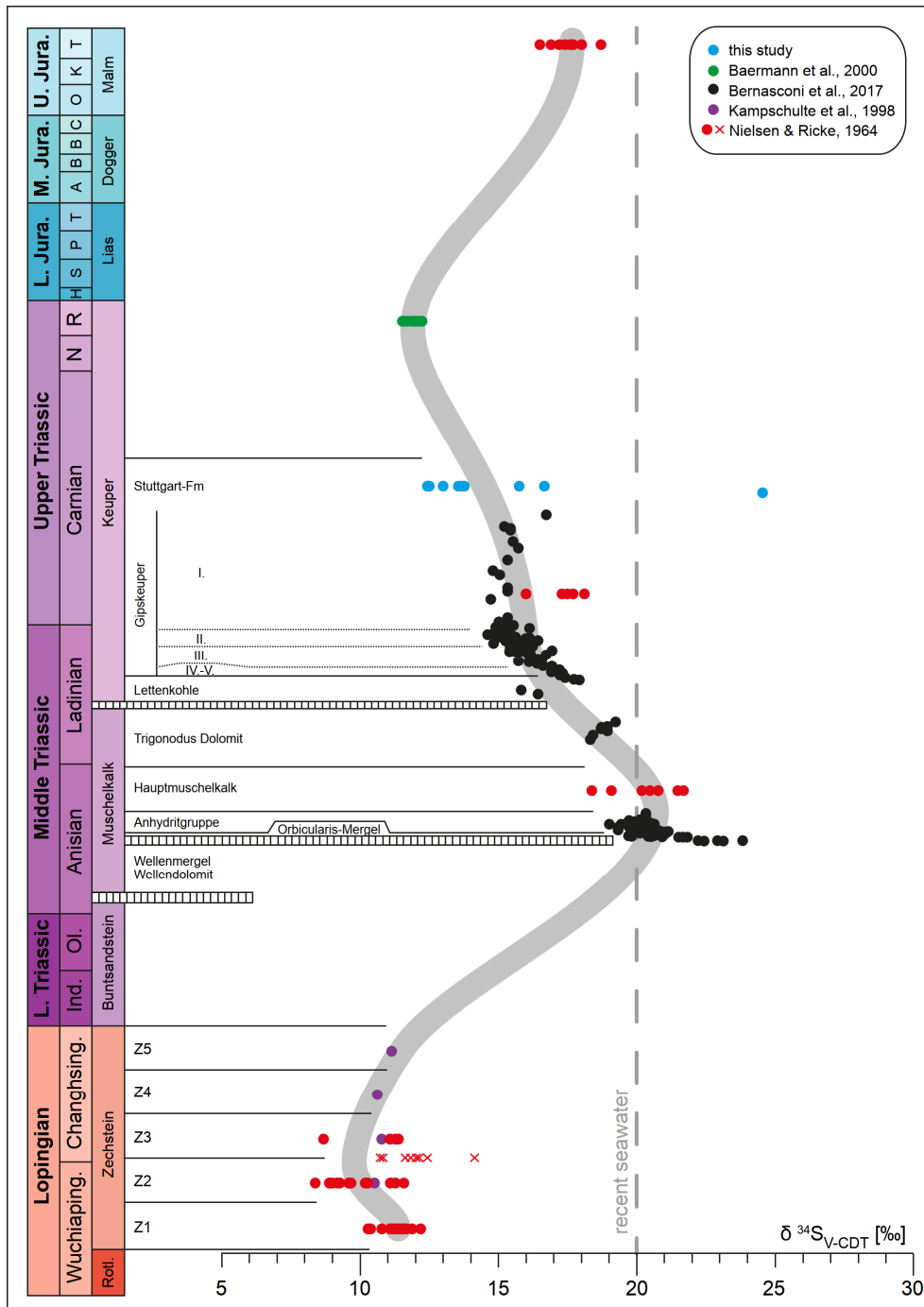


Fig. 4.11:  $\delta^{34}\text{S}$  values of oceanic sulphate. Black areas represent values of evaporite sulphates mainly from Central Europe. Grey areas represent values obtained from evaporite basins of presumably not completely marine origin (after Nielsen 1968). Red circle: values in core samples from Allermoehe 1 (Baermann et al. 2000). Green diamonds: values in core samples of five wells in the North German Basin. The grey curve is the sulphur trend of sulphate from the German Basin.

#### 4.4.3 Origin of authigenic analcime

The formation of analcime was already discussed in chapter 3.5.1.3. According to this, thermal degradation of volcanic ash, which started in the eogenetic regime (see Hay, 1966, 1978; Hay and Sheppard, 2001; Weibel et al., 2019), finally led to the precipitation of analcime in the mesogenetic regime.

The simplified model verifies only that the precipitation of analcime is favoured by the diagenetic degradation of volcanic detritus. The mesogenetic formation is not supported by the reactive transport modelling, as the model suggests a precipitation in the eogenetic regime.

In general, the model is limited regarding to the integration of e.g. influx of pore waters and uplift during diagenetic or basin evolution. Reactive transport modelling should therefore be considered more as a tool to show trends in mineral precipitation.

#### 4.4.4 Explanation for higher formation temperatures

In chapter 2.6.3 the conflict between the low to intermediate grain packaging and the burial history of the Stuttgart Formation was noted. Furthermore, based on the documented diagenetic pathways and parageneses of the Schilfsandstein, maximum burial temperatures and depths as well as a possible burial history are offered in chapter 3.5.2.

The following reasons could explain the higher formation temperatures compared to the recent burial depths of the Schilfsandstein: (1) stretching of fluid inclusions, (2) higher paleogeothermal gradient, and/or (3) the sediments were buried deeper than previously known.

##### (1) stretching of fluid inclusions

Total homogenisation temperature ( $T_{ht}$ ) of dolomite was obtained in the range between 86 and 137 °C. Stretching may explain the higher homogenisation temperatures, i.e. internal pressure causes the crystal to plastically deform (stretch) resulting in a shift of 10–20 °C. The fluid inclusions in quartz homogenise at higher temperatures, between 110 and 139 °C. Goldstein (1986) states that stretched (but not decrepitated) inclusions still retain their chemical composition. On the other hand, Burruss (1987) assumed that stretched inclusions yield a poor record of the low-temperature history, but they correspond to maximum temperatures experienced during rock evolution. The

calculated formation temperatures of stable isotopes argue for stretching of fluid inclusions to explain the high formation temperatures. But the temperatures were detected in two different authigenic minerals (dolomite and quartz), which argue against stretching.

## (2) higher paleogeothermal gradient

Another possible explanation for the conflict is, that the geothermal palaeogradient must have been higher than the current geothermal gradient. According to Hornung et al. (2007), temperatures of c. 20 °C were present in the Julian. To reach formation temperatures of about 120–200 °C (quartz and dolomite) at a present depth of the Schilfsandstein of 785.1 to 754.5 m (Wolgast well), a geothermal palaeogradient of about 129.9–233.8 K per km would have been essential. This is not consistent with the known geothermal gradients of 32–90 K per km of depth (Wolfgramm et al., 2014 and Duschl, 2018) and can therefore be excluded.

Such discrepancies between maximum burial depth and measured temperature are known in the North German Basin (e.g. Hoth, 1997; Friberg, 2001 and discussed therein). So, these high temperatures may have been realised during a Mesozoic thermal event during the Cimmerian tectonic activity (Wolfgramm et al., 2018; Wolfgramm, 2005; Wolfgramm and Schmidt-Mumm, 2001). Hoth (1997) describes anomalous diagenetic modifications in Mesozoic sediments, resulting from multiphase intrusive bodies, which were effected subsequently a convective heat transport caused by pore water circulation at fault zones.

## (3) sediments were buried deeper than previously known

In sedimentary rocks the fluid inclusion data delimit the highest temperature reached during diagenesis. Isochore calculations indicate a minimum depth of fluid trapping at c. 2.4 km (Fig. 4.4) for the Stuttgart Formation considering a palaeogeothermal gradient of c. 40 K/km (Wolfgramm and Schmidt-Mumm, 2001; Japsen et al., 2007; Duschl et al., 2016) and 20 °C palaeosurface temperature (see discussion in Lippmann, 2012).

A minimum uplift of c. 1.6 km is assumed, taking in account that the samples from the Wolgast well originate from c. 2.4 km depth (Fig. 4.4). The calculated burial maximum of about 2.4 km corresponds to the present-day burial depth of 2.5–2.8 km of the Stuttgart Formation in the axial part of the eastern North German Basin (Hoth et



al., 1993). The shallower present day burial depth of 785.1 to 754.5 m in the Wolgast well located to the North of the basin axis is herein related to substantial uplift and erosion during the basin differentiation and inversion stage. The maximum burial temperature of the Stuttgart Formation (120–200 °C) is largely consistent with published thermal maturity and thermochronological data of the Lower–Middle Keuper. Reported vitrinite reflectance (VRr) values of Bachmann et al. (2002, South Germany), Rodon and Littke (2005, NW Germany) and Beyer (2015, Thuringia) were related to burial temperatures of 70–100 °C (Rodon and Littke, 2005; Beyer, 2015). These temperatures correspond roughly to burial history modelling based on apatite fission track data of Lower–Middle Keuper sandstones from Thuringia (von Eynatten et al., 2021). Slightly higher maximum burial temperatures of 85–135 °C for the Stuttgart Formation were suggested by Norden and Frykman (2013) at Ketzin CO<sub>2</sub> storage site (NE Germany), resulting from vitrinite reflectance. The paragenetic sequence of authigenic minerals in the Stuttgart Formation is also consistent with this temperature range (see discussion in Niegel et al., 2023; chapter 3.5). The comparable thermal maturity of Keuper strata points to balanced subsidence pattern in larger parts of the Central European Basin System (CEBS) during the late basin fill stage, followed by the uplift in the northern CEBS and uplift/exhumation of Triassic strata in southern parts of the CEBS.

A calculated maximum subsidence of c. 4.5 km with a subsequent uplift of 3.7 km is not known in the literature and can therefore be excluded for the eastern North German Basin. Furthermore, a thermal event must have additionally influenced these high temperatures.

## **Acknowledgement**

The author acknowledges funding by the Federal Ministry for Economic Affairs and Climate Action (BMWK, grant numbers 0325920). The Geological State Surveys of Brandenburg and Mecklenburg-Vorpommern kindly provided access to core repositories. The support of Graciela M. Sosa, Alfons M. van den Kerkhof (University of Göttingen), Christian Buse (Geothermie Neubrandenburg GmbH), Armin Zeh and Aratz Beranoaguirre (Karlsruhe Institute of Technology) with Cathodoluminescence, XRD, SEM-EDX and U/PB dating analyses is gratefully acknowledged. The sulphate preparation by Benny Fischer and the support of Ulrich Maier with the reactive transport modelling (University of Göttingen) are gratefully acknowledged. The author

acknowledges supervision and valuable discussions with Matthias Franz (University of Göttingen) and Markus Wolfgramm (Schwerin).

## References

- Allison, J. D., Brown, D. S., Novo-Gradac, K. J., 1991. MINTEQA2/PRODEFA2, a geochemical assessment model for environmental systems: version 3.0 user's manual. Environmental Research Laboratory, Office of Research and Development, US Environmental Protection Agency.
- Baermann, A., Kröger, J. Zarth, M. 2000. Anhydritzemente im Rhätsandstein Hamburgs - Röntgen- und Kernspintomographische Untersuchungen und Lösungsversuche. *Zeitschrift für angewandte Geologie*, 46 (3), 144–152.
- Bakker, R. J., 2003. Package FLUIDS 1. Computer programs for analysis of fluid inclusion data and for modelling bulk fluid properties. *Chemical Geology*, 194 (13), 3–23.
- Bao, Z., Haberer, C. M., Maier, U., Amos, R. T., Blowes, D. W., Grathwohl, P., 2017. Modeling controls on the chemical weathering of marine mudrocks from the Middle Jurassic in Southern Germany. *Chemical Geology*, 459, 112. <https://doi.org/10.1016/j.chemgeo.2017.03.021>.
- Bath, A.H., Milodowski, A.E., Spiro, B., 1987. Diagenesis of carbonate cements in Permo-Triassic sandstones in the Wessex and East Yorkshire-Lancashire Basin, UK: a stable isotope study. – In: Marshall, J. D. (ed.): *Diagenesis of sedimentary sequences*. – Spec. Publ. Geol. Soc. London, 36, 174–190.
- Bernasconi, S. M., Meier, I., Wohlwend, S., Brack, P., Hochuli, P. A., Bläsi, H., Wortmann, U. G., Ramseyer, K., 2017. An evaporite-based high-resolution sulfur isotope record of Late Permian and Triassic seawater sulfate. *Geochimica et Cosmochimica Acta*, 204, 331–349. <http://dx.doi.org/10.1016/j.gca.2017.01.047>.
- Beyer, D., 2015. Evolution of reservoir properties in the Lower Triassic aquifer sandstones of the Thuringian Syncline in Central Germany (Doctoral dissertation).
- Bodnar R. J., 2003. Reequilibration of fluid inclusions. – In: Samson, I., Anderson, A., Marshall, D. (Eds.), *Fluid Inclusions: Analysis and Interpretation*. Mineral. Assoc. Canada, Short Course 32, 213–230.

- Bodnar, R. J., 1994. Synthetic fluid inclusions: XII. The system H<sub>2</sub>O-NaCl. Experimental determination of the halite liquidus and isochores for a 40 wt% NaCl solution. *Geochimica et Cosmochimica Acta*, 58 (3), 1053–1063.
- Burruss, R. C., 1987. Diagenetic palaeotemperatures from aqueous fluid inclusions: re-equilibration of inclusions in carbonate cements by burial heating. *Mineralogical Magazine*, 51(362), 477–481.
- Cao, B., Luo, X., Zhang, L., Sui, F., Lin, H., Lei, Y., 2017. Diagenetic heterogeneity of deep sandstones and its relationship to oil emplacement: a case study from the middle Jurassic toutunhe formation in the Fukang Sag, central Junggar Basin (NW China). *Geofluids*, 2017. <https://doi.org/10.1155/2017/4292079>.
- Dockter, J., Langbein, R., Seidel, G., 1967. Keuper in Thüringen. Abschlussbericht (unpublished).
- Duschl, F., 2018. Structural control on fluid migration in inverted sedimentary basins (Doctoral dissertation, Georg-August-Universität Göttingen).
- Duschl, F., Van den Kerkhof, A.M., Sosa, G., Leiss, B., Wiegand, B., Vollbrecht, A., Sauter, M., 2016. Fluid inclusion and microfabric studies on Zechstein carbonates (Ca<sub>2</sub>) and related fracture mineralizations – New insights on gas migration in the Lower Saxony Basin (Germany). *Marine and Petroleum Geology* 77, 300–322. <http://dx.doi.org/10.1016/j.marpetgeo.2016.06.020>.
- Förster, A., Schöner, R., Förster, H.-J., Norden, B., Blaschke, A.-W., Luckert, J., Beutler, G., Gaupp, R., Rhede, D., 2010. Reservoir characterization of a CO<sub>2</sub> storage aquifer: The Upper Triassic Stuttgart Formation in the Northeast German Basin. *Marine and Petroleum Geology* 27, 2156–2172. <https://doi.org/10.1016/j.marpetgeo.2010.07.010>.
- Friberg, L. J., 2001. Untersuchungen zur Temperatur- und Absenkungsgeschichte sowie zur Bildung und Migration von Methan und molekularem Stickstoff im Nordostdeutschen Becken. Ber. Forschungszentrum Jülich 3914, 1–248.
- Friedman, I., O'Neil, J. R., 1977. Data of Geochemistry: Compilation of stable isotope fractionation factors of geochemical interest. Chapter KK (Vol. 440). US Government Printing Office.
- Fritz, P., Smith, D. G. W., 1970. The isotopic composition of secondary dolomites. *Geochimica et Cosmochimica Acta*, 34 (11), 1161–1173.
- Füchtbauer, H., 1988. *Sedimente und Sedimentgesteine*. E. Schweizerbart'sche Verlagsbuchhandlung, Stuttgart.

- Gerdes, A., Zeh, A., 2006. Combined U–Pb and Hf isotope LA-(MC-)ICP-MS analyses of detrital zircons: comparison with SHRIMP and new constraints for the provenance and age of an Armorican metasediment in Central Germany. *Earth Planet Sci. Lett.* 249, 47–61.
- Gerdes, A., Zeh, A., 2009. Zircon formation versus zircon alteration – new insights from combined U-Pb and Lu-Hf in-situ La-ICP-MS analyses of Archean zircons from the Limpopo Belt. *Chem. Geol.* 261, 230–243.
- Goldstein, R. H., 1986. Reequilibration of fluid inclusions in low-temperature calcium-carbonate cement. *Geology*, 14 (9), 792–795.
- Goldstein, R. H., Reynolds, T. J., 1994. Systematics of fluid inclusions in diagenetic minerals.
- Hay R. L., 1978. Zeolites in sedimentary rocks. *Sedimentology*. Encyclopedia of Earth Science. Springer, Berlin, Heidelberg. [https://doi.org/10.1007/3-540-31079-7\\_251](https://doi.org/10.1007/3-540-31079-7_251).
- Hay, R. L., 1966. Zeolites and zeolitic reactions in sedimentary rocks. *Geological Society of America Special Paper 85*, 1–130. <https://doi.org/10.1130/SPE85-p1>.
- Hay, R. L., Sheppard, R.A., 2001. Occurrence of zeolites in sedimentary rocks: An overview. *Reviews in mineralogy and geochemistry*, 45 (1), 217–234. <https://doi.org/10.2138/rmg.2001.45.6>.
- Heling, D., 1965. Zur Petrographie des Schilfsandsteins. *Beiträge zur Mineralogie und Petrographie* 11, 272–296. <https://doi.org/10.1007/BF01172137>.
- Hesse, R., Gaupp, R., 2021. *Diagenese klastischer Sedimente*. Springer Spektrum, Berlin, Heidelberg. <https://doi.org/10.1007/978-3-662-59685-2>.
- Hornung, T., Brandner, R., Krystyn, L., Joachimski, M. M., Keim, L. 2007. Multistratigraphic constraints on the NW Tethyan “Carnian crisis”. *The Global Triassic*, 41, 59–67.
- Hoth, K., Rusbült, J., Zagora, K., Beer, H., Hartmann, O., 1993. Die tiefen Bohrungen im Zentralabschnitt der Mitteleuropäischen Senke – Dokumentation für den Zeitabschnitt 1962–1990. *Schriftenreihe für Geowissenschaften 2*, Gesellschaft für Geowissenschaften e. V. (i. G.), Berlin.
- Japsen, P., Green, P. F., Nielsen, L. H., Rasmussen, E. S., Bidstrup, T., 2007. Mesozoic–Cenozoic exhumation events in the eastern North Sea Basin: a multi-disciplinary study based on palaeothermal, palaeoburial, stratigraphic and seismic

- data. *Basin Research*, 19, 451–490. <https://doi.org/10.1111/j.1365-2117.2007.00329.x>.
- Kampschulte, A., Buhl, D., Strauss, H., 1998. The sulfur and strontium isotopic compositions of Permian evaporites from the Zechstein basin, northern Germany. *Geologische Rundschau*, 87, 192–199.
- Khalifa, M., Morad, S., 2012. Impact of structural setting on diagenesis of fluvial and tidal sandstones: The Bahi Formation, Upper Cretaceous, NW Sirt Basin, North Central Libya. *Marine and Petroleum Geology* 38 (1), 211–231. <https://doi.org/10.1016/j.marpetgeo.2011.05.006>.
- Lippmann, R., 2012. Diagenesis in Rotliegend, Triassic and Jurassic clastic hydrocarbon reservoirs of the Central Graben, North Sea. (Doctoral Thesis) Friedrich-Schiller-Universität Jena, Germany.
- Maier, U., Tatomir, A., Sauter, M., 2022. Hydrogeochemical modeling of mineral alterations following CO<sub>2</sub> injection. *Applied Geochemistry*, 136, 105–151. <https://doi.org/10.1016/j.apgeochem.2021.105151>.
- Mansurbeg, H., Morad, S., Salem, A., Marfil, R., El-Ghali, M. A. K., Nystuen, J. P., Caja, M. A., Amorosi, A., Garcia, D. La Iglesia, A., 2008. Diagenesis and reservoir quality evolution of palaeocene deep-water, marine sandstones, the Shetland-Faroes Basin, British continental shelf. *Marine and Petroleum Geology*, 25 (6), 514–543. <https://doi.org/10.1016/j.marpetgeo.2007.07.012>.
- Mao, S., Duan, Z., 2008. The P, V, T, x properties of binary aqueous chloride solutions up to T= 573 K and 100 MPa. *The Journal of Chemical Thermodynamics*, 40 (7), 10461063. doi:10.1016/j.jct.2008.03.005.
- Mayer, K. U., 1999. A multicomponent reactive transport model for variably saturated media, Department of Earth Sciences (Doctoral dissertation, PhD Thesis, University of Waterloo, Ontario, Canada.[in page nr.: 5]).
- Mayer, K. U., Frind, E. O., Blowes, D. W., 2002. Multicomponent reactive transport modeling in variably saturated porous media using a generalized formulation for kinetically controlled reactions. *Water Resources Research*, 38 (9), 131.
- McBride, E. F., 1963. A classification of common sandstones. *Journal of Sediment Petrology* 33, 664–669. <https://doi.org/10.1306/74D70EE8-2B21-11D7-8648000102C1865D>.
- McNeil, B., Shaw, H. F., Rankin, A. H., 1995. Diagenesis of the Rotliegend Sandstones in the V-Fields, southern North Sea: a fluid inclusion study. Geological Society,

- London, Special Publications, 86 (1), 125–139.  
<https://doi.org/10.1144/GSL.SP.1995.086.01.10>.
- Moore, C. H., Druckmann, Y., 1981. Burial diagenesis and porosity evolution, Upper Jurassic Smackover, Arkansas and Louisiana - AAPG, 65, 597–628.
- Neuser, R. D., Bruhn, F., Götze, J., Habermann, D., Richter, D. K., 1995. Kathodolumineszenz: Methodik und Anwendung. Zentralblatt für Geologie und Paläontologie Teil I, H. 1/2, 287–306.
- Niegel, S., Franz, M., 2023. Depositional and diagenetic controls on porosity evolution in sandstone reservoirs of the Stuttgart Formation (North German Basin). *Marine and Petroleum Geology*, 106157. <https://doi.org/10.1016/j.marpetgeo.2023.106157>.
- Nielsen, H., 1968. Sulphur isotopes and the formation of evaporite deposit. – In: *Proceed. Geol. of saline deposits; Hannover*.
- Nielsen, H., Ricke, W., 1964. Schwefelisotopenverhältnisse von Evaporiten aus Deutschland; Ein Beitrag zur Kenntnis von  $\delta^{34}\text{S}$  im Meerwassersulfat. *Geochimica et Cosmochimica Acta*, 28 (5), 577–591.
- Norden, B., Frykman, P., 2013. Geological modelling of the Stuttgart Formation at Ketzin CO<sub>2</sub> storage site, Germany. *International Journal of Greenhouse Gas Control*, 19, 756–774. <https://doi.org/10.1016/j.ijggc.2013.04.019>.
- Parkhurst, D. L., Appelo, C. A. J., 2013. Description of input and examples for PHREEQC version 3 a computer program for speciation, batch-reaction, one-dimensional transport, and inverse geochemical calculations. *US geological survey techniques and methods*, 6 (A43), 497.
- Patel, S. S., Sahoo, S., 2021. Investigation of water quality of Damanganga estuary using water quality index, south Gujarat, India. *Sustainability, Agri, Food and Environmental Research*, 9 (2), 148–167.
- Plein, E., 1993. Bemerkungen zum Ablauf der paläogeographischen Entwicklung im Stefan und Rotliegend des Norddeutschen Beckens.- *Geol. Jb.*, A131, 99116.
- Portnyagin, M. V., Ponomareva, V. V., Zelenin, E. A., Bazanova, L. I., Pevzner, M. M., Plechova, A. A., Garbe-Schönberg, D., 2020. TephraKam: geochemical database of glass compositions in tephra and welded tuffs from the Kamchatka volcanic arc (northwestern Pacific). *Earth System Science Data*, 12 (1), 469–486.

- Rasbury, E. T., and Cole, J. M., 2009. Directly dating geologic events: U-Pb dating of carbonates: *Reviews of Geophysics*, v. 47, p. 1–27. <https://doi.org/10.1029/2007RG000246>.
- Rieken, R., 1988. Lösungszusammensetzung und Migrationsprozesse von Paläo-Fluidsystemen in Sedimentgesteinen des Norddeutschen Beckens.- Göttinger Arbeit. *Z. Geol. u. Paläont.*, 37, 116 S.
- Rigo, M., Joachimski, M. M., 2010. Palaeoecology of Late Triassic conodonts: Constraints from oxygen isotopes in biogenic apatite. *Acta Palaeontologica Polonica*, 55 (3), 471–478.
- Rodon, S., Littke, R., 2005. Thermal maturity in the Central European Basin system (Schleswig-Holstein area): results of 1D basin modeling and new maturity maps. *International Journal of Earth Sciences*, 94 (5), 815–833. <http://dx.doi.org/10.1007/s00531-005-0006-1>.
- Rosenbaum, J., Sheppard, S. M. F., 1986. An isotopic study of siderites, dolomites and ankerites at high temperatures. *Geochimica et cosmochimica acta*, 50 (6), 1147–1150.
- Steele-MacInnis, M., Bodnar, R. J., Naden, J., 2011. Numerical model to determine the composition of H<sub>2</sub>O–NaCl–CaCl<sub>2</sub> fluid inclusions based on microthermometric and microanalytical data. *Geochimica et Cosmochimica Acta*, 75 (1), 21–40.
- Sullivan, M. D., Haszeldine, R. S., Fallick, A. E., 1990. Linear coupling of carbon and strontium isotopes in Rotliegend sandstone, North Sea: evidence for crossformational fluid flow. – *Geology*, 18, 1215–1218.
- Tucker, M. E., 1985. Einführung in die Sedimentpetrologie. Ferdinand Enke Verlag, Stuttgart.
- Van den Kerkhof, A. M., Hein, U. F., 2001. Fluid inclusion petrography. *Lithos*, 55 (14), 27–47.
- von Eynatten, H., Kley, J., Dunkl, I., Hoffmann, V. E., Simon, A., 2021. Late Cretaceous to Paleogene exhumation in central Europe – localized inversion vs. large-scale domal uplift. *Solid Earth*, 12, 935–958. <https://doi.org/10.5194/se-12-935-2021>.
- Weibel, R., Olivarius, M., Jakobsen, F. C., Whitehouse, M., Larsen, M., Midtgaard, H., Nielsen, K., 2019. Thermogenetic degradation of early zeolite cement: An important process for generating anomalously high porosity and permeability in deeply buried sandstone reservoirs?. *Marine and Petroleum Geology*, 103, 620–645. <https://doi.org/10.1016/j.marpetgeo.2019.02.006>.

- Wentworth, C., 1922. A scale of grade and class terms for clastic sediments. *Journal of Geology* 30, 377–392.
- Wolfgramm, M., Franz, M. Agemar, T., 2014. Explorationsstrategie tiefer geothermischer Ressourcen am Beispiel des Norddeutschen Beckens [Exploration strategy of deep geothermal Resources on the Example of the North German Basin]. – In: Bauer, M., Freeden, W., Jacobi, H., Neu, T. (Eds.), *Handbuch Tiefe Geothermie*. Springer, Berlin, 463–505.
- Wolfgramm, M., Kuempel, H.-J. (editor), Roehling, H.-G. (editor), Steinbach, V. (editor), 2012. Deep geothermal waters in the North German Basin (Geothermische Tiefenwaesser im Norddeutschen Becken), *Schriftenreihe der Deutschen Gesellschaft für Geowissenschaften Bd. 80*, 209.
- Wolfgramm, M., 2005. Fluidentwicklung und Diagenese im Norddeutschen Becken – Petrographie, Mikrothermometrie und Geochemie stabiler Isotope. *Hallesches Jb.*, B, Beiheft 20.
- Wolfgramm, M., Schmidt-Mumm, A., 2001. Die zeitliche Einordnung diagenetischer und hydrothermaler Fluidphasen im Nordostdeutschen Becken (NEDB). In: *Zbl. Geol. Paläont. Nummer I (3/4)*, 237–256
- World Health Organization (WHO), 2005. *Nutrients in Drinking Water*, 196 p.
- Zeh, A., Franz, M., Obst, K., 2021. Zircon of Triassic Age in the Stuttgart Formation (Schilfsandstein)—Witness of Tephra Fallout in the Central European Basin and New Constraints on the Mid-Carnian Episode. *Frontiers in Earth Science* 9, 15 p. <https://doi.org/10.3389/feart.2021.778820>



# Chapter V

## 5 Diagenetic controls on sandstone reservoirs of the Exter Formation (Rhaetian) – preliminary results

The petrography and diagenesis of the Exter Formation (Rhaetian) was also investigated during the project *GeoPoNDD*. This chapter presents the preliminary results of this study and will be published in the future. Following, a short overview of the Rhaetian reservoirs is given to show that the diagenetic evolution of the Schilfsandstein equally applies to other Mesozoic reservoirs.

**Authors' edited topics:** This chapter was mainly conceptualized and written by Sebastian Niegel. Discussions were made with Matthias Franz.

The sandstones of the Exter Formation (Rhaetian) are the reservoirs with the highest potential for hydrothermal use in the North German Basin. The reason for this is that the Rhaetian sandstones deposited in high thicknesses and are located at an average depth where temperatures are sufficiently high for geothermal uses. In addition, the sandstones at this depth are in most cases only insignificantly affected by diagenetic modifications (decreasing porosity). In Neubrandenburg, Neustadt-Glewe and Waren the municipal suppliers operate these reservoirs for seasonal heat storage or district heating (Franz et al., 2018a).

The Rhaetian reservoir complex (Upper Keuper) comprises distributive fluvial and deltaic depositional systems (Fig. 5.1) (Franz and Wolfgramm, 2008; Bachmann et al., 2010; Barth et al., 2014; Gaupp, 1991). The Rhaetian distributive fluvial system forms the Rhaetian reservoirs A and B (previously the Postera Sandstone) and the deltaic system forms the Rhaetian reservoirs C–F (previously the Contorta Sandstone) (Franz et al., 2018a).

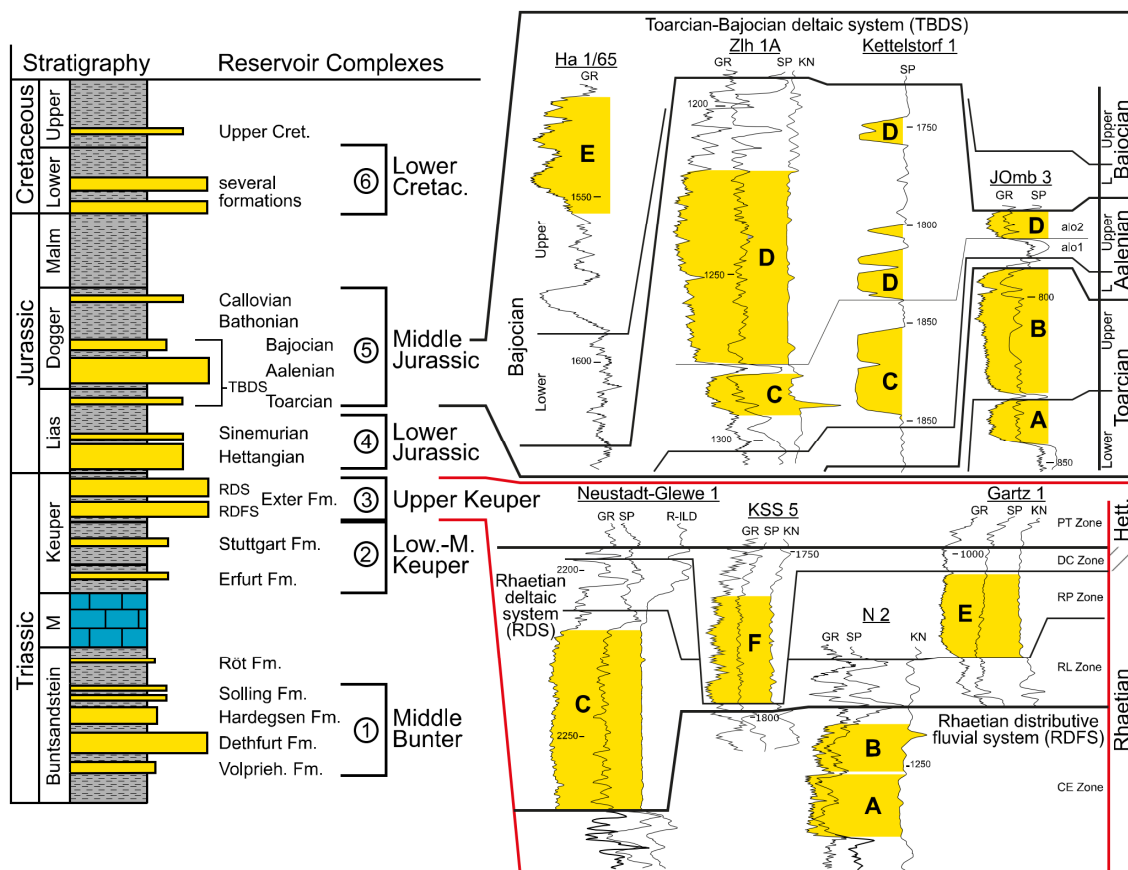


Fig. 5.1: Mesozoic reservoir complexes with examples of the Rhaetian Deltaic System, modified after Franz et al. (2018a).

Subsurface facies of the Rhaetian deltaic system (Fig. 5.2) revealed environments prograding from northern and southern margins towards the subsidence centre, which was fed by Scandinavian sources.

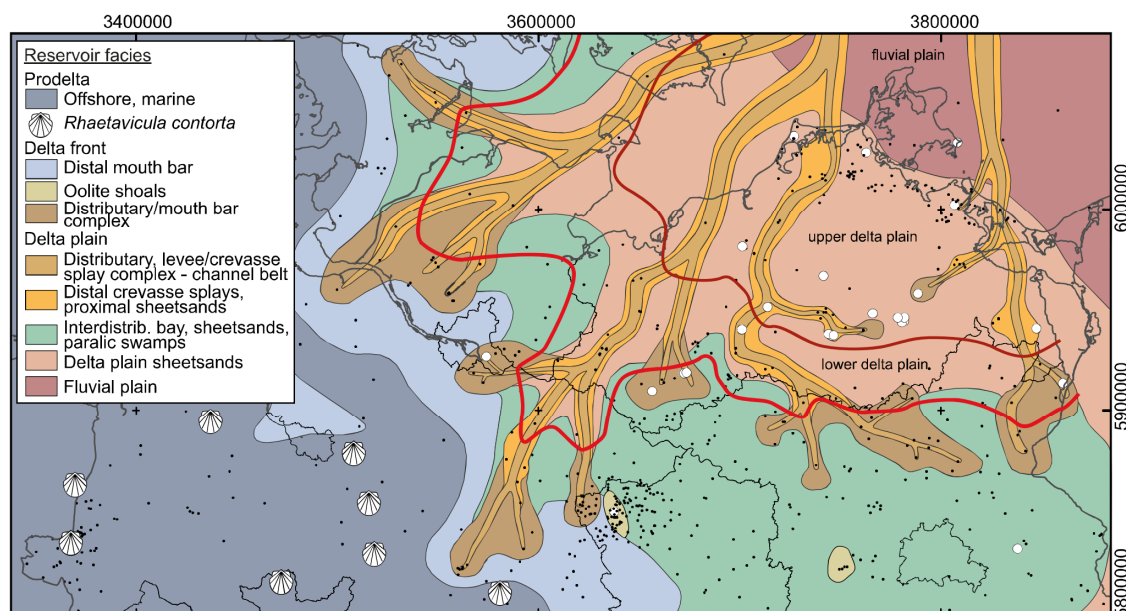


Fig. 5.2: The Rhaetian deltaic system. Subsurface facies map of the high-constructive fluvial-dominated Rhaetian deltaic system; red lines represent the margins of the upper and lower deltaic plains; post-sedimentary erosion not shown, modified after Franz et al. (2018a).

The samples contained herein were already part of a previous study of Niegel and Franz (2023; chapter III) and Franz et al. (2018b) and are buried at depths between 629 and 3257 m. The median grain sizes of Rhaetian sandstones (198 samples) range from 0.6 to 4.4 Phi (Folk and Ward 1957). On detail, grain size and skewness of sandstones are subject to noticeable changes which can be related to facies shifts and associated changes from bedload to suspension load processes (Fig. 5.3). According to the grain size classes of Wentworth (1922), the samples are classified as coarse sand to coarse silt. The majority of the samples are characterised medium to fine sand (1–3 Phi).

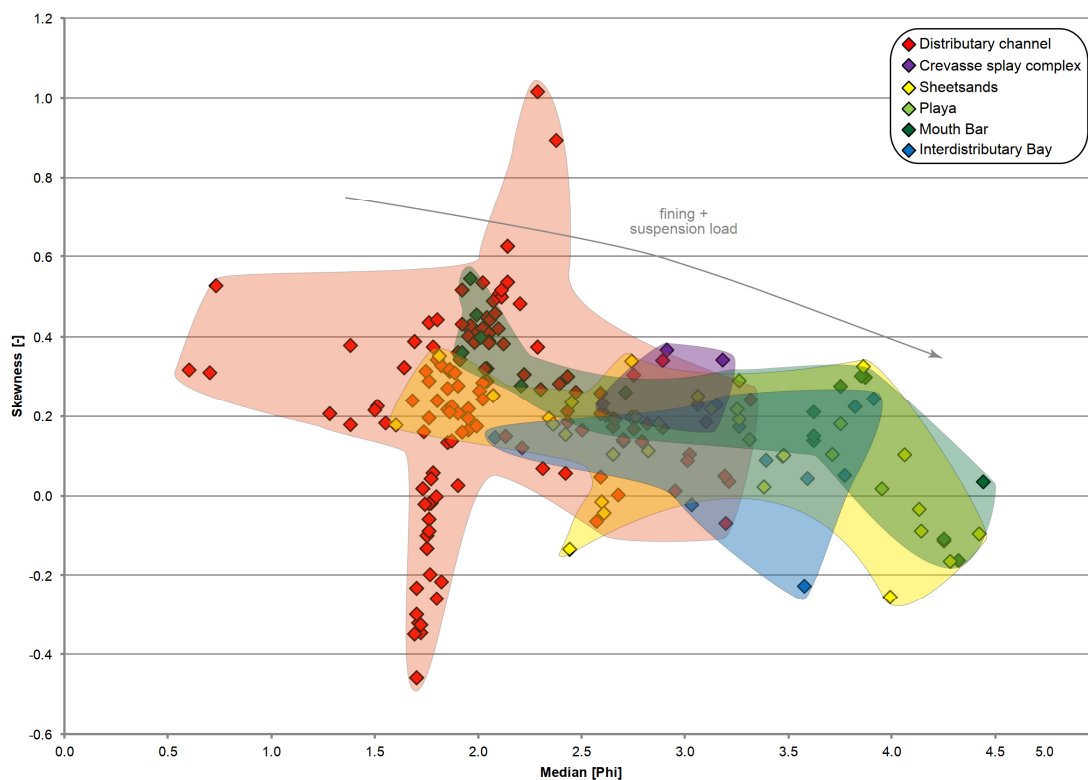


Fig. 5.3: Granulometry of the Exter Formation (198 samples), median (Phi) and skewness according to Folk and Ward (1957).

The quality of the Rhaetian reservoirs is favoured by the generally high compositional maturity of sandstones being subarkoses and quartzarenites (Fig. 5.4) and the mostly low content of detrital matrix within pores and substantial diagenetic cementation (Fig. 5.5).

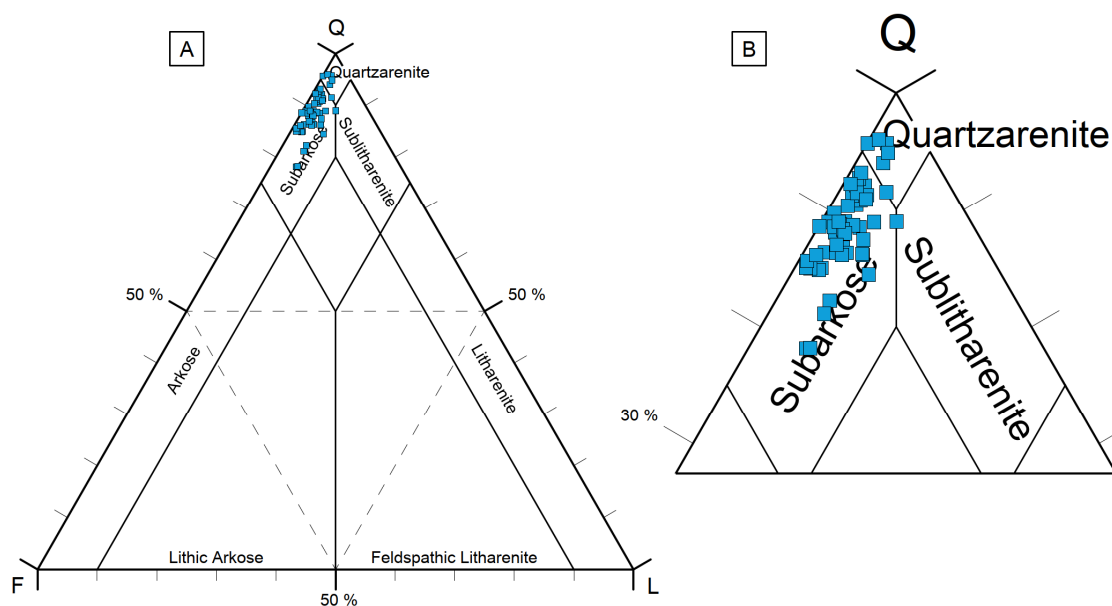


Fig. 5.4: Detrital mineralogy of the Exter Formation. **(A)** Ternary plot (McBride, 1963) showing the 54 samples investigated in this study. Q – mono- and polycrystalline quartz and chert, F – feldspar, L – lithics; **(B)** Detail of (A).

The mechanical compaction of the investigated sandstones is remarkably low. The grain fabrics are dominated by point contacts, whereas long-contacts and convex-concave contacts are present in low abundance (Fig. 5.5).

The qualitative and quantitative analyses of grain contacts resulted in values of contact strength (Füchtbauer, 1988) ranging from 1.1 to 2.0 (median 1.5) for 36 samples.

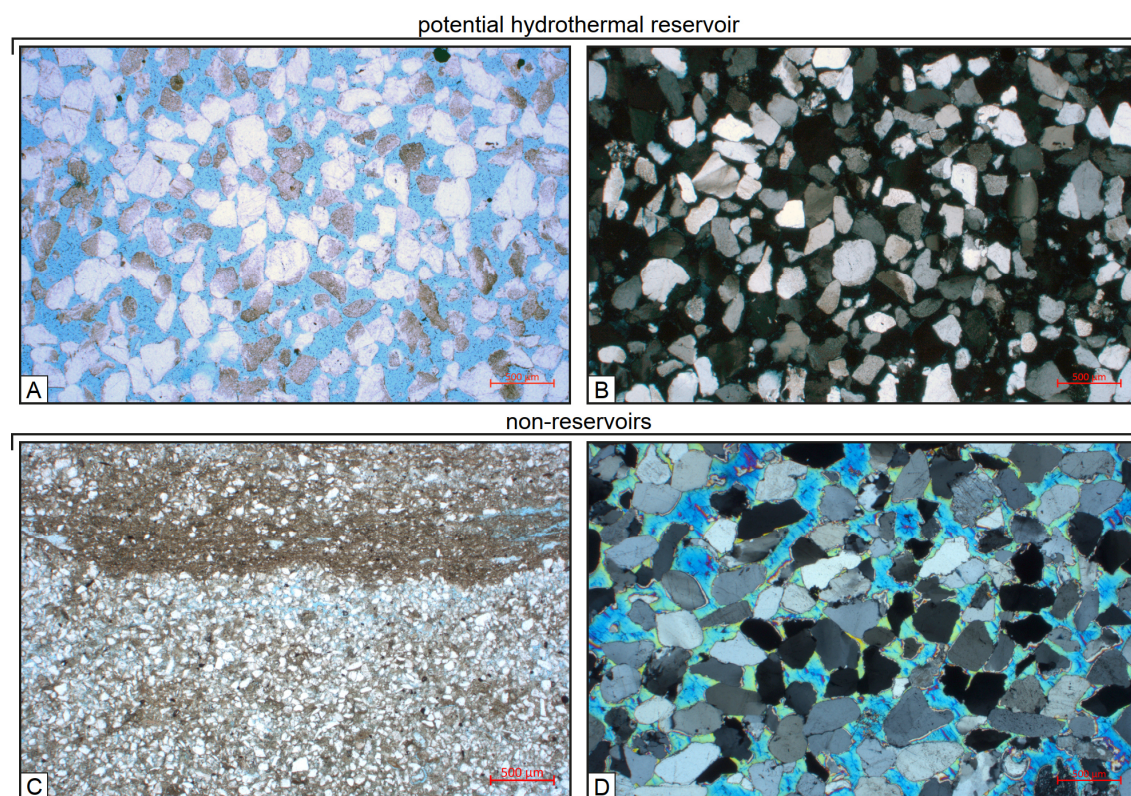


Fig. 5.5: Thin section examples. **Potential hydrothermal reservoirs:** (A) Gartz 1/65, sample 13-24 (depth 1044.15): distributary channel fill showing floating grains, point contacts and open pore space (stained blue); scale is 500 µm, parallel nicols (B) As before, scale is 500 µm, crossed nicols. **Non-reservoirs:** (C) Tarnow 1/65, sample 11-02 (depth 917.1 m): matrix-rich laminated very fine-grained sandstone to siltstone of a wet playa; scale is 500 µm, parallel nicols (D) Hamburg Allermoehe 1, sample 11-06 (depth 3251.2 m): distributary channel fill with pore-filling sulphate; scale is 500 µm, crossed nicols.

Intergranular volumes calculated according to Houseknecht (1987) and Ehrenberg (1989) range from 10.2 to 49.3 % for all samples (Fig. 5.6). For the channel deposits, intergranular volumes > 22 % were noted. Remarkable are ten sandstones with high intergranular volumes of more than 40 % corresponding to assumed initial porosities (Atkins and McBride, 1992). Comparable values were recorded for the Schilfsandstein Members in Niegel and Franz (2023).

The high intergranular volumes and low contact strength of channel sandstones indicate a cementation-controlled diagenesis during which early cementation supported the grain fabric and prevented significant mechanical compaction (Fig. 5.6).

Calculated after Ehrenberg (1989), 0–70 % of the original porosity of these channel sandstones was destroyed by cementation but only 0–55 % by mechanical compaction (Fig. 5.6).

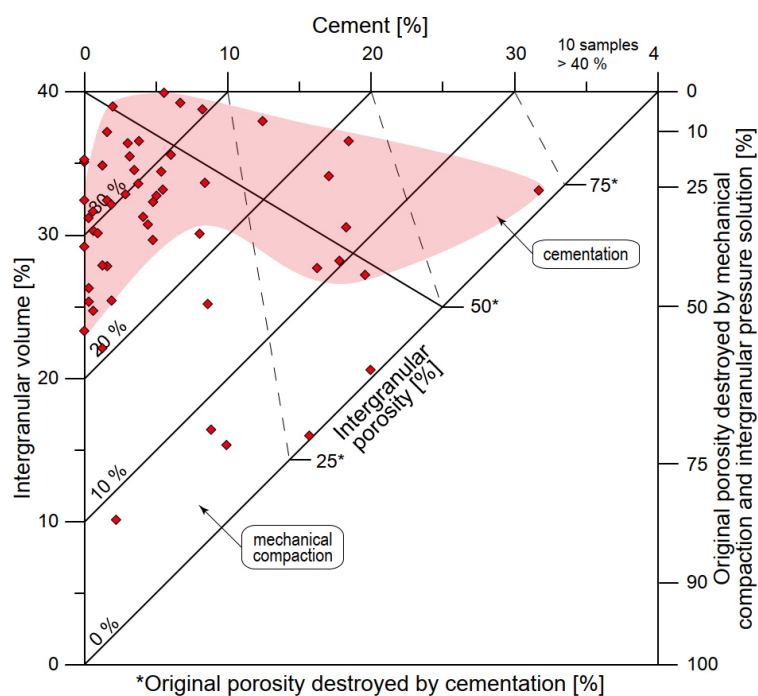


Fig. 5.6: Intergranular and cement volumes (Houseknecht, 1987; Ehrenberg, 1989); red area represents channel deposits.

Considering all samples, the secondary porosity of 0–40.8 % (median 26.9 %), which presents the recent porosity, is mainly formed of intergranular pores, whereas intragranular pores and oversized pores are less abundant.

The diagenesis of the Exter Formation is characterised by typical paragenetic sequences of authigenic minerals. The abundance of authigenic minerals derived from modal analyses varies from 0 to 38.1 % (median 4.6 %) for all investigated samples. The paragenetic sequence typically includes carbonate and quartz overgrowths, which were subsequently formed in eo- to mesogenetic regimes (Fig. 5.7). Pyrite, clay cutans, kaolinite, analcime, chlorite, siderite and sulphate were subordinately and locally present (Fig. 5.8).

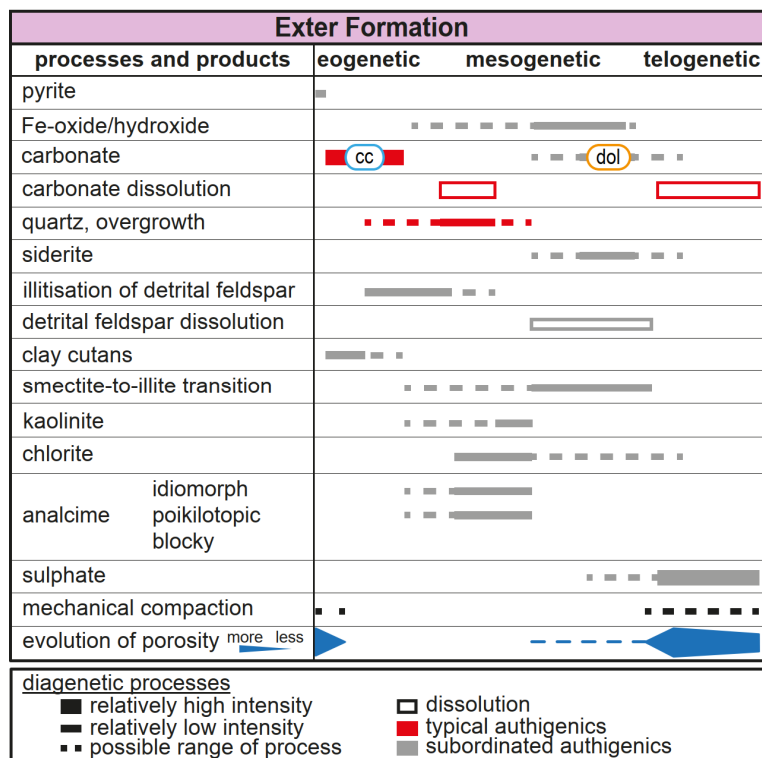
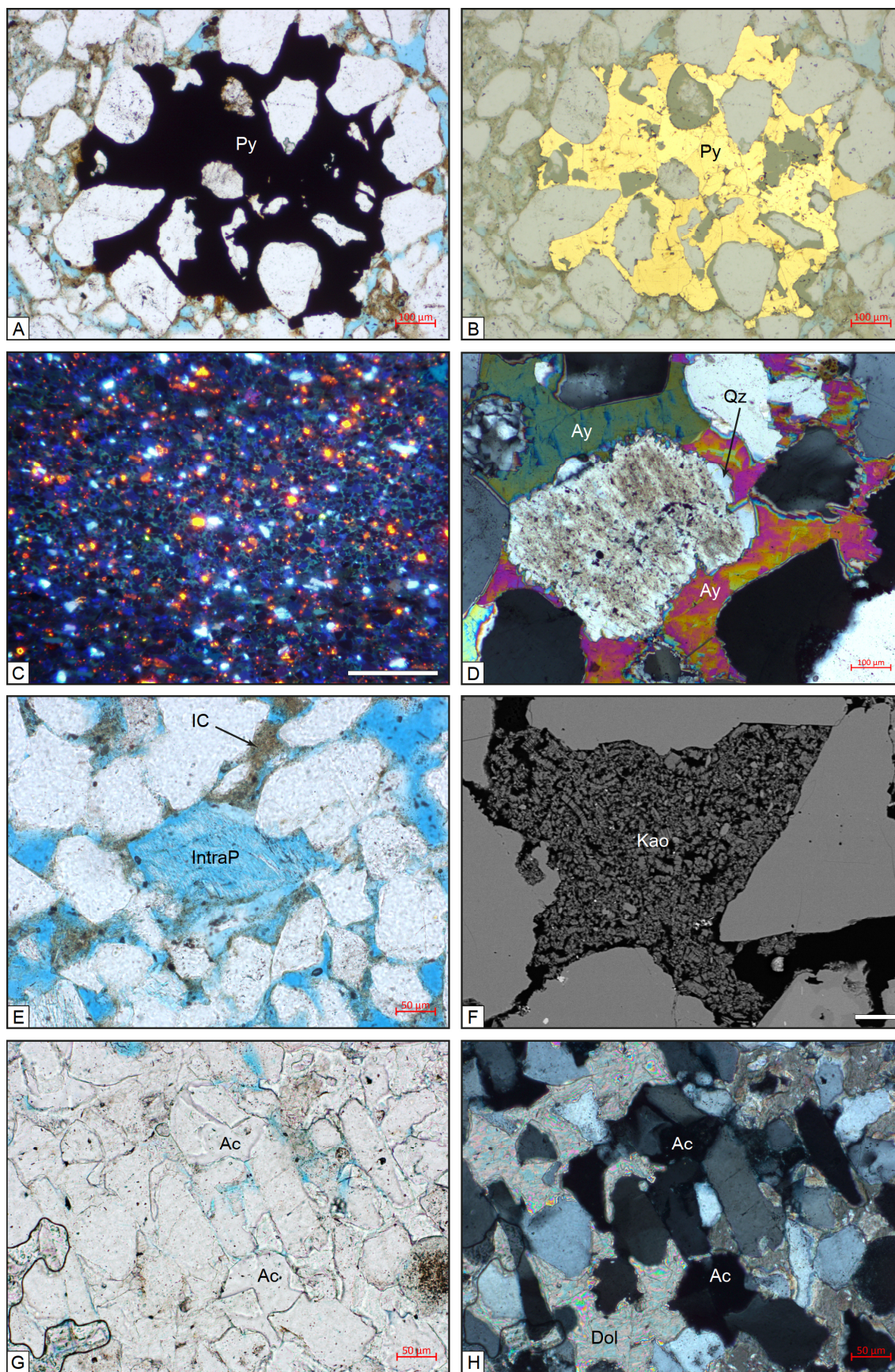


Fig. 5.7: Schematic paragenetic sequences of diagenetic processes and products reconstructed for the Exter Formation.

Fig. 5.8 (**facing page**): Thin section examples of authigenic mineralogy. (A) Eogenetic pyrite (Py); scale is 100 µm, Barth 10/65 (sample 11-16), parallel nicols. (B) As before, scale is 100 µm, reflected light. (C) Residues of eogenetic carbonate showing bright orange luminescence; scale is 500 µm, Wolgast 1/1A/63 (sample 11-34). (D) Detrital feldspar grain with quartz overgrowth and pore-filling anhydrite; scale is 100 µm, Hamburg Allemoehe 1 (sample 11-04), crossed nicols. (E) Dissolution of feldspar grain resulting in intragranular porosity (IntraP) and clay cutans (IC) on detrital grains; scale is 20 µm, KSS 5/66 (sample 11-26), parallel nicols. (F) SEM image showing kaolinite booklets (Kao); scale is 20 µm, KSS 5/66 (sample 11-09). (G) Idiomorphic analcime crystals (Ac) predating pore-filling dolomite (Dol); scale is 50 µm, Siedenlangenbeck 1/84 (sample 11), parallel nicols. (H) As before, scale is 50 µm, crossed nicols.





The study of the Rhaetian sandstones has shown undercompacted grain fabrics, low abundance of authigenic minerals (median 4.6 %) and large secondary porosity volumes (median 26.9 %). The discrepancy of undercompacted grain fabrics and porosity volumes of >20 % at depth of up to c. 1,800 m represents the same phenomenon was documented for the sandstones of the Stuttgart Formation (Niegel and Franz, 2023; chapter III). The proposed model for the Stuttgart Formation of cementation-controlled burial diagenesis, followed by dissolution-controlled retrograde diagenesis (uplift) and low to moderate reburial can also be applied for the Exter Formation (Niegel and Franz, 2023; see chapter 3.5.2.2). Thus, depending on the typical depositional systems of the Mesozoic (fluvial, deltaic), the diagenesis model can be applied to predictions of other reservoirs within the Mesozoic succession of the North German Basin.

## **Acknowledgement**

The author acknowledges funding by the Federal Ministry for Economic Affairs and Climate Action (BMWK, grant numbers 0325920). The Geological State Surveys of Brandenburg, Mecklenburg-Vorpommern and Hamburg kindly provided access to core repositories. The support of Graciela M. Sosa, Alfons M. van den Kerckhof (University of Göttingen) and Christian Buse (Geothermie Neubrandenburg GmbH) with Cathodoluminescence, XRD and SEM-EDX analyses is gratefully acknowledged. The author acknowledges supervision and valuable discussions with Matthias Franz (University of Göttingen).

## **References**

- Atkins, J. E., McBride, E. F., 1992. Porosity and packing of Holocene river, dune, and beach sands: AAPG Bulletin, v. 76, 339–355. <https://doi.org/10.1306/BDF87F4-1718-11D7-8645000102C1865D>.
- Bachmann, G. H., Geluk, M. C., Warrington, G., Becker-Roman, A., Beutler, G., Hagdorn, H., Hounslow, M. W., Nitsch, E., Röhling, H.-G., Simon, T., Szulc, A., with contributions by Dusar, M., Nielsen, L. H., Barnasch, J., Franz, M., 2010: Triassic. – In: Doornenbal, J.C., Stevenson, A. G. (Eds.), Petroleum Geological Atlas of the Southern Permian Basin Area, Houten (EAGE Publ.), pp. 149–173.
- Barth, G., Franz, M., Heunisch, C., Kustatscher, E., Thies, D., Vespermann, J., Wolfgramm, M., 2014. Late Triassic (Norian–Rhaetian) brackish to freshwater

- habitats at a fluvial-dominated delta plain (Seinstedt, Lower Saxony, Germany). *Palaeobiology and Palaeoenvironments*, 94, 495–528. Gaupp, 1991.
- Ehrenberg, S. N., 1989. Assessing the relative importance of compaction processes and cementation to reduction of porosity in sandstones: discussion; compaction and porosity evolution of Pliocene sandstones, Ventura Basin, California: discussion. *American Association of Petroleum Geologists Bulletin* 73, 1274–1276. <https://doi.org/10.1306/44B4AA1E-170A-11D7-8645000102C1865D>.
- Folk, R. L., Ward, W. C., 1957. Brazos River bar: a study in the significance of grain size parameters. *Journal of Sedimentary Petrology* 27, 3–26. <http://dx.doi.org/10.1306/74D70646-2B21-11D7-8648000102C1865D>.
- Franz, M. Wolfgramm, M., 2008. Sedimentologie, Petrologie und Fazies geothermischer Reservoirs des Norddeutschen Beckens am Beispiel der Exter-Formation (Oberer Keuper, Rhaetium) NE-Deutschlands [Sedimentology, petrology and facies of geothermal reservoirs of the North German Basin on the example of the Exter Formation (Upper Keuper, Rhaetian)]. *Zeitschrift für geologische Wissenschaften*, 36, 223–248.
- Franz, M., Barth, G., Zimmermann, J., Budach, I., Nowak, K., Wolfgramm, M., 2018a. Geothermal resources of the North German Basin: exploration strategy, development examples and remaining opportunities in Mesozoic hydrothermal reservoirs. *Geological Society, London, Special Publications*, 469 (1), 193–222. <https://doi.org/10.1144/SP469.11>.
- Franz, M., Nowak, K., Niegel, S., Seidel, E., Wolf, M., Wolfgramm, M., 2018b. Deep geothermal resources of the North German Basin: The hydrothermal reservoirs of the Stuttgart Formation (Schilfsandstein, Upper Triassic). *Zeitschrift der Deutschen Gesellschaft für Geowissenschaften* 169 (3), 353–387. <https://doi.org/10.1127/zdgg/2018/0164>.
- Füchtbauer, H., 1988. *Sedimente und Sedimentgesteine*. E. Schweizerbart'sche Verlagsbuchhandlung, Stuttgart.
- Houseknecht, D. W., 1987. Assessing the relative importance of compaction processes and cementation to reduction of porosity in sandstones. *AAPG Bulletin* 71, 633–642.
- McBride, E. F., 1963. A classification of common sandstones. *Journal of Sediment Petrology* 33, 664–669. <https://doi.org/10.1306/74D70EE8-2B21-11D7-8648000102C1865D>.

Niegel, S., Franz, M., 2023. Depositional and diagenetic controls on porosity evolution in sandstone reservoirs of the Stuttgart Formation (North German Basin). *Marine and Petroleum Geology*, 106157. <https://doi.org/10.1016/j.marpetgeo.2023.106157>.

Wentworth, C., 1922. A scale of grade and class terms for clastic sediments. *Journal of Geology* 30, 377–392.

## Curriculum Vitae

Name Sebastian Niegel  
Geburtsdatum 14. Mai 1987  
Geburtsort Borna

### Ausbildung und berufliche Karriere

1993–1997 Grundschule Borna-Ost  
1997–2005 Pestalozzi-Gymnasium, Borna  
2006–2010 Bachelor-Studiengang in Geologie und Mineralogie,  
Technische Universität Bergakademie Freiberg  
2010–2014 Master-Studiengang in Geowissenschaften,  
Technische Universität Bergakademie Freiberg  
2015–2016 Ingenieurgeologe, Anlagenprüforganisation GEOPOHL AG,  
Chemnitz  
2016–2019 Wissenschaftlicher Mitarbeiter am FuE-Verbundvorhaben  
"Geothermische Potenziale Norddeutschlands (GeoPoNDD)",  
Georg-August-Universität Göttingen  
2016–2023 Promotionsstudiengang in Geoscience,  
Georg-August-Universität Göttingen  
seit 2019 Projektingenieur, IBES Baugrundinstitut Freiberg GmbH  
(Mitglied der BPM-Gruppe)